Finite and infinite element method applied to water wave diffraction problems

Baghbani, Alireza

Finite and Infinite Element Method Applied to Water Wave Diffraction Problems

Alireza Baghbani
(M.Sc., B.Sc.)

A thesis submitted for the degree of Doctor of Philosophy
in the Faculty of Science, University of Durham

School of Engineering
The University of Durham, UK
May 1999

To Lucy and my daughter

Acknowledgements

I acknowledge with thanks the invaluable help and advice received from my supervisors Dr David Gregory-Smith and Professor Peter Bettess of School of Engineering. Professor Bettes and his wife Jackie kindly allowed me to adopt their wave program and mesh generators for the purpose of my research.

I extend my gratitude to Professor Grant Hearn for his advice on hydrodynamics, Dr Raj Subramani for his mesh plotting program, Dr Christos Atalianis and Professor and Mrs Bettess for their code of analytical solution for elliptical cylinder diffraction problem, Dr Phil Clark for his wave programs and mesh generator, him, Dr Edmond Chadwick and Dr Omar Laghrouche for their help and useful discussions on different aspects of the infinite element method and Dr Woodford for his help on computer programming. I would also thank Dr Rob de Jue for his collaboration on developing the analytical solution and the mesh generator for multiple body diffraction problem and for his invaluable discussions on different mathematical aspects of the research.

I would like to thank the secretarial and I.T.S. staff of the school of Engineering at Durham University, as well as the Department of Marine Technology at the University of Newcastle upon Tyne for their help and support during my PhD.

I benefited from support, advice and discussions with friends and colleagues especially Professor and Mrs Batho, Professor Mike Petty, Mrs Christine Ramshaw, Mr Ehsan Mesbahi, Miss Suzan Duxbury, Dr Hollie Marsden, Miss Nicky Fry, Mr Alan Proctor, Dr Fiona O'Carroll, Mr Jonathan Hartland and Mr Dave Bell.

I acknowledge the Ministry of Culture and Higher Education of Iran for the partial financial support of this research.

Finally, I am deeply indebted to my parents and my daughter for their invaluable moral support and patient.

Declaration

The material contained within this thesis has not previously been submitted for a degree at the University of Durham or any other university. The research reported within this thesis has been conducted by the author unless indicated otherwise.

Finite and Infinite Element Method Applied to Water Wave Diffraction Problems

Alireza Baghbani, Ph.D. Thesis, 1999

Abstract

In this work, three types of infinite elements are developed to solve the problem of linear water wave diffraction by objects in a 2D unbounded domain. The infinite elements, which model the far field wave potential stretching to infinity, are coupled to conventional finite elements, which model the near field wave potential. This coupling greatly economises the finite element analysis.

The original mapped infinite element, due to Zienkiewicz *et al* [102], is improved to model objects of large aspect ratio more economically. This infinite element (Type 1) can now be used on the exterior of an ellipse (or other shapes) rather than a circle circumscribing the object. The element is validated by solving the problem of diffraction of water waves by an ellipse with different angles of wave incidence. The results are compared with their equivalent analytical solutions and the errors are very small being less than 1.0%.

The wave envelope approach, due to Astley *et al* [9], is employed to develop a simple mapped wave envelope infinite element. The element mass, stiffness and damping matrices are derived from first principles using the weighted residual approach. This element (Type 2) can also be used on the exterior of any shapes. The element is validated by solving the problem of wave diffraction by circular and elliptical vertical cylinders for different angles of wave incidence. The results are compared with their equivalent analytical solutions and again the errors are very small.

The problem of wave diffraction by multiple objects is also considered. A new wave envelope mapped infinite element (Type 3) is developed to tackle such a problem. Examples involving diffraction of water waves by arrays of circular and elliptical cylinders are solved. For circular cylinders, the results are compared with their equivalent analytical solutions which show excellent agreement.

A comparison is made between the three types of infinite elements by solving the diffraction of waves by circular and elliptical vertical cylinders. The results show that all three types of infinite elements can give accurate results in the near field for a given single diffracting object. Type 1 would be a preferable choice in situations where computing resource is the main concern and reliable solutions are required only in the near field. Type 2 or 3 would give very accurate solutions both in the near and far fields. Type 3 is the most suitable choice for modelling any number, shape and configuration of bodies.

Contents

List of Figures

Chapter 1

Introduction

Continuum problems may be modelled by a set of differential equations subjected to some boundary conditions. These equations can be solved to obtain the solutions. The best way obviously is to solve them analytically. However, as this is not possible in the majority of practical cases, experimental and numerical techniques are the only way to tackle such problems. Experimental studies are expensive and time consuming and are advisable either to validate a numerical model or to solve problems that are not solvable otherwise. Various numerical techniques have been developed, over years, such as the Finite Difference Method (FDM), Boundary Element Method (BEM) and Finite Element Method (FEM).

In some cases the domain of interest is unbounded. Although this is not physically the case, in the numerical solution process, it is convenient to assume that the domain extends to infinity. One example of this is the interaction of fluid with structures, such as ships or oil rigs, located in an open water. This is one of the practical problem faced by the offshore industry where it is required to predict the

environmental loads including wind, current and wave loads applied to the structures. The wave effect by far is the largest one on most offshore structures (see the standard texts, e.g. Morgan [85]) and so will be considered here. The fluid (water) will be assumed incompressible and inviscid (no viscosity) and the flow will be assumed irrotational (no vorticity).

When an incoming wave is incident upon object(s), its pattern changes which is often called wave diffraction or scattering. This in turn exerts some forces on the object(s) and the resulting movement of the objects generates some additional waves radiating away from the objects. This is often called wave radiation (see e.g. Wu and Eatock Taylor [112]) but will not be considered here as the objects will be assumed stationary. The amount of the change due to the presence of the objects and so the resulting forces depend on the characteristic length of the objects relative to the wave length. Guidelines are given by different authors (e.g. Hogben and Standing [66], Garrison [57], Mei [84]) as the distinction is necessary because of the limitation of fundamental assumptions; invisid fluid and linear irrotational (potential) flow (see chapter 2). For small objects the change is small and so the wave diffraction effect is negligible and viscous effect (due to flow separation) becomes dominant. Morison's equation [86] can be used to estimate the wave forces (see e.g. Morgan [85]) but this will not be considered here. Morison's equation is based on the assumption that wave forces can be written as the sum of drag and inertia forces. The drag forces are due to wave fluid velocity and the inertia forces are due to wave acceleration. For an oscillatory wave flow the drag forces are dominated by the separation of flow behind the diffracting object and

formation of large vortices. The exception in this case is when the ratio of the incident wave amplitude, A, over the object diameter, D, is small. As Morgan [85] points out, when $A/D < 0.75$ the wave flow is not unidirectional long enough for a substantial vortex flow to develop, and so the drag forces are very small, and the inertia forces are dominant. In this case, the potential flow diffraction theory can be used to predict the wave forces with confidence. For large objects the pattern of an incoming wave is changed significantly by the presence of the object(s) and so diffraction effects become dominant and diffraction analysis must be carried out, which will be considered in this research. Wave diffraction analysis is also referred as calculation of wave loads on large bodies in standard text books. The analysis involves the solution of a non-linear boundary value problem (see chapter 2). Although, much of current research has been focused on the non-linear wave diffraction problems (e.g. Eatock Taylor [52] or Greaves *et al* [62]), the present model will only be applied to the linear wave diffraction problem for the sake of simplicity, firstly to test the proposed numerical model and secondly because linear solutions can be applied to a wide range of large bodies, such as ships, barges, offshore platforms, harbours and so on.

Diffraction analysis can also provide information for many other purposes such as determining the location and type of objects, determining ocean depth and locating schools of fish. The present numerical model will be developed only for linear water wave diffraction by large fixed vertical bottom mounted structures, such as oil rigs, located in the middle of an ocean with a gradually varied water depth (The model will only be validated for constant depth).

Two main classes of numerical methods that have been applied to water wave diffraction problems are the FEM and the BEM which are very similar in their computational steps. In the FEM, the governing equation is transformed into integral equations defined over the entire fluid domain. The domain is then subdivided into subdomains and the integrals are calculated over them numerically by the use of some known functions (see chapter 4). In the BEM, however, the governing integral equation defined only on the boundary and therefore the full 3D domain is reduced to a 2D one to be subdivided into subdomains as in FEM. A review of these techniques is given by different authors, e.g. Mei [84] or Bando *et al* [17].

The BEM has been widely used by practitioners both in industry and research in solving wave diffraction problems, because of its computational efficiency since only the boundary rather than the entire domain needs to be meshed. Examples of applications of the method are given by Faltinsen and Michelsen [56], Garrison [57], Kormeyer *et al* [75]. There are however areas of potential difficulties, such as the problem of irregular frequencies (see John [72]) in using the method. More importantly, the BEM becomes expensive for modelling wave diffraction by objects of complex shapes or by multiple objects because of its dense unsymmetric matrix structure. Recent research has been focused on the development of higher order BEMs to tackle complex shape of the diffraction objects more efficiently. Examples are papers by Liu *et al* [79], Eatock Taylor and Chau [54], Eatock Taylor and Teng [53], Teng and Eatock Taylor [96].

The FEM, on the other hand, has the capability of modelling both objects of complex shapes and multiple objects very easily and does not suffer the problem

of irregular frequencies. On the other hand, it is widely accepted that in the finite element analysis of wave problems at least ten nodes per wavelength are needed to model the oscillatory variation of the wave potential with reasonable accuracy. Hence, a prohibitively large number of elements and so a large amount of computing time is needed to model the entire domain. Various techniques have been suggested to tackle such problems. Some of them are, truncation (e.g. Harari and Hughes [63] or Thompson and Pinsky [97]), dampers (e.g. Bando, Bettess and Emson [18]) matching to a far field analytical solution (e.g. Chen and Mei [40] or Bai and Yeung [16]), coupled finite and boundary element and the infinite element method. A good survey of these techniques is given by Zienkiewicz, Bettess, Chiam and Emson [104]. Truncation and different boundary conditions imposed on the truncating surface to replace the radiation boundary condition at infinity are discussed and compared by Shirron [94]. Some recent works on unbounded domain problems (e.g. by Athanassoulis [12]) were presented in a symposium dedicated to these type of problems [58].

A marriage between the two techniques (FEM and BEM) appeared to be an efficient solution to the problem of wave diffraction in general. In this process the entire domain is subdivided into two regions. The finite region, which surrounds the diffracting object(s) of any shape(s), is modelled with FEM, while the outer infinite region is modelled with BEM. This technique has been called Coupled Finite and Boundary Element Method (e.g. Zienkiewicz *et al* [105, 106] or Zietsman and Eatock Taylor [110]), Hybrid Method (e.g. Atalianis [10]) or Localised Finite Element Method (e.g. Eatock Taylor and Zietsman [55] or Zietsman [109]).

The infinite element method is perhaps most naturally coupled with the finite element method to tackle unbounded problems. This is because the philosophy and computational details associated with their use are very similar. In this process the conventional finite elements, which model the near field potential, are coupled to the infinite elements which model the wave potential stretching to infinity. The infinite element is stretched to infinity in one or more directions and the shape function is chosen with a prior knowledge of the behaviour of the solution in the far field. In this sense, the infinite element method is similar to the method of matching to a far field analytical solution. As the analytical solution in the far field is not always known, the behaviour of the solution is guessed and incorporated into the shape function.

The debate over whether FEM or BEM is superior for modelling unbounded wave problems has been longstanding. Practitioners who used both methods such as Burnett [36], Demkowicz [49] or Shirron [94] concluded that F/IEM is typically more efficient than the BEM. For detailed discussion the reader is referred to the above references. The development of infinite elements is reviewed below.

Infinite elements can be generally classified to three groups, as *decay function*, *mapped* and *wave envelope* infinite elements.

For *decay function* infinite element, the finite domain is extended to infinity in one or more directions by multiplying the conventional finite element shape function by a decay function (Ungless [98], Anderson and Ungless [2], Zienkiewicz and Bettess [107], Bettess [34, 33]). To increase the accuracy of the infinite element for a particular problem, the decay function must be chosen such that it models a

realistic behaviour of the far field solution. Therefore for wave problems, an extra term of the form $exp(ikr)$ is added to the shape function to model the harmonic variation of the wave potential (Bettess and Zienkiewicz [35]). Although the resulting element matrix remains symmetric, which is of interest, the determination of the resulting integral expression becomes complicated and a special integration scheme is required (see the above reference). This type of infinite element has been applied to many unbounded problems. A good survey of the literature is given in a book by Bettess [28]. By the separation of variables in different directions, the radial (or infinite) direction integration can be carried out analytically which greatly economises the infinite element (Burnett [36]). The integration in other directions are carried out using the standard Guass-Legendre numerical scheme. A recent convergence study of this infinite element (Shirron [94]) shows the element gives very accurate solutions only in the near field.

The frequency dependent characteristic of the finite/infinite element mesh is a disadvantage of this method. For shorter waves a finer mesh in the circumferential direction is required. A frequency-independent infinite element (Yang, Kuo and Hung [99]) can tackle such problems.

For *mapped* infinite elements, special geometry mapping functions are used to map a finite to the infinite element (Zienkiewicz *et al* [104], Beer and Meek [19]) (see section 5.2). By mapping the conventional finite element shape function, a new polynomial is obtained which decays to zero at infinity (see the above references and also Zienkiewicz, Emson and Bettess [103], Pissanetzky [91]). Similar to the first group, an extra term is added to the shape function (Bettess, Emson and

Chiam [31]) to model the harmonic behaviour of the wave potential (see section 5.3). Again, a new integration scheme is required to calculate the element integrals. A much simpler finite to infinite mapping procedure is introduced (Marques and Owen [81]) which makes the finite and infinite element methods more similar. For two dimensional wave problems, the shape function of the above reference [31] was modified to consider a more correct rate of attenuation of wave amplitude towards infinity by multiplying the original shape function by an extra term, i.e. $\sqrt{r}$ (Zienkiewicz, Bando, Bettess, Emson and Chiam [102]). More accurate results were achieved. This is another successful attempt to use a shape function that models the behaviour of a particular problem more realistically. The mapped infinite elements have been used on the exterior of a circle circumscribing the diffracting objects. Burnett [36] pointed out that, for diffracting objects with large aspect ratio, such as a submarine, the element becomes inefficient.

A new idea of choosing a special weighting function to simplify the infinite element formulation generated a new class of elements. This can be applied to both decay function and mapped infinite elements. In the residual equation the weighting functions may be chosen to be the complex conjugate of the shape functions. This eliminates harmonic terms from the element integrals and therefore makes possible the use of the Gauss-Legendre numerical scheme in the calculation of these integrals. This method, the so-called *wave envelope approach*, originated in the study of in-duct acoustical propagation by Astley and Eversman [9]. The method was then used to solve acoustic wave radiation and scattering problems [8, 6]. It was extended to model unbounded wave type problems by Bettess [29].

Unfortunately the simple model equation used by Bettess to test the theory displayed rather simple behaviour towards infinity. Astley pointed out that in real unbounded wave problems an extra term, the line integral at infinity, omitted by Bettess, must be included. Astley went on to develop infinite wave envelope elements for acoustic applications [5].

The method was then used to solve progressive wave examples by Bettess and Chadwick [26]. It was later used to model bounded domain problems by choosing the governing equation for the wave envelope (and phase) rather than for the potential by Chadwick and Bettess [37]. This reduces the size of the mesh and consequently enhances the economy of the model since the limitation of ten nodes per wavelength no longer exists. Chadwick and Bettess later presented a new infinite element using the above idea to model short wave diffraction problems [38].

Shirron [94] presented a wave envelope version of Burnett infinite element and called these two types of infinite elements as unconjugated and conjugated infinite elements. In the unconjugated (Burnett's) formulation, the weighting function (test function in their terminology) is chosen to be the same as the shape function, whereas in the conjugated version, it is a complex conjugate of the shape function. He compared unconjugated and conjugated infinite elements against each other and against the other boundary conditions and concluded that the unconjugated formulation gives more accurate solutions in the near field but the solutions become very inaccurate for the far field. Whereas the conjugated infinite element gives accurate solutions both in the near and far fields. Following Burnett, Gerdes [59] also used the idea of the separation of variables and applied wave envelope

approach to Helmholtz and Laplace equations. He carried out a convergence study of the method which shows the reliability of the wave envelope infinite element. He used the infinite elements on the exterior of the circumscribing sphere. This results in computing inefficiency in modeling objects with large aspect ratio. Astley [3] recently developed a spheroidal axisymmetric mapped wave envelope infinite element for acoustic scattering which offers a more efficient element compared to the above reference. Oslon and Bathe [89] applied the infinite element to transient problems. More recently, Astley [4] applied the wave envelope infinite element method to transient acoustic problems. Zienkiewicz and Taylor pointed out that "Unfortunately the method has not been fully tested for surface waves and it is possible that there will be unforseen difficulties" [101].

1.1 Aim of the thesis

The aim [1] of this study is therefore to develop a series of infinite elements to be used in conjunction with the conventional finite elements to solve the problem of linear water wave diffraction by large objects, in particular large offshore structures.

- The first objective, from Burnett [36], is to improve the existing mapped infinite element, due to Zienkiewicz *et al* [102], so that it can model objects of large aspect ratio, say a submarine, more economically.

[1] The original aim of the research was to develop and insert the new infinite elements into 3D non-linear wave programs, FEMWV3 and FEMWV5, of Dr. P Clark and Prof. P Bettess [43]. After detailed comparison with the analytical solutions and the other 3D linear wave programs, WAVE and WAVEM, of Prof. P Bettess, Mrs. J Bettess, Mr H Hara and Mr S Karaiosifidis, the non-linear codes appeared unreliable for this work and therefore the new infinite elements were inserted to a 2D wave program, SMAWAVE, of Prof. Peter Bettess and Mrs. Jackie Bettess.

- The second and the main objective, from Zienkiewicz and Taylor [101], is to apply the idea of the wave envelope approach, due to Astley [9], to surface waves to develop a simple and efficient infinite element which produces accurate solutions in the far field as well as the near field.

- As the global matrix resulting from this method is unsymmetric, the third objective is to amend the existing unsymmetric solver (Hood [67]) and to insert it into the wave program.

- The fourth objective is to code some existing analytical solutions to be the basis of validation of the infinite elements.

- The final objective is to develop a finite/infinite element mesh generator to solve the problem of wave diffraction by multiple objects.

A number of assumptions have been made to simplify the problem. They are explained in chapter 2. Three main assumptions have been to ignore the non-linear and viscous effects and to reduce the problem to two-dimensions with gradually varying water depth. The governing equation then become the well known Mild-Slope wave equation subjected to the natural and radiation boundary conditions.

As was mentioned above, the model developed in this thesis can solve the linear wave diffraction by large objects in a gradually varying water depth. However, the model was validated only for problems with constant water depth as all the analytical solutions presented in this thesis had been developed for water of constant depth. In the time available it would not have been possible to code other analytical solutions to validate the model for varying water depth problems.

1.2 Plan of the thesis

In the next chapter the mathematical description of the problem of wave diffraction by objects is given. The governing equation and the relevant boundary conditions are explained. Assumptions and limitations of the present study are outlined. By making some assumptions, the general model is simplified to a two-dimensional model.

In chapter 3 the analytical solutions of the problem for constant water depth for some simple shape of the diffracting objects are discussed. These are the diffraction of water waves by a vertical circular cylinder, by a vertical elliptical cylinder and by arrays of vertical circular cylinders.

In chapter 4 the problem is solved for any arbitrary shape and configuration of the diffracting objects by using the coupled finite and infinite element method. Various parts of the method are explored. The finite and infinite element matrix equations are derived from the basic principles using the weighted residual approach. A simple procedure is introduced for developing infinite elements for other unbounded problems.

In chapter 5 other aspects of infinite elements, which depend on the type of elements, are explored. Finite to infinite geometry mapping procedure is explained both for 1D and 2D. The mapping functions for different infinite elements are derived. The construction of the basic shape and weighting functions for an infinite element is explained. The procedure is explained for improving mapped infinite element taken from the literature. The development of two other new infinite

elements is then given. Extension to 3D is outlined.

In chapter 6 different example problems involving the diffraction of water waves by objects in water of constant depth are solved in order to validate the three types of infinite elements. The results are compared with their equivalent analytical solutions. The errors are calculated and plotted. A comparison is made between the three infinite elements.

Finally in chapter 7 the discussion of the results and the advantages and disadvantages of each infinite element is given, concluding remarks are made and further research is discussed.

Chapter 2

Mathematical Formulation of the Problem

2.1 Introduction

The mathematical formulation which describes the problem of diffraction of surface water waves is given in this chapter. Later this will be solved to achieve the required solutions. First the general formulation (i.e. three-dimensional) is described. This will then be restricted to two-dimensional formulation which will be solved using the finite/infinite element method.

An arbitrary body is subjected to incoming plane waves of heading θ_I, amplitude A and angular frequency ω. A Cartesian coordinate system (x, y, z) is fixed at the still water level, with coordinate z pointing vertically upwards. Definition sketches of the problem are given in Figures 2.1 and 2.2.

A number of assumptions were made to simplify the formulation as follow:

- The fluid is assumed to be ideal, i.e. inviscid (no viscosity), incompressible and homogeneous;
- the flow is irrotational which leads to a potential formulation;
- there is no underlying current (see e.g. Kirby [74]);
- the flow is simple harmonic in time;
- waves are of small amplitude, i.e. the wave amplitude is much smaller than the wavelength so that the wave slope is small which leads to a linearised free surface boundary condition;
- a constant gravity force field exists;
- the structures (diffracting objects) are assumed large, stationary and rigid with impermeable surfaces;
- the sea bed is assumed to be rigid, impermeable and frictionless (see e.g. Zienkiewicz *et al* [101] , page 265);
- the surface tension is negligible (see e.g. Sarpkaya [92], page 22);

The finite/infinite element model given in chapter 4 can be used to solve the problem of wave diffraction by objects of any shape and size. However, to maintain the inviscid fluid assumption, the characteristic diameter of the diffracting object (D), must be significant compared to the incoming wave length (L) and amplitude (A).

Guidelines are given by different authors (see e.g. Morgan [85] or Sarpkaya and Isaacson [92]) as:

$$\frac{D}{L} > 0.2 \ (ka > 0.2\pi) \tag{2.1}$$

where k is the wavenumber and a is radius (=D/2) of the diffracting object. In the above range the diffraction effects become dominant, rather than the viscous effects in which case Morison equation [86] can be used to calculate the wave effects (see e.g. the above referrences). The exception is that when $A/D < 0.75$ the wave forces can be predicted by the potential flow diffraction theory regardless of the parameter D/L (see chapter 1). Hence the present model can also be used in this case.

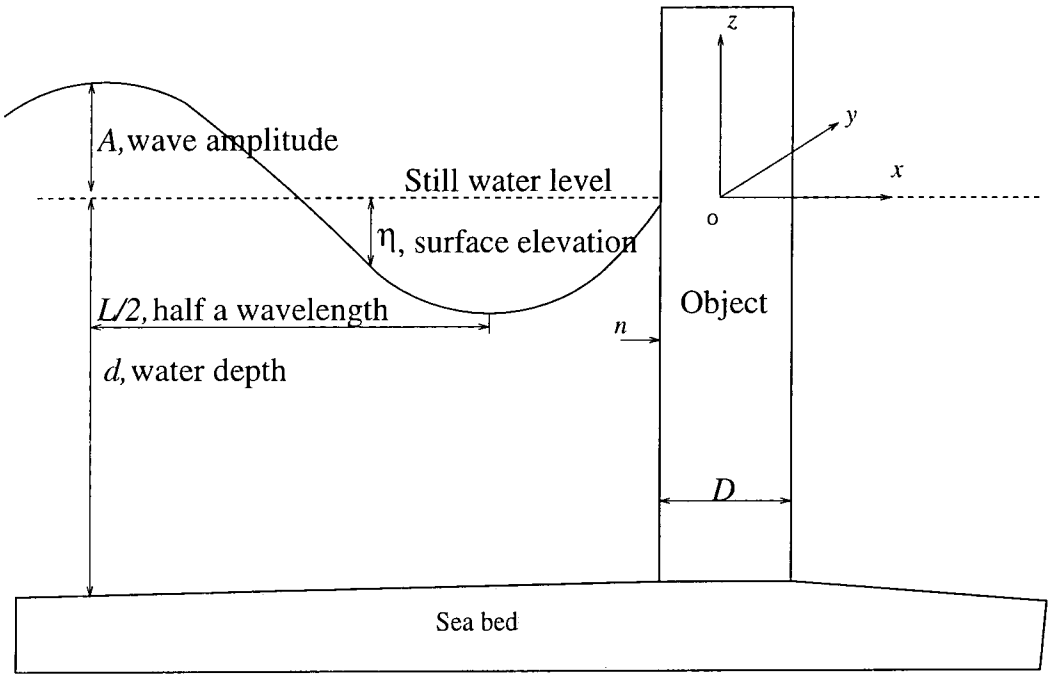

Figure 2.1: x-z Definition sketch and coordinate system

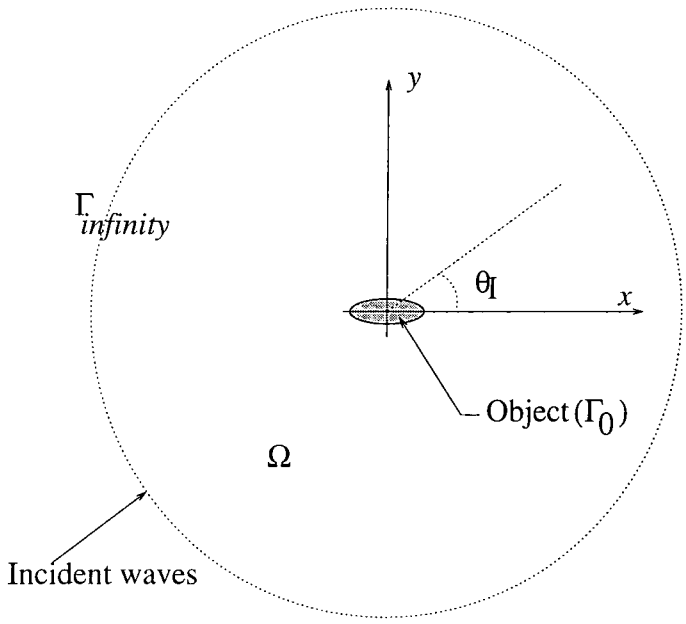

Figure 2.2: x-y Definition sketch of the boundary value problem

2.2 Governing equation

The governing equations can be derived from the fundamental laws of conservation of mass and momentum. This is given by number of authors (see e.g. Lamb [76]). For an inviscid and incompressible fluid (water), the conservation of mass gives [76]

$$\frac{\partial u}{\partial x} + \frac{\partial v}{\partial y} + \frac{\partial w}{\partial z} = 0 \tag{2.2}$$

where u, v and w are the velocity component in x, y and z directions respectively. By assuming the flow to be irrotational, the velocity can be defined as the gradient of a scalar Φ

$$u = \frac{\partial \Phi}{\partial x}, \quad v = \frac{\partial \Phi}{\partial y}, \quad w = \frac{\partial \Phi}{\partial z} \tag{2.3}$$

By substitution, equation (2.2) leads to a linear second order differential equation, known as the Laplace equation

$$\frac{\partial^2\Phi}{\partial x^2} + \frac{\partial^2\Phi}{\partial y^2} + \frac{\partial^2\Phi}{\partial z^2} = \nabla^2\Phi = 0 \tag{2.4}$$

where ∇ is the gradient operator in three dimensions and Φ is often called the velocity potential.

The conservation of momentum upon integration with respect to the space variables leads to the Bernoulli equation (Lamb [76])

$$-\frac{p}{\rho} = gz + \frac{\partial\Phi}{\partial t} + \frac{1}{2}(\nabla\Phi)^2 \tag{2.5}$$

where p is the total pressure, ρ is the water density, g is acceleration due to gravity and t is time. The first term on the right hand side, gz, is the hydrostatic contribution and the rest is the hydrodynamic contribution to the total pressure.

2.3 Boundary conditions

The boundary conditions must be applied to obtain a unique solution to the governing equation. The boundaries involved in the problem are:

- air-water interface (free surface)
- water-sea bed interface
- water-body interface

- surface at infinity (radiation surface)

2.3.1 Free surface condition

At the free surface a kinematic boundary condition can be applied. This ensures that the fluid particles at the boundary move only tangentially and never cross it. By assuming that the wave steepness is small (small amplitude wave theory), the non-linear terms can be omitted giving (see e.g. Berkhof [20])

$$\frac{\partial \eta}{\partial t} - \frac{\partial \Phi}{\partial z} = 0 \tag{2.6}$$

where η is the free surface elevation which is an unknown. Therefore another condition is sought for this boundary. By taking the atmospheric pressure as zero at the free surface and assuming that the motion is slow a linearised dynamic condition can be achieved from the Bernoulli equation (2.5) giving

$$\eta + \frac{1}{g}\frac{\partial \Phi}{\partial t} = 0 \tag{2.7}$$

The above two equations can be combined by eliminating η to give the equation

$$\frac{\partial \Phi}{\partial z} + \frac{1}{g}\frac{\partial \Phi}{\partial t} = 0 \tag{2.8}$$

Now if the problem is periodic, i.e.

$$\Phi = \phi \exp(-i\omega t) \tag{2.9}$$

then equation (2.8) becomes

$$\frac{\partial \phi}{\partial z} + \frac{\omega^2}{g}\phi = 0 \tag{2.10}$$

2.3.2 Sea bed condition

The boundary condition for a fixed, rigid and impermeable sea bed can be written as (see e.g. Berkhof [20])

$$\frac{\partial \phi}{\partial z} + \frac{\partial \phi}{\partial x}\frac{\partial (d+\eta)}{\partial x} + \frac{\partial \phi}{\partial y}\frac{\partial (d+\eta)}{\partial y} = 0 \tag{2.11}$$

2.3.3 Natural boundary condition

Since the structures (diffracting objects) are assumed to be stationary, impermeable and rigid, the natural boundary condition is that the velocity on the solid boundaries is zero, that is

$$\frac{\partial \Phi}{\partial n} = 0 \tag{2.12}$$

where n is the outward normal to the surface.

2.3.4 Radiation boundary condition

The diffracting bodies are subjected to incoming plane waves which may be diffracted by and reflected from the objects and refracted in the vicinity of the objects and

then radiate away towards infinity. Therefore, the radiation boundary condition, which is applied at the surface at infinity, must be applied to the radiated part of the wave. This may be considered by applying the Sommerfeld radiation boundary condition [95] to periodic problems. This may be written as

$$\lim_{r\to\infty} r^{\frac{m-1}{2}} \left(\frac{\partial \phi_s}{\partial r} - ik\phi_s \right) = 0 \tag{2.13}$$

where m is the dimension of the problem, i is the square root of -1, r is the radius and ϕ_s is the radiated part of the velocity potential (see section 2.4).

Zienkiewicz and Newton [108] developed the condition for transient problems, for plane waves giving

$$\frac{\partial \Phi_s}{\partial n} + \frac{1}{c}\frac{\partial \Phi_s}{\partial t} = 0 \tag{2.14}$$

Now if the problem is periodic, equation (2.9), then the equation becomes

$$\frac{\partial \phi_s}{\partial n} - ik\phi_s = 0 \tag{2.15}$$

This plane wave form of the boundary condition will become more accurate as the radius, r, increases.

For further details of the wave equations and boundary conditions, the reader is referred to standard texts (see e.g. Lamb [76]). The radiation boundary condition is applied to the radiated part of the wave, whereas the other boundary conditions are applied to the total wave. Therefore, it is necessary to separate the wave

into incident and radiated waves. This is explained by a number of authors. One explanation is given by Bettess and Zienkiewicz [35]. An outline is given below.

2.4 The incident and scattered waves

The free surface, sea bed and the natural boundary conditions are applied to the total wave whereas the radiation condition must be applied to the radiated part of the wave. Therefore, the linearization of the problem permits the velocity potential to be separated into two parts as

$$\phi = \phi_I + \phi_s \tag{2.16}$$

where ϕ is the total velocity potential, ϕ_I is the incident velocity potential and ϕ_s is the scattered velocity potential. The incident wave is defined by some known functions and the scattered wave is the unknown which includes diffracted and reflected waves from fixed objects and refracted waves due to varied water depth.

The incident wave is a known function satisfying the governing equation as well as the boundary conditions. In this work this is chosen to be a monochromatic plane wave. This is given by number of authors (e.g. Sarpkaya and Isaacson [92] or Chen and Mei [40]) as

$$\phi_I = -\frac{igH}{2\omega} Z(z) \exp(ikr\cos(\theta - \theta_I)) \tag{2.17}$$

which can be rewritten as

$$\phi_I = -\frac{igH}{2\omega} Z(z) \exp(ik(x\cos\theta_I + y\sin\theta_I)) \tag{2.18}$$

where the depth function, Z(z), is given by (see e.g. Sarpkaya *et al* [92])

$$Z(z) = \frac{\cosh k(d+z)}{\cosh kd} \tag{2.19}$$

g is acceleration due to gravity, d is the water depth, ω is the wave angular frequency, H $(= 2A)$ is the wave height defined as the vertical distance between a wave crest and its trough, θ_I is the angle of wave incidence, the anticlockwise angle from the positive x axis in $x - y$ plane and k is the wavenumber derived from the linear dispersion relation. This relation can be derived from the combined linear free surface boundary condition equation and the incident wave equation as (see e.g. [92])

$$\omega^2 = gk\tanh kd \tag{2.20}$$

2.5 Wave other parameters

For a given wave frequency, ω, the wave number must be calculated from the above equation 2.20. Then the other wave parameters can easily be found. The wave celerity, c, is given by $c = \omega/k$ and the wave group velocity, c_g is given by

$c_g = nc$ where n is given by (see e.g. Newman [87])

$$n = \frac{1}{2}(1 + \frac{2kd}{\sinh 2kd}) \tag{2.21}$$

The wavelength is given by $L = 2\pi/k$, the wave period is given by $T = 2\pi/\omega$ and the wave frquency is given by $f = \omega/2\pi$.

2.6 Simplified formulation (2D)

In some practical engineering cases, say large offshore structures, the diffracting objects are usually selected to be vertical cylinders extending from the sea bed to above the free surface. Therefore, the incident waves are scattered in $x - y$ plane which allows separation of depth, z, variation from the velocity potential giving (see e.g. Sarpkaya *et al* [92])

$$\phi(x, y, z) = Z(z)\phi(x, y) \tag{2.22}$$

where $Z(z)$ is the depth variation function given by equation (2.19). A new governing equation can then be sought to express the velocity potential for two-dimensions which is as follows.

The propagation of periodic, small amplitude (linear) surface gravity waves over a variable depth sea bed of mild slope is governed by the Mild-Slope wave equation which was first derived by Berkhoff [22, 21] using the governing equation (2.4), the linear free surface boundary condition, equation (2.10), and the sea bed boundary

condition, equation (2.11), as

$$\nabla \left(cc_g \nabla \phi \right) + \frac{c_g}{c} \omega^2 \phi = 0 \tag{2.23}$$

in Ω, where

Ω is the unbounded two-dimensional (x-y) domain,

∇ is the gradient operator in two dimensions, $[\frac{\partial}{\partial x}, \frac{\partial}{\partial y}]$

ϕ is the time independent complex velocity potential at the free surface,

ω is the angular frequency,

c is the wave celerity,

c_g is the wave group velocity,

and g is acceleration due to gravity.

For shallow water ($kd < \pi/10$) kd is small and so $\tanh kd \cong kd$ and $\sinh 2kd \cong 2kd$, therefore $n = 1$, equation (2.21), and so the wave group velocity $c_g = c = \sqrt{gd}$, then the equation reduces to the linear shallow water wave equation as

$$\nabla \left(d \nabla \phi \right) + \frac{\omega^2}{g} \phi = 0 \tag{2.24}$$

where k is the wavenumber and d is the water depth.

For constant depth this reduces to the Helmholtz equation

$$\nabla^2 \phi + k^2 \phi = 0 \tag{2.25}$$

where ∇^2 is two-dimensional Laplace operator.

As the free surface and sea bed boundary conditions are explicitly satisfied in the above wave equation the only boundary conditions that need to be applied are the natural and radiation boundary conditions. The incident wave function for two-dimensions is derived simply by omiting the depth function from equation (2.18) giving

$$\phi_I = -\frac{igH}{2\omega} \exp(ik(x\cos\theta_I + y\sin\theta_I)) \tag{2.26}$$

2.7 Physical variables

Once the solution, velocity potential function ϕ, has been found, all physical quantities of interest can be computed, e.g.:

The harmonic free surface elevation can be found using equation (2.7) giving

$$\eta(x,y) = Re[\frac{i\omega}{g}\phi] \tag{2.27}$$

The linear hydrodynamic pressure is given by

$$p_d = i\rho\omega\phi = \rho g\eta \tag{2.28}$$

By dividing the vertical cylinder into j sections, the sectional hydrodynamic horizontal force can be found by integrating the pressure over the section j of the

surface of the diffracting object giving

$$F_j = -\int_0^{2\pi} p_d \hat{n} r d\theta \tag{2.29}$$

where $\hat{n}$ is the normal to the surface. The overturning moment is given by

$$M = \int_{-d}^{0} F_j(z+d)dz \tag{2.30}$$

The total horizontal force is then given by

$$F = \int_{-d}^{0} F_j dz \tag{2.31}$$

The horizontal diffraction coefficient is given by

$$C_h = \frac{|F|}{|F_k|} \tag{2.32}$$

where F_k is Froude-Krylov force which is the hydrodynamic force in the absence of any diffracting object [92]. It can be calculated by equation (2.28) and (2.31) by simply using incident potential ϕ_I instead of ϕ.

The time dependent physical variable, say for surface elevation, can be simply found by equation (2.9) giving

$$\eta(x,y,t) = Re[\frac{i\omega}{g}\phi \exp(-iwt)] \tag{2.33}$$

and the phase angle can be found by

$$phase = \arctan[\frac{Re(\phi)}{Im(\phi)}] \tag{2.34}$$

were Re and Im denote the real and imaginary parts of the variable respectively.

2.8 Summary

The mathematical description of the problem of linear water wave diffraction was given in this chapter. The governing equation and relevant boundary conditions were described. The assumptions and so restrictions of the present model were mentioned. By an assumption the formulation was transformed to two-dimensions allowing simplification in mesh generation later in the numerical solution chapter 4.

Chapter 3

Some Analytical Solutions

3.1 Introduction

In this chapter, analytical solutions for problems of water wave diffraction by some objects of simple shape are given. First, the special case of wave diffraction by a circular cylinder and then by an elliptical cylinder are discussed. Finally, the solution for the more practical problem, i.e. multiple circular cylinders wave diffraction problem, is presented. These analytical solutions firstly give some insight into the wave diffraction problem and more importantly later will be used to establish the accuracy of the numerical method described in this thesis.

3.2 Wave diffraction by a circular cylinder

Circular piling is a very common structural element in maritime structures, such as offshore platforms, shore protection and harbours. The problem of diffraction

of plane water waves from a vertical bottom mounted circular cylinder was first presented by Havelock [64] for the special case of infinite depth and later by MacCamy and Fuchs [80] for finite depth. They found a very good agreement with the experiments performed in a wave channel by Morison [86]. Therefore this problem may help to establish the accuracy of the other analytical solutions as well as the numerical method. An outline of the mathematical solution by MacCamy and Fuchs [80] is given below.

It was pointed in section 2.4 that the incident wave equation (2.26) is a solution to the two-dimensional boundary value problem. The cylinder of radius a is assumed to lie along the z axis (see Figure 2.1) and plane waves are incident from the negative x direction ($\theta_I = 0$, see Figures 2.1 and 2.2). The equation then may be written as

$$\phi_I = -\frac{igH}{2\omega}\exp(ikx) = -\frac{igH}{2\omega}\exp(ikr\cos\theta) \tag{3.1}$$

where r and θ are cylindrical polar coordinates. The exponential term of this equation may be expanded as an infinite series of Bessel functions [1]

$$\phi_I = -\frac{igH}{2\omega}\sum_{n=0}^{\infty} i^n \varepsilon_n J_n(kr)\cos(n\theta) \tag{3.2}$$

where $J_n(kr)$ is Bessel function of the first kind and n^{th} order (see Apendix D), $\varepsilon_0 = 1$ and $\varepsilon_n = 2$ for $n = 1, 2, 3, \ldots$. When programming the solution, the series can be truncated when sufficient accuracy has been obtained. Six terms have been used in this study which gives accuracy to four significant figures.

A similar expansion which satisfies the governing equation (2.25) as well as the radiation boundary condition equation (2.13) may be written as [80]

$$\phi_s = -\frac{igH}{2\omega}\sum_{n=0}^{\infty} i^n \varepsilon_n B_n H_n(kr)\cos(n\theta) \tag{3.3}$$

where $H_n(kr)$ is Hankel function of the first kind and n-th order (see Apendix D) given by

$$H_n(kr) = J_n(kr) + iY_n(kr) \tag{3.4}$$

where $Y_n(kr)$ is Bessel function of the second kind and n-th order (see Apendix D).

The only unknown in equation (3.3) is the coefficient B_n. By considering that the diffracting object has a circular cross section, the natural boundary condition, equation (2.12) and (2.16) may be written as

$$\left[\frac{\partial \phi_I}{\partial r}\right]_{r=a} = -\left[\frac{\partial \phi_s}{\partial r}\right]_{r=a} \tag{3.5}$$

By differentiating equations (3.2) and (3.3) with respect to r and substituting into the above equation, the coefficient can be obtained as

$$B_n = -\frac{J_n'(ka)}{H_n'(ka)}$$

The total velocity potential thus may be written as the sum of incident and

diffracted waves

$$\phi = -\frac{igH}{2\omega}\sum_{n=0}^{\infty} i^n \varepsilon_n [J_n(kr) - \frac{J_n'(ka)}{H_n'(ka)} H_n(kr)] \cos(n\theta) \tag{3.6}$$

This is given by MacCamy and Fuchs [80] with a different notation[1]. The surface elevation can then be computed by using equation (2.27).

A plot of real and imaginary parts of incident, diffracted and total velocity potential around the circular cylinder at the still water level ($z = 0$) are illustrated in Figures 3.1, 3.2 and 3.3. The real and imaginary parts of surface elevations around the cylinder are also illustrated in Figure 3.4. The radius of the cylinder, the water depth, the acceleration due to gravity and the wave number are all chosen to be equal to one unit and the wave height is chosen to be equal to two units.

3.3 Wave diffraction by an elliptical cylinder

The ellipse can represent a large variety of shapes from a circular cylinder, to a hull, to a long thin breakwater. It is therefore a very useful test case for the numerical method. In this section the mathematical solution of the problem of diffraction of plane water waves by a bottom mounted elliptical cylinder in shallow water of constant depth is presented. This was originally given by Chen and Mei [39] for the

[1]This solution was coded by Orphanidou under supervision of Prof. P. Bettess at the Department of Marine Tech., University of Newcastle Upon Tyne [88]. In this work, the solution was also coded by Excell to test and validate the FORTRAN code written by Orphanidou.

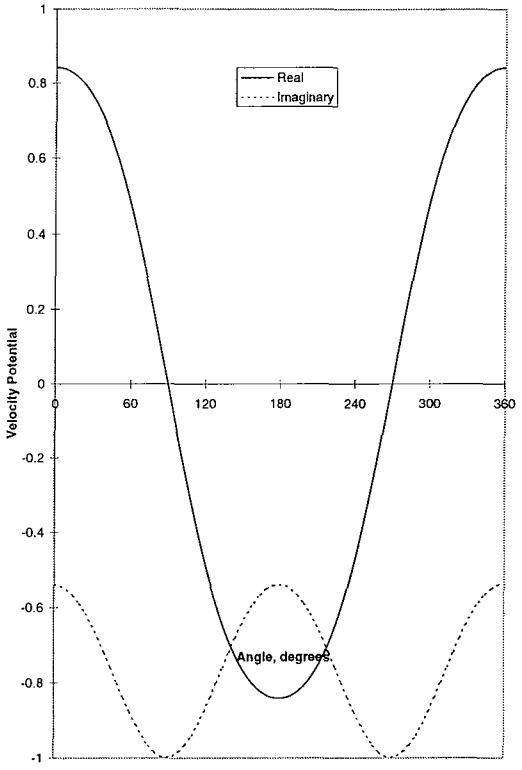

Figure 3.1: Incident velocity potential around the circular cylinder (radius, $r = 1$ unit)

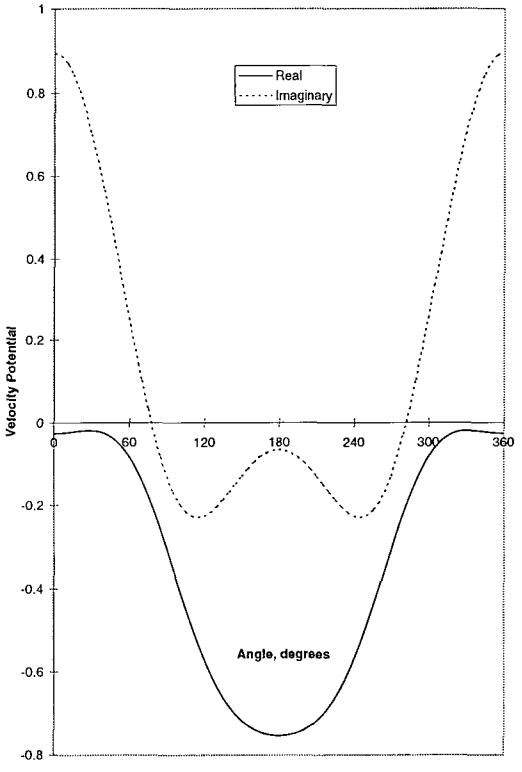

Figure 3.2: Analytical diffracted velocity potential around the circular cylinder ($r = 1$ unit)

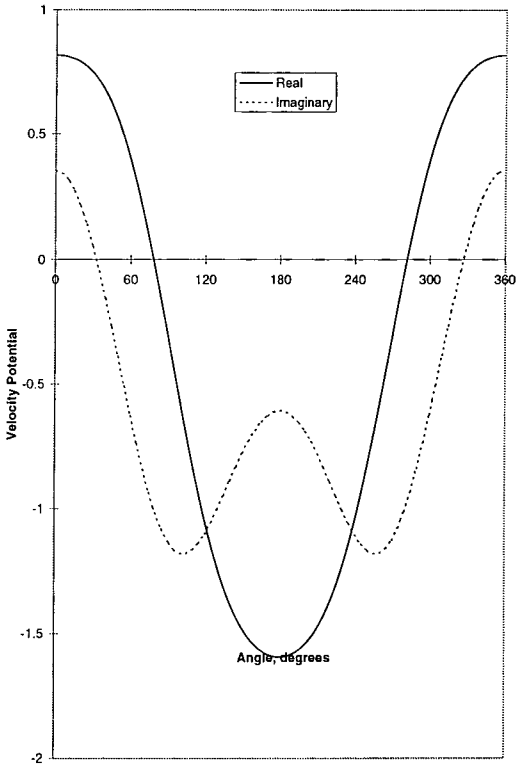

Figure 3.3: Analytical total velocity potential around the circular cylinder ($r = 1$ unit)

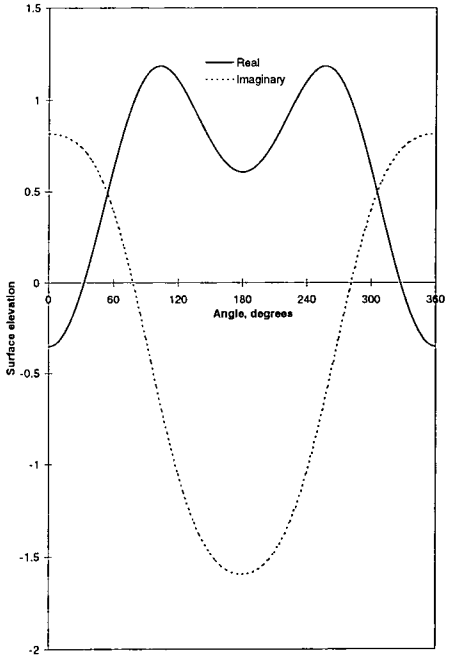

Figure 3.4: Analytical total surface elevations around the circular cylinder ($r = 1$ unit)

case of a floating bodies and coded by Atalianis [11] [2, 3]. A full explanation of the problem is given by Atalianis [10]. An outline of the mathematical solution given by Chen and Mei is first given below. The solutions then are checked against the existing solutions by MacCamy and Fuchs [80] presented in the previous section by assuming equal semi-major and semi-minor axes lengths for the elliptical cylinder. An example problem is finally solved and the solutions are plotted.

This problem is similar to the previous problem except that the diffracting object is an elliptical cylinder and therefore the natural boundary condition can no longer simply be expressed as equation(3.5) . Thus the elliptical coordinate system is employed. The governing equation for shallow water with constant depth is the Helmholtz equation (2.25) which in elliptical coordinate system can be written (Chen *et al* [39])

$$\frac{\partial^2\phi}{\partial\xi^2} + \frac{\partial^2\phi}{\partial\eta^2} + 2q(\cosh 2\xi - \cos 2\eta)\phi = 0 \tag{3.7}$$

where ξ and η are the elliptical co-ordinates and $q = (kh/2)^2$, k is the wavenumber for shallow water $k = \omega/\sqrt{gd}$ and $h = (a^2 - b^2)^{1/2}$ where a and b are the lengths of the semi-major and semi-minor axes.

The exponential term of the plane incident wave equation (2.26) can now be

[2]This code was developed under supervision of Prof. P. Bettess at the Department of Marine Tech., University of Newcastle upon Tyne, UK, 1990.

[3]Further work was necessary to produce satisfactory surface elevations around the cylinder which was carried out in collaboration with Mrs J. Bettess under supervision of Prof. P. Bettess at Durham University, UK, 1995.

expanded by using an infinite series of Mathieu functions (Chen *et al* [39])

$$\begin{aligned}\phi_I = -\frac{igH}{2\omega}\sum_{n=0}^{\infty}&(-1)^n Mc_{2n}^{(1)}(\xi,q)ce_{2n}(\eta,q)ce_{2n}(\theta_I,q)\\ &+(-1)^n iMc_{2n+1}^{(1)}(\xi,q)ce_{2n+1}(\eta,q)ce_{2n+1}(\theta_I,q)\\ &+(-1)^n iMs_{2n+1}^{(1)}(\xi,q)se_{2n+1}(\eta,q)se_{2n+1}(\theta_I,q)\\ &+(-1)^{n+1}Ms_{2n+2}^{(1)}(\xi,q)se_{2n+2}(\eta,q)se_{2n+2}(\theta_I,q)\end{aligned} \tag{3.8}$$

where $ce_n(\eta,q)$ and $se_n(\eta,q)$ are the periodic Mathieu functions and $Mc_n^{(1)}(\xi,q)$ and $Ms_n^{(1)}(\xi,q)$ are the radial Mathieu functions (see Appendix D). When programming the solution, the series can be truncated when sufficient accuracy has been obtained. Thirteen terms has been used in this study which gives accuracy to four significant figures.

A similar expansion which satisfies the governing equation (3.7) may be written for the diffracted wave as (Chen *et al* [39])

$$\begin{aligned}\phi_s = -\frac{igH}{2\omega}\sum_{n=0}^{\infty}&(-1)^n Ac_{2n}Mc_{2n}^{(3)}(\xi,q)ce_{2n}(\eta,q)ce_{2n}(\theta_I,q)\\ &+(-1)^n iAc_{2n+1}Mc_{2n+1}^{(3)}(\xi,q)ce_{2n+1}(\eta,q)ce_{2n+1}(\theta_I,q)\\ &+(-1)^n iAs_{2n+1}Ms_{2n+1}^{(3)}(\xi,q)se_{2n+1}(\eta,q)se_{2n+1}(\theta_I,q)\\ &+(-1)^{n+1}As_{2n+2}Ms_{2n+2}^{(3)}(\xi,q)se_{2n+2}(\eta,q)se_{2n+2}(\theta_I,q)\end{aligned} \tag{3.9}$$

where $Mc_m^{(3)}$ and $Ms_m^{(3)}$ are again the radial Mathieu functions (see Appendix D) and give outgoing waves and so satisfy the radiation boundary condition. Ac and

As are some sets of coefficients which can be found using the natural boundary condition, equation(2.12). This in elliptical coordinate system can be written

$$\left[\frac{\partial \phi_I}{\partial \xi}\right]_{\xi=\xi_0} = -\left[\frac{\partial \phi_s}{\partial \xi}\right]_{\xi=\xi_0} \tag{3.10}$$

By differentiating equations (3.8) and (3.9) with respect to ξ and substituting into the above equation, the coefficients can be obtained as

$$Ac_{2n} = -\frac{M'c_{2n}^{(1)}(\xi_0, q)}{M'c_{2n}^{(3)}(\xi_0, q)}$$

$$Ac_{2n+1} = -\frac{M'c_{2n+1}^{(1)}(\xi_0, q)}{M'c_{2n+1}^{(3)}(\xi_0, q)}$$

$$As_{2n+1} = -\frac{M's_{2n+1}^{(1)}(\xi_0, q)}{M's_{2n+1}^{(3)}(\xi_0, q)}$$

$$As_{2n+2} = -\frac{M's_{2n+2}^{(1)}(\xi_0, q)}{M's_{2n+2}^{(3)}(\xi_0, q)}$$

A comparison between the solutions produced by the present method for an elliptical cylinder of unit aspect ratio ($b/a = 0.99999$) and the equivalent solutions produced by the method described in section 3.2 is illustrated in Figure 3.5. The agreement between two methods is very good, the difference being less than 1.0E-5. A plot of incident, diffracted and total velocity potential around the elliptical cylinder ($b/a = 2$) at the still water level ($z = 0$) for zero angle of incidence ($\theta_I = 0$) are illustrated in Figures 3.6, 3.7 and 3.8. A plot of the surface elevations around the cylinder are also illustrated in Figure 3.9. The water depth, the acceleration due to gravity and the wave number are all chosen to be 1 unit and the wave height is

chosen to be 2 units.

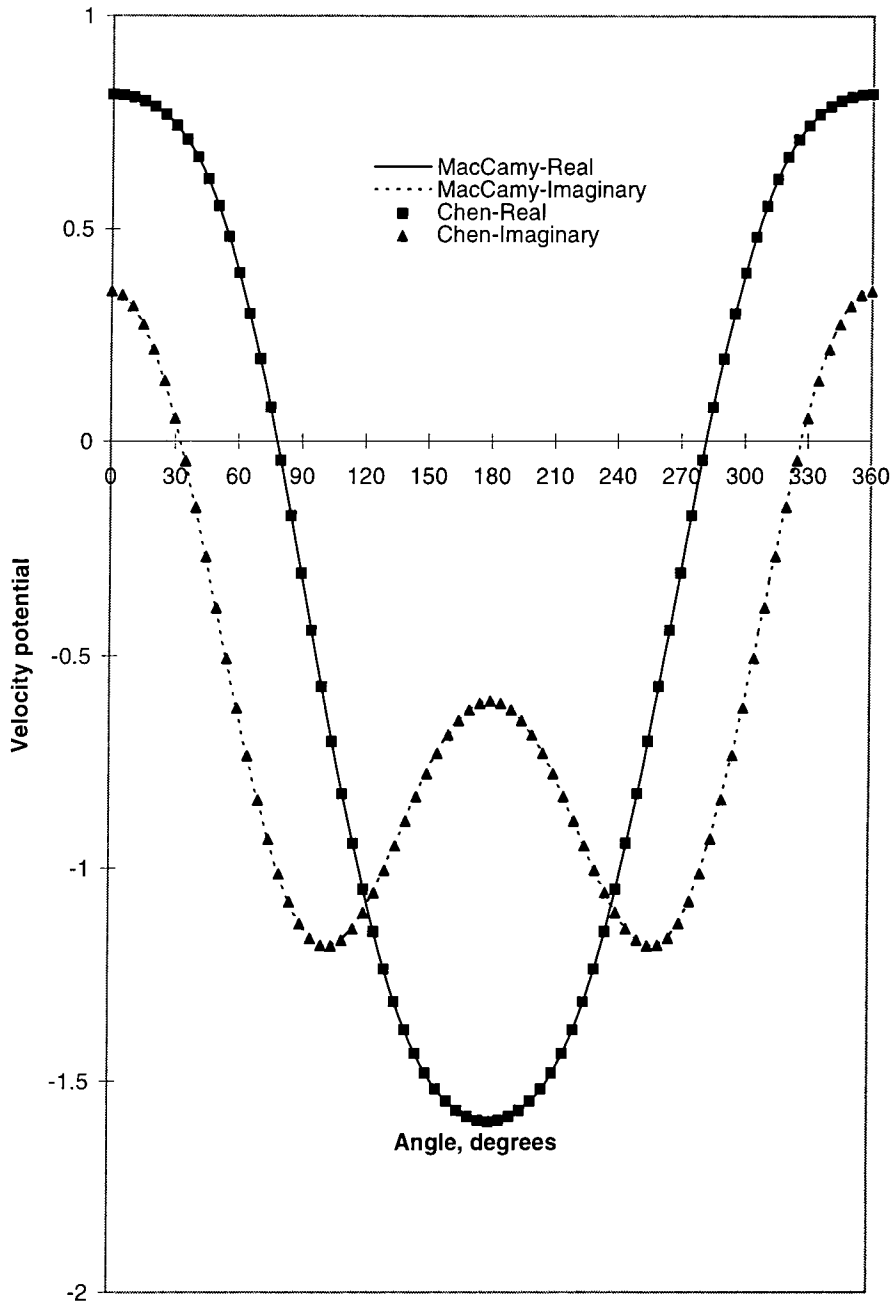

Figure 3.5: A comparison between Chen and MacCamy analytical methods (angle of incidence, $\theta_I, = 0^o$, aspect ratio, $b/a = 2$)

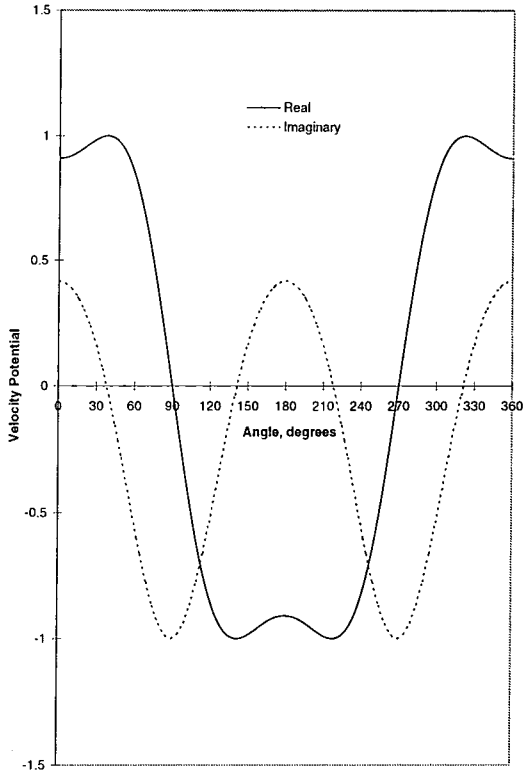

Figure 3.6: Incident velocity potential around the elliptical cylinder ($\theta_I = 0^o$, $b/a = 2$)

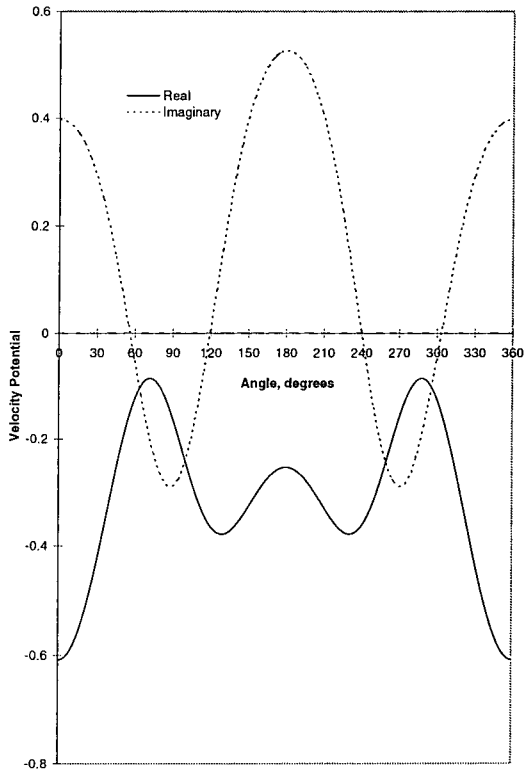

Figure 3.7: Analytical diffracted velocity potential around the elliptical cylinder ($\theta_I = 0^o$, $b/a = 2$)

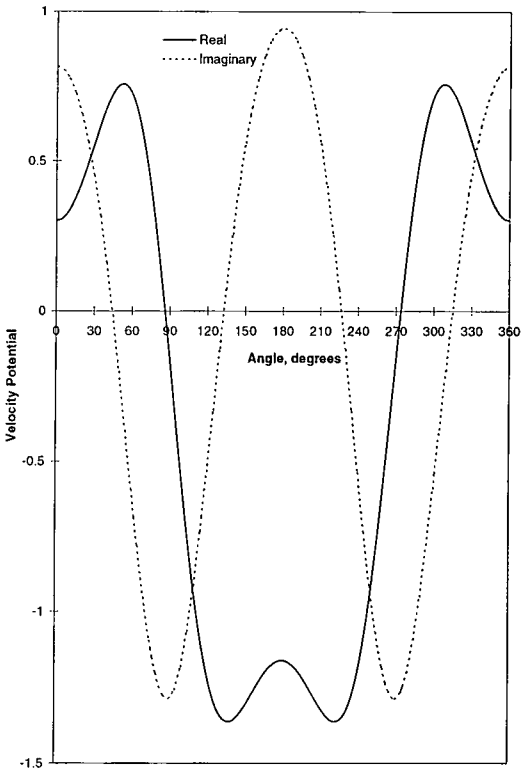

Figure 3.8: Analytical total velocity potential around the elliptical cylinder ($\theta_I = 0^o$, $b/a = 2$)

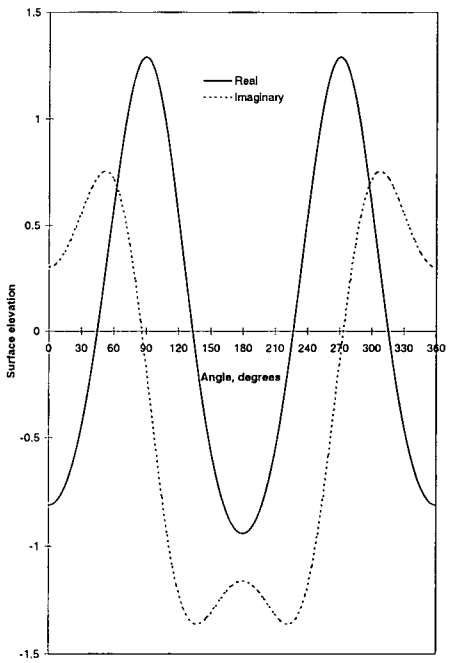

Figure 3.9: Analytical surface elevations around the elliptical cylinder ($\theta_I = 0^o$, $b/a = 2$)

3.4 Wave diffraction by multiple circular cylinders

An offshore structure, such as an oil rig, consists of a number of legs on which some form of structure is mounted. Therefore, the diffraction of water waves by arrays of circular cylinders may help to test the numerical method which in turn can be used to solve the problem for any shape of the diffracting objects.

A number of attempts were made to solve the problem one of which is given by Linton and Evans [78]. Their theory is widely accepted as correct. However their wave contours showed a lack of the expected symmetry. This was also reported by Bettess and Bettess [27] and Baghbani [13]. For the present work, their analytical solution was programmed in Maple. This gave satisfactory answers and symmetrical wave elevations. In this section, an outline of the mathematical solution [78] is presented which will be shown that it recovers the analytical solution given by MacCamy and Fuchs [80] for a special case of wave diffraction by a single circular cylinder. The other example problems are then solved and the results are plotted.

Consider an array of N bottom mounted vertical circular cylinders which are located in the middle of an ocean and are subjected to a plane wave which makes an angle of θ_I with the x axis as shown in Figure 3.10. By assuming there are no diffracting objects in the water, the only contribution to velocity potential is from the incident wave which is given by equation (2.26). The equation is now rewritten to express the incident velocity potential in terms of local polar coordinates (r_j, θ_j)

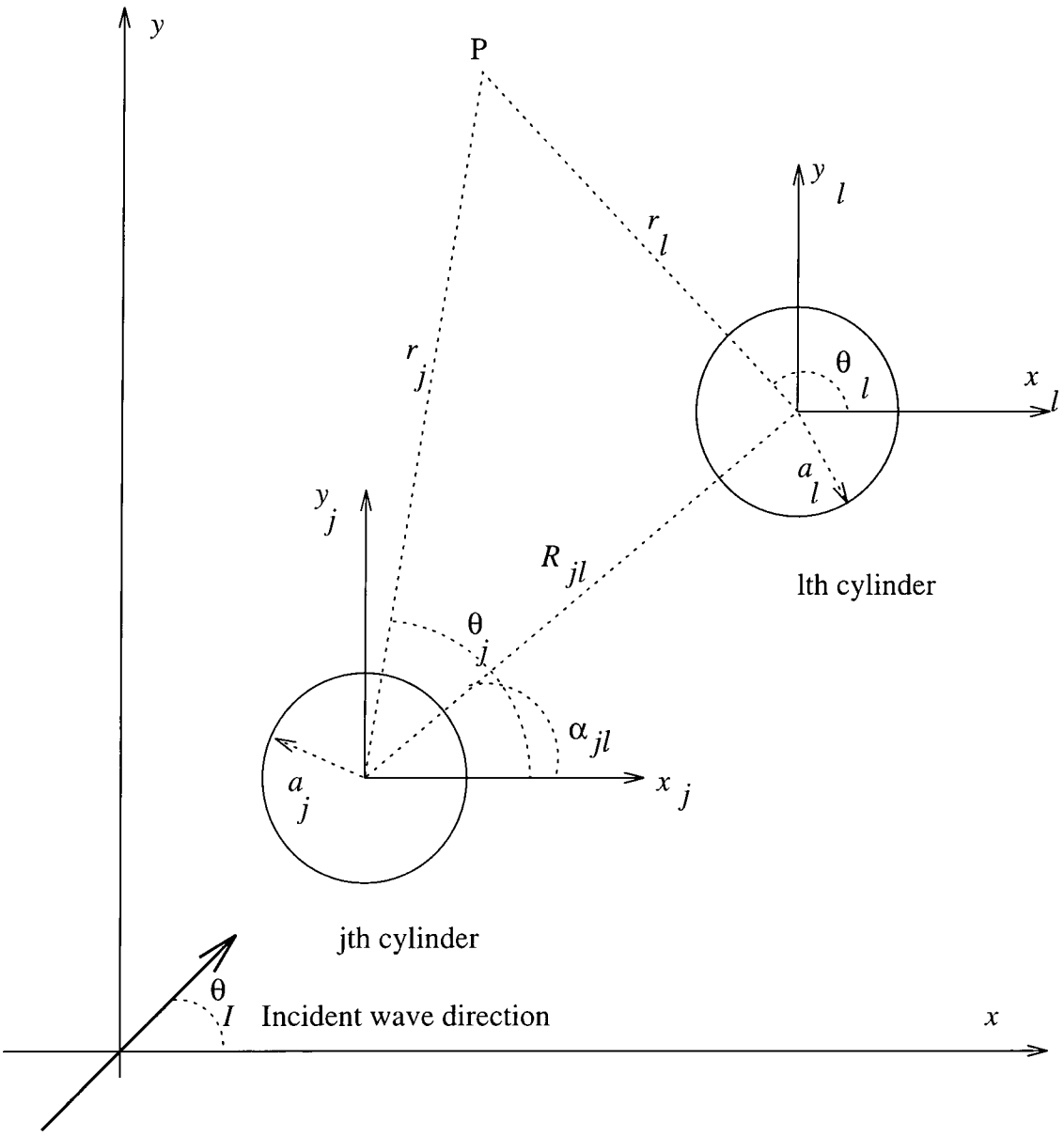

Figure 3.10: Plan view of multiple cylinders diffraction problem

associated with the jth cylinder as [78]

$$\phi_I = -\frac{igH}{2\omega} I_j \exp(ikr_j \cos(\theta_j - \theta_I)) \tag{3.11}$$

where I_j is a phase factor associated with the jth cylinder given by

$$I_j = \exp(ik(x_j \cos\theta_I + y_j \sin\theta_I)) \tag{3.12}$$

where x_j and y_j are the coordinates of the centre of jth cylinder. Similar to section 3.2, the exponential term of the equation (3.11) can now be expanded by using an infinite series of Bessel function [61, 78] giving

$$\phi_I = -\frac{igH}{2\omega} I_j \sum_{n=0}^{\infty} J_n(kr_j) \exp(in(\pi/2 - \theta_j + \theta_I)) \tag{3.13}$$

A similar expansion which satisfies the governing equation (2.25) as well as the radiation boundary condition equation (2.13) is now sought for the diffracted part of the wave. This for the cylinder j may be expressed as [78]

$$\phi_s = -\frac{igH}{2\omega} \sum_{n=0}^{\infty} B_n^j H_n(kr_j) \exp(in\theta_j) \tag{3.14}$$

where B_n^j are some sets of coefficients which can be found using the natural boundary condition on cylinder j. As the cylinders are assumed to have circular shape the natural boundary condition, equation (2.12), can be written as

$$\left[\frac{\partial \phi_I}{\partial r}\right]_{r=a_j} = -\left[\frac{\partial \phi_s}{\partial r}\right]_{r=a_j} \tag{3.15}$$

where a_j is the radius of cylinder j. By differentiating equations (3.13) and (3.14) with respect to r and substituting into the above equation, the coefficient can be obtained as

$$B_n^j = -\frac{J_n'(ka_j)}{H_n'(ka_j)} \tag{3.16}$$

The incident wave is diffracted by a cylinder and produces a diffracted wave

which travels towards other cylinders. Therefore, each cylinder is subjected to different waves. A full explanation of all the possible interactions is given by McIver and Evans [82] and Linton *et al.* [78]. A general form for the diffracted wave radiating away from the cylinder j is given as [78]

$$\phi_s = -\frac{igH}{2\omega} \sum_{n=0}^{\infty} A_n^j B_n^j H_n(kr_j) \exp(in\theta_j) \tag{3.17}$$

The total velocity potential can then be computed by adding the incident and diffracted components

$$\phi = \phi_I + \sum_{j=1}^{N} \phi_s^j \tag{3.18}$$

where N is the number of cylinders. In order to compute the coefficients A_n^j, the natural boundary condition on the cylinders can be written as

$$\left[\frac{\partial \phi_I}{\partial r}\right]_{r=a_l} = -\left[\frac{\partial \phi_s}{\partial r}\right]_{r=a_l} \tag{3.19}$$

for $l = 1, ..., N$, where a_l is the radius of cylinder l. As Linton *et al* [78] showed, by using the Bessel addition theorem, differentiating equations (3.13) and (3.17) with respect to r and substituting into the above equation, an infinite systems of equations can be obtained

$$A_m^l + \sum_{\substack{j=1 \\ j \neq l}}^{N} \sum_{n=-\infty}^{\infty} A_n^j B_n^j \exp(i(n-m)\alpha_{jl}) H_{n-m}(kR_{jl}) = I_l \exp(im(\pi/2 - \theta_i)) \tag{3.20}$$

for $l = 1, ..., N$ and $m = -\infty, ..., \infty$. As Linton *et al* [78] stated "in order to evaluate the constants A_n^l the infinite system is truncated to an $N(2M+1)$ system of equations in $N(2M+1)$ unknowns"

$$A_m^l + \sum_{\substack{j=1 \\ j \neq l}}^{N} \sum_{n=-M}^{M} A_n^j B_n^j \exp(i(n-m)\alpha_{jl}) H_{n-m}(kR_{jl}) = I_l \exp(im(\pi/2 - \theta_i)) \tag{3.21}$$

for $l = 1, ..., N$ and $m = -M, ..., M$. This set of equations can be expressed as a matrix equation which can be solved to evaluate A_n^j. This was done using Maple and the solutions were computed by equation (3.18) for different number of cylinders. Greater accuracy may be achieved by increasing M. In this work, M is taken to be six which gives accuracy to four significant figures.

The above equation is now solved for a single cylinder ($N = 1$). The centre of the cylinder is taken to be at the origin ($x_1 = 0$, $y_1 = 0$) and the angle of incidence ($\theta_I = 0$) chosen to be zero. The incident wave equation will then become the same as equation(3.1). The coefficients are then found as

$$A_m^1 = -i^m \tag{3.22}$$

Substituting this into equation (3.17) gives the same values for the diffracted part of the wave as MacCamy and Fuchs [80]. Therefore, the total wave predicted by this method for a single circular cylinder is exactly the same as MacCamy and Fuchs's.

3.4.1 Example problems

Wave diffraction by a single cylinder

The problem of of wave diffraction by a single circular cylinder standing in shallow water of constant depth is solved. The radius of the cylinder is one unit and the angle of incident wave (θ_I, see Figure 3.10) is taken to be zero. The water depth, the acceleration due to gravity and the wave number are all chosen to be equal to one unit and the wave height is chosen to be equal to two units. A contour plot of real and imaginary [4] parts of the surface elevations around the cylinder is illustrated in Figures 3.11 and 3.12.

Wave diffraction by a pair of cylinders

Now two cylinders of radius one unit are standing in shallow water of constant depth ($d = 1$ unit) and subjected to a plane wave of zero angle of incidence ($\theta_I = 0$, see Figure 3.10). The interaction effects of the two cylinders on the wave pattern may be seen by plotting the surface elevations around the cylinders. A contour plot [5] of real and imaginary components of the surface elevations is shown in Figure 3.13 and 3.14. Again, the water depth, the acceleration due to gravity and the wave number are all chosen to be equal to one unit and the wave height is chosen to be equal to two units.

[4] Solutions at nodal points were calculated by the Maple program and then these solutions were used to generate contour plots. Unimap software package was used for contour ploting. Slight unsymmetry can be seen from the Figure 3.12 which is an artifact of the contouring.

[5] Small boxes that appear on some plots are an artifact of the contouring.

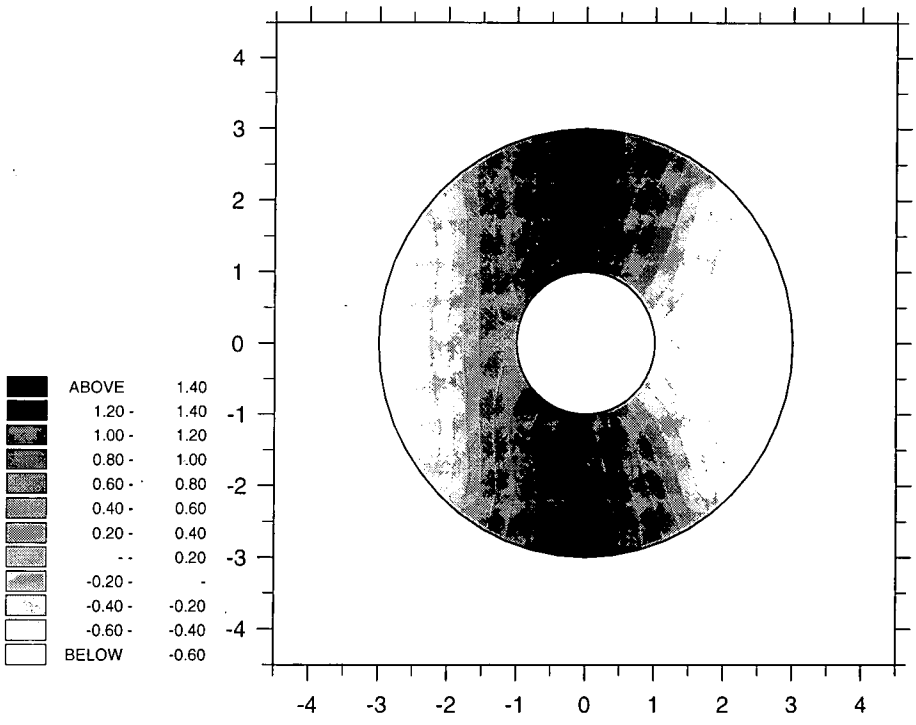

Figure 3.11: A contour plot of analytical total surface elevations around the circular cylinder, real part

3.5 Other analytical solutions

In all the analytical solutions presented in this work , it is assumed that the water depth is constant. However, in real engineering problems this may not always be the case. The programmer then has to check his software for more general problems. Homma [69] gave an analytical solution for the problem of wave diffraction-refraction by a circular island with a parabolic bottom. Further work is required to program this mathematical solution to be used to test the numerical method. Another useful test problem is the problem of wave diffraction by a break water. This is a useful test, because a singularity occurs at the tip of the breakwater. In this research, the mathematical solution given by Penney and Price [90] is coded using FORTRAN and the solutions on the breakwater are plotted (Baghbani [13]).

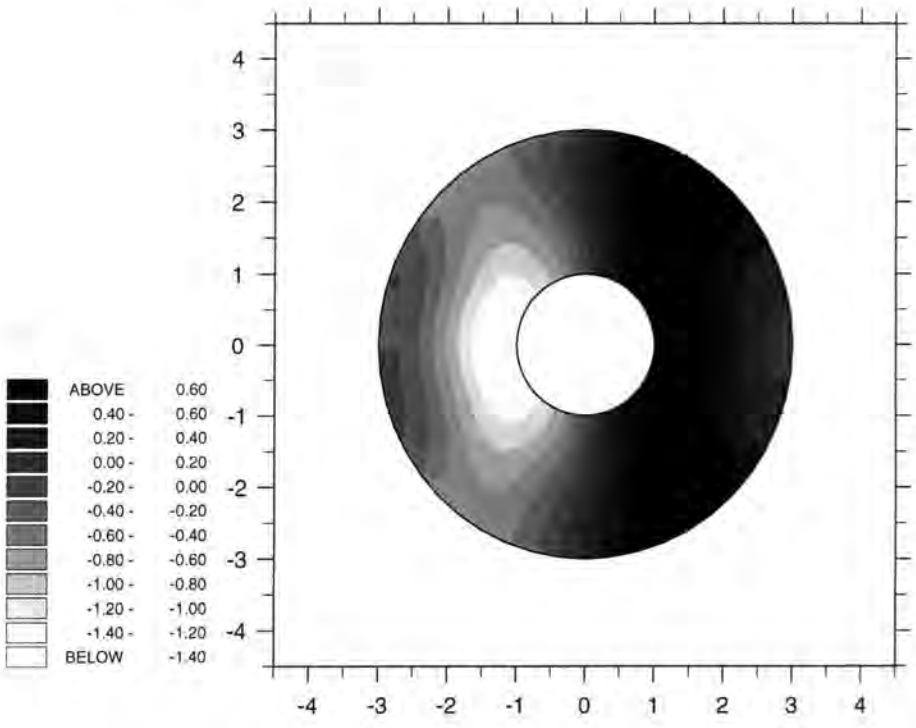

Figure 3.12: A contour plot of analytical total surface elevations around the circular cylinder, imaginary part

3.6 Summary

Some analytical solutions for the problems of water wave diffraction by some simple shape of the diffracting objects were presented in this chapter. The existing FORTRAN program for the problem of wave diffraction by a circular cylinder was first checked and modified to be the base of other problems. Then the existing FORTRAN program for the problem of wave diffraction by an elliptical cylinder was modified and debugged to give correct velocity potentials and surface elevations by comparing with other existing solutions. Finally, the problem of wave diffraction by multiple circular cylinders were discussed and programmed in Maple. The predicted solutions for all cases were plotted to be the basis of comparison for the solutions predicted by the numerical method.

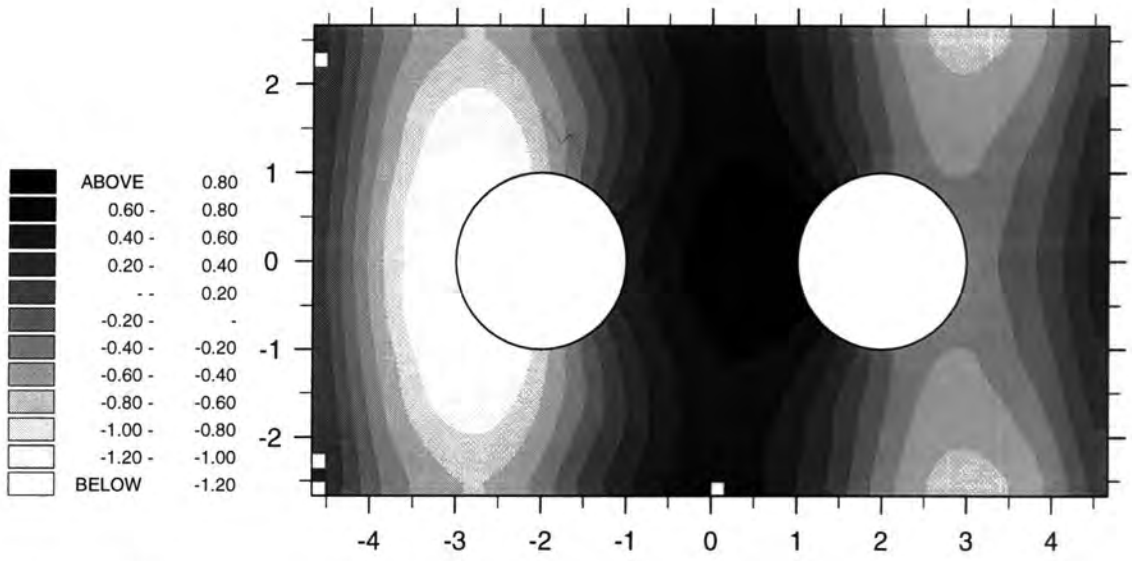

Figure 3.13: A contour plot of analytical total surface elevations around two cylinders, real part

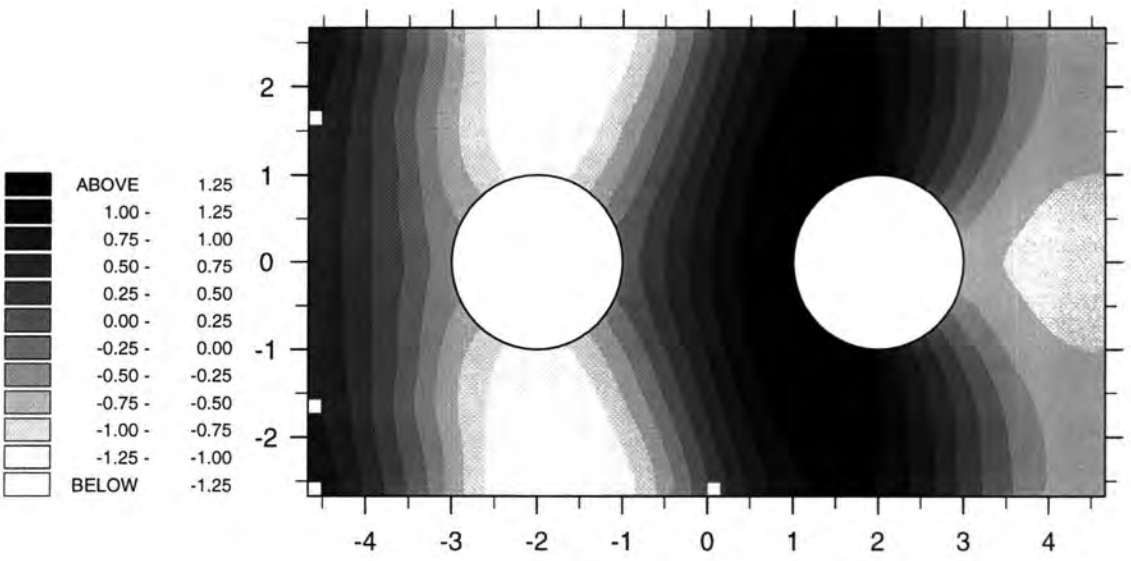

Figure 3.14: A contour plot of analytical total surface elevations around two cylinders, imaginary part

Chapter 4

Coupled Finite and Infinite Element Solution

4.1 Introduction

Problems of diffraction of water waves by some scatterers of simple shape were treated analytically in Chapter 3. In real engineering problems the shape of the scatterer may be very complex, as in a submarine, for which no such analytical solution is available so far. In this chapter, a method based on coupling of *Finite* and *Infinite Element Methods* (F/IEM) is given to tackle such problems. The differential governing equation, for given boundary conditions, is solved using this method. The mathematical base of the method is explored and the implementation of the FORTRAN program is described and a flowchart is given.

The Finite Element Method (FEM) is one of the well-known numerical tech-

niques for solving boundary value problems. However, as it is still not a well-known procedure to combine the finite and infinite element methods, some details are given which are pertinent to this study, so as to make the material self-contained. For further details of the FEM, the reader is referred to standard texts (see e.g. Huebner [70] or Zienkiewicz and Taylor [100, 101]) and for further details of IEM the reader is referred to standard texts (see e.g. Zienkiewicz and Taylor [100] or Bettess [28]).

In F/IE analysis of wave problems, the domain of interest is divided by lines, surfaces or volumes (depending on the dimension of the problem) into a finite number of nonoverlapping subdomains which are called *elements* (finite and infinite). The solution is then approximated within each element by suitable interpolation (shape) functions in terms of a finite number of unknown parameters. In this work, the unknown parameters are the velocity potentials at a finite number of points on the edge of the element which are called *nodes*. The element matrix equations for the unknown parameters are then established. The boundary conditions are imposed. The relations for individual elements are combined into a system of equations for all the unknown parameters by using the assembling procedure. By this method, the original continuum domain problem, which results in infinite degrees of freedom, is transformed into a problem with finite degrees of freedom. The assembled matrix equation is then solved and the solutions are found. The physical quantities of interest are then computed.

The F/IEM procedure employed in this work may be summarized as:

- *Discretize the domain*: The unbounded solution domain, Ω, is subdivided

into two regions, Ω_1 and Ω_2, with a common boundary Γ as shown in Figure 4.1. The finite region Ω_1 being the vicinity of the structure where physical features are of interest for the analyst. The infinite region Ω_2, although, is not physically important, but has to be considered so as to model mathematically the problem correctly. Quadrilateral finite elements are used in the region Ω_1 and a ring of infinite elements are used to model the infinite region Ω_2. The number of finite elements in the radial direction and the number of elements in the circumferential direction and so the number of nodes is a matter of engineering judgment. In general, when the element size becomes smaller, the number of nodes becomes larger which in turn result in the larger number of degrees of freedom for the model. Thus the discretization error of the field variable decreases and so more accurate solutions can be obtained. In wave analysis, it is widely accepted that ten finite element nodes per wavelength give reasonably accurate solutions.

- *Select interpolation (shape) function*: The shape function represents the variation of the velocity potential over the element. For finite elements, this is selected to be a quadratic polynomial which can be easily differentiated and integrated. For infinite elements, however, this is very complex and is selected to be a combination of a polynomial, a decay function and a complex exponential (harmonic) function. This will be discussed in detail later in Chapter 5.

- *Find the element matrices*: Having established the finite and infinite element model, the element matrix equations can be determined. There are

different ways of doing this task. Other researchers, such as Chen and Mei [40], Bai and Yeung [16], Bettess and Zienkiewicz [35], Eatock Taylor and Zietsman [55] and Wu and Eatock Taylor [113], used the variational principle to derive the element matrix equations. In this study, a more general approach, the weighted residual approach is employed to derive the element matrix equations. In this process, the weighting function is selected to be the same as the shape function for the finite element and this is the Bubnov-Galerkin method. For the infinite element, the weighting function is taken to be either the same as the element shape function or multiples of the complex conjugate of it. This gives different types of infinite element which will be discussed in detail later in Chapter 5.

- *Impose the boundary conditions*: Before the element matrix is ready to be assembled to the global matrix, the possible contributions due to the boundary conditions are calculated and are added to the element matrix and its right hand side vector. Two boundary conditions must be considered, the natural and radiation boundary conditions. The first one, which means zero velocity on the diffracting object(s), has no contribution to the element matrix equation. The latter is imposed on a boundary away from the object(s). The first condition is applied to the total wave, whereas the latter is applied to the diffracted wave. Therefore the field variable must be changed at some boundary to maintain these conditions. This change in turn brings the incident wave into the formulation and adds two other contributions to the right hand side of the element matrix equation. These are explained later in this

chapter.

- *Assemble the element matrices*: The element matrix equations which express the behaviour of the elements are combined to form a system matrix expressing the behaviour of the entire domain. The infinite elements matrices are assembled into the system matrix exactly as are the other finite elements matrices. The FE assembling procedure is fully explained in standard texts (see e.g. Huebner [70] or Zienkiewicz and Taylor [100, 101]) and will not be repeated here.

- *Solve the global matrix equation*: The assembling process gives a matrix equation containing a set of simultaneous equations. These are solved to obtain the nodal velocity potentials. As the element matrix resulting from two (out of three) infinite elements developed in this study are unsymmetric, the system matrix becomes unsymmetric. An appropriate (symmetric or unsymmetric) solver is employed to solve the matrix equation.

- *Compute the physical features of interest*: Having calculated the nodal velocity potentials, the other physical quantities of interest may be calculated. The main concern of this study is the prediction of the free surface elevations around the diffracting objects. Computation of the other physical features, such as pressure or force, is straight forward.

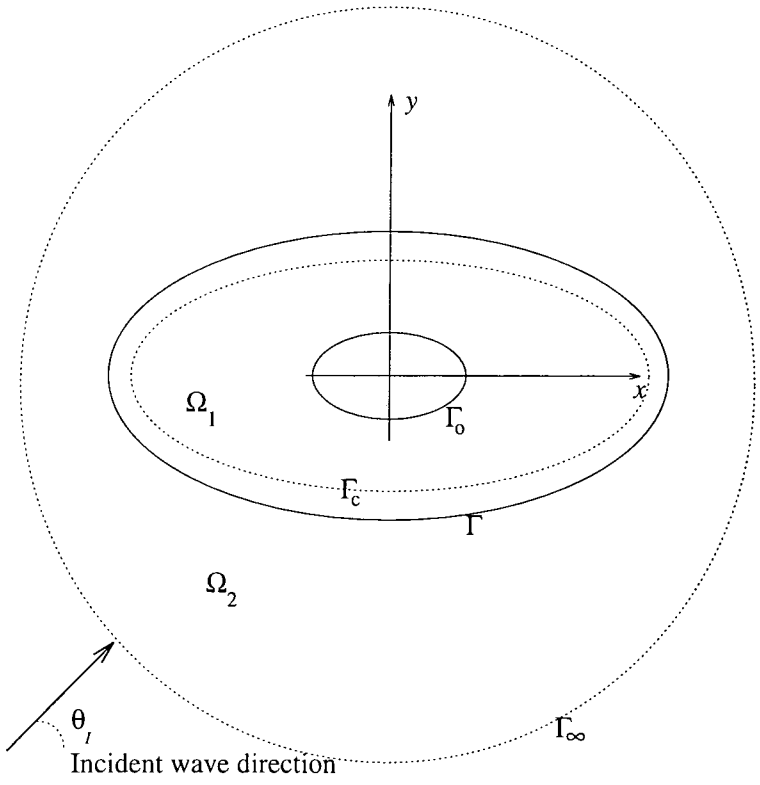

Figure 4.1: Definition sketch of the boundary value problem

4.2 Weighted residual approach

In this section by employing the weighted residual approach and applying the integration by parts the weak form of the governing equation will be obtained. This will be the basis of the finite and infinite element solution.

As was discused in section 2.6, the fluid is governed by the Mild-Slope equation (2.23). By applying the weighted residuals approach for the boundary value problem, equation (2.23) can be written

$$\iint_{\Omega} W\nabla\left(cc_g\nabla\phi_s\right)dxdy + \iint_{\Omega} W\frac{c_g}{c}\omega^2\phi_s dxdy = 0 \tag{4.1}$$

where W is a weighting function. Integration by parts may now be employed to obtain the weak form of the above equation. Integration by parts in two dimensions

can be written as (Huebner [70])

$$\iint_{\Omega} u(\nabla.v)d\Omega = \oint_{\Gamma} u(v.\hat{n})d\Gamma - \iint_{\Omega} v.\nabla u d\Omega \tag{4.2}$$

where u and v are functions of x and y in the Cartesian coordinate system and $\hat{n}$ is the normal vector to the boundary surface. Equation (4.1) may now be written as

$$\iint_{\Omega} \nabla W c c_g \nabla \phi dx dy - \iint_{\Omega} W \frac{c_g}{c} \omega^2 \phi dx dy - \oint_{\Gamma} W c c_g \frac{\partial \phi}{\partial n} d\Gamma = 0 \tag{4.3}$$

This equation includes the weak form of the governing equation (2.23) as well as the boundary conditions which form the basis of finite/infinite element approximations to the wave diffraction problem. The last term is a line integral along the boundaries of the domain which brings the boundary conditions into the formulation. The free surface and sea bed boundary conditions are explicitly satisfied in the governing equation. The natural boundary condition is zero velocity on the surface of the diffracting object(s), equation(2.12), and therefore the line integral on the object(s) vanishes. When the velocity is not zero then the line integral must be considered. This is explained by number of authors such as Bettess and Zienkiewicz [35], Eatock Taylor and Zietsman [55] and Wu and Eatock Taylor [113]. The line integral must also be evaluated on the outer surface of the domain (Γ_∞, see Figure 4.1). This brings the radiation condition into the formulation. Having discretized the domain, the second and third terms of the above equation give the stiffness and mass matrices for the individual elements respectively.

The fluid domain, Ω, is now subdivided into two regions, Ω_1 and Ω_2. In region Ω_1, which surrounds the diffracting object(s) (see Figure 4.1), due to zero velocity on the object(s), the line integral disappears from equation (4.3) giving

$$\iint_{\Omega_1} \nabla W c c_g \nabla \phi dx dy - \iint_{\Omega_1} W \frac{c_g}{c} \omega^2 \phi dx dy = 0 \tag{4.4}$$

In region Ω_2, equation (4.3) can be written as

$$\iint_{\Omega_2} \nabla W c c_g \nabla \phi dx dy - \iint_{\Omega_2} W \frac{c_g}{c} \omega^2 \phi dx dy - \oint_{\Gamma_\infty} W c c_g \frac{\partial \phi}{\partial n} d\Gamma = 0 \tag{4.5}$$

where the line integral brings the radiation matrix into the formulation.

4.3 Development of finite element matrix equation

The determination of the finite element matrix equation is discussed here [1]. The fluid in region Ω_1 is now divided into finite elements. The velocity potential, ϕ, at a given point inside a finite element can be found by interpolating in terms of its nodal values by using the finite element shape functions as

$$\phi = \sum_{i=1}^{n} P_i \phi_i \tag{4.6}$$

[1] The finite element matrix equation was already coded to the SMAWAVE program by Prof. P. Bettess and his wife Mrs J. Bettess using the variational functional given by Bettess and Zienkiewicz [35]. An alternative and a more general approach is to use the weighted residual approach which is developed by the author for this study.

where ϕ_i is the value of ϕ at the i^{th} node in the finite element, P_i is the corresponding finite element shape function and n is the number of nodes used in the finite element. Substituting this into equation (4.4) and taking the weighting function to be the same as the finite element shape function ($W = P$) gives

$$(\iint_{\Omega^e} (\nabla \mathbf{P})^T c c_g \nabla \mathbf{P} dxdy - \omega^2 \iint_{\Omega^e} \mathbf{P}^T \frac{c_g}{c} \mathbf{P} dxdy)\boldsymbol{\phi}^e = \mathbf{0} \tag{4.7}$$

where e is the finite element number, Ω^e is its area, $\mathbf{P}$ is a vector of finite element shape functions and $\boldsymbol{\phi}^e$ is a vector of nodal variables, ϕ_i, for the element. The above equation in a matrix form can be written as

$$\mathbf{A}^e \boldsymbol{\phi}^e = (\mathbf{K}^e - \omega^2 \mathbf{M}^e)\boldsymbol{\phi}^e = \mathbf{0} \tag{4.8}$$

where $\mathbf{A}^e$ is the element matrix and $\mathbf{K}^e$ is the element stiffness matrix,

$$\mathbf{K}^e = \iint_{\Omega^e} (\nabla \mathbf{P})^T c c_g \nabla \mathbf{P} dxdy \tag{4.9}$$

and $\mathbf{M}^e$ is the element mass matrix

$$\mathbf{M}^e = \iint_{\Omega^e} \mathbf{P}^T \frac{c_g}{c} \mathbf{P} dxdy \tag{4.10}$$

The element shape functions are expressed in local coordinate system, $\xi - \eta$, giving

$$\nabla \mathbf{P}_{(x,y)} = \mathbf{J}^{-1} \nabla \mathbf{P}_{(\xi,\eta)} \tag{4.11}$$

were $\mathbf{J}^{-1}$ is the inverse matrix of the jacobian matrix, $\mathbf{J}$, given below and $\nabla\mathbf{P}_{(\xi,\eta)}$ can be expanded as

$$\nabla\mathbf{P}_{(\xi,\eta)} = \begin{bmatrix} \frac{\partial P_1}{\partial \xi} & \frac{\partial P_1}{\partial \eta} \\ \frac{\partial P_2}{\partial \xi} & \frac{\partial P_2}{\partial \eta} \\ \cdots & \cdots \\ \frac{\partial P_n}{\partial \xi} & \frac{\partial P_n}{\partial \eta} \end{bmatrix} \tag{4.12}$$

and therefore the element stiffness and mass matrices in the $\xi-\eta$ coordinate system need to be written as

$$\mathbf{K}^e = \int_{-1}^{+1}\int_{-1}^{+1} (\nabla\mathbf{P})^T\mathbf{J}^{-1}cc_g\mathbf{J}^{-1}\nabla\mathbf{P}|\mathbf{J}|\,d\xi\,d\eta \tag{4.13}$$

$$\mathbf{M}^e = \int_{-1}^{+1}\int_{-1}^{+1} \mathbf{P}^T\frac{c_g}{c}\mathbf{P}|\mathbf{J}|\,d\xi\,d\eta \tag{4.14}$$

These integrals can now be easily calculated using the Gauss-Legendre numerical integration scheme which gives

$$\mathbf{K}^e = \sum_{i=1}^{ni}\sum_{j=1}^{nj} (\nabla\mathbf{P})^T_{(\xi_i,\eta_j)}\mathbf{J}^{-1}_{(\xi_i,\eta_j)}cc_g\mathbf{J}^{-1}_{(\xi_i,\eta_j)}\nabla\mathbf{P}_{(\xi_i,\eta_j)}|\mathbf{J}_{(\xi_i,\eta_j)}|w_iw_j \tag{4.15}$$

$$\mathbf{M}^e = \sum_{i=1}^{ni}\sum_{j=1}^{nj} \mathbf{P}^T_{(\xi_i,\eta_j)}\frac{c_g}{c}\mathbf{P}_{(\xi_i,\eta_j)}|\mathbf{J}_{(\xi_i,\eta_j)}|w_iw_j \tag{4.16}$$

where w_i and w_j denote Gauss-Legendre weights, ξ_i and η_j denote the integration points and ni and nj are the number of integration points in two directions. The details of the numerical integration scheme are given in standard texts (see e.g. Lewis [77]). In the above equations $|\mathbf{J}|$ is the determinant of $\mathbf{J}$.

$$\mathbf{J} = \begin{bmatrix} \sum_{i=1}^{n} \frac{\partial P_i}{\partial \xi} x_i & \sum_{i=1}^{n} \frac{\partial P_i}{\partial \xi} y_i \\ \\ \sum_{i=1}^{n} \frac{\partial P_i}{\partial \eta} x_i & \sum_{i=1}^{n} \frac{\partial P_i}{\partial \eta} y_i \end{bmatrix} \tag{4.17}$$

x_i and y_i are Cartesian coordinates of node i, and P_i are the mapping functions taken to be the same as finite element shape functions. The construction of finite element shape functions is explained in standard texts (see e.g. Zienkiewicz [100] or Huebner [70]).

4.4 Development of infinite element matrix equation

In this section, the infinite element matrix equation will be derived. As will be explained in section 4.6, the field variable changes from total to diffracted wave potential for the infinite elements. Substituting equation (2.16) into the governing equation (2.23) gives

$$\nabla \left(c c_g \nabla (\phi_I + \phi_s) \right) + \frac{c_g}{c} \omega^2 (\phi_I + \phi_s) = 0 \tag{4.18}$$

this can be rewritten as

$$\nabla \left(cc_g \nabla \phi_I\right) + \frac{c_g}{c}\omega^2 \phi_I + \nabla \left(cc_g \nabla \phi_s\right) + \frac{c_g}{c}\omega^2 \phi_s = 0 \tag{4.19}$$

As was explained in section 2.4, the incident wave potential, ϕ_I, is a solution to the governing equation and therefore the terms involving ϕ_I in the above equation vanish giving

$$\nabla \left(cc_g \nabla \phi_s\right) + \frac{c_g}{c}\omega^2 \phi_s = 0 \tag{4.20}$$

The field variable is now the diffracted wave potential, rather than the total wave potential. The total velocity potential at each point then is the sum of known incident and computed diffracted waves.

The infinite element matrix equation is now derived. The weighted residuals equation derived above, equation (4.5), is used but with the field variable now being the diffracted wave, ϕ_s. In this process, the concept of shape, weighting and mapping functions is used by analogy with the finite element procedure. These functions, however, are more complicated and will be discussed later in Chapter 5. The fluid in the infinite region, Ω_2, is now subdivided into a ring of infinite elements. For individual infinite elements, ϕ_s can be approximated using a set of infinite element shape functions, N_i, as

$$\phi_s = \sum_{i=1}^{n} N_i \phi_{si} \tag{4.21}$$

where ϕ_{si} is the value of ϕ_s at the i^{th} node in the infinite element and n is the number of nodes used in the infinite element. Substituting this equation into equation (4.5) gives

$$(\iint_{\Omega^e} (\nabla \mathbf{W})^T cc_g \nabla \mathbf{N} dxdy - \omega^2 \iint_{\Omega^e} \mathbf{W}^T \frac{c_g}{c} \mathbf{N} dxdy - \oint_{\Gamma^e_\infty} \mathbf{W}^T cc_g \frac{\partial \mathbf{N}}{\partial n} d\Gamma)\boldsymbol{\phi}_s = \mathbf{0} \tag{4.22}$$

where Ω^e is now the area of individual infinite elements and $\boldsymbol{\phi}_s^e$ is a vector of an infinite element's nodal variables, ϕ_{si}. The above equation in a matrix form can be written as

$$\mathbf{A}^e {\phi_s}^e = (\mathbf{K}^e - \omega^2 \mathbf{M}^e - \mathbf{R}^e)\boldsymbol{\phi}_s^e = \mathbf{0} \tag{4.23}$$

$\mathbf{A}^e$ is now the infinite element matrix and $\mathbf{K}^e$ is the element stiffness matrix,

$$\mathbf{K}^e = \iint_{\Omega^e} (\nabla \mathbf{W})^T cc_g \nabla \mathbf{N}\, dx\, dy \tag{4.24}$$

$\mathbf{M^e}$ is the element mass matrix as

$$\mathbf{M}^e = \iint_{\Omega^e} \mathbf{W}^T \frac{c_g}{c} \mathbf{N}\, dx\, dy \tag{4.25}$$

and $\mathbf{R}^e$ is the element radiation or damping matrix as

$$\mathbf{R}^e = \int_{\Gamma^e_\infty} \mathbf{W}^T cc_g \frac{\partial \mathbf{N}}{\partial n} d\Gamma \tag{4.26}$$

where $\mathbf{N}$ and $\mathbf{W}$ are vectors of the infinite element shape and weighting functions,

respectively. These functions are derived in Chapter 5.

The shape and weighting functions are expressed in a local coordinate system $\xi - \eta$, therefore the element matrices need to be rewritten in this coordinate system giving

$$\mathbf{K}^e = \int_{-1}^{+1} \int_{-1}^{+1} (\nabla \mathbf{W})^T \mathbf{J}^{-1} c c_g \mathbf{J}^{-1} \nabla \mathbf{N} |\mathbf{J}| \, d\xi \, d\eta \tag{4.27}$$

$$\mathbf{M}^e = \int_{-1}^{+1} \int_{-1}^{+1} \mathbf{W}^T \frac{c_g}{c} \mathbf{N} |\mathbf{J}| \, d\xi \, d\eta \tag{4.28}$$

where $\mathbf{J}$ is the Jacobian matrix, $\mathbf{J}^{-1}$ its inverse and $|\mathbf{J}|$ its determinant.

$$\mathbf{J} = \begin{bmatrix} \sum_{i=1}^{n} \frac{\partial M_i}{\partial \xi} x_i & \sum_{i=1}^{n} \frac{\partial M_i}{\partial \xi} y_i \\ \sum_{i=1}^{n} \frac{\partial M_i}{\partial \eta} x_i & \sum_{i=1}^{n} \frac{\partial M_i}{\partial \eta} y_i \end{bmatrix} \tag{4.29}$$

x_i and y_i are Cartesian coordinates of node i, n is the number of nodes, and M_i are the corresponding mapping functions. The construction of these functions depends on the type of the infinite element being employed in the model and therefore will be explained later in chapter 5.

Three types of infinite element are developed later in Chapter 5 and are called Type 1, Type 2 and Type 3 infinite elements (Type 1 has only been improved to tackle more general problems, see section 5.4). For the Type 1 infinite element, the weighting function is the same as the shape function. The resulting element matrix is symmetric but the Gauss-Legendre numerical scheme can no longer be used to compute the element integrals and a new integration scheme is required. Full

explanation of development and computation of the Type 1 infinite element matrix, $\mathbf{A}^e$, is given elsewhere (see Zienkiewicz *et al* [102, 100]) and will not be repeated here. For Types 2 and 3 infinite elements, the weighting functions are chosen to be multiple complex conjugates of the shape functions (see Chapter 5), therefore, the harmonic terms from the element integrals are eliminated. The resulting integrals have a polynomial form (though they are complex). This makes possible the use of the standard Gauss-Legendre numerical scheme in the calculation of these integrals as was explained in equations (4.15) and (4.16).

4.5 Finite and infinite elements coupling

Infinite element shape functions are chosen such that the finite and infinite elements are compatible at the outset (Γ boundary, as shown in Figure 4.1). This is fully explained in section 5.3.3. Therefore the infinite elements are coupled to finite elements just as are finite elements to other finite elements.

4.6 Inclusion of the boundary conditions

The inclusion of the boundary conditions into the finite/infinite element model is discussed in this section [2]. As was explained in Chapter 2, the natural boundary condition is in terms of the total wave potential whereas the radiation condition is in terms of the diffracted wave potential. Therefore, at some boundary in the

[2]This was already coded to the SMAWAVE program by Prof. P. Bettess and his wife Mrs J. Bettess. It was altered to suit the present study. An explanation is given here in detail for easy access.

domain the field variable must be changed from the total wave potential, ϕ, to the diffracted one, ϕ_s. This boundary can be chosen anywhere between the boundary of the object attached to the finite element, Γ_o^e, and the outer boundary of the infinite element Γ_∞^e inclusive (see Figure 4.2). As the present finite/infinite model has been developed for the Mild-Slope wave equation, the water depth can gradually vary over the domain. In this study the incident wave is taken to be a plane wave, therefore for problems with varying water depth, Γ_c (see Figure 4.1) must be placed outside a domain where the water depth varies so that the incident wave remains a plane wave. For example, if the water depth varies everywhere then Γ_c must be placed on Γ_∞.

The change in the variable has two effects on the model. Firstly it gives rise to a line integral which brings the incident wave into the formulation. Secondly, it leads to a contribution to the right hand side vector. In order to clarify the effects of the change, Γ_c^e will now be taken, as an example, to be the inner edge of an exterior finite element as shown in Figure 4.2 (Γ_c^e is the elemental part of Γ_c in Figure 4.1). The two effects will be explained below.

Consider the equation (4.4) with the total wave, ϕ, being its field variable. Some algebra (see Appendix B) leads to the following equation

$$\iint_{\Omega_{12}} \nabla W c c_g \nabla \phi_s dx dy - \iint_{\Omega_{12}} W \frac{c_g}{c} \omega^2 \phi_s dx dy = \oint_{\Gamma_c} W c c_g \left(\frac{\partial \phi_I}{\partial x} dy - \frac{\partial \phi_I}{\partial y} dx \right) \tag{4.30}$$

where Ω_{12} is a part of Ω_1 where the field variable has been changed from ϕ to ϕ_s. The left hand side of the above equation is exactly the same as the equation (4.4)

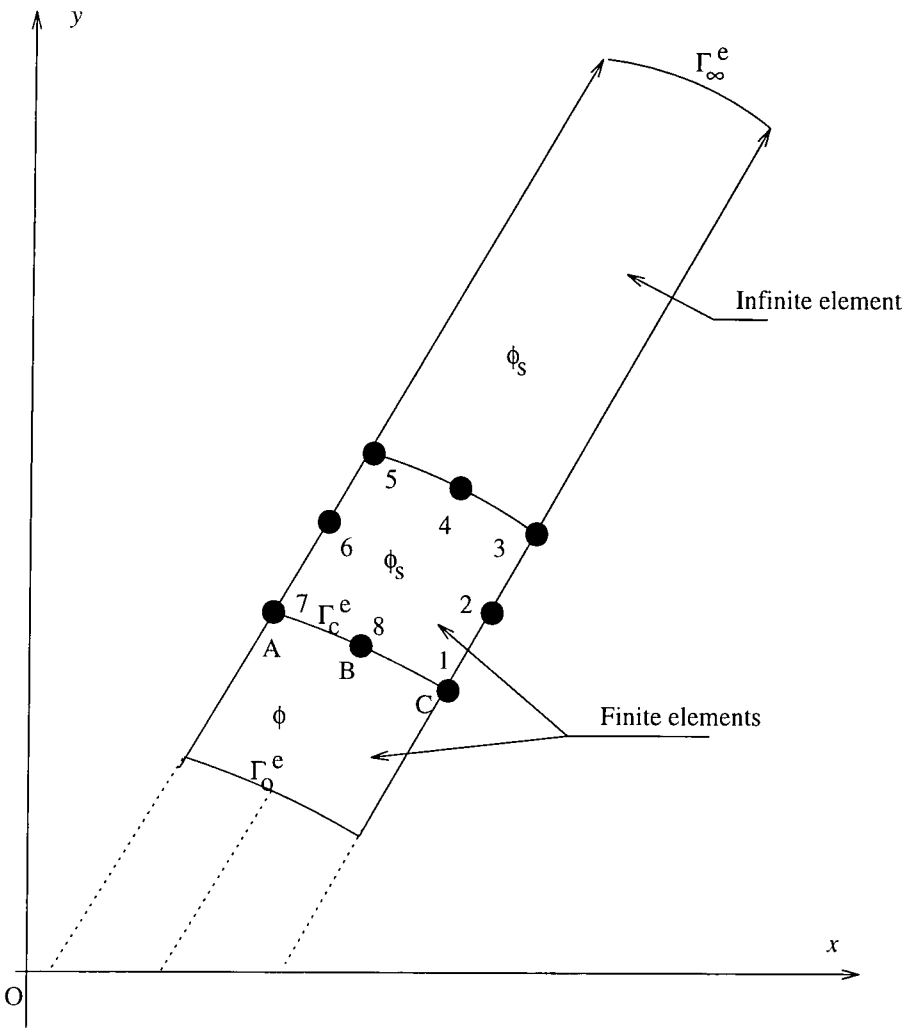

Figure 4.2: Definition sketch of finite/infinite element coupling

with the field variable now being the diffracted wave, ϕ_s. Hence with the same procedure as before, the equation (4.30) in a matrix form can be written as

$$\mathbf{A}^e\boldsymbol{\phi}_s^e = (\mathbf{K}^e - \omega^2\mathbf{M}^e)\boldsymbol{\phi}_s^e = \mathbf{b}^e \tag{4.31}$$

where $\mathbf{A}^e$ is again the finite element matrix, $\mathbf{K}^e$ and $\mathbf{M}^e$ are again the element stiffness and mass matrices defined already by equations (4.9) and (4.10). $\mathbf{b}^e$ is the

element right hand side vector due to the incident wave defined as

$$\mathbf{b}^e = cc_g \int_{\Gamma_c^e} \mathbf{P} \left(\frac{\partial \phi_I}{\partial x} dy - \frac{\partial \phi_I}{\partial y} dx \right) \tag{4.32}$$

where $\boldsymbol{\phi}_I$ is a vector of nodal incident wave potentials, ϕ_I, and $\mathbf{P}$ is now a vector of shape functions for a line element on the edge of the finite element located on the Γ_c^e boundary (see Figure 4.2). The explanation of how the calculation of the line integral is carried out is given below.

4.6.1 Calculation of the line integral due to the incident wave

The calculation of the right hand side vector is discussed in this section[3]. In equation (4.32) ϕ_I is the incident wave potential defined by equation (2.26), therefore its derivatives can be derived as

$$\frac{\partial \phi_I}{\partial x} = ik \cos\theta_I \phi_I$$

$$\frac{\partial \phi_I}{\partial y} = ik \sin\theta_I \phi_I \tag{4.33}$$

[3]This was already coded to the SMAWAVE program by Prof. P. Bettess and his wife Mrs J. Bettess. It was altered to suit the present study. An explanation is given here in detail for easy access.

In the finite element process, the nodes in the $\xi - \eta$ plane may be mapped into corresponding nodes in the $x - y$ plane by the use of the shape functions as

$$x = \sum_{i=1}^{n} P_i(\xi, \eta) x_i$$

$$y = \sum_{i=1}^{n} P_i(\xi, \eta) y_i \tag{4.34}$$

For the line element located on the edge of the element (see Figure 4.3) the shape functions are only functions of η giving

$$x = \sum_{i=1}^{3} P_i(\eta) x_i$$

$$y = \sum_{i=1}^{3} P_i(\eta) y_i \tag{4.35}$$

Individual terms of the shape function $P_i(\eta)$ can be written as

$$\begin{aligned} P_1(\eta) &= 0.5\eta(\eta - 1) \\ P_2(\eta) &= (1 + \eta)(1 - \eta) \\ P_3(\eta) &= 0.5\eta(\eta + 1) \end{aligned} \tag{4.36}$$

Now dx and dy may be written as

$$dx = \frac{\partial x}{\partial \eta} d\eta = \sum_{i=1}^{3} \frac{\partial P_i(\eta)}{\partial \eta} x_i d\eta = f_x(\eta) d\eta$$

$$dy = \frac{\partial y}{\partial \eta} d\eta = \sum_{i=1}^{3} \frac{\partial P_i(\eta)}{\partial \eta} y_i d\eta = f_y(\eta) d\eta \tag{4.37}$$

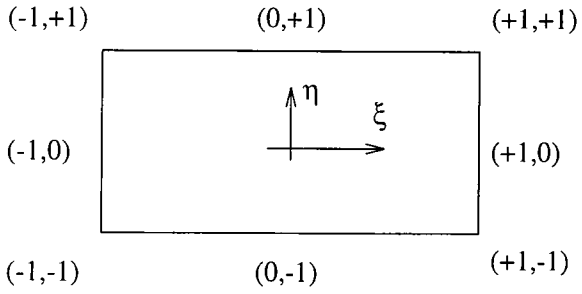

Figure 4.3: Definition sketch of a finite element and its local co-ordinate system

Substituting equations (4.33) and (4.37) into equation (4.32) gives

$$b_j = ikcc_g \int_{-1}^{+1} P_l \left[\cos\theta_I f_y(\eta) - \sin\theta_I f_x(\eta)\right] \phi_{Ij} d\eta \tag{4.38}$$

$l = 1, 2, 3$ and $j = 1, 7, 8$ for the present node numbering as shown in Figure 4.2. These integrals can now be easily performed using the Guass-Legendre numerical integration scheme as explained above.

4.6.2 Change of the variable - contribution to the right hand side vector

The second effect of the change of the variable on Γ_c^e (see Figure 4.2) boundary to the model is discussed here [4]. On this boundary, there are two types of variables, ϕ on the interior, and ϕ_s on the exterior (see Figure 4.2). The nodal variable on this boundary must therefore be transformed to a unique value, say ϕ. This results in a new solution vector as well as a new right hand side vector for the element matrix equation.

[4]This is given by Zienkiewicz ([101], page 629-630) and was already coded to the SMAWAVE program by Prof. P. Bettess and his wife Mrs J. Bettess. It was altered to suit the present study. An explanation is given here in detail for easy access.

The element matrix equation derived for the exterior finite element, equation (4.31), can be expanded as

$$\begin{bmatrix} a_{11} & a_{12} & \dots & a_{18} \\ a_{21} & a_{22} & \dots & a_{28} \\ a_{31} & a_{32} & \dots & a_{38} \\ a_{41} & a_{42} & \dots & a_{48} \\ a_{51} & a_{52} & \dots & a_{58} \\ a_{61} & a_{62} & \dots & a_{68} \\ a_{71} & a_{77} & \dots & a_{78} \\ a_{81} & a_{87} & \dots & a_{88} \end{bmatrix} \begin{bmatrix} \phi_{s1} \\ \phi_{s2} \\ \phi_{s3} \\ \phi_{s4} \\ \phi_{s5} \\ \phi_{s6} \\ \phi_{s7} \\ \phi_{s8} \end{bmatrix} = \begin{bmatrix} b_1 \\ b_2 \\ b_3 \\ b_4 \\ b_5 \\ b_6 \\ b_7 \\ b_8 \end{bmatrix} \tag{4.39}$$

Nodes 1, 7 and 8 (according to the present node numbering scheme, see Figure 4.2) are located on Γ_c^e boundary and therefore their variable must be changed from ϕ_s to ϕ. The equation (2.16) may be rewritten as

$$\phi_s = \phi - \phi_I \tag{4.40}$$

Substituting this into equation (4.39) and rearranging the matrix equation gives

$$\begin{bmatrix} a_{11} & a_{12} & \dots & a_{18} \\ a_{21} & a_{22} & \dots & a_{28} \\ a_{31} & a_{32} & \dots & a_{38} \\ a_{41} & a_{42} & \dots & a_{48} \\ a_{51} & a_{52} & \dots & a_{58} \\ a_{61} & a_{62} & \dots & a_{68} \\ a_{71} & a_{77} & \dots & a_{78} \\ a_{81} & a_{87} & \dots & a_{88} \end{bmatrix} \begin{bmatrix} \phi_1 \\ \phi_{s2} \\ \phi_{s3} \\ \phi_{s4} \\ \phi_{s5} \\ \phi_{s6} \\ \phi_7 \\ \phi_8 \end{bmatrix} = \begin{bmatrix} b_1 \\ b_2 \\ b_3 \\ b_4 \\ b_5 \\ b_6 \\ b_7 \\ b_8 \end{bmatrix} + \begin{bmatrix} (a_{11} + a_{17} + a_{18})\phi_{I1} \\ (a_{21} + a_{27} + a_{28})\phi_{I2} \\ (a_{31} + a_{37} + a_{38})\phi_{I3} \\ (a_{41} + a_{47} + a_{48})\phi_{I4} \\ (a_{51} + a_{57} + a_{58})\phi_{I5} \\ (a_{61} + a_{67} + a_{68})\phi_{I6} \\ (a_{71} + a_{77} + a_{78})\phi_{I7} \\ (a_{81} + a_{87} + a_{88})\phi_{I8} \end{bmatrix} \tag{4.41}$$

As can be seen, the element matrix has remained the same, but the solution vector as well as the right hand side vector have been altered. The solver therefore produces ϕ for the nodes located in the interior of Γ_c and ϕ_s for the others. Therefore ϕ_I has to be added to the latter nodal values to achieve the final velocity potential, ϕ everywhere.

4.7 Solving the global matrix equation

Individual finite and infinite element matrices and their right hand side vectors are calculated and assembled to the global matrix equation leading to a linear system of equation

$$\mathbf{A}_{m\times m}\boldsymbol{\phi}_{m\times 1} = \mathbf{b}_{m\times 1} \tag{4.42}$$

where m is the total number of nodes used in the F/IE mesh, $\mathbf{A}$ is the global matrix, $\boldsymbol{\phi}$ is the global solution vector and $\mathbf{b}$ is the global right hand side vector defined as

$$\mathbf{A} = \sum_{e=1}^{ne} \mathbf{A}^e \qquad \boldsymbol{\phi} = \sum_{e=1}^{ne} \boldsymbol{\phi}^e \qquad \mathbf{b} = \sum_{e=1}^{ne} \mathbf{b}^e \tag{4.43}$$

where ne is the total number of finite and infinite elements used in the mesh.

The matrix, $\mathbf{A}^e$, resulting from Type 2 and Type 3 infinite elements, equations (4.23), are unsymmetric, resulting in an unsymmetric matrix for the global matrix equation. An unsymmetric frontal solver was presented by Hood [67, 68] to solve such a matrix equation. Since the element matrix and right hand side vector entries produced in the present work are complex numbers, the solver has been suitably modified (Appendix C) to deal with such problems.

4.8 Implementation

First the key operation structure of the finite/infinite element program is given below. Then a simple procedure for developing an infinite element routine, which can be inserted into an existing FE code, is given.

The structure of key operations of the **F/IE** code may be summarised as follows:

- Initialise problem independent matrices, vectors and variables.
- Read and store problem dependent data including finite/infinite element mesh data

- Do for all elements

  Call appropriate (finite or infinite) element routine to generate element matrix ($\mathbf{A}^e$)

  Call routines to generate the right hand side vector ($\mathbf{b}^e$)

- End Do

- Assemble them into the global matrix equation

- Call the solver and find the nodal solutions

- Compute and output nodal free surface elevations

- Stop

The description of an **infinite element routine** may be summarised as follows:

- Initialise element matrix and its right hand side (r.h.s.) vector

- Get wave parameters

- Given the coordinates of the nodes, calculate the radii of internal nodes of the element and their angles (r_{0i}, θ_i)

- Do for all Gauss-Legendre integration points in η direction (4 points)

  Get integration weights and points (w_j, η_j)

  Calculate $r_0(\eta_j), \theta(\eta_j)$

  Do for all Gauss-Legendre integration points in ξ direction (8 points)

  Get integration weights and points (w_i, ξ_i)

Call appropriate routine to generate mapping functions derivatives , $\frac{\partial \mathbf{M}}{\partial \xi}$, $\frac{\partial \mathbf{M}}{\partial \eta}$

Calculate Jacobian matrix, its determinant and its inverse matrix

Call appropriate routine to generate shape functions and their derivatives ($\mathbf{N}$, $\frac{\partial \mathbf{N}}{\partial \xi}$, $\frac{\partial \mathbf{N}}{\partial \eta}$)

Call appropriate routine to generate weighting functions and their derivatives ($\mathbf{W}$, $\frac{\partial \mathbf{W}}{\partial \xi}$, $\frac{\partial \mathbf{W}}{\partial \eta}$)

Calculate the global shape and weighting functions derivatives ($\frac{\partial \mathbf{N}}{\partial \mathbf{x}}$, $\frac{\partial \mathbf{N}}{\partial \mathbf{y}}$, $\frac{\partial \mathbf{W}}{\partial \mathbf{x}}$, $\frac{\partial \mathbf{W}}{\partial \mathbf{y}}$)

Calculate element mass and stiffness matrices ($\mathbf{K}^e$ and $\mathbf{M}^e$)

Calculate element damping matrix ($\mathbf{R}^e$)

- Calculate element matrix ($\mathbf{A}^e = \mathbf{K}^e - \omega^2 \mathbf{M}^e - \mathbf{R}^e$)
- End

For developing a new infinite element, the routines which generate the mapping, shape and weighting functions and their derivatives must be up-dated.

4.9 A technique to test an element routine

Different techniques have been suggested to test the infinite element routines (see e.g Bettess [32]). With the development of advanced mathematical computer software, the easiest and safest way to test a numerical routine is probably to calculate the element integrals and so element matrices using these mathematical software. For most cases the integrals can be performed analytically. In this work the Maple

mathematical software was used. Having produced the same element matrices with the FORTRAN routine, it was then inserted to the main program.

4.10 Summary

In this chapter the problem of diffraction of water waves by some arbitrary shape of diffraction objects located in open water with gradually varying depth is solved using a coupled finite and infinite element method. Although the water depth can vary, the boundary, at which the field variable changes from the total to the diffracted wave potential must be set outside the region of varying water depth. The incident plane wave can then be applied at this boundary. In this technique, conventional finite elements, which model the near field potential, are coupled to infinite elements which model the far field potential stretching to infinity. The mathematical base of the model is fully explained in a simple way. A straight forward procedure is introduced for developing new infinite elements which can be used to model other unbounded boundary value problems.

Chapter 5

Different Types of Mapped Infinite Elements

5.1 Introduction

The coordinates of nodes of a finite element are expressed in its local coordinate system (ξ, η) (see Figure 4.3). The element is then mapped to the global coordinate system (x, y) in order to cover a more general shape of the domain and sometimes curved boundary domains. In the local-global coordinate mapping process, the mapping functions are selected to be the same as the finite element shape functions. A full explanation of this can be found in standard texts (see e.g. Zienkiewicz [101] or Huebner[70]). An outline is given in section 4.6.1, equation (4.34).

In the local-global mapping process, the mapping functions may be selected in such a way that the mapped element covers a large part of the domain stretching

to infinity in one direction. This new type of element is called a *mapped infinite element* and was first introduced by Zienkiewicz *et al* [104] and by Beer *et al* [19]). The infinite element covers a large part of the physical domain, and at the same time it only produces one element matrix equation which is assembled into the global matrix equation. This in terms of computing resources means that a large part of the domain is being modelled using more or less the same amount of resources as for a single finite element. The question then arises how the behaviour of the field variable can be modelled within this large domain by the use of the shape functions. This is fully explained in section 5.3.

Just as different types of finite elements can be generated, different types of infinite elements can be produced depending on their parent finite elements. New types of infinite element may also be produced depending on how the shape and weighting functions are adopted which in turn depends on the differential equations governing the problem and the relevant boundary conditions. Three types of infinite element are explained later in this chapter. The finite to infinite geometry mapping procedure is explained below.

5.2 Finite to infinite geometry mapping

5.2.1 One dimensional

Consider a one-dimensional quadratic finite element as shown in Figure 5.1-a. This element may be mapped from its local coordinate to the global coordinate which extends to infinity in the x direction as shown in Figure 5.1-b. This local to global

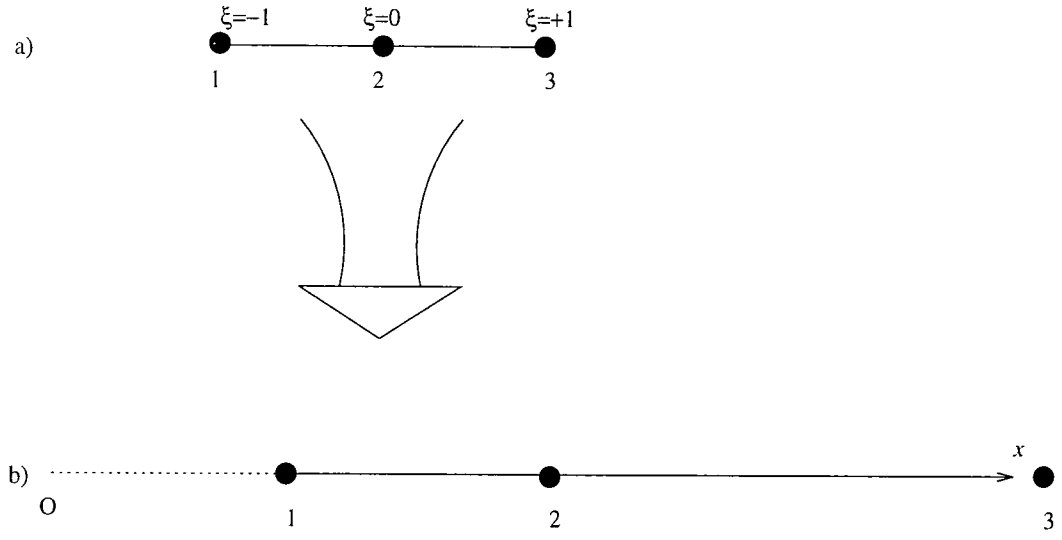

Figure 5.1: Finite to infinite geometry mapping

mapping may be written as

$$x = \sum_{i=1}^{n} Q_i(\xi) x_i \tag{5.1}$$

where $Q_i(\xi)$ are the special mapping functions given by Marques and Owen [81] for a quadratic element as

$$\begin{aligned} Q_1(\xi) &= \frac{-2\xi}{1-\xi} \\ Q_2(\xi) &= \frac{1+\xi}{1-\xi} \\ Q_3(\xi) &= 0 \end{aligned} \tag{5.2}$$

An explanation of these mapping functions is also given by Bettess [28]. The corresponding nodes in the two coordinate systems may be identified as

$$\begin{aligned} \xi &= -1 \quad \rightarrow \quad x = x_1 \\ \xi &= 0 \quad \rightarrow \quad x = x_2 \\ \xi &= +1 \quad \rightarrow \quad x = \infty \end{aligned} \tag{5.3}$$

where x_1 and x_2 are the coordinates of the nodes 1 and 2 as shown in Figure 5.1-b.

5.2.2 Two dimensional

Now consider a two dimensional quadratic finite element as shown in Figure 4.3. The element is now mapped to a new element which is stretched to infinity in the radial direction (see Figure 5.2). Therefore, for the ξ direction, the finite to infinite mapping functions are employed. For the η direction, the conventional finite element shape functions are employed. Similar to finite element procedure, the local global coordinate mapping can now be written as

$$\begin{aligned} x &= \sum_{i=1}^{n} M_i(\xi, \eta) x_i \\ y &= \sum_{i=1}^{n} M_i(\xi, \eta) y_i \end{aligned} \tag{5.4}$$

where

$$M_i(\xi, \eta) = Q_j(\xi) P_k(\eta) \tag{5.5}$$

where $i = 1, ..., 9$, $j = 1, 2, 3$, $k = 1, 2, 3$, $P_k(\eta)$ are the quadratic finite element

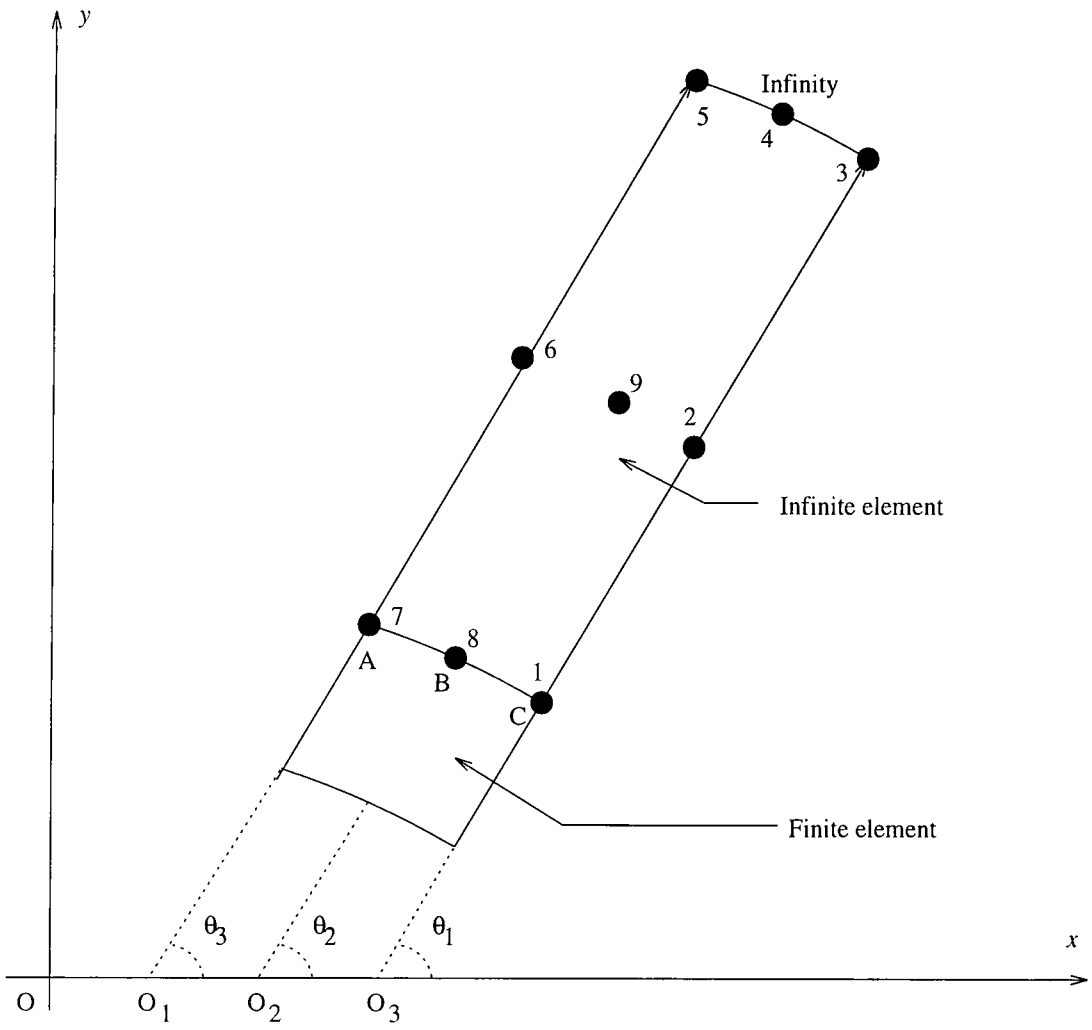

Figure 5.2: Finite/infinite element coupling and 9-node infinite element (Type 2) node numbering scheme

shape functions in the η direction given by equation (4.36), and $Q_j(\xi)$ are the finite to infinite geometry mapping functions given by equation (5.2). In order to derive the individual terms, a node numbering scheme must be adopted. Two such schemes are used in this study. The first is the 9-node element as shown in Figure

5.2 and the corresponding mapping functions are

$$
\begin{aligned}
M_1(\xi,\eta) &= Q_1(\xi)P_1(\eta) = (\frac{-2\xi}{1-\xi})\frac{\eta}{2}(\eta-1) \\
M_2(\xi,\eta) &= Q_2(\xi)P_1(\eta) = (\frac{1+\xi}{1-\xi})\frac{\eta}{2}(\eta-1) \\
M_6(\xi,\eta) &= Q_2(\xi)P_3(\eta) = (\frac{1+\xi}{1-\xi})\frac{\eta}{2}(\eta+1) \\
M_7(\xi,\eta) &= Q_1(\xi)P_3(\eta) = (\frac{-2\xi}{1-\xi})\frac{\eta}{2}(\eta+1) \\
M_8(\xi,\eta) &= Q_1(\xi)P_2(\eta) = (\frac{-2\xi}{1-\xi})(1-\eta)(\eta+1) \\
M_9(\xi,\eta) &= Q_2(\xi)P_2(\eta) = (\frac{1+\xi}{1-\xi})(1-\eta)(\eta+1)
\end{aligned}
\tag{5.6}
$$

and the mapping functions for nodes 3, 4, and 5 are zero.

A new infinite element will be presented in section 5.8 to model multiple body diffraction problems. For this element, the nodes at the infinite edge of the element are no longer required. A new node numbering scheme is adopted and shown in Figure 5.3. The corresponding mapping functions are (Bettess [28])

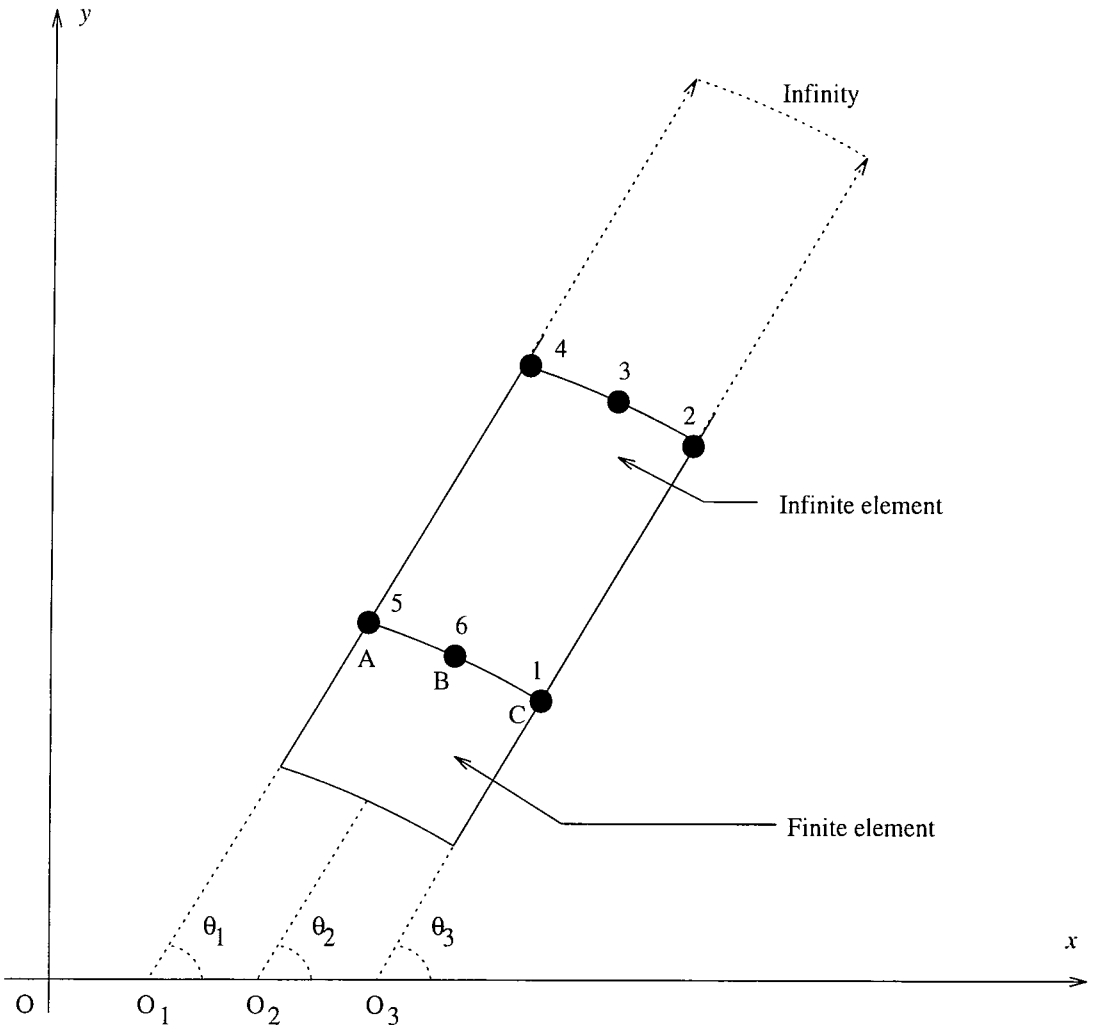

Figure 5.3: Finite/infinite element coupling and 6-node infinite element (Type 1/Type 3) node numbering scheme

$$
\begin{aligned}
M_1(\xi,\eta) &= Q_1(\xi)P_1(\eta) = (\frac{-2\xi}{1-\xi})\frac{\eta}{2}(\eta-1) \\
M_2(\xi,\eta) &= Q_2(\xi)P_1(\eta) = (\frac{1+\xi}{1-\xi})\frac{\eta}{2}(\eta-1) \\
M_3(\xi,\eta) &= Q_2(\xi)P_2(\eta) = (\frac{1+\xi}{1-\xi})(1-\eta)(\eta+1) \\
M_4(\xi,\eta) &= Q_2(\xi)P_3(\eta) = (\frac{1+\xi}{1-\xi})\frac{\eta}{2}(\eta+1) \\
M_5(\xi,\eta) &= Q_1(\xi)P_3(\eta) = (\frac{-2\xi}{1-\xi})\frac{\eta}{2}(\eta+1) \\
M_6(\xi,\eta) &= Q_1(\xi)P_2(\eta) = (\frac{-2\xi}{1-\xi})(1-\eta)(\eta+1) \qquad (5.7)
\end{aligned}
$$

The derivatives of the mapping functions can now be easily obtained as

$$\frac{\partial M_i(\xi,\eta)}{\partial \xi} = \frac{\partial Q_j(\xi)}{\partial \xi} P_k(\eta)$$

$$\frac{\partial M_i(\xi,\eta)}{\partial \eta} = Q_j(\xi) \frac{\partial P_k(\eta)}{\partial \eta} \tag{5.8}$$

and substituted into equation (4.29) to calculate the Jacobian matrix.

5.2.3 Extension to three dimensions

The mapping functions for a three dimensional element are simply derived by multiplying the mapping functions of the two dimensional element by the corresponding finite element shape function for the third, the ζ, direction giving

$$M_i(\xi,\eta,\zeta) = Q_j(\xi) P_k(\eta) P_l(\zeta) \tag{5.9}$$

where $P_l(\zeta)$ are the conventional finite element shape functions for ζ direction.

5.3 Construction of the shape and weighting functions

As was explained above, element shape functions are used to model the behaviour of the field variable over the element. The diffracted wave behaves harmonically and its amplitude decays to zero at infinity. Therefore the shape functions of an infinite element which may cover many wavelengths must have these two characteristics.

The infinite element shape functions must also satisfy the compatibility criteria with the finite element shape functions at the interface.

5.3.1 Amplitude decay

In the mapped infinite element concept, the parent finite element shape functions are mapped to obtain the infinite element shape functions. Consider a quadratic one dimensional finite element shape function (The shape function of node 1 of the element shown in Figure 5.1-a)

$$P(\xi) = -0.5\xi(1-\xi) \tag{5.10}$$

By choosing $x_2 = 2x_1$, the finite to infinite geometry mapping, equation (5.1), may now be rewritten as [102]

$$r = \frac{2r_0}{1-\xi} \qquad or \qquad \xi = 1 - \frac{2r_0}{r} \tag{5.11}$$

where $r_0 = x_2 - x_1 = x_1$ (see Figure 5.1-b). Substituting equation (5.11) into equation (5.10) gives

$$P(r) = -\frac{r_0}{r} + \frac{2r_0^2}{r^2} \tag{5.12}$$

Therefore, in using a quadratic polynomial as a parent shape function in the infinite direction, a decay of r^{-1} and r^{-2} is achieved for the resulting shape function.

As was explained in section 3.2, Hankel functions of the first kind and mth

order, $H_m(kr)$, are solutions of the two-dimensional wave diffraction problems. For zero order (m=0) and large values of r, the function may be approximated as (MacCamy *et al* [80])

$$H_0(kr) \approx \alpha r^{-1/2} \exp(ikr) \tag{5.13}$$

where α is a constant. Hence, for two dimensional problems the amplitude of the diffracted wave may decay approximately as $r^{-1/2}$. Therefore, an appropriate infinite element shape function may be achieved (see Appendix E) by multiplying the shape function, equation (5.12), by a factor of $r^{1/2}$, giving

$$N(r) = P(r)r^{1/2} \tag{5.14}$$

where $N(r)$ is the infinite element shape function.

5.3.2 Harmonic variation

To model the harmonic variation of the diffracted wave, a periodic term of the form $\exp(ikr)$, see again equation (5.13), is introduced to the shape function giving

$$N(r) = P(r)r^{1/2} \exp(ikr) \tag{5.15}$$

5.3.3 Compatibility of the Finite and Infinite elements

The infinite element models the potential of the far field and the finite element models the potential of the near field. In order to maintain continuous behaviour between these two fields, the shape functions of finite and infinite elements must be continuous at the interface, where $\xi = -1$ and $r = r_0$. To acheive this, the absolute value of the infinite element shape function must be unity and the phase must be zero. Therefore the appropriate shape function becomes

$$N(r) = P(r)\left(\frac{r}{r_0}\right)^{1/2} \exp(ik(r - r_0)) \tag{5.16}$$

Substituting equation (5.11) into this equation gives the shape function in the local coordinate system

$$N(\xi) = P(\xi)\left(\frac{2}{1-\xi}\right)^{1/2} \exp\left(ikr_0\frac{1+\xi}{1-\xi}\right) \tag{5.17}$$

For two dimensional elements for which the element is stretched to infinity in the ξ direction, the η variation must be introduced to the shape function giving

$$N(\xi,\eta) = P(\xi,\eta)\left(\frac{2}{1-\xi}\right)^{1/2} \exp\left(ikr_0\frac{1+\xi}{1-\xi}\right) \tag{5.18}$$

By assuming that the infinite elements are used on the exterior of a circle, the radii of inner nodes of an element become constant, r_0. The derivatives of the shape

function with respect to ξ and η can then be written as

$$\frac{\partial N}{\partial \xi} = \left(\frac{\partial P}{\partial \xi} + \frac{P}{2(1-\xi)} + \frac{i2kr_0P}{(1-\xi)^2}\right)\left(\frac{2}{1-\xi}\right)^{1/2} \exp\left(ikr_0\frac{1+\xi}{1-\xi}\right) \tag{5.19}$$

$$\frac{\partial N}{\partial \eta} = \frac{\partial P}{\partial \eta}\left(\frac{2}{1-\xi}\right)^{1/2} \exp\left(ikr_0\frac{1+\xi}{1-\xi}\right) \tag{5.20}$$

This is the final mapped infinite element formulation which is given by Zienkiewicz *et al* [102, 101] and other references (e.g. Bettess [28]) with a different notation.

5.3.4 Weighting functions

The weighting functions are a set of arbitrary functions that need to be introduced when applying the weighted residuals approach, equation (4.5). The weighting functions can be taken to be the same as the shape functions which leads to *the mapped infinite element* formulation given in the above references (see also section 5.4). The standard numerical scheme can no longer be used to calculate the element integrals, equation (4.23). A new integration scheme is presented to calculate the integrals (see the above references). Alternatively, the weighting functions can be chosen to be the complex conjugate of the shape functions resulting in a new type of infinite element (which has been called *the mapped wave envelope infinite element*). This eliminates the exponential terms from the element integrals and hence the standard Gauss-Legendre numerical scheme can be used to calculate the infinite element integrals, equation (4.23). The shape and weighting functions of

this type of infinite element are fully explained in sections 5.6 and 5.8.

5.3.5 Extension to three dimensions

The shape function for a three dimensional element, stretched to infinity in ξ direction, is simply derived by multiplying the function of the two dimensional element by the corresponding finite element shape function for the third, ζ, direction giving

$$S(\xi, \eta, \zeta) = N(\xi, \eta)P(\zeta) \tag{5.21}$$

where $P(\zeta)$ are the conventional finite element shape functions for ζ direction.

5.4 Mapped infinite element for elliptical meshes (Type 1 infinite element)

The original mapped infinite element presented by Zienkiewicz *et al* [102, 100] and others (e.g. Bettess [28]) is intended to be usable for solving diffraction of waves by any shape of diffracting object. From equation (5.20) it can be noticed that when taking the derivative of the shape function with respect to η, the term involving the variation of r_0 (i.e. $\frac{\partial r_0}{\partial \eta}$) is being neglected. This implies that the radii of all infinite elements, r_{0i}, are assumed to be constant (in the above reference's notation $A_i = 2r_{0i}$ are assumed to be constant). As Burnett [36] pointed out, this implies that the 'radial' sides of all infinite elements emanate from a single point. In other words, the original infinite elements must be used on the exterior of a circle

circumscribing the object as shown in Figure 5.4. Since the fluid region between the

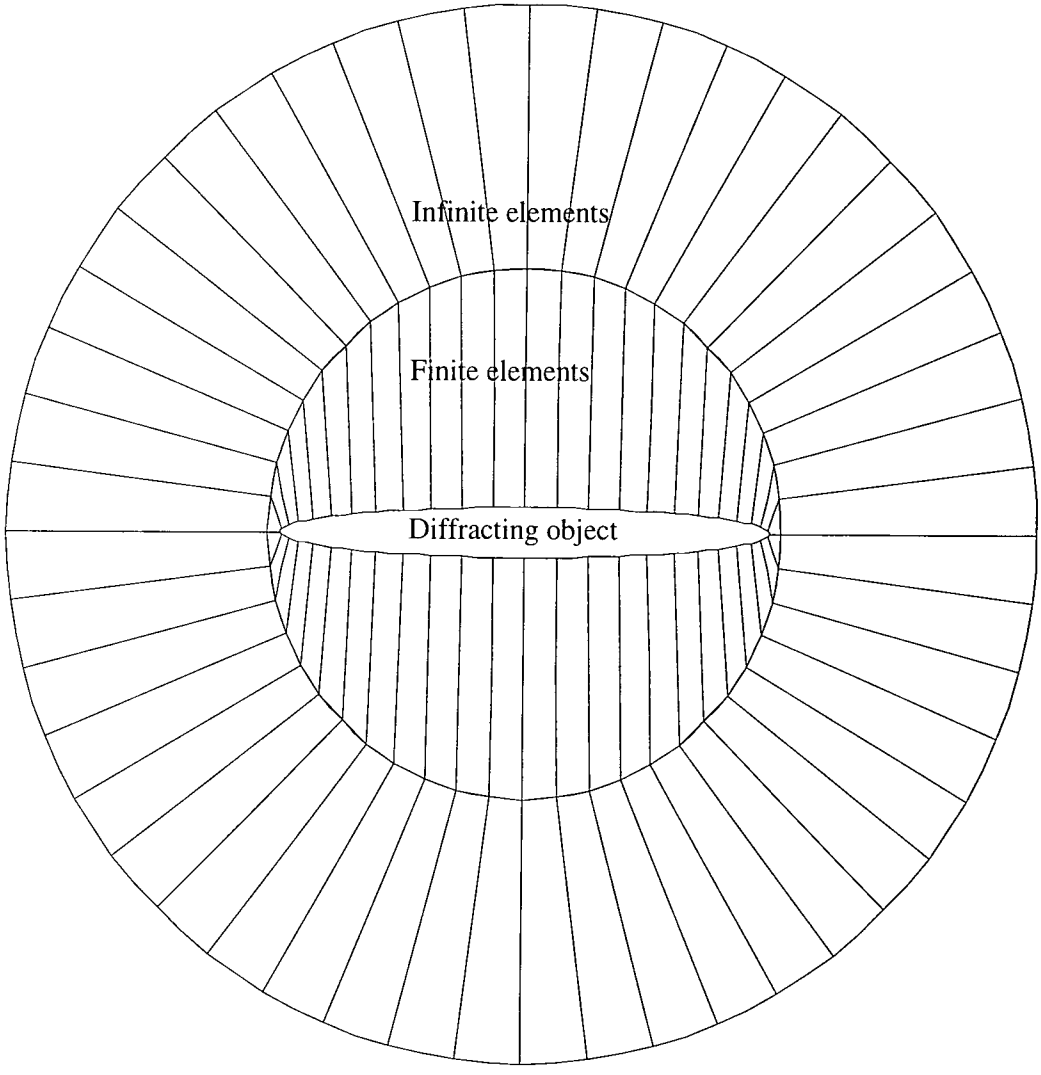

Figure 5.4: A circular mesh of finite and infinite elements (Type 1) for elliptical cylinder (b/a=10)

circumscribing circle and the object is modelled with the finite elements, the total number of elements would become very large for an object of large aspect ratio to maintain the limitation of at least ten finite element nodes per wavelength. This is computationally inefficient and so expensive particularly for shorter wavelengths, which is contrary to the primary goal of introducing the infinite elements. A remedy would be to reformulate the infinite element so that it can be used on the exterior

of any shape, say an ellipse, circumscribing the object as shown in Figure 5.5. The radial sides of the infinite elements now emanate from their virtual sources located on the semi-major axis of the ellipse.

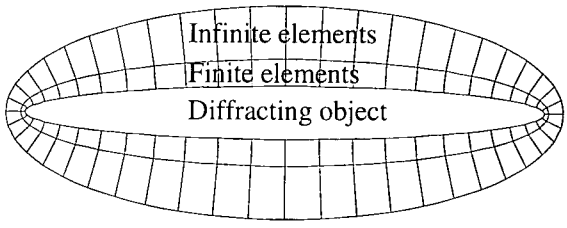

Figure 5.5: An elliptical mesh of finite and infinite elements (Type 1) for elliptical cylinder (b/a=10)

In this work, an investigation was carried out to test the original infinite element for elliptical meshes in which the elements are used on the exterior of an ellipse. This revealed that significant errors were associated with the original formulation when the computed results were compared with the analytical solutions. This error was considered to arise from the variation in r_0 which had been neglected in the original formulation. Therefore a modification to the original infinite element was to produce a more accurate mapped infinite element for any shape of the diffracting object.

Two methods of carrying out this modification were employed. The first method, termed approach 1, was to use the averaged value of the lengths of the radial sides of all infinite elements used in the mesh as a constant value for r_0 in the formulation of equations (5.18), (5.19) and (5.20)). This surprisingly gave very accurate results. Because, so far, there is no theoretical justification for this behaviour, a second method, termed approach 2, was used which considered the variation of the radii of infinite elements in the η direction. Approach 2 is explained below.

5.4.1 New shape function

The new shape function can be written as

$$N(r) = P(\xi,\eta)\left(\frac{r(\xi,\eta)}{r_0(\eta)}\right)^{1/2}\exp\left(ik[r(\xi,\eta)-r_0(\eta)]\right) \tag{5.22}$$

where $P(\xi,\eta)$ is a conventional quadratic finite element shape function and r is the radial distance measured from 'virtual' sources at point A, B and C (see Figure 5.2) given by the mapping as

$$r(\xi,\eta) = \frac{2r_0(\eta)}{1-\xi} \qquad or \qquad \xi = 1 - \frac{2r_0(\eta)}{r(\xi,\eta)} \tag{5.23}$$

By substituting r from this equation into equation (5.22), the shape function in the local coordinates (ξ,η) can be written as

$$N(\xi,\eta) = P(\xi,\eta)\left(\frac{2}{1-\xi}\right)^{1/2}\exp\left(ikr_0(\eta)\frac{1+\xi}{1-\xi}\right) \tag{5.24}$$

It can be seen that the shape function behaves asymptotically as $(1/r)^{1/2}\exp(ikr)$. A plot of the real and imaginary parts of the shape function over an element and the domain are illustrated in Figures 5.6 and 5.7.

Note that for two dimensional infinite elements which are used on the exterior of a shape other than a circle, r_0 is no longer a constant, as originally given by Zienkiewicz *et al*, equations 5.11 and 5.18, but is a function of η. The new mapping, equation 5.23, which considers the variation of r_0 in the η direction is used by different researchers (e.g Astley and Coyette [6], Cremers and Fyfe [46]. In the

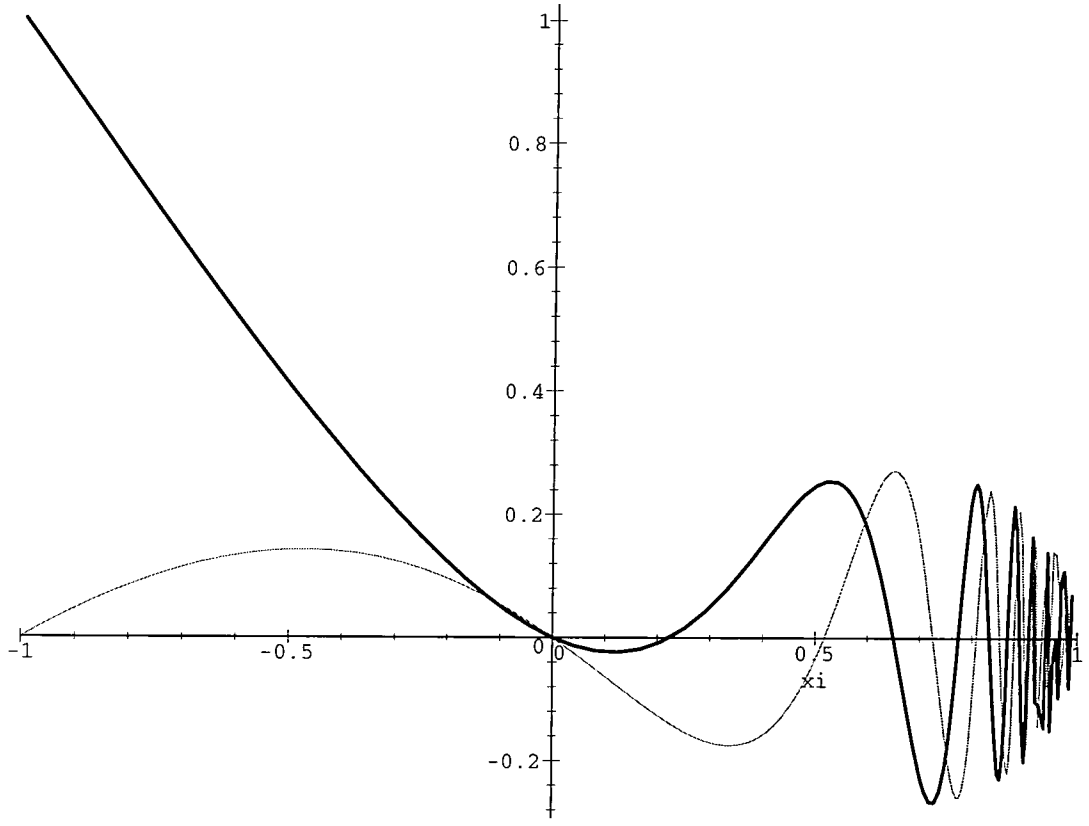

Figure 5.6: Variation of real (bold line) and imaginary parts of a Type 1 infinite element shape function over an element

present thesis, quadratic finite elements have been employed and therefore the infinite elements have quadratic variation in the η direction. In equations 5.22 onwards, $r_0(\eta)$ for quadratic variation in η is therefore given by

$$r_0(\eta) = \sum_{i=1}^{3} P_i(\eta) r_i = P_1(\eta) r_1 + P_2(\eta) r_2 + P_3(\eta) r_3 \tag{5.25}$$

where $P_i(\eta)$ are the finite element shape functions in the η direction given by equation (4.36), r_1, r_2 and r_3 are equal to O_3C, O_2B and O_1A as shown in Figure 5.2.

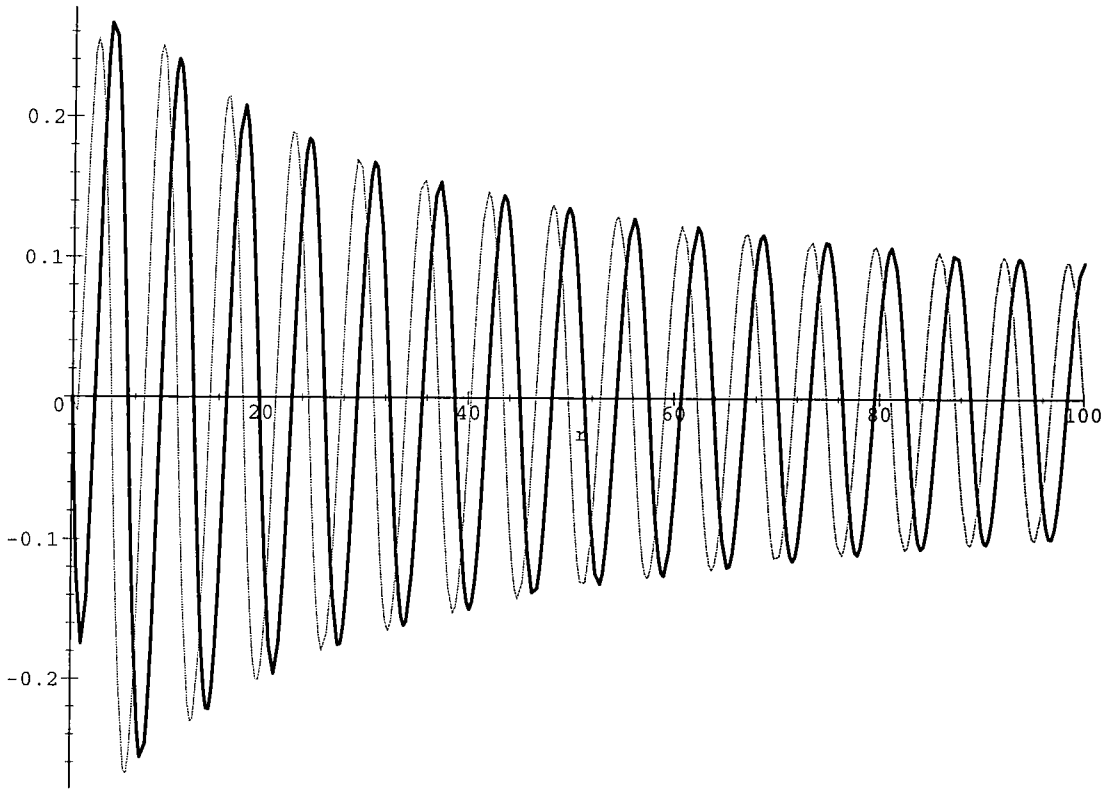

Figure 5.7: Variation of real (bold line) and imaginary parts of a Type 1 infinite element shape function over the domain

The shape function derivatives can be written as

$$\frac{\partial N}{\partial \xi} = \left(\frac{\partial P}{\partial \xi} + \frac{P}{2(1-\xi)} + \frac{i2kr_0P}{(1-\xi)^2}\right)\left(\frac{2}{1-\xi}\right)^{1/2} \exp\left(ikr_0\frac{1+\xi}{1-\xi}\right)$$

$$\frac{\partial N}{\partial \eta} = \left(\frac{\partial P}{\partial \eta} + \frac{ik(1+\xi)P}{(1-\xi)}\frac{\partial r_0}{\partial \eta}\right)\left(\frac{2}{1-\xi}\right)^{1/2} \exp\left(ikr_0\frac{1+\xi}{1-\xi}\right) \qquad (5.26)$$

Comparing $\frac{\partial N}{\partial \eta}$ in the above equation and the one in the original formulation, equation 5.20, it can be seen that an extra term has been added to the derivative of the shape function. It can also be seen that in all the new equations r_0 is now a function of η rather than being a constant. The term $\frac{\partial r_0}{\partial \eta}$ can be derived from the

equation 5.25 as

$$\frac{\partial r_0(\eta)}{\partial \eta} = \sum_{i=1}^{3} \frac{\partial P_i(\eta)}{\partial \eta} r_i \tag{5.27}$$

5.5 Radiation or Damping matrix for Type 1 infinite element

The calculation of the line integral which gives the radiation or damping matrix for this infinite element is fully explained elsewhere (Astley *et al* [7]). The contribution to the line integral from its upper limit is undefined. The difficulty is resolved by the authors by neglecting the undefined term altogether. Although this is difficult to be justified mathematically, it gives results which compare well with the analytical solutions both in the original work (Zienkiewicz *et al* [102, 100]) for circular meshes and in this thesis for elliptical meshes. A simple justification is that the exponential term has been added to the infinite element shape functions to consider the harmonic behaviour of the wave amplitude over the element (see section 5.3.2). At infinity the wave amplitude no longer has harmonic variation and so the term involving exponential term at infinity may as well be discarded from the formulation.

5.6 Mapped infinite wave envelope element (Type 2 infinite element)

5.6.1 Introduction

In the process of finite and infinite element analysis, the weighting function is adopted to be the same as the shape function. For infinite elements this leads to a complex integration procedure (see e.g. Zienkiewicz *et al* [102]). A remedy is to use the complex conjugate of the shape function as the weighting function so that the exponential terms cancel from the element integrals leaving a polynomial function to be integrated over the element. This is the so-called *wave envelope approach* which was first introduced by Astley [9]. In this section the appropriate shape and weighting functions are presented for a 2D Lagrangian element (9-node) for the analysis of water wave diffraction problems. The calculation of the Radiation/Damping matrix for this infinite element will also be fully explained.

5.6.2 Shape and weighting functions

The base shape function is chosen so that it takes the value unity where it is coupled to the finite element (at $\xi = -1$), decays to zero at infinity (at $\xi = +1$) and incorporates an outward travelling wave-like term. The procedure of constructing any infinite element shape function is explained in section 5.3 and in Appendix E. For this infinite element, the shape function is adopted to decay more rapidly (compared with the Type 1 infinite element) so that the line integral remains

integrable (see the discussion, section 7.2). An appropriate shape function (see equation E.5) may therefore be [1]

$$N(r) = P(\xi,\eta)\left(\frac{r_0(\eta)}{r(\xi,\eta)}\right)^{1/2}\exp\left(ik[r(\xi,\eta)-r_0(\eta)]\right) \tag{5.28}$$

where $P(\xi,\eta)$ is a conventional quadratic finite element shape function and r is the radius given by the mapping, equation (5.23), and r_0 is given by equation (5.25). By substituting r from equation (5.23), the shape functions in local coordinates (ξ,η) can be written as

$$N(\xi,\eta) = P(\xi,\eta)\left(\frac{1-\xi}{2}\right)^{1/2}\exp\left(ikr_0(\eta)\frac{1+\xi}{1-\xi}\right) \tag{5.29}$$

It can be seen that this shape function behaves asymptotically as $\frac{1}{r\sqrt{r}}\exp(ikr)$. A plot of the real and imaginary parts of the shape function over an element and the domain are illustrated in Figures 5.8 and 5.9 which show that this infinite element shape function decays more rapidly than the Type 1 infinite element shape function.

Following Astley [9, 8, 5], the weighting function is chosen to be the complex conjugate of the shape functions so that

$$W(r) = P(\xi,\eta)\left(\frac{r_0(\eta)}{r(\xi,\eta)}\right)^{1/2}\exp\left(-ik[r(\xi,\eta)-r_0(\eta)]\right) \tag{5.30}$$

By substituting r from equation (5.23), the weighting function in local coordinates

[1] The idea of similar shape function was suggested to the author by Dr. Phil Clark [44].

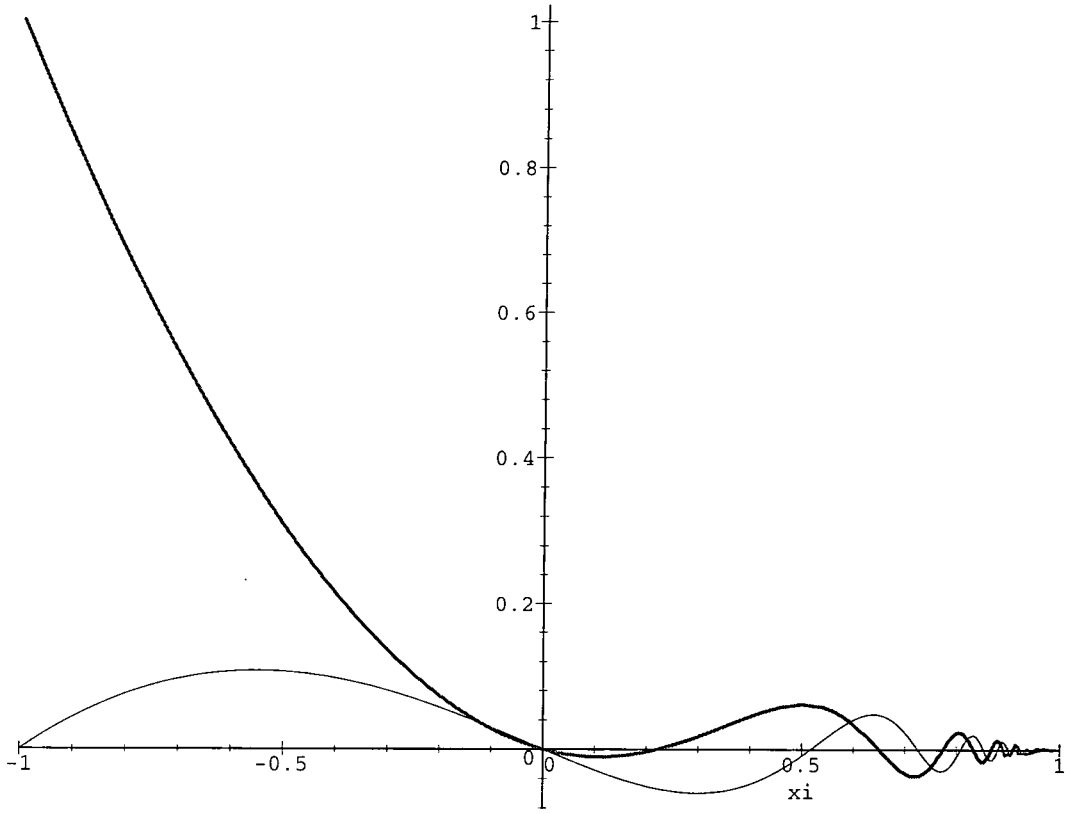

Figure 5.8: Variation of real (bold line) and imaginary parts of a Type 2 infinite element shape function over an element

(ξ, η) can be written as

$$W(\xi,\eta) = P(\xi,\eta)\left(\frac{1-\xi}{2}\right)^{1/2} \exp\left(-ikr_0(\eta)\frac{1+\xi}{1-\xi}\right) \tag{5.31}$$

The shape and weighting functions derivatives then can be written as

$$\begin{aligned}
\frac{\partial N}{\partial \xi} &= \left(\frac{\partial P}{\partial \xi} - \frac{P}{2(1-\xi)} + \frac{i2kr_0P}{(1-\xi)^2}\right)\left(\frac{1-\xi}{2}\right)^{1/2} \exp\left(ikr_0\frac{1+\xi}{1-\xi}\right) \\
\frac{\partial W}{\partial \xi} &= \left(\frac{\partial P}{\partial \xi} - \frac{P}{2(1-\xi)} - \frac{i2kr_0P}{(1-\xi)^2}\right)\left(\frac{1-\xi}{2}\right)^{1/2} \exp\left(-ikr_0\frac{1+\xi}{1-\xi}\right) \\
\frac{\partial N}{\partial \eta} &= \left(\frac{\partial P}{\partial \eta} + \frac{ik(1+\xi)P}{(1-\xi)}\frac{\partial r_0}{\partial \eta}\right)\left(\frac{1-\xi}{2}\right)^{1/2} \exp\left(ikr_0\frac{1+\xi}{1-\xi}\right) \\
\frac{\partial W}{\partial \eta} &= \left(\frac{\partial P}{\partial \eta} - \frac{ik(1+\xi)P}{(1-\xi)}\frac{\partial r_0}{\partial \eta}\right)\left(\frac{1-\xi}{2}\right)^{1/2} \exp\left(-ikr_0\frac{1+\xi}{1-\xi}\right)
\end{aligned} \tag{5.32}$$

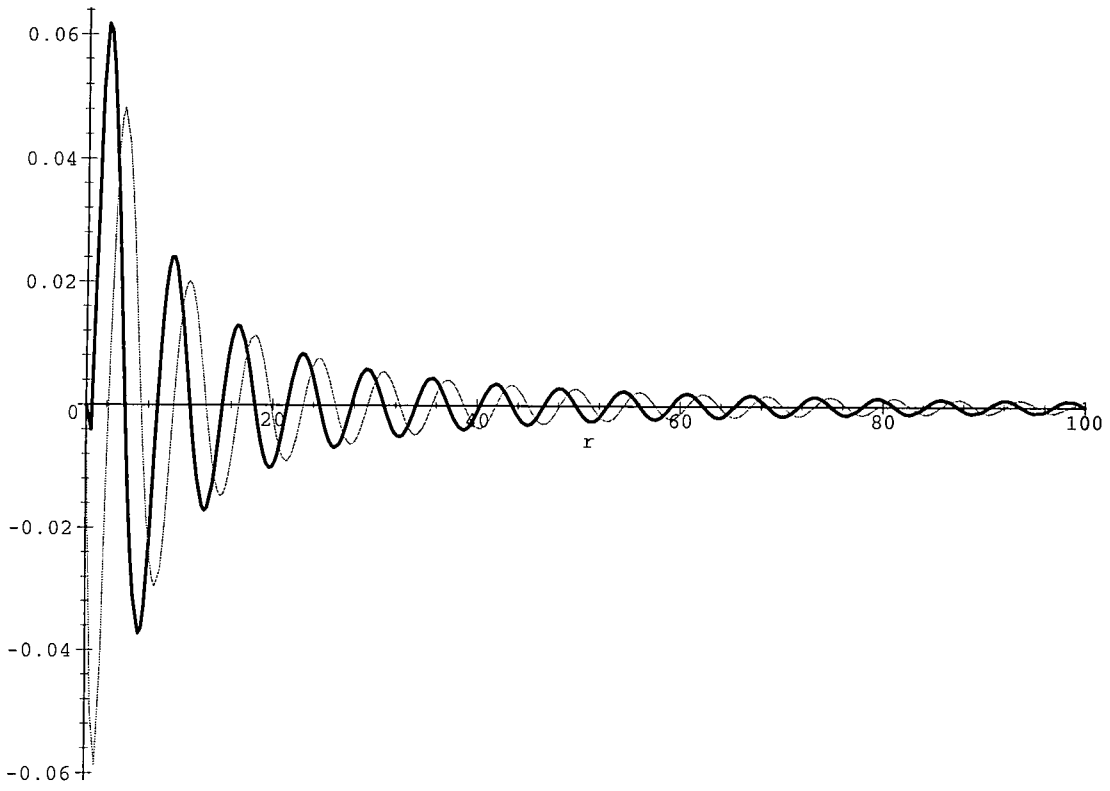

Figure 5.9: Variation of real (bold line) and imaginary parts of a Type 2 infinite element shape function over the domain

The term $\frac{\partial r_0}{\partial \eta}$ can be calculated by equation 5.27. These equations can then be substituted into equations (4.27) and (4.28) to calculate the element stiffness and mass matrices. The exponential terms cancel when calculating the element integrals. Therefore the Gauss-Legendre numerical scheme may be used to calculate these integrals. The calculation of the element radiation matrix is explained below.

5.7 Radiation or Damping matrix for Type 2 infinite element

As was shown in section 4.4, this term, which is a line integral along the infinite boundary, arises when applying the integration by parts to derive the weak form of

the weighted residuals equation. This term will now be calculated in two different ways, using infinite mapped wave envelope elements shape and weighting functions directly and using the radiation boundary condition discussed above (section 2.3.4). The former does not use any assumptions in calculating the radiation boundary condition contribution to the element matrix.

5.7.1 Direct approach

Since nodes 3, 4, and 5 are located at the infinite boundary (Figure 5.2), ϕ_s can now be approximated by using a set of infinite mapped wave envelope element shape functions, N_i

$$\phi_s = \sum_{i=3}^{5} N_i \phi_{si} \tag{5.33}$$

Substituting this into equation (4.26) gives

$$R_{ij}^e = \int_{\Gamma_\infty^e} W_j c c_g \frac{\partial N_i}{\partial n} d\Gamma \tag{5.34}$$

where i and j=3, 4 and 5 and N_i and W_j are the infinite element shape and weighting functions given by equations (5.28) and (5.30) (subscripts omitted for simplification). The parent Lagrangian finite element shape function P in these equations can be written as

$$P(\xi, \eta) = P^*(\eta) P^{"}(\xi) \tag{5.35}$$

For the line element located at the infinite edge of the infinite element, this can be written as

$$P(\xi,\eta) = P^*(\eta)P_3^{"}(\xi) \tag{5.36}$$

where P^* is the finite element shape function for a quadratic line element in the η direction given by equation (4.36) and $P_3^{"}$ is the finite element shape function for a quadratic line element in the ξ direction (i.e. shape function for node 3 in Figure 5.1). $P_3^{"}$ is therefore

$$P_3^{"}(\xi) = 0.5\xi(1+\xi) \tag{5.37}$$

Substituting finite to infinite geometry mapping equation (5.23) in this gives

$$P^{"}(r) = 1 - \frac{3r_0}{r} + \frac{2r_0^2}{r^2} \tag{5.38}$$

and its derivative is

$$\frac{\partial P^{"}}{\partial r} = \frac{3r_0}{r^2} - \frac{4r_0^2}{r^3} \tag{5.39}$$

The equation (5.36) can be rewritten as

$$P = P^*(\eta)P^{"}(r) \tag{5.40}$$

and similarly equations (5.28) and (5.30) as

$$N(r) = P^* P^{"} \left(\frac{r_0}{r}\right)^{1/2} \exp\left(ik(r - r_0)\right) \tag{5.41}$$

and

$$W(r) = P^* P^{"} \left(\frac{r_0}{r}\right)^{1/2} \exp\left(-ik(r - r_0)\right) \tag{5.42}$$

Considering equation (5.41), $\frac{\partial N}{\partial n}$ can be written as

$$\frac{\partial N}{\partial n} \approx \frac{\partial N}{\partial r} = P^* \left(\frac{\partial P^{"}}{\partial r} - \frac{P^{"}}{2r} + ikP^{"}\right) \left(\frac{r_0}{r}\right)^{1/2} \exp\left(ik(r - r_0)\right) \tag{5.43}$$

If the outer boundary is assumed to be circular, then

$$d\Gamma = r d\theta \tag{5.44}$$

Substituting this and equations (5.43) and (5.42) into equation (5.34) and taking into account that at infinity r tends to ∞ gives

$$\mathbf{R}^e = \int_{\Gamma^e_\infty} \mathbf{P}^{*T} c c_g ikr_0 \mathbf{P}^* d\theta \tag{5.45}$$

This is a new radiation boundary condition contribution to the element matrix which resulted directly from integration by parts by using the wave envelope infinite element theory. It will be shown later (section 5.7.2) that the same matrix can be

achieved by using the radiation boundary condition.

In the above equation θ is the anticlockwise angle from the horizontal axis (x) (see Figure 5.2) and can be interpolated along the edge of the element using P^*

$$\theta = \sum_{i=1}^{3} P_i^* \theta_i = 0.5\eta(\eta - 1)\theta_1 + (1 - \eta)(1 + \eta)\theta_2 + 0.5\eta(\eta + 1)\theta_3 \tag{5.46}$$

where θ_1, θ_2 and θ_3 are the angles at $\eta = -1$, 0 and $+1$. Therefore $d\theta$ can now be written as

$$d\theta = \sum_{i=1}^{3} \frac{\partial P_i^*}{\partial \eta} \theta_i d\eta = [(\eta - 0.5)\theta_1 + 2\eta\theta_2 + (\eta + 0.5)\theta_3]d\eta \tag{5.47}$$

Now the final matrix resulting from the line integral at the infinite boundary of the infinite element, or the radiation matrix, can be written as

$$\mathbf{R}^e = \int_{-1}^{+1} \mathbf{P}^{*T} c c_g i k r_0(\eta)[(\eta - 0.5)\theta_1 + 2\eta\theta_2 + (\eta + 0.5)\theta_3]\mathbf{P}^* d\eta \tag{5.48}$$

These integrals are evaluated using the Gauss-Legendre numerical scheme.

5.7.2 Using radiation boundary condition

The radiation boundary condition due to Zienkiewicz and Newton [108], equation (2.15), can be rewritten as

$$\frac{\partial \phi_s}{\partial n} = ik\phi_s \tag{5.49}$$

Substituting this and equation (5.33) into (4.26) gives

$$\mathbf{R}^e = \int_{\Gamma_\infty^e} \mathbf{W}^T cc_g ik \mathbf{N} d\Gamma \tag{5.50}$$

Now by substituting equations (5.41), (5.42) and 5.44 into this gives

$$\mathbf{R}^e = \int_{\Gamma_\infty^e} \mathbf{P}^{*T} cc_g ikr_0 \mathbf{P}^* d\theta \tag{5.51}$$

which is exactly the same as equation (5.45).

5.8 Mapped infinite wave envelope element for multiple body diffraction problems (Type 3 infinite element)

5.8.1 Introduction

The problem of wave diffraction by arrays of diffracting bodies is an important problem in many scientific and engineering disciplines, such as the offshore industry. The analytical solution of the problem was presented for circular diffracting bodies in section 3.4. In this section, a new infinite element is presented which can be used to solve the problem of wave diffraction by arrays of bodies with arbitrary shapes. The definition sketch of the problem is illustrated in Figure 5.10.

The governing equation obviously remains the same, but the boundary condi-

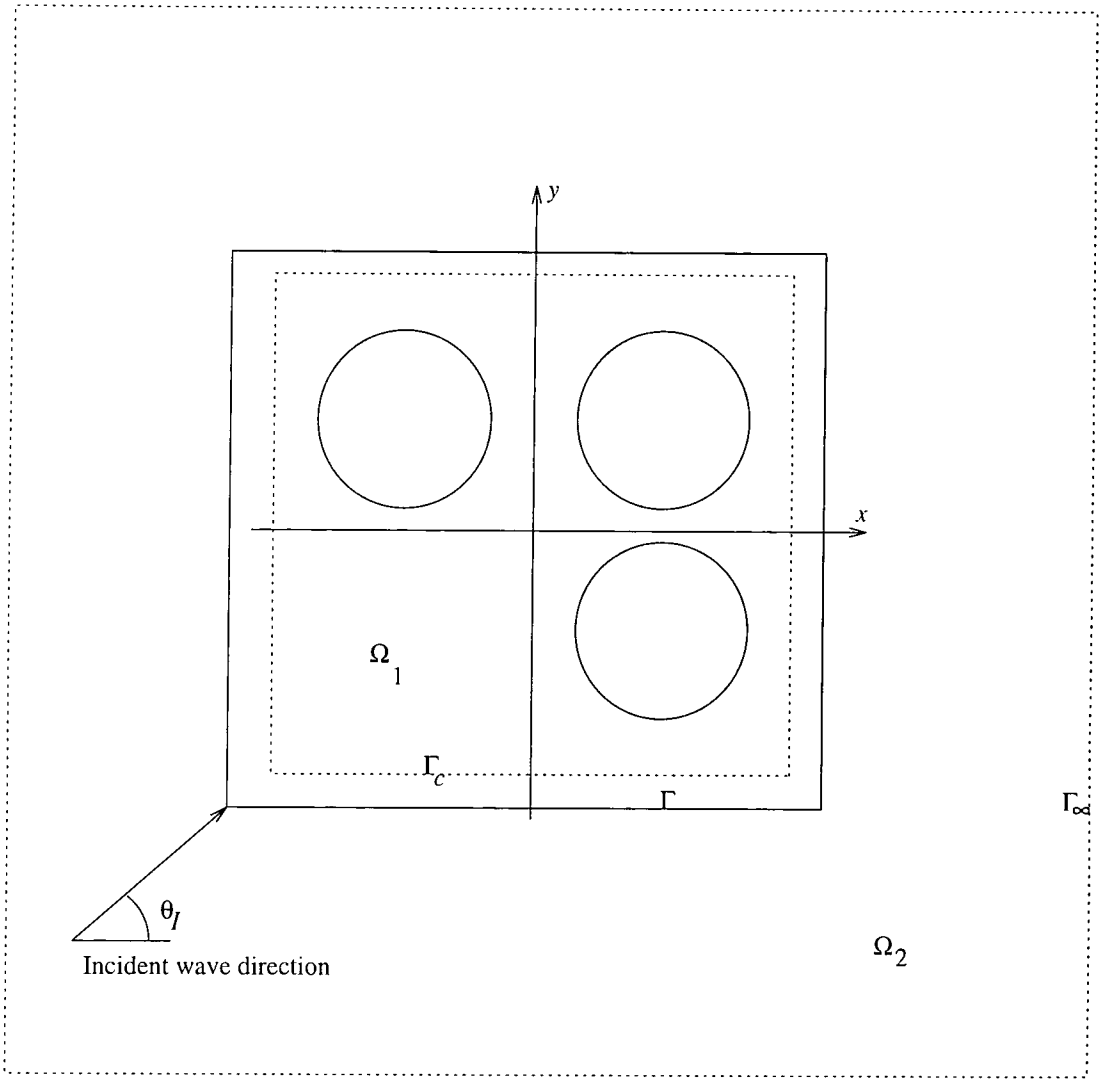

Figure 5.10: Definition sketch of multiple body diffraction problem

tions must be reconsidered. Comparing the above definition sketch and the one given for a single diffracting body, Figure 2.2, it is obvious that the radiation boundary condition remains also the same. The only difference here is that the natural boundary condition must be applied to multiple bodies rather than a single body. However, by placing the Γ_c boundary (see section 4.6) outside the diffracting objects and considering that the velocity on the objects is assumed to be zero (see section 2.3.3) this boundary condition has no contribution to the finite and infinite element model. Therefore, the overall modelling remains the same.

5.8.2 Shape and weighting functions

The shape function is now chosen in such a way that it can model the correct rate of attenuation of the wave amplitude towards infinity. The weighting function is then adopted such that the line integral at the infinite boundary vanishes so that the outer boundary of the infinite elements is no longer required to be a circle (equation (5.44)). As usual, the base shape function is chosen so that it takes the value unity where it is coupled to the finite element (at $\xi = -1$), decays to zero at infinity (at $\xi = +1$) and incorporates an outward travelling wave-like term. As was explained above (see equation 5.13), for 2D water wave problems, the amplitudes of the diffracted waves decay approximately as $\frac{1}{\sqrt{r}}$. Therefore, an appropriate shape function can be chosen the same as the Type 1 infinite element shape function given by equations (5.22) and (5.24).

An appropriate weighting function is adopted based on multiples of the complex conjugates of the shape functions so that

$$W(r) = P(\xi,\eta)\left(\frac{r_0(\eta)}{r(\xi,\eta)}\right)^2 \exp\left(-ik[r(\xi,\eta) - r_0(\eta)]\right) \tag{5.52}$$

which behave asymptotically as $(1/r)^{-3}\exp(-ikr)$. This ensures that the element radiation matrix ($\mathbf{R}^e$ in equation 4.23) vanishes (see section 5.9).

Substituting r from equation (5.23), the weighting function in local coordinates (ξ,η) can be written as

$$W(\xi,\eta) = P(\xi,\eta)\left(\frac{1-\xi}{2}\right)^2 \exp\left(-ikr_0\frac{1+\xi}{1-\xi}\right) \tag{5.53}$$

The weighting function derivatives can then be written as

$$\frac{\partial W}{\partial \xi} = \left(\frac{\partial P}{\partial \xi} - \frac{2P}{1-\xi} - \frac{i2kr_0P}{(1-\xi)^2}\right)\left(\frac{1-\xi}{2}\right)^2 \exp\left(-ikr_0\frac{1+\xi}{1-\xi}\right)$$

$$\frac{\partial W}{\partial \eta} = \left(\frac{\partial P}{\partial \eta} - \frac{ik(1+\xi)P}{(1-\xi)}\frac{\partial r_0}{\partial \eta}\right)\left(\frac{1-\xi}{2}\right)^2 \exp\left(-ikr_0\frac{1+\xi}{1-\xi}\right) \quad (5.54)$$

These equations and equations 5.24 to 5.26 can now be substituted into equations (4.27) and (4.28) to calculate Type 3 infinite element stiffness and mass matrices. With the present choice of weighting function, although the radiation matrix vanishes, the element matrix still becomes unsymmetric. The exponential terms, again, cancel when calculating the element integrals as in section 5.6.2. Therefore the Gauss-Legendre numerical scheme may be used to calculate these integrals.

5.9 Radiation or Damping matrix for Type 3 infinite element

It can easily be seen that the radiation matrix resulting from the line integral vanishes ($\mathbf{R}^e = 0$ in equation 4.23) leaving the element matrix to consist of only stiffness and mass matrices (i.e. $\mathbf{A}^e = \mathbf{K}^e - \omega^2\mathbf{M}^e$). This can be proved both with the direct approach presented in this work and the boundary condition given by Zienkiewicz and Newton [108].

5.9.1 Direct approach

Now consider the term at infinity, equation (4.26), which requires the calculation of $\frac{\partial N}{\partial n}$. Considering equations (5.22) and (5.40), this can be written as

$$\frac{\partial N}{\partial n} \approx \frac{\partial N}{\partial r} = P^* \left(\frac{\partial P_i^{"}}{\partial r} + \frac{P_i^*}{2r} + ikP_i^{"} \right) \left(\frac{r}{r_0} \right)^{1/2} \exp ik(r - r_0) \tag{5.55}$$

Substituting this and equation (5.52) into equation (4.26) gives

$$\mathbf{R}^e = \int_{\Gamma_\infty^e} \mathbf{P}^{*T} cc_g ik \left(\frac{\partial P^{"}}{\partial r} + \frac{P^{"}}{2r} + ikP^{"} \right) \left(\frac{r_0}{r} \right)^{3/2} \mathbf{P}^* d\Gamma \tag{5.56}$$

Note that P^* and $P^{"}$ are the finite element shape functions in η and ξ directions respectively as explained in equations (5.35) to (5.40). At infinity r tends to ∞ and therefore the line integral is equal to zero. The radiation boundary condition therefore is implied in the formulation with the present choice of shape and weighting functions. This is another advantage of this (Type 3) infinite element.

5.9.2 Using radiation boundary condition

Substituting the shape and weighting functions into equation (5.50), the line integral calculated using the radiation boundary condition due to Zienkiewicz and Newton [108], gives

$$\mathbf{R}^e = \int_{\Gamma_\infty^e} \mathbf{P}^{*T} cc_g ik \left(\frac{r_0}{r} \right)^{3/2} \mathbf{P}^* d\Gamma \tag{5.57}$$

which is obviously zero as r tends to infinity.

5.10 Summary

In this chapter, three types of two-dimensional infinite element, for the analysis of water wave diffraction problems are given. First the original mapped infinite element is further improved so that it can model the diffraction of waves by large aspect ratio bodies more economically. A simple explanation is given to justify why the undefined term of the line integral can simply be ignored to give satisfactory results. Then a new infinite element is developed using the so-called wave envelope approach which leads to a much more simple formulation. Hence the element integrals can be integrated by a standard integration scheme such as Gauss-Legendre numerical integration scheme. The shape and weighting functions for the element are given. The calculation of the line integral for this element is given in detail. Then a third infinite element is developed to model the diffraction of water waves by arrays of objects more accurately. The shape and weighting functions for this element are chosen such that the line integral becomes zero. The extension to thr three-dimensional formulation is outlined. Table 5.1 illustrates the shape and weighting functions for the different types of infinite elements and Table 5.2 shows the asymptotic behaviour of these functions.

Table 5.1: Shape and weighting functions for different infinite elements

infinite element	shape function	weighting function
Type 1	$N = P(\frac{r}{r_0})^{0.5} \exp ik(r - r_0)$	$W = P(\frac{r}{r_0})^{0.5} \exp ik(r - r_0)$
Type 2	$N = P(\frac{r_0}{r})^{0.5} \exp ik(r - r_0)$	$W = P(\frac{r_0}{r})^{0.5} \exp -ik(r - r_0)$
Type 3	$N = P(\frac{r}{r_0})^{0.5} \exp ik(r - r_0)$	$W = P(\frac{r_0}{r})^{2} \exp -ik(r - r_0)$

Table 5.2: Asymptotic behaviour of different infinite elements shape and weighting functions

infinite element	shape function	weighting function
Type 1	$N \approx r^{-0.5} \exp ikr$	$W \approx r^{-0.5} \exp ikr$
Type 2	$N \approx r^{-1.5} \exp ikr$	$W \approx r^{-1.5} \exp -ikr$
Type 3	$N \approx r^{-0.5} \exp ikr$	$W \approx r^{-3.0} \exp -ikr$

Chapter 6

Results and Comparison

An application of finite/infinite element analysis of wave diffraction is in the prediction of waves on the surface of water. Also it can be used to predict the wave pressure or forces acting on diffracting objects. Three types of infinite elements have been developed in this work which are as follows:

Type 1: Improved mapped infinite element for elliptical meshes (described in section 5.4 and by Bettess *et al* [24, 25])

Type 2: Mapped infinite wave envelope element (described in section 5.6 and by Baghbani [14])

Type 3: Mapped infinite wave envelope element for multiple body diffraction problems (described in section 5.8 and by Baghbani *et al* [15])

As a test for these new infinite elements, example problems were solved involving water wave diffraction by

- A circular cylinder
- An elliptical cylinder
- An array of circular cylinders

The analytical solutions are presented in sections 3.2, 3.3 and 3.4 respectively.

Finite/infinite element (**F/IE**) solutions on the diffracting objects were compared to their analytical (**Theory**) equivalents, and their relative errors are evaluated and plotted. The error is defined as

$$\varepsilon = \frac{|\eta_a| - |\eta|}{A} \times 100 \tag{6.1}$$

where η_a is the analytical surface elevation, η is the surface elevation calculated by the finite/infinite element model and A is the incident wave amplitude. The other comparison is based on the contour plot of the real and imaginary parts of water surface elevations in the vicinity of cylinder(s) for the finite/infinite element and their equivalent analytical solutions [1]. All the given parameters were made dimensionless by using a dimension of the diffracting object. The resulting free surface elevations are divided by the incident wave amplitude in order to obtain the non-dimensional surface elevations (η/A).

[1]The Unimap software package was used for contour plotting. Small boxes that appear on some plots are an artifact of the contouring

6.1 Finite and infinite element mesh design

In designing a mesh of finite and infinite elements three criteria were considered. First at least ten finite element nodes per wavelength were used both in the radial and circumferential directions to model the oscillatory behaviour of the wave reasonably accurately. Secondly the mesh was designed such that the finite elements remained approximately square. In other words, the lengths of the sides of the finite elements remained approximately equal and less than one fifth of the wavelength. Finally sharp corner elements were avoided. These ensured that the errors resulting from finite elements were minimised so that the accuracy of the different infinite elements could be examined. Three types of meshes were used in this work, circular, elliptical and square meshes. The existing mesh generators [24], which generate circular and elliptical meshes for single body diffraction problems, were modified to generate the required finite and infinite element meshes for this study. In this work a new mesh generator was also developed using Maple to generate square meshes of finite and infinite elements for arrays of circular or elliptical cylinders.

6.2 Results for Type 1 infinite element

The element was originally tested for some special cases of wave diffraction problems [102]. In this work, first the problem of wave diffraction by an elliptical cylinder was solved using circular and elliptical meshes. Two approaches, 1 and 2, described in section 5.4 to improve the infinite element for the latter meshes

were tested. Then other example problems were solved using the robust approach, approach 2, for this infinite element.

An elliptical cylinder standing in open water with a plane surface wave incident upon it was analysed. The non-dimensional parameters for this problem were as follows:

$$b/a=2$$

$$d/a=1$$

$$\theta_I = 0^o, 30^o \text{ and } 90^o$$

$$ka = 1\ (> 0.2\pi)$$

where

b is Semi-major axis length of the ellipse

a is Semi-minor axis length of the ellipse

A is The incident wave amplitude

d is The water depth

θ_I is Angle of the incident wave

k is The wave number

This problem was solved using two types of meshes, circular and elliptical meshes. They are illustrated in Figures 6.1 and 6.2 respectively.

First the original (Zienkiewicz *et al*'s [102]) formulation, equation (5.18), was examined. Figures 6.3 and 6.4 show the comparison between the numerical and analytical solutions on the surface of the cylinder for both real and imaginary parts of the free surface elevations. The relative errors are shown in Figures 6.5 and 6.6. As can be seen the elliptical mesh gives larger errors.

Two approaches were presented in section 5.4 to improve the formulation of

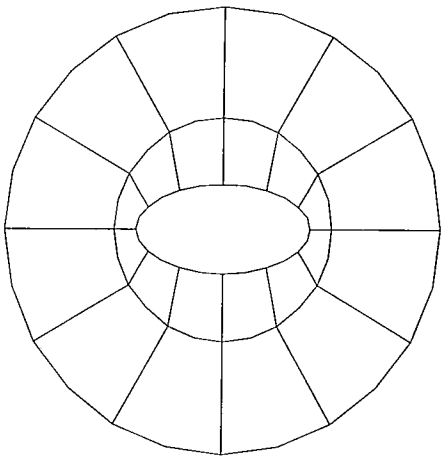

Figure 6.1: Circular mesh of finite and Type 1 infinite elements for elliptical cylinder, b/a=2

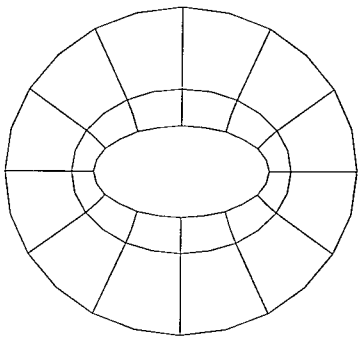

Figure 6.2: A coarse elliptical mesh of finite and Type 1 infinite elements for elliptical cylinder, b/a=2 (Mesh1)

the mapped infinite element for elliptical meshes. Approach 1 was examined first. The real and imaginary parts of relative errors are shown in Figures 6.7 and 6.8 respectively. Case a is the Zienkiewicz *et al*'s [102] formulation and case b is approach 1. As can be seen the results of the elliptical mesh using approach 1 improved and this mesh now gives better results than the circular mesh.

Approach 2, which is a robust formulation of the mapped infinite element for elliptical meshes, was then examined. The real and imaginary parts of relative errors are shown in Figures 6.9 and 6.10 respectively. As can be seen, the elliptical mesh again gives better results than the circular mesh. From here onwards, approach 2

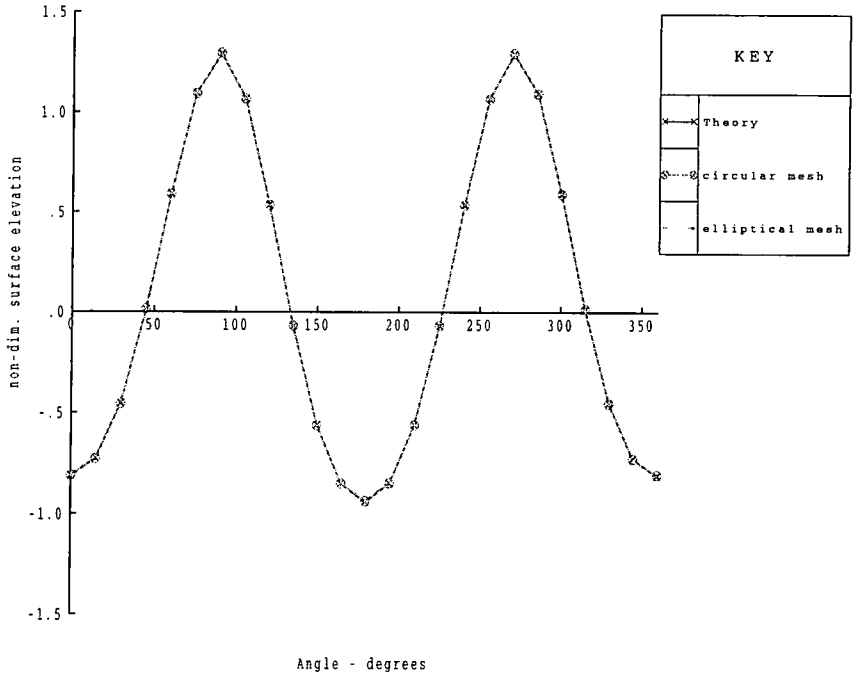

Figure 6.3: Real part of the surface elevations (η/A) on elliptical cylinder as a function of angle around the cylinder ($b/a = 2$, $\theta_I = 0^o$)

was then used to solve other example problems.

The mesh design in the circumferential direction was then considered. A mesh of finite and infinite elements, Mesh1, is illustrated in Figure 6.2 and the other mesh, Mesh2, in which the infinite elements are located at a greater distance from the cylinder, is illustrated in Figure 6.11. The relative errors are shown in Figures 6.12 and 6.13. As can be seen the errors for Mesh2 are larger than the ones for Mesh1. This unexpected tendency resulted from not using an adequate number of finite element nodes (at least 10 nodes per wavelength) circumferentially. In the next example problem this is investigated. A revised mesh with 24 elements in the circumferential direction was then constructed. The coarse and fine mesh are illustrated in Figures 6.14 and 6.15. The relative errors are shown in Figures 6.16 and 6.17 which show that the errors decrease to less than 0.1 percent for the fine

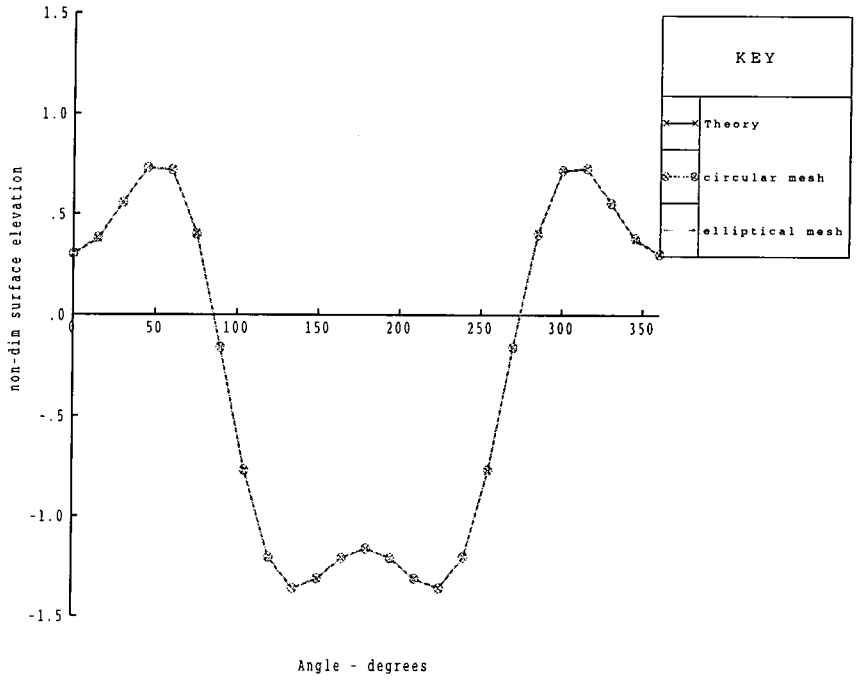

Figure 6.4: Imaginary part of the surface elevations on elliptical cylinder as a function of angle around the cylinder ($b/a = 2$, $\theta_I = 0^o$)

mesh.

The analysis was repeated using the coarse mesh, Figure 6.14, for angles of incidence of 30 and 90 degrees and results are shown in Figures 6.18, 6.19, 6.20 and 6.21. As can be seen from these figures the errors are small being not greater than 0.25 percent.

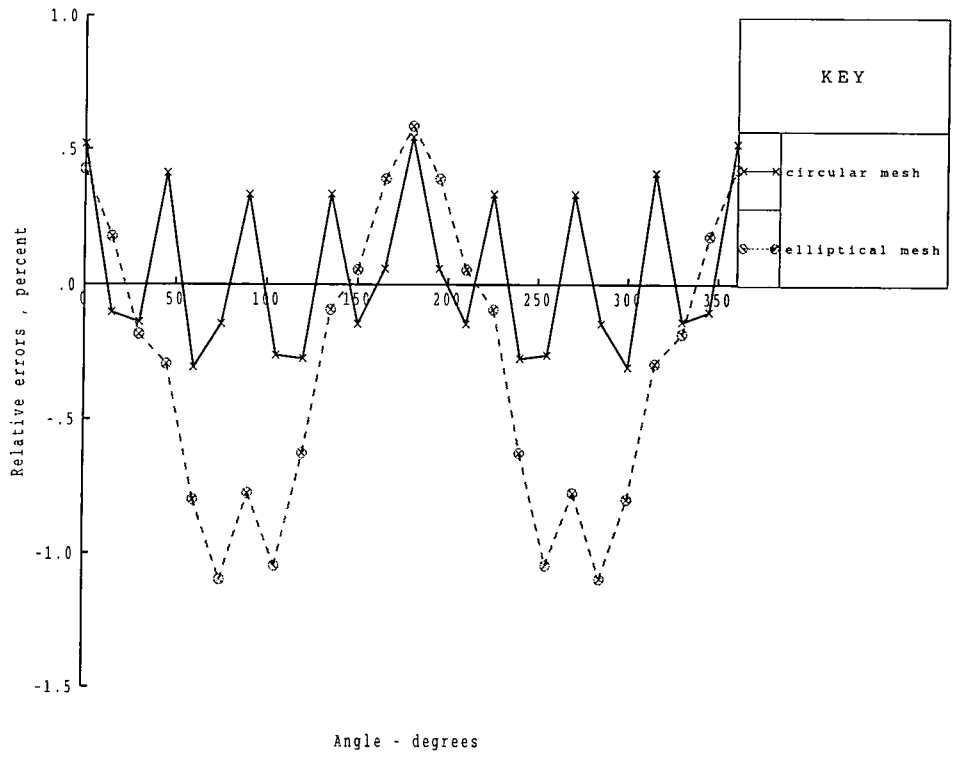

Figure 6.5: Comparison of errors in real part of the solutions produced by two types of mesh ($b/a = 2$, $\theta_I = 0^o$)

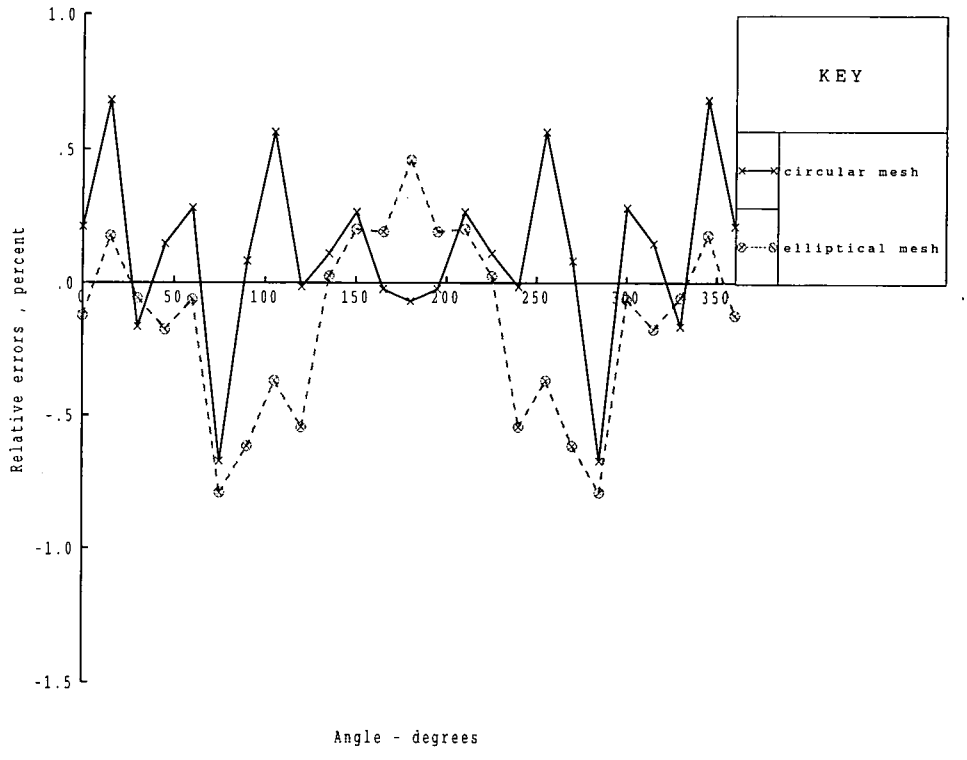

Figure 6.6: Comparison of errors in imaginary part of the solutions produced by two types of mesh ($b/a = 2$, $\theta_I = 0^o$)

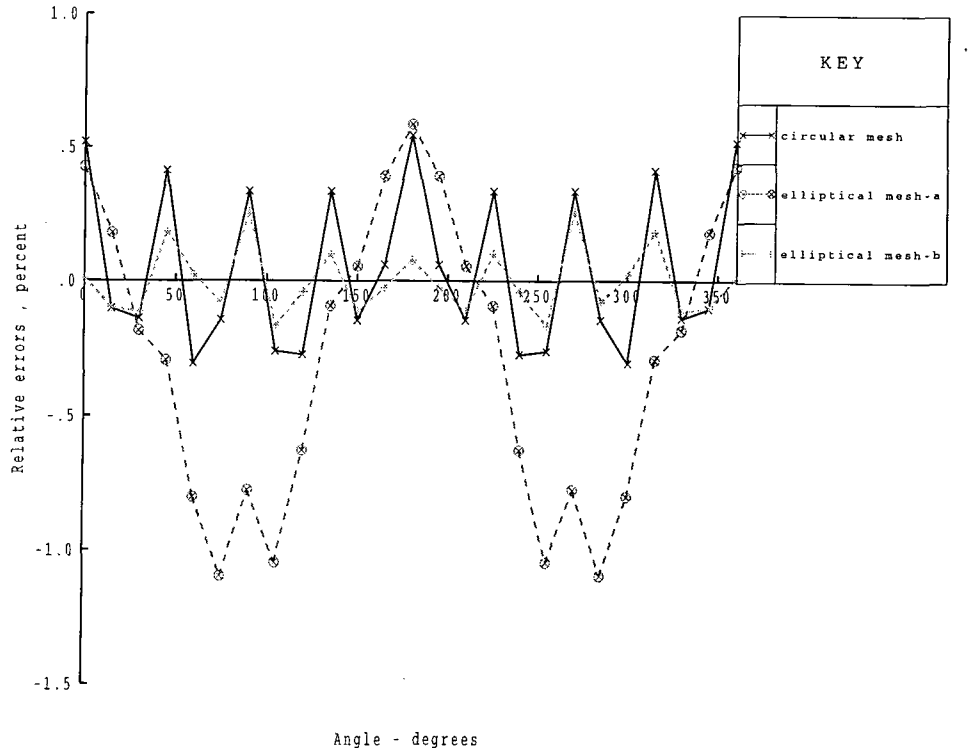

Figure 6.7: Comparison of errors in real part of the solutions produced by two types of mesh ($b/a = 2$, $\theta_I = 0^o$)

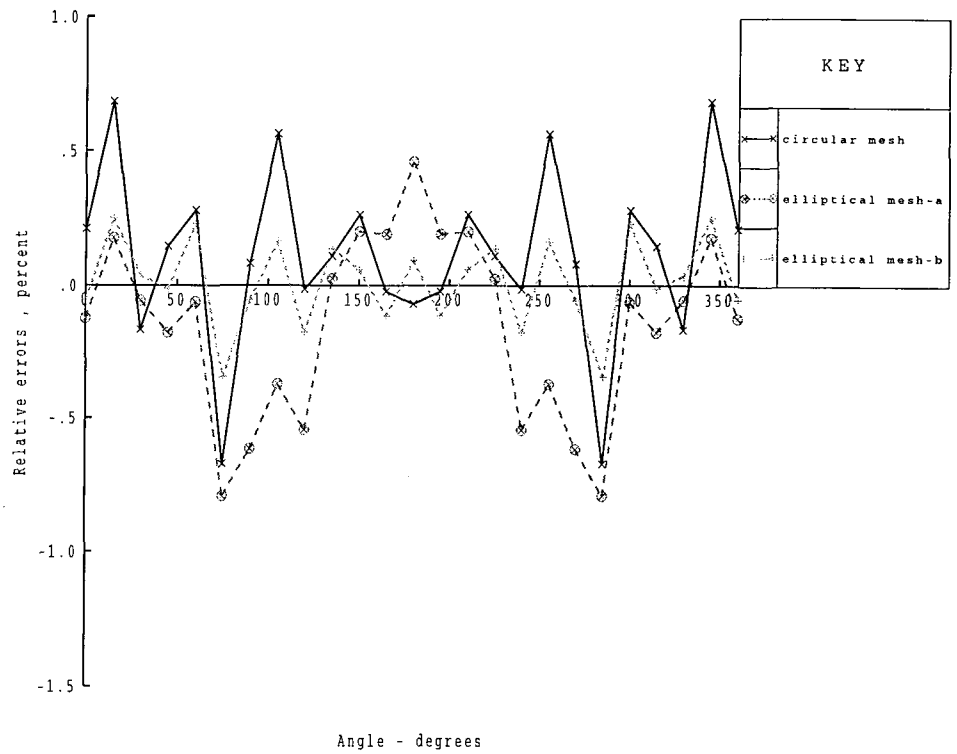

Figure 6.8: Comparison of errors in imaginary part of the solutions produced by two types of mesh ($b/a = 2$, $\theta_I = 0^o$)

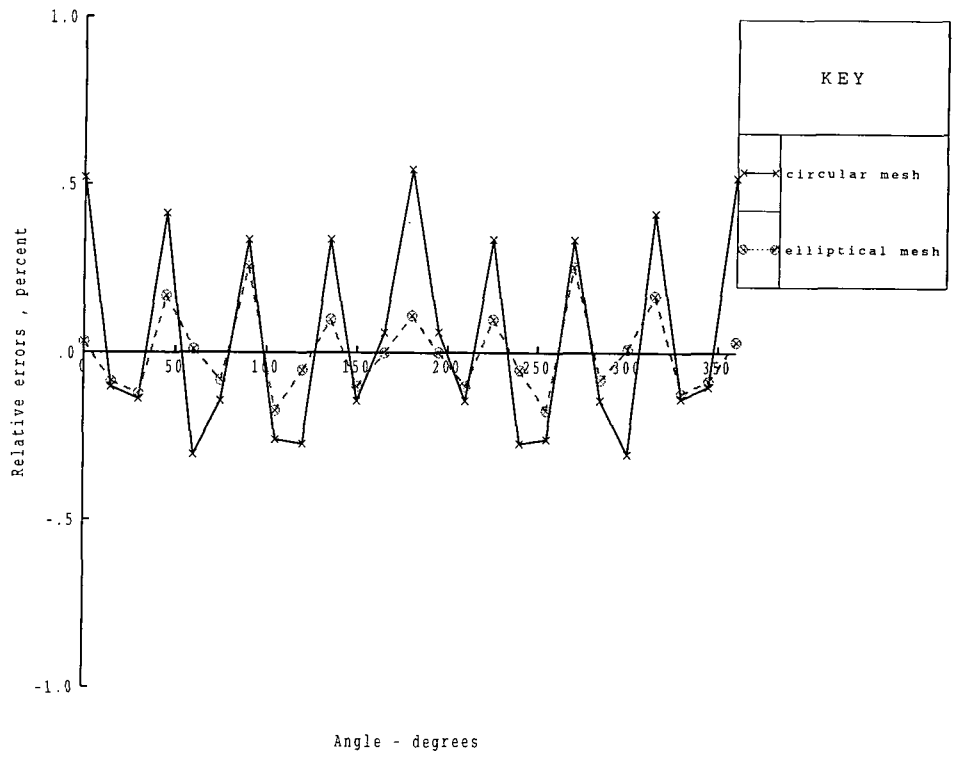

Figure 6.9: Comparison of errors in real part of the solutions produced by two types of mesh ($b/a = 2$, $\theta_I = 0^o$)

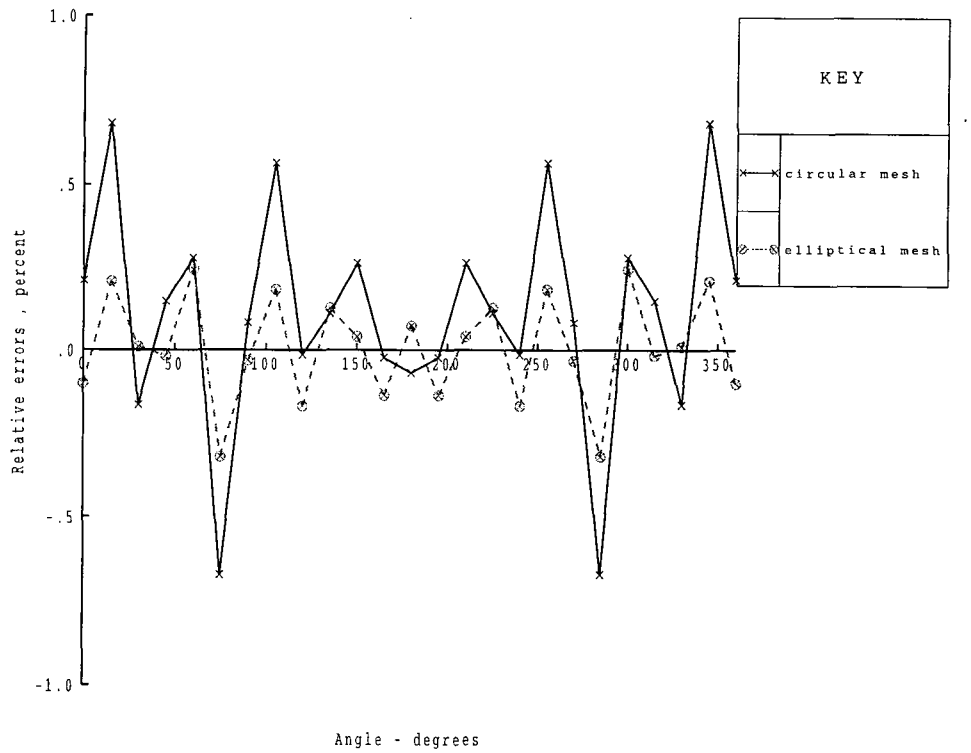

Figure 6.10: Comparison of errors in imaginary part of the solutions produced by two types of mesh ($b/a = 2$, $\theta_I = 0^o$)

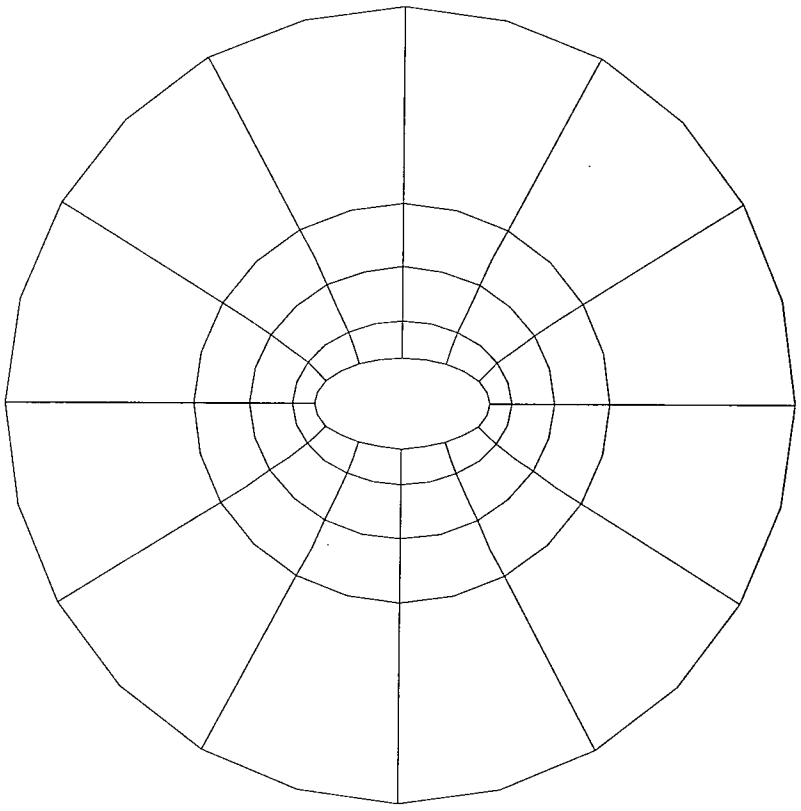

Figure 6.11: A mesh of finite and Type 1 infinite elements for elliptical cylinder, b/a=2 (Mesh2)

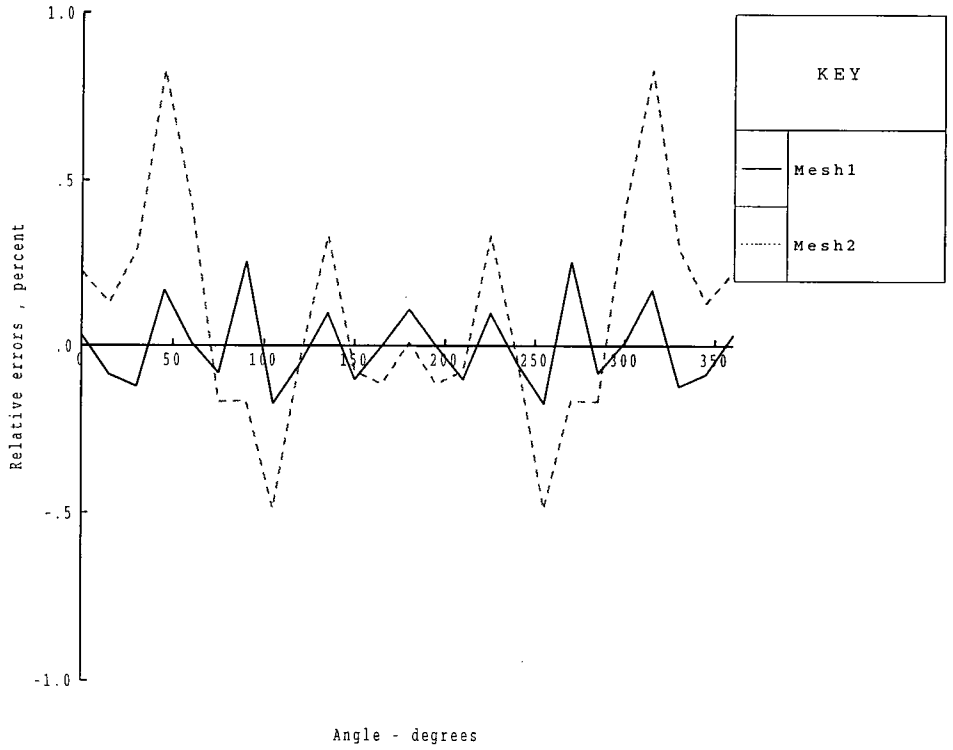

Figure 6.12: Comparison of errors in real part of the solutions on the cylinder produced by Mesh1 and Mesh2 ($b/a = 2$, $\theta_I = 0^o$)

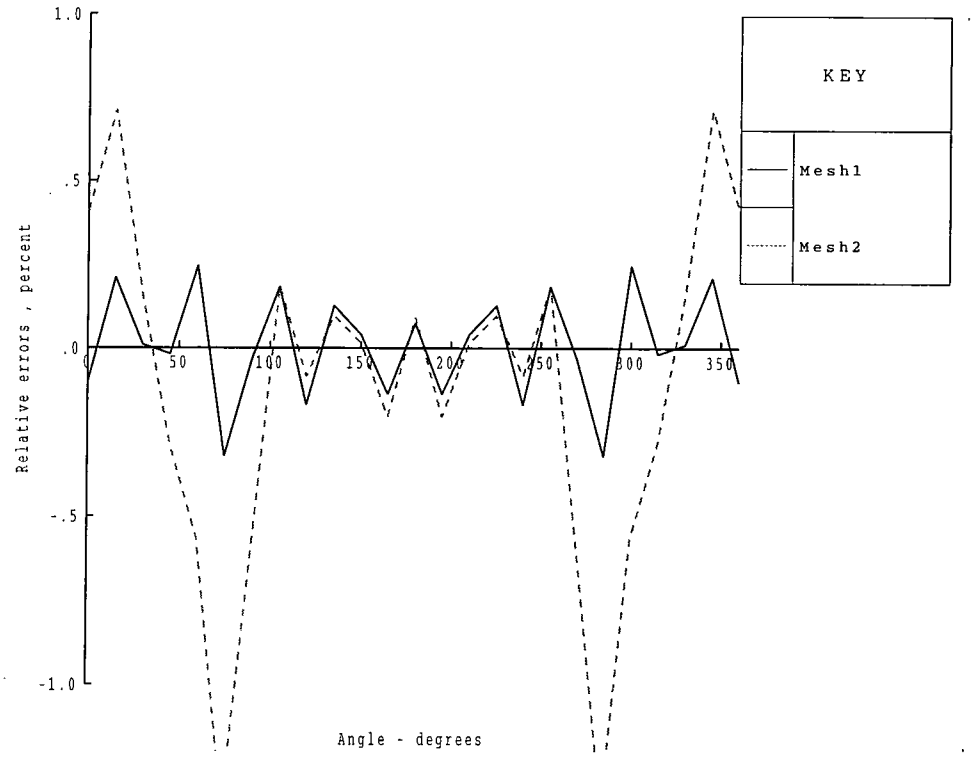

Figure 6.13: Comparison of errors in imaginary part of the solutions produced by Mesh1 and Mesh2 ($b/a = 2$, $\theta_I = 0^o$)

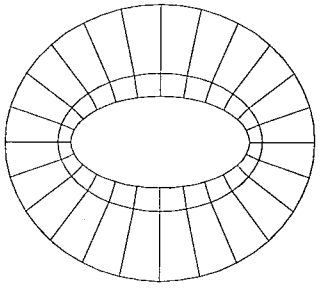

Figure 6.14: Coarse mesh of finite and Type 1 infinite elements for elliptical cylinder, b/a=2

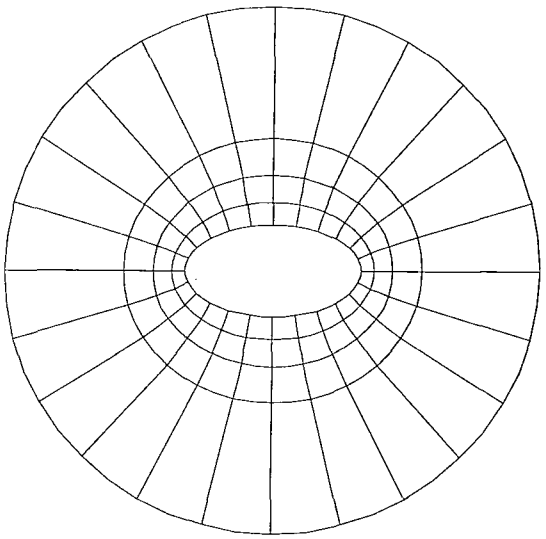

Figure 6.15: Fine mesh of finite and Type 1 infinite elements for elliptical cylinder, b/a=2

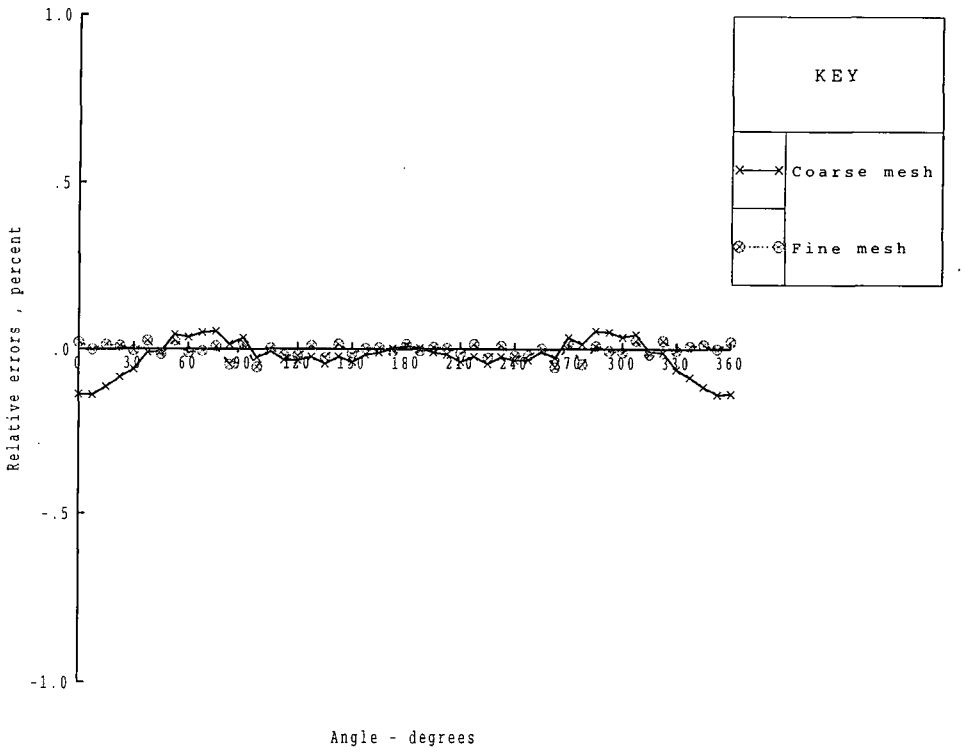

Figure 6.16: Comparison of errors in real part of the solutions on the cylinder produced by coarse and fine meshes ($b/a = 2$, $\theta_I = 0^o$)

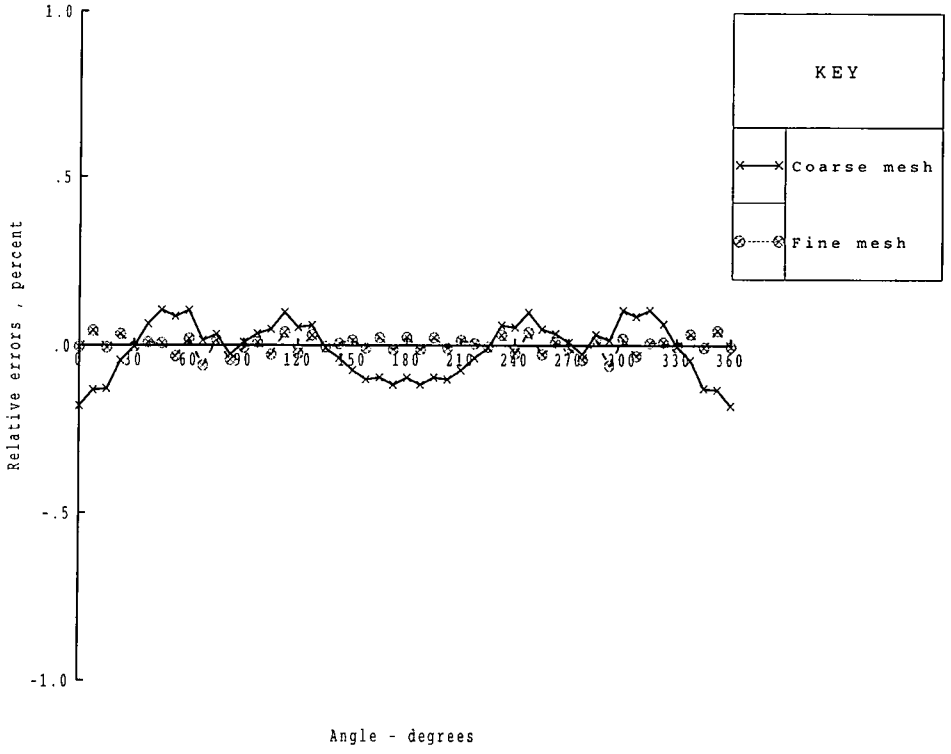

Figure 6.17: Comparison of errors in imaginary part of the solutions on the cylinder produced by coarse and fine meshes ($b/a = 2$, $\theta_I = 0^o$)

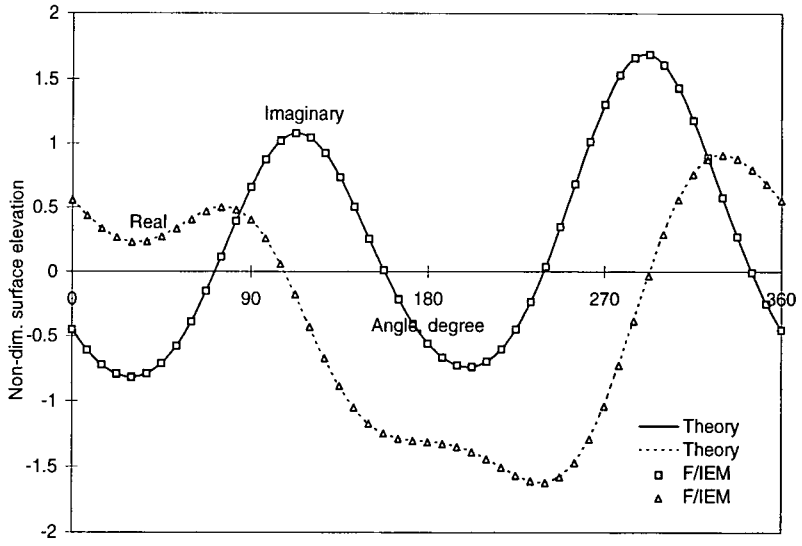

Figure 6.18: Real and imaginary part of surface elevations on elliptical cylinder as a function of angle around the cylinder ($b/a = 2$, $\theta_I = 30^o$)

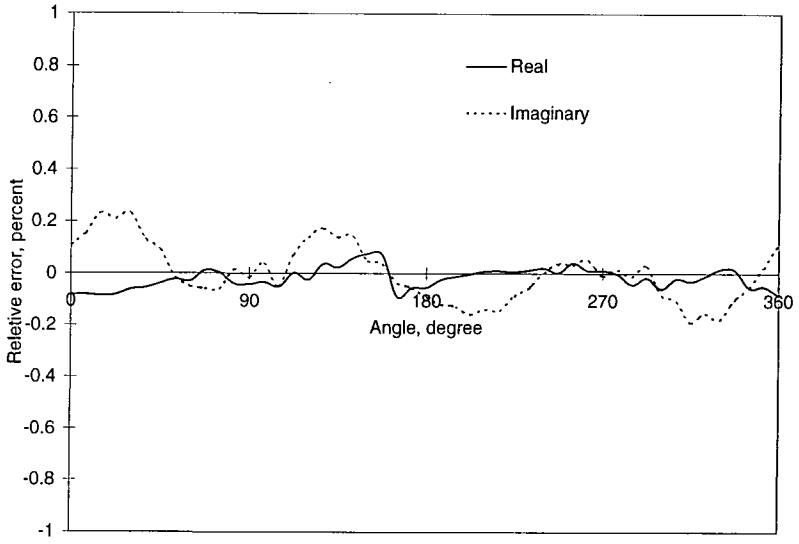

Figure 6.19: Errors in the real and imaginary parts of the solutions on on the cylinder ($b/a = 2$, $\theta_I = 30^o$)

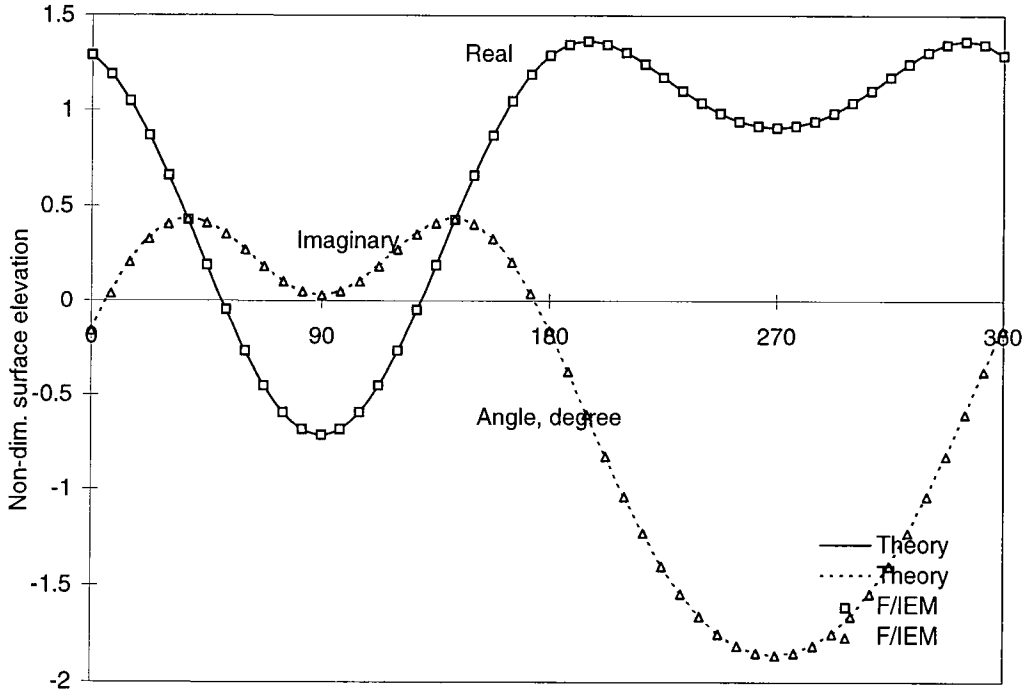

Figure 6.20: Real and imaginary part of surface elevations on elliptical cylinder as a function of angle around the cylinder ($b/a = 2$, $\theta_I = 90^o$)

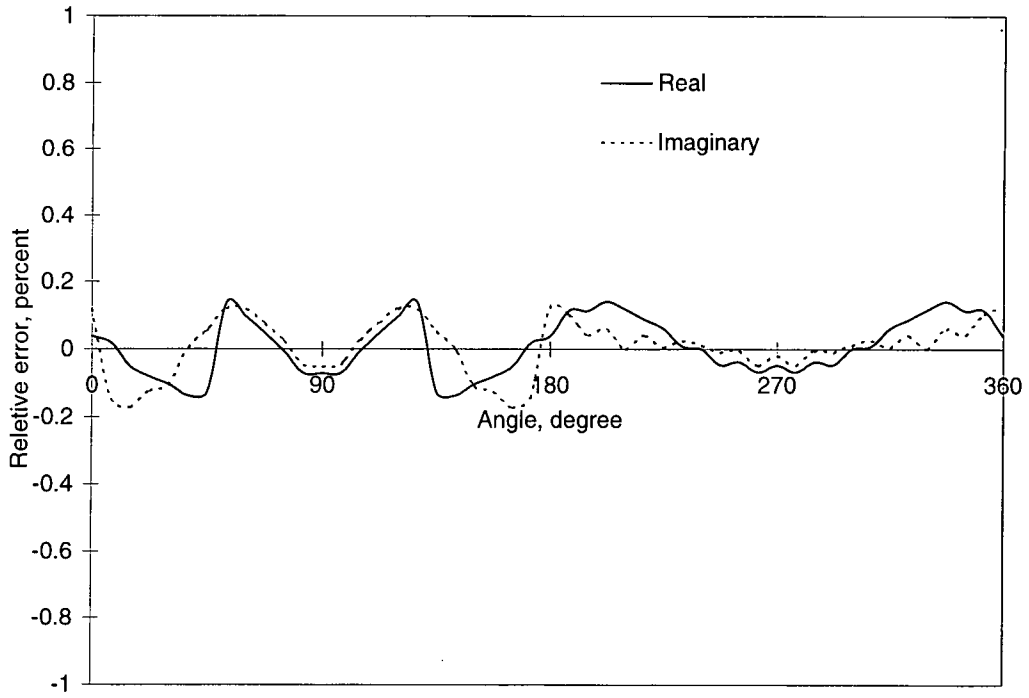

Figure 6.21: Errors in the real and imaginary parts of the solutions on the cylinder ($b/a = 2$, $\theta_I = 90^o$)

6.3 Results for Type 2 infinite element

In this section two problems were solved using Type 2 infinite elements. First the basic problem of wave diffraction by a circular cylinder was solved and the solutions were compared with their analytical equivalents presented in section 3.2. Secondly the problem of wave diffraction by an elliptical cylinder was solved and the solutions were compared with their analytical equivalents presented in section 3.3. For the latter case, the problem was solved for different angles of incidence and different aspect ratios.

6.3.1 Problem of wave diffraction by a circular cylinder

A circular cylinder with radius a standing in open water with a plane surface wave incident upon it was analysed. The parameters for this problem were as follows:

$$d/a=1$$

$$\theta_I = 0^o$$

$$ka=1$$

A coarse mesh of finite and infinite elements is illustrated in Figure 6.22. It consists of one ring of finite elements and one ring of infinite elements (24 elements circumferentially). The infinite elements are located at a half length of the radius away from the object.

Figure 6.23 shows the comparison between the numerical and analytical solutions on the surface of the cylinder for both real and imaginary parts of the free surface elevations. Figure 6.24 shows the relative errors around the cylinder which for the real part are not more than 0.4 percent and for the imaginary part are not

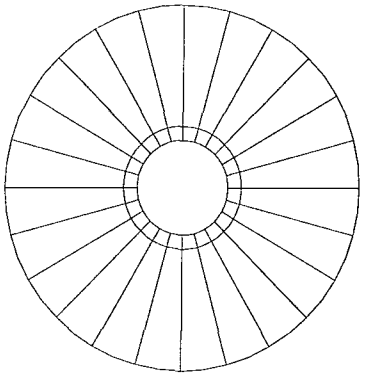

Figure 6.22: A coarse mesh of finite and Type 2 infinite elements for circular cylinder, a=1

more than 0.5 percent. This shows that the model gives very accurate results even for such a coarse mesh.

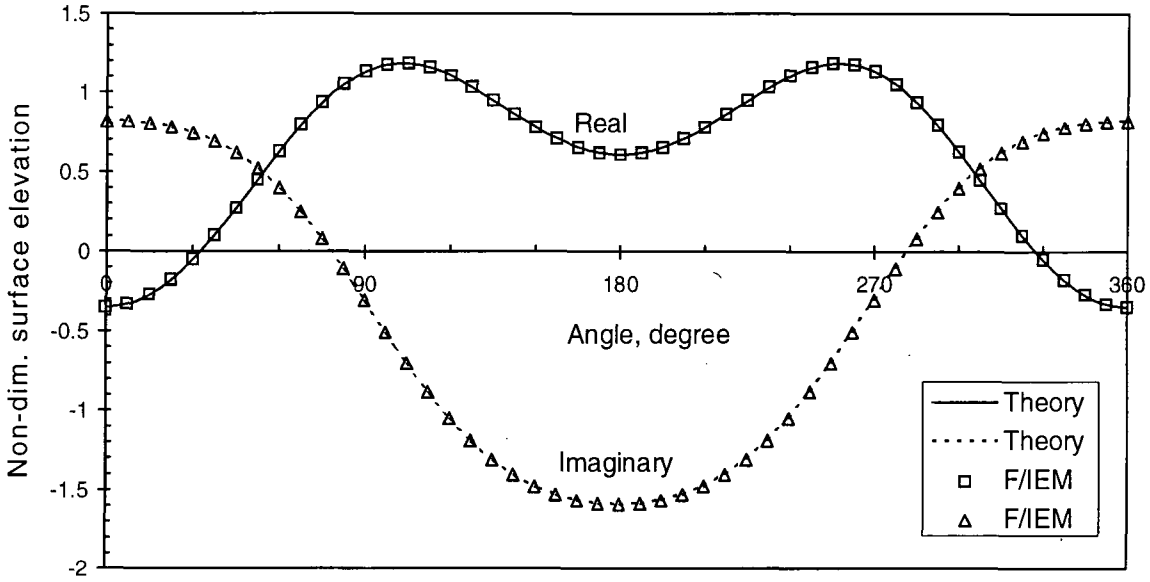

Figure 6.23: Real and imaginary parts of the surface elevations on circular cylinder as a function of angle around the cylinder, a=1

6.3.2 Problem of wave diffraction by elliptical cylinders

An elliptical cylinder standing in open water with a plane surface wave incident upon it was analysed. The parameters for this problem were as follows:

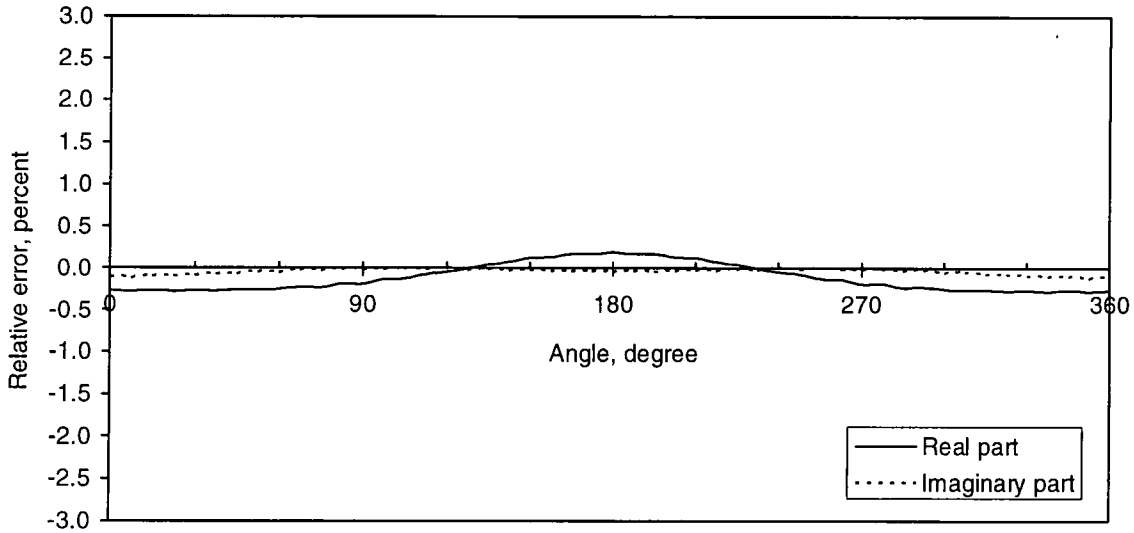

Figure 6.24: Errors in the real and imaginary parts of the solutions around the cylinder, a=1

b/a=2

d/a=1

$\theta_I = 0^o$

ka=1

A coarse mesh of finite and infinite elements is illustrated in Figure 6.25 which again consists of only one ring of finite and one ring of infinite elements (24 elements circumferentialy). The real and imaginary parts of the numerical solutions are compared to their analytical equivalents in Figure 6.26. The relative errors for real and imaginary components are plotted in Figure 6.27. As can be seen the errors are not greater than 2.2 percent for the real part and not more than 1.3 percent for the imaginary part. A revised mesh was constructed with the infinite elements being located reasonably far from the diffracting object (i.e. at a distance close to the half length of the semi-major axis of the ellipse) to achieve more accurate results. The finer mesh of finite and infinite elements (three rings of finite and one ring of infinite elements) is illustrated in Figure 6.28. The relative errors for

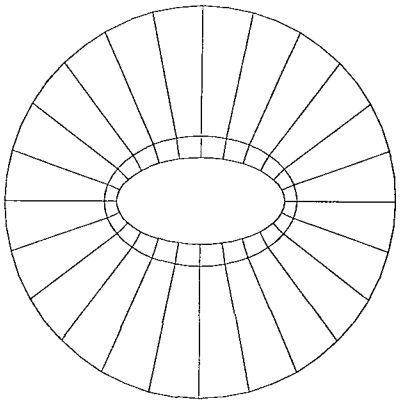

Figure 6.25: A coarse mesh of finite and Type 2 infinite elements for elliptical cylinder, b/a=2

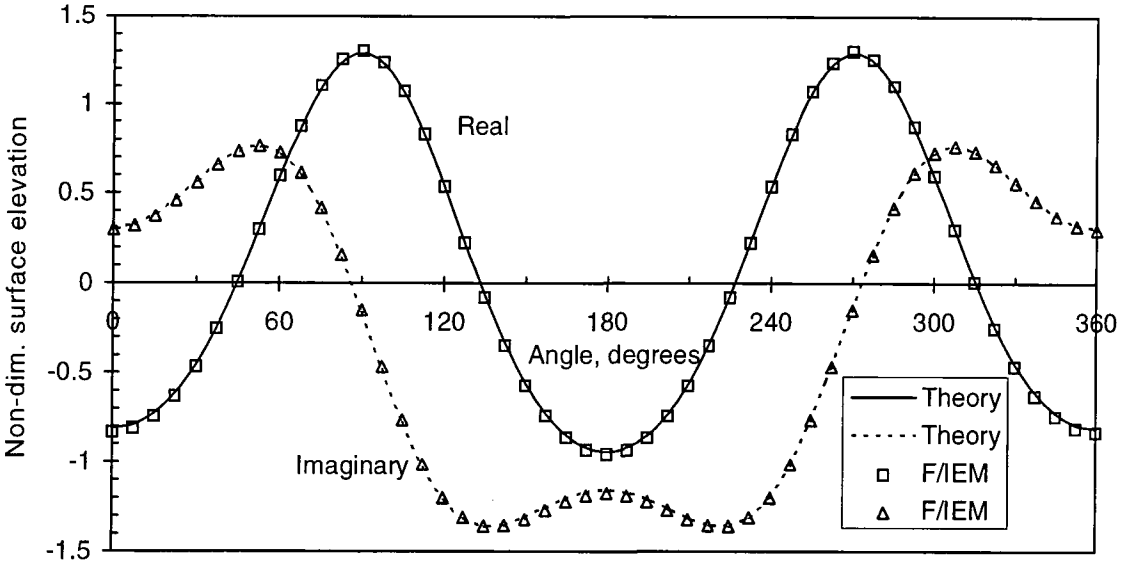

Figure 6.26: Real and imaginary parts of the surface elevations on elliptical cylinder as a function of angle around the cylinder ($b/a = 2$, $\theta_I = 0^o$)

the real and imaginary parts are shown in Figure 6.29 which shows that the errors decrease and are now not more than 0.25 percent.

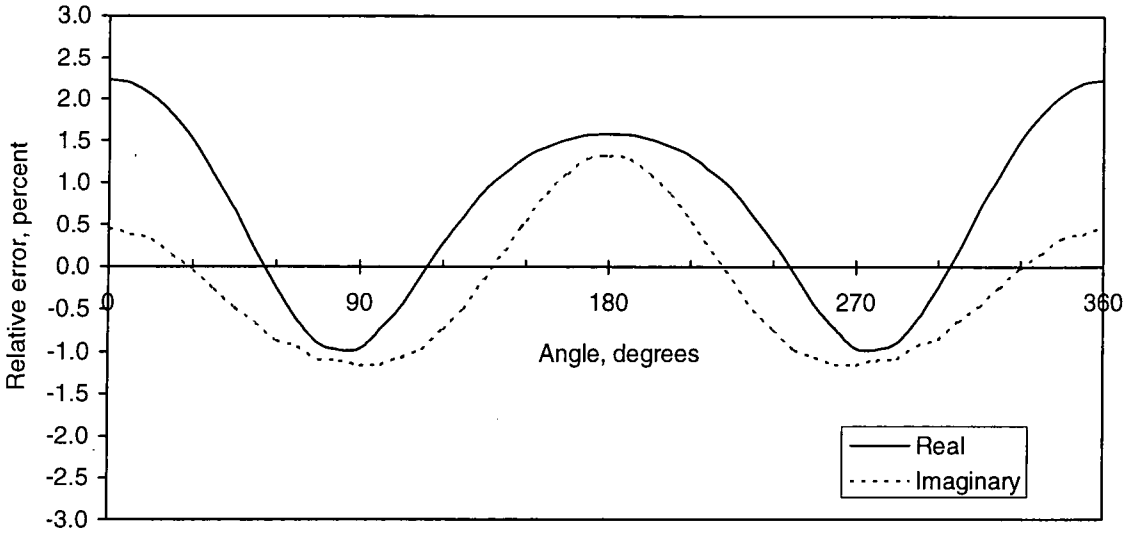

Figure 6.27: Errors in the real and imaginary parts of the solutions on the waterline nodes ($b/a = 2$, $\theta_I = 0^o$)

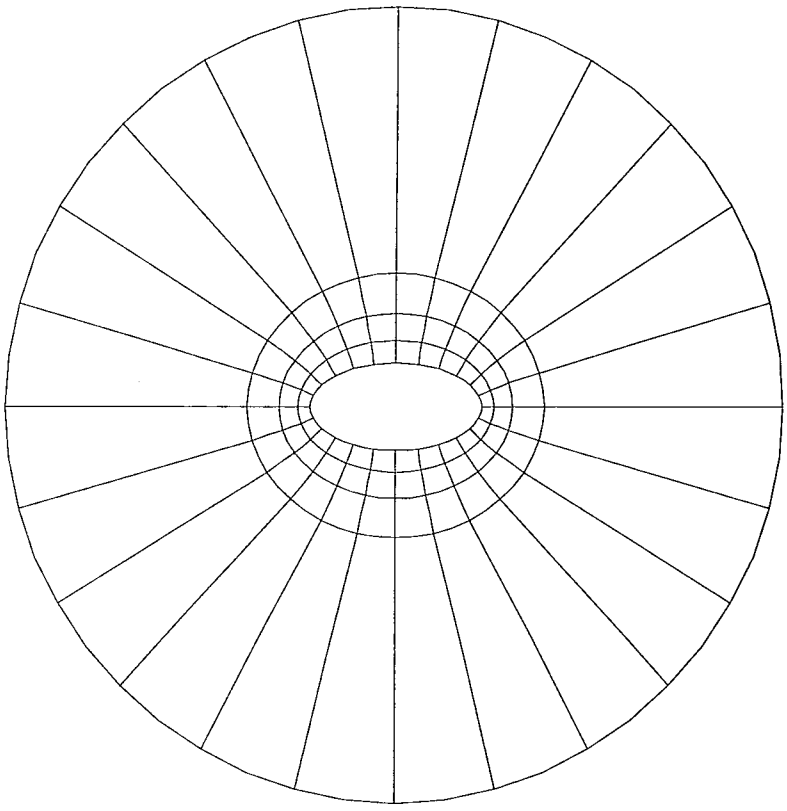

Figure 6.28: A fine mesh of finite and Type 2 infinite elements for elliptical cylinder, b/a=2

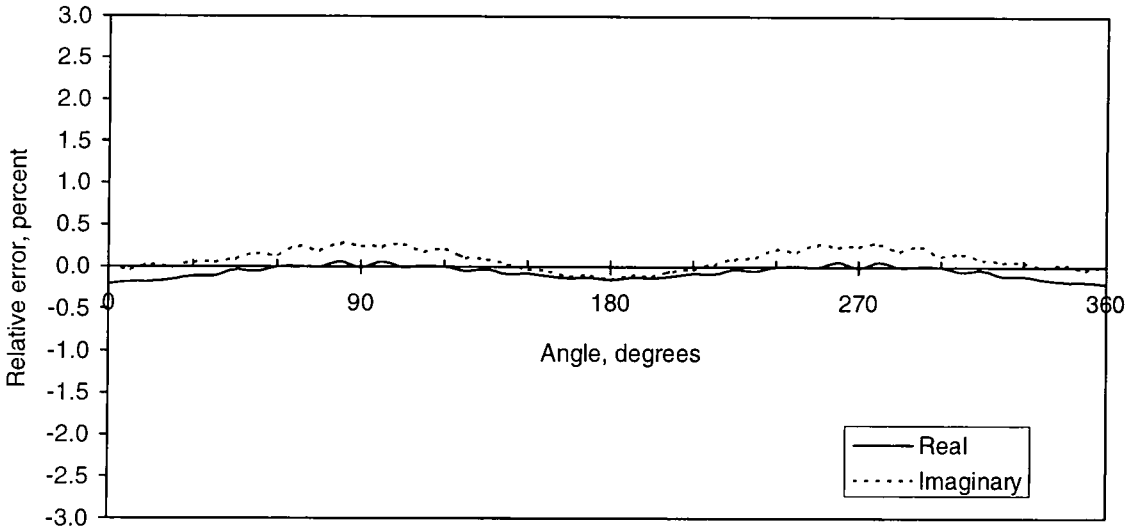

Figure 6.29: Errors in the real and imaginary parts of the solutions on the cylinder ($b/a = 2$, $\theta_I = 0^o$)

Next the infinite element was tested for different cases of elliptical cylinder diffraction problem. The above problem was solved with the new following parameters:

b/a=3

d/a=1

$\theta_I = 0^o, 30^o, 45^o$ and 90^o

ka=1

A mesh of finite and infinite elements is illustrated in Figure 6.30. The real and imaginary parts of the numerical solutions are compared to their analytical equivalent in Figure 6.31. The relative errors for real and imaginary parts are plotted in Figure 6.32. As can be seen the errors are slightly greater than before (however not greater than 0.7 percent). Since the aspect ratio of the ellipse increased from 2 to 3, the number of elements used in the circumferential direction (24) needs to be increased to maintain the same accuracy. A contour plot of the free surface elevations around the cylinder is shown in Figures 6.33 and 6.34 for real and imaginary parts

respectively. An example of a three-dimensional view of the free surface elevations is also shown in Figures 6.35 and 6.36 for real and imaginary parts respectively.

The same analysis was repeated for angles of incidence of 30, 45, and 90 degrees and results are shown in Figure 6.37 to 6.48. Figures 6.32, 6.38, 6.42 and 6.46 demonstrate that the accuracy of the method remains almost the same for the different angles of incidence.

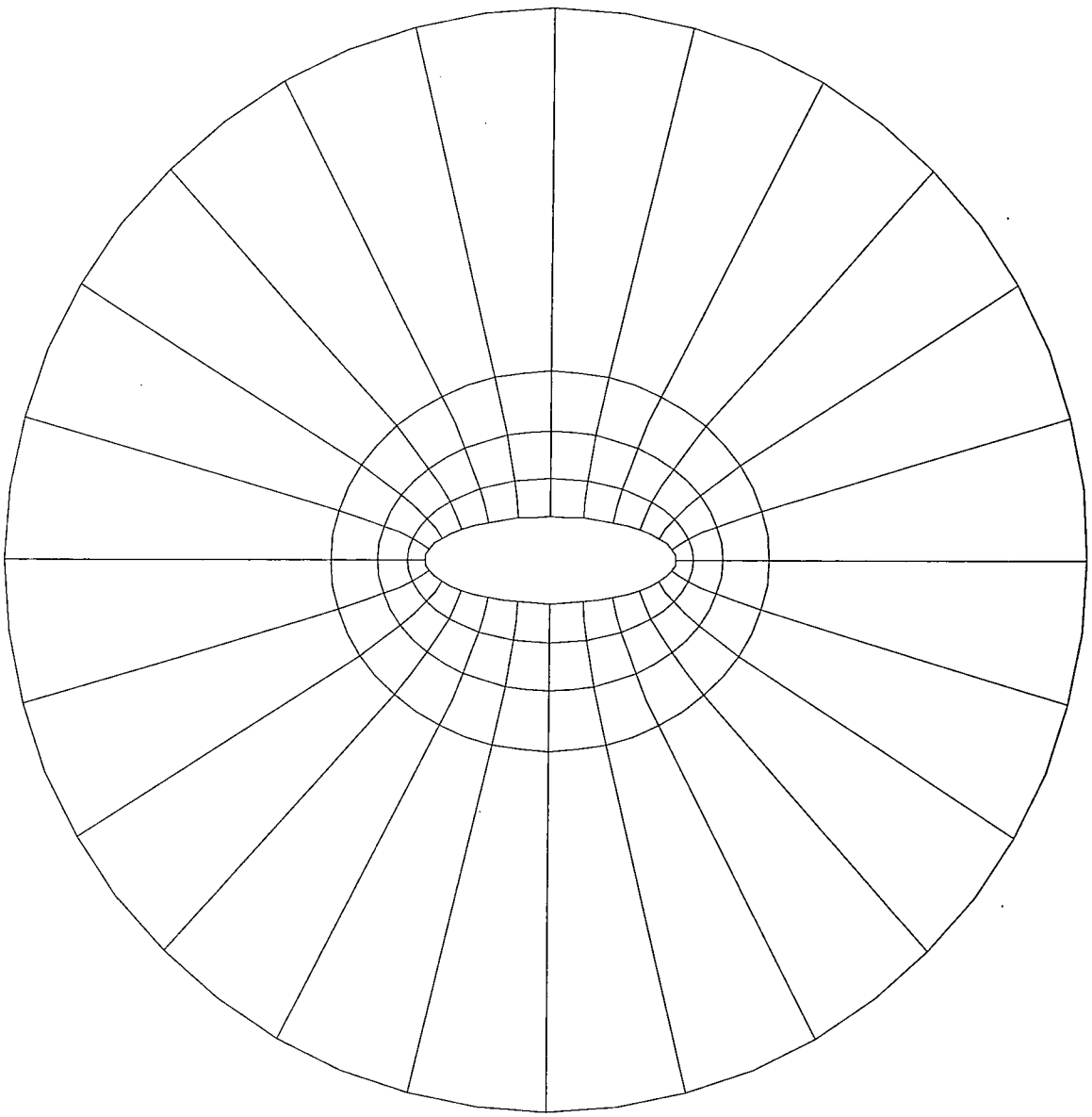

Figure 6.30: Mesh of finite and Type 2 infinite elements for elliptical cylinder (b/a=3)

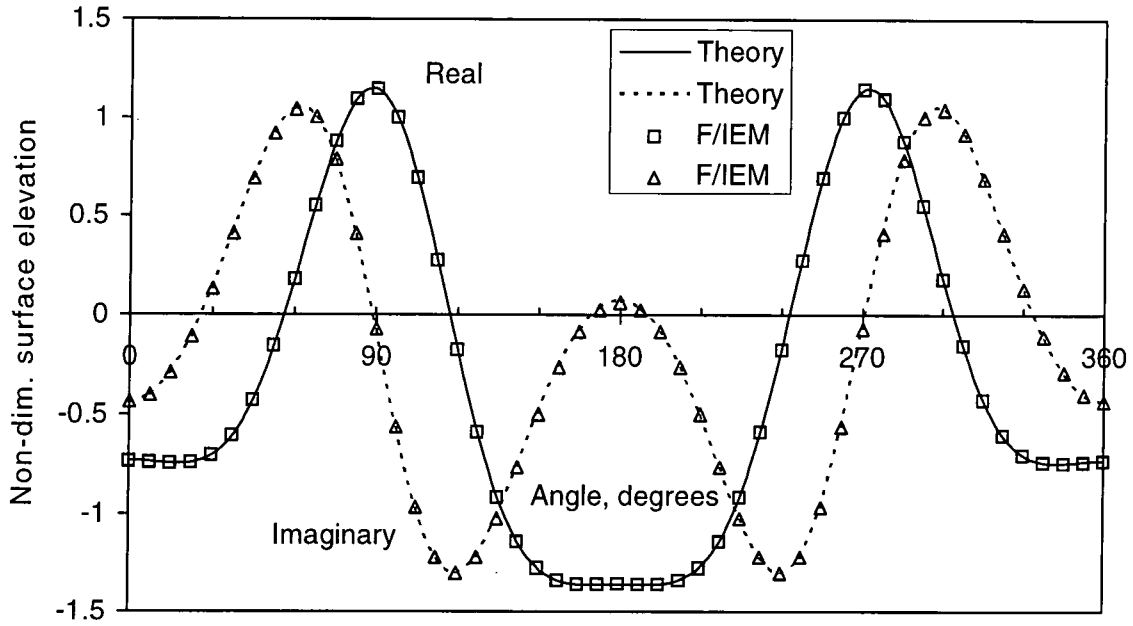

Figure 6.31: Real and imaginary parts of the surface elevations on elliptical cylinder as a function of angle around the cylinder ($b/a = 3$, $\theta_I = 0^o$)

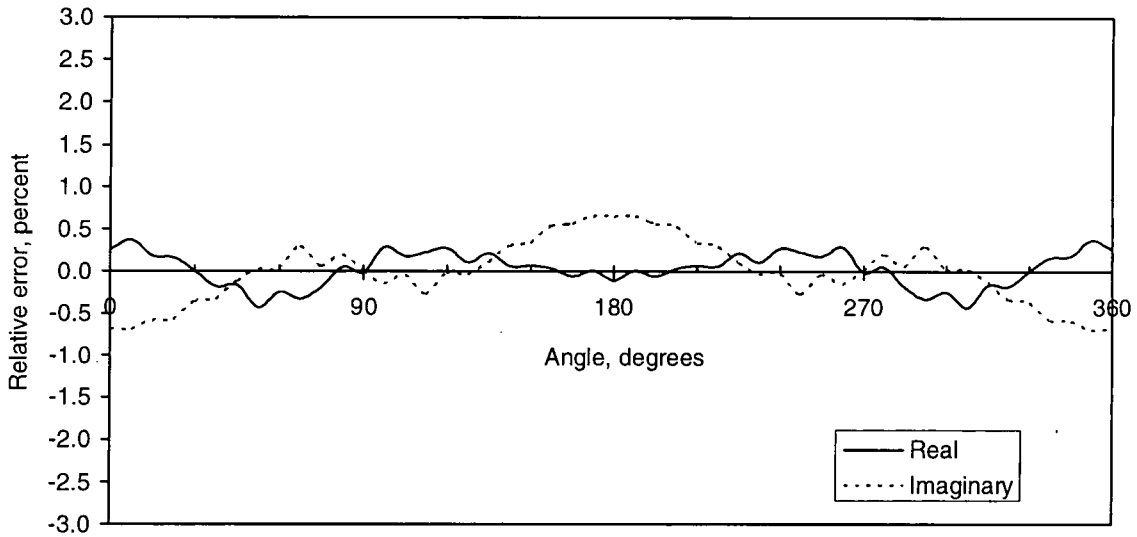

Figure 6.32: Errors in the real and imaginary parts of the solutions on the waterline nodes ($b/a = 3$, $\theta_I = 0^o$)

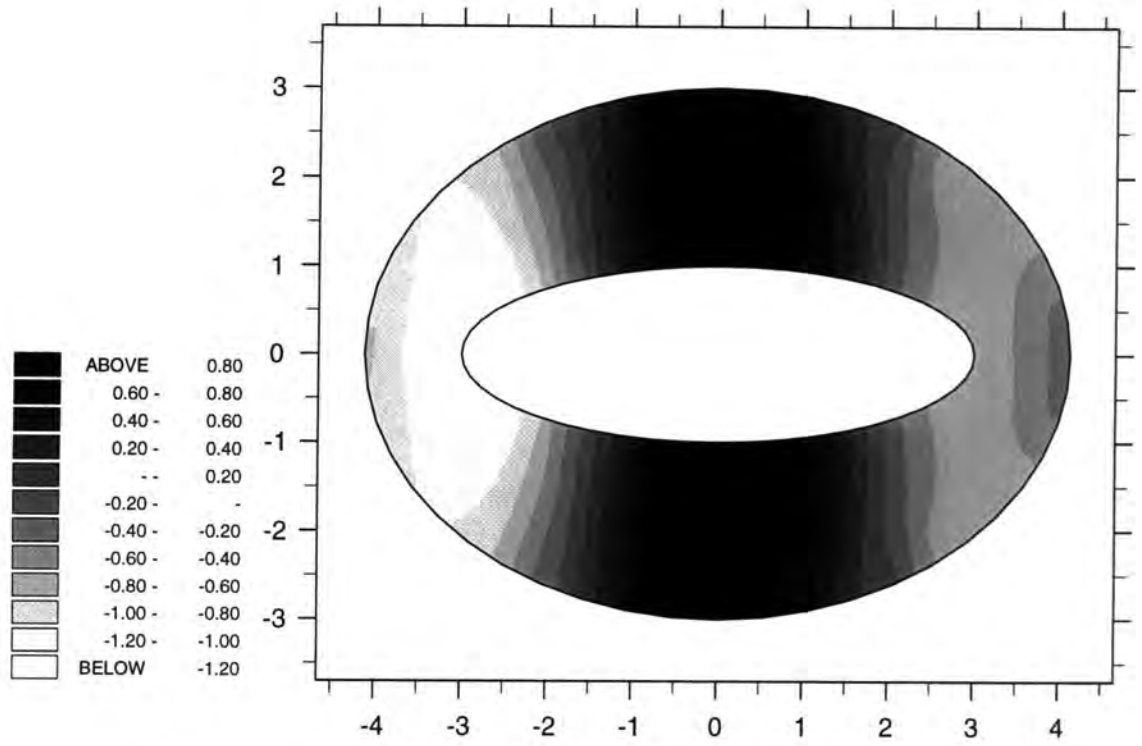

Figure 6.33: A contour plot of the non-dim. free-surface elevation around the cylinder, real part ($b/a = 3$, $\theta_I = 0^o$)

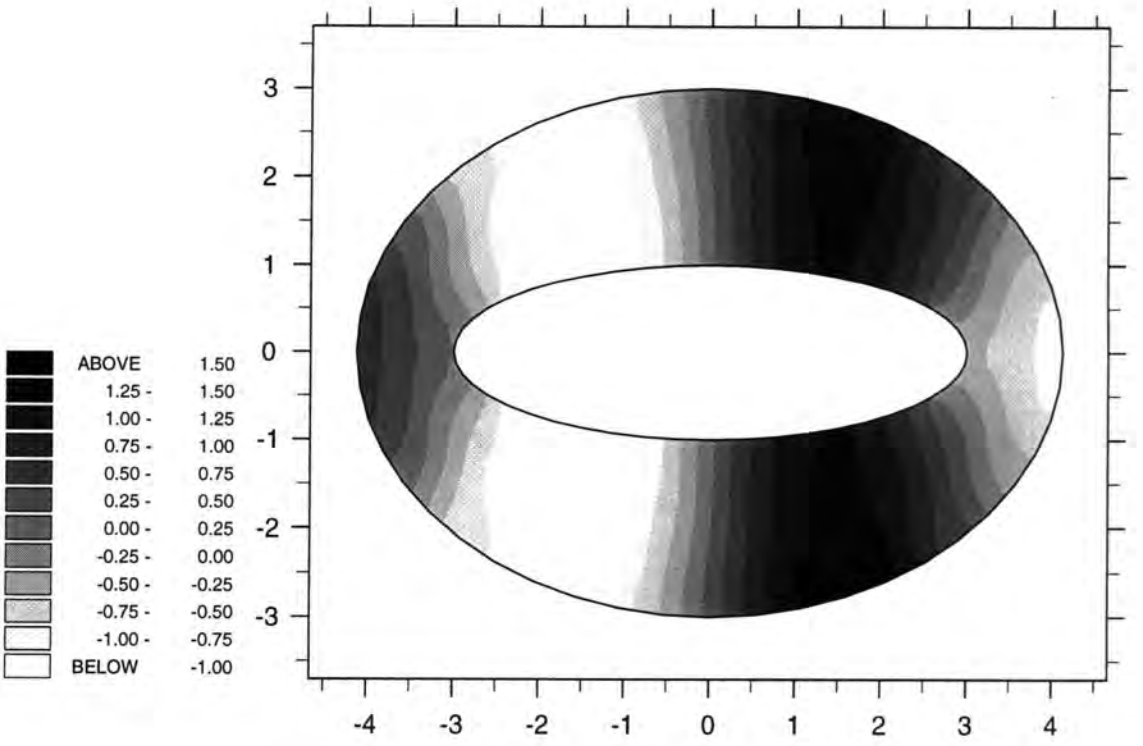

Figure 6.34: A contour plot of the non-dim. free-surface elevation around the cylinder, imaginary part ($b/a = 3$, $\theta_I = 0^o$)

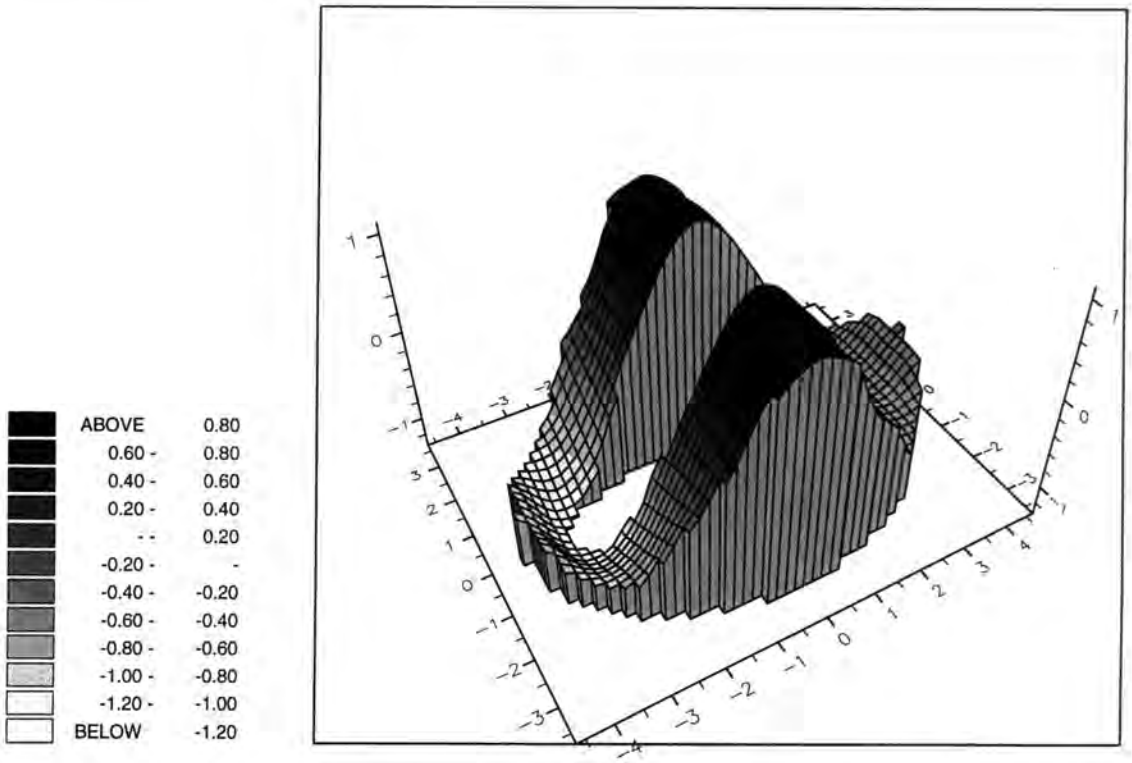

Figure 6.35: A three dimensional perspective view of the non-dim. free-surface elevation, real part ($b/a = 3$, $\theta_I = 0^o$)

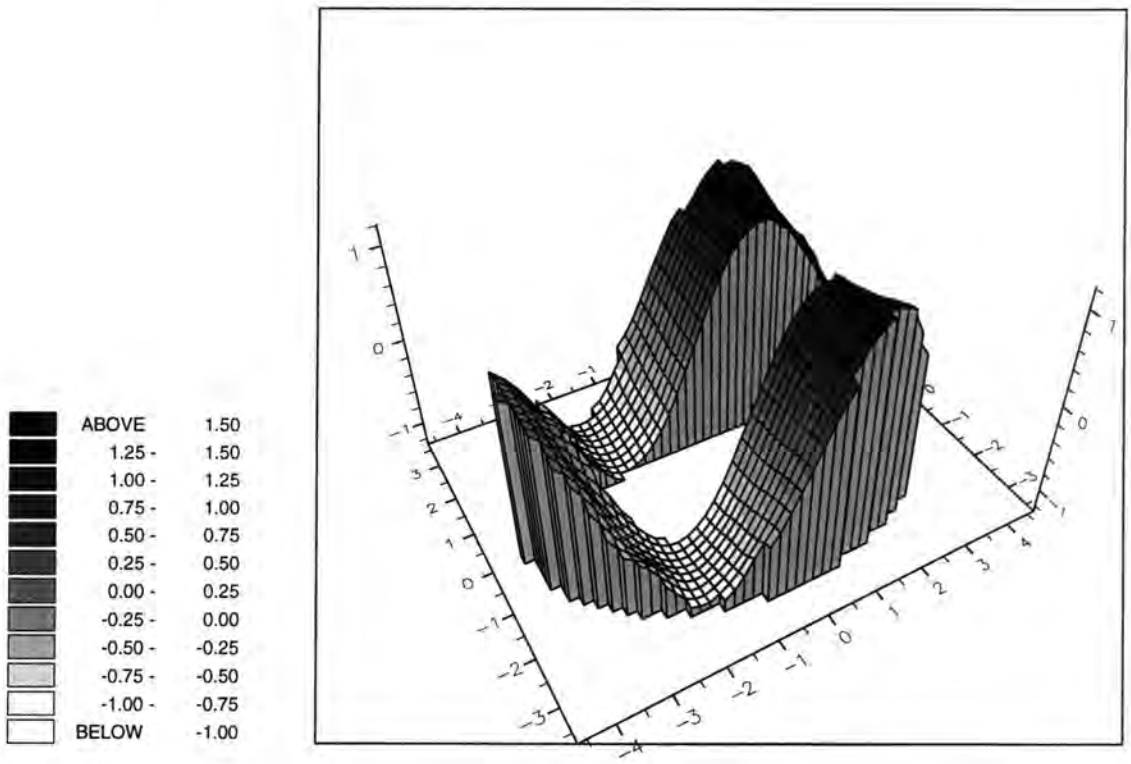

Figure 6.36: A three dimensional perspective view of the non-dim. free-surface elevation, imaginary part ($b/a = 3$, $\theta_I = 0^o$)

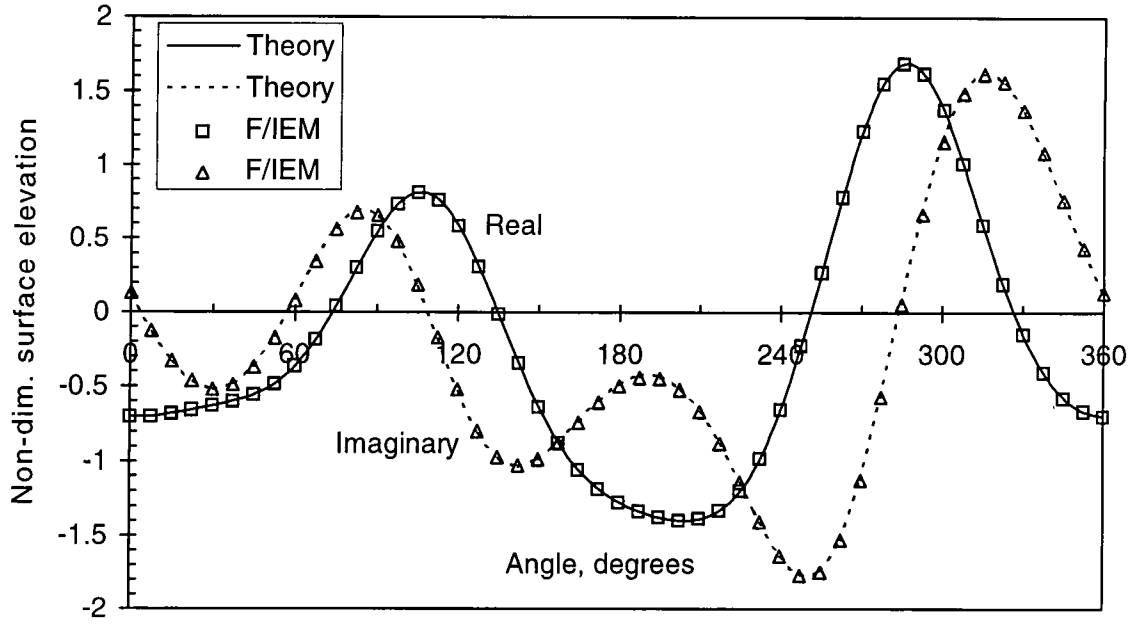

Figure 6.37: Real and imaginary parts of the surface elevations on elliptical cylinder as a function of angle around the cylinder ($b/a = 3$, $\theta_I = 30^o$)

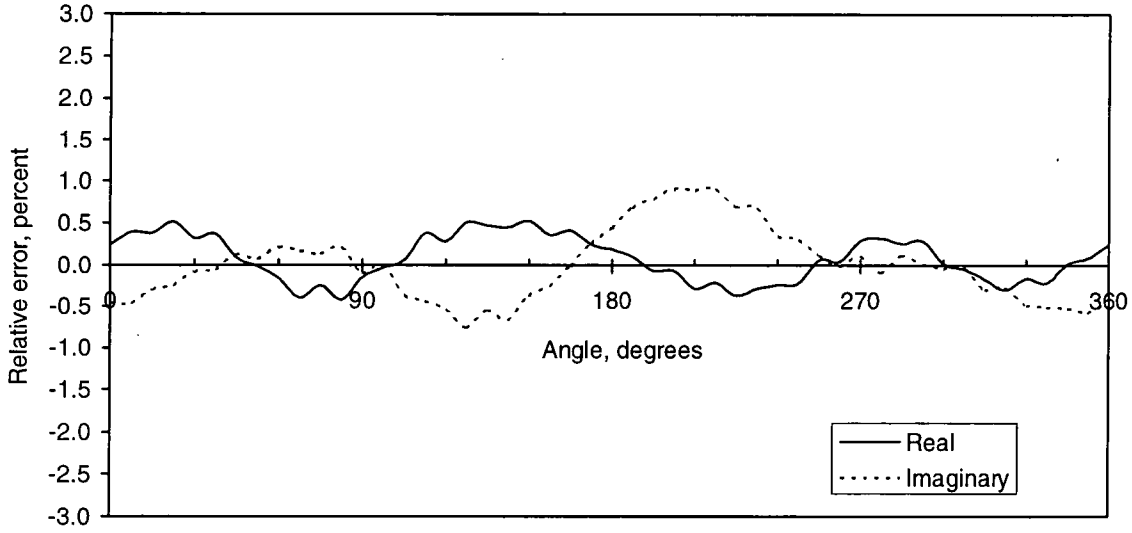

Figure 6.38: Errors in the real and imaginary parts of the solutions on the cylinder ($b/a = 3$, $\theta_I = 30^o$)

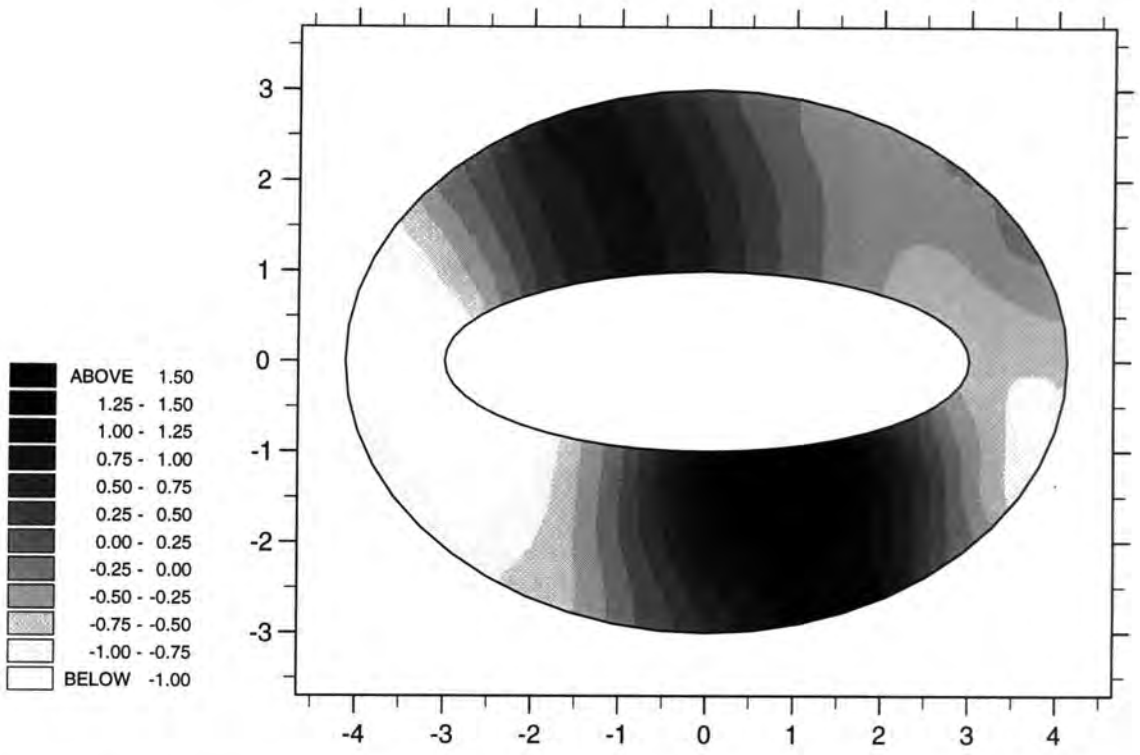

Figure 6.39: A contour plot of the non-dim. free-surface elevation around the cylinder, real part ($b/a = 3$, $\theta_I = 30^o$)

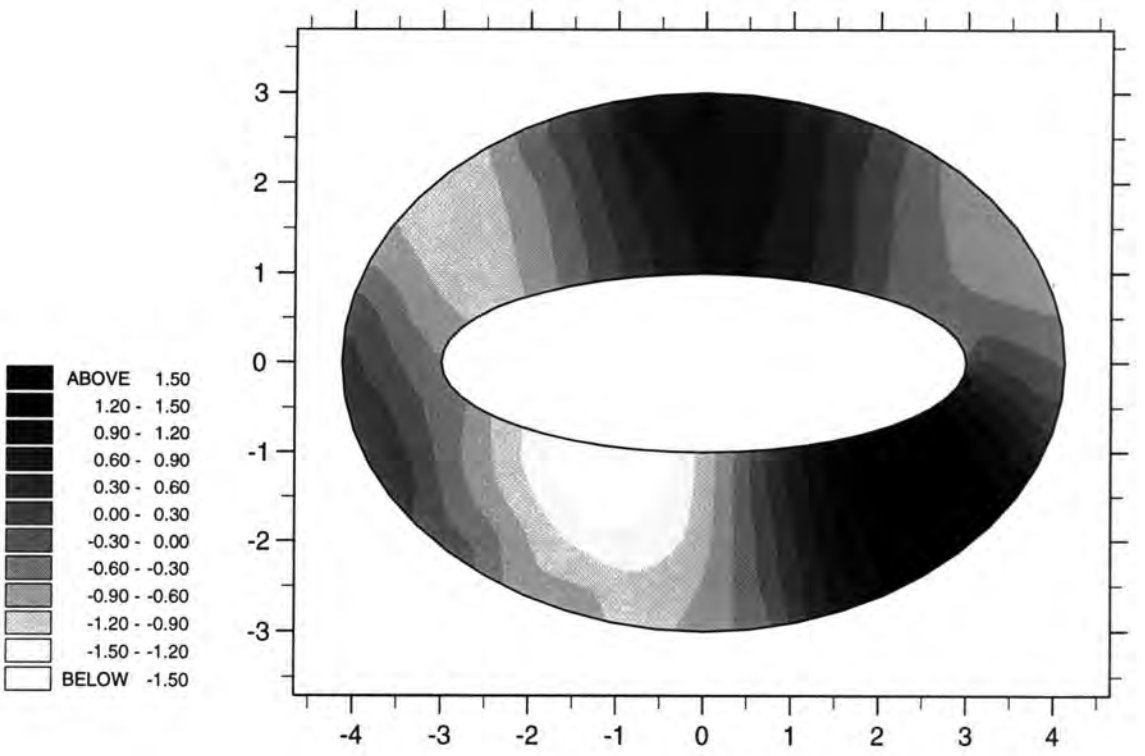

Figure 6.40: A contour plot of the non-dim. free-surface elevation around the cylinder, imaginary part ($b/a = 3$, $\theta_I = 30^O$)

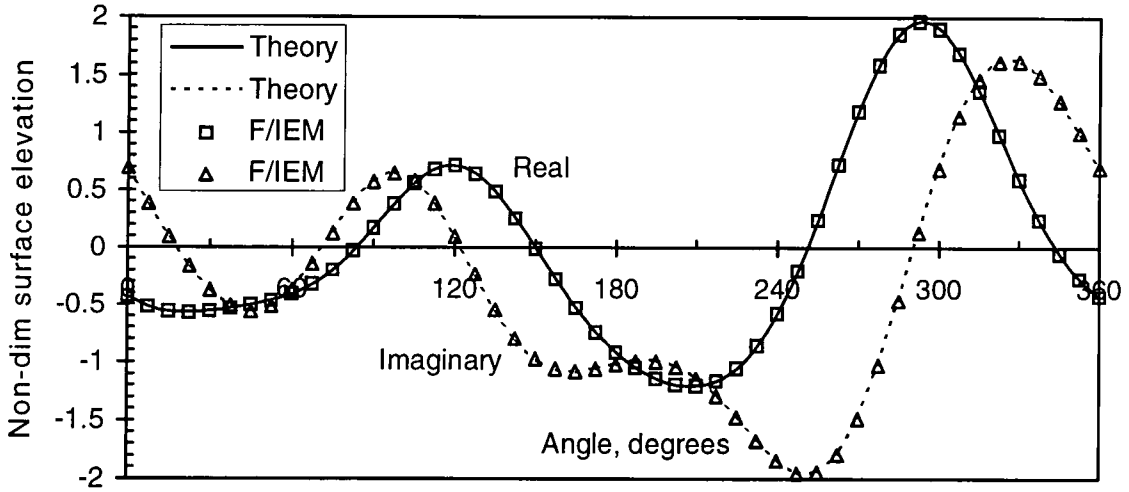

Figure 6.41: Real and imaginary parts of the surface elevations on elliptical cylinder as a function of angle around the cylinder ($b/a = 3$, $\theta_I = 45^o$)

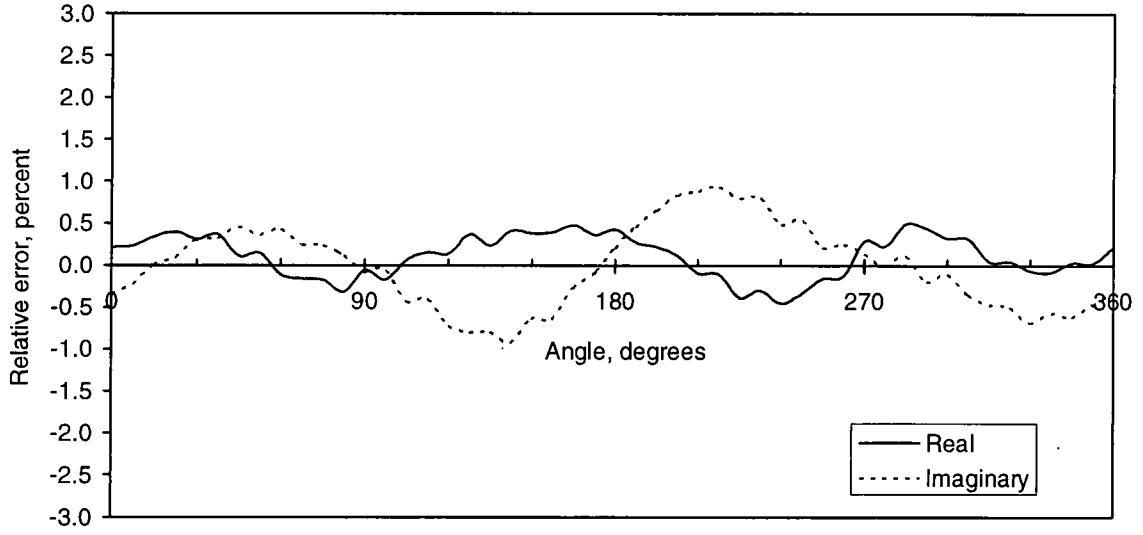

Figure 6.42: Errors in the real and imaginary parts of the solutions on the cylinder ($b/a = 3$, $\theta_I = 45^o$)

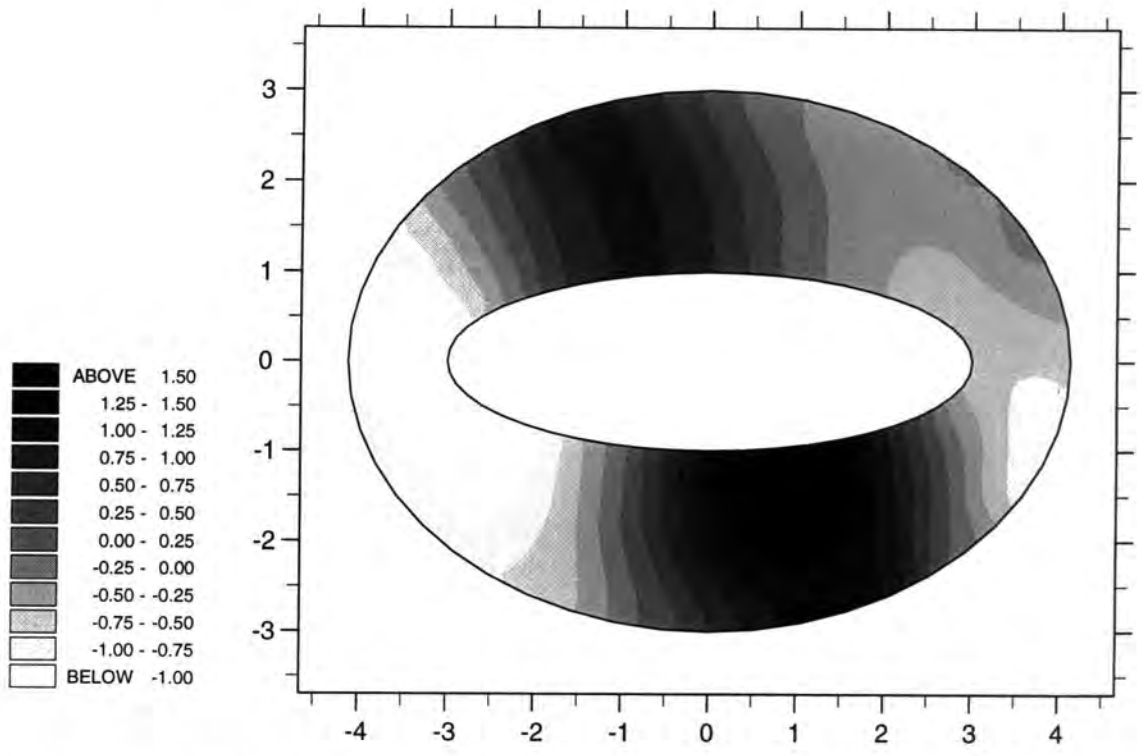

Figure 6.43: A contour plot of the non-dim. free-surface elevation around the cylinder, real part ($b/a = 3$, $\theta_I = 45^o$)

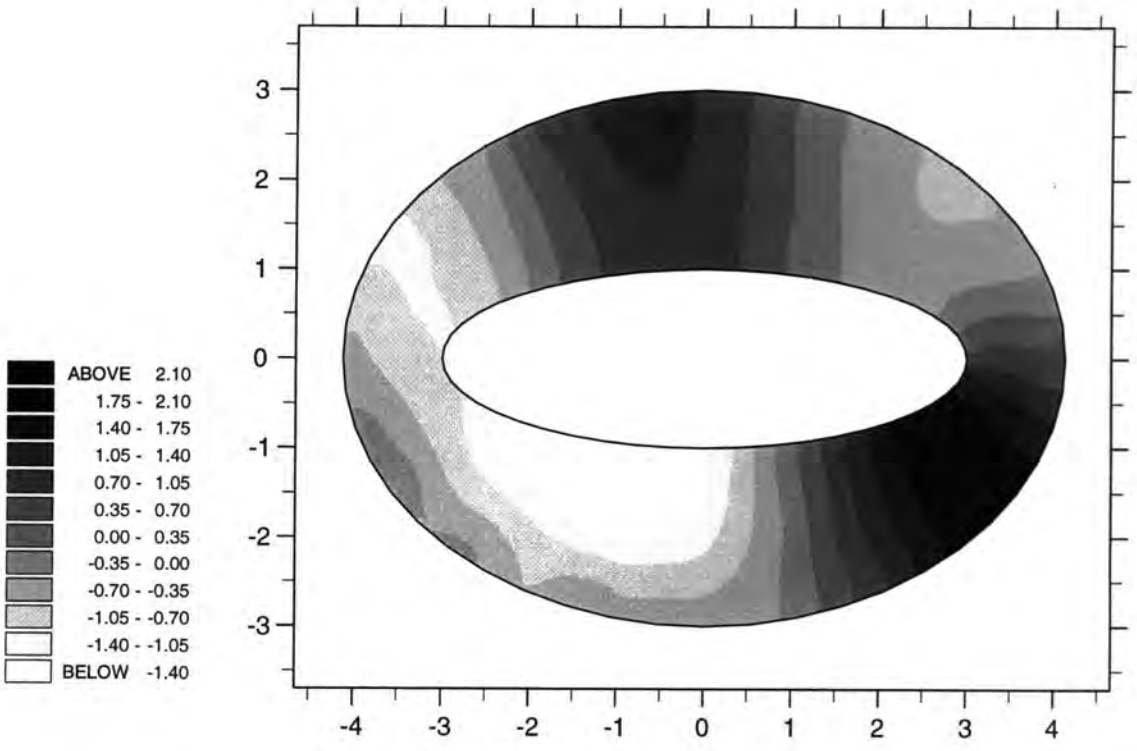

Figure 6.44: A contour plot of the non-dim. free-surface elevation around the cylinder, imaginary part ($b/a = 3$, $\theta_I = 45^o$)

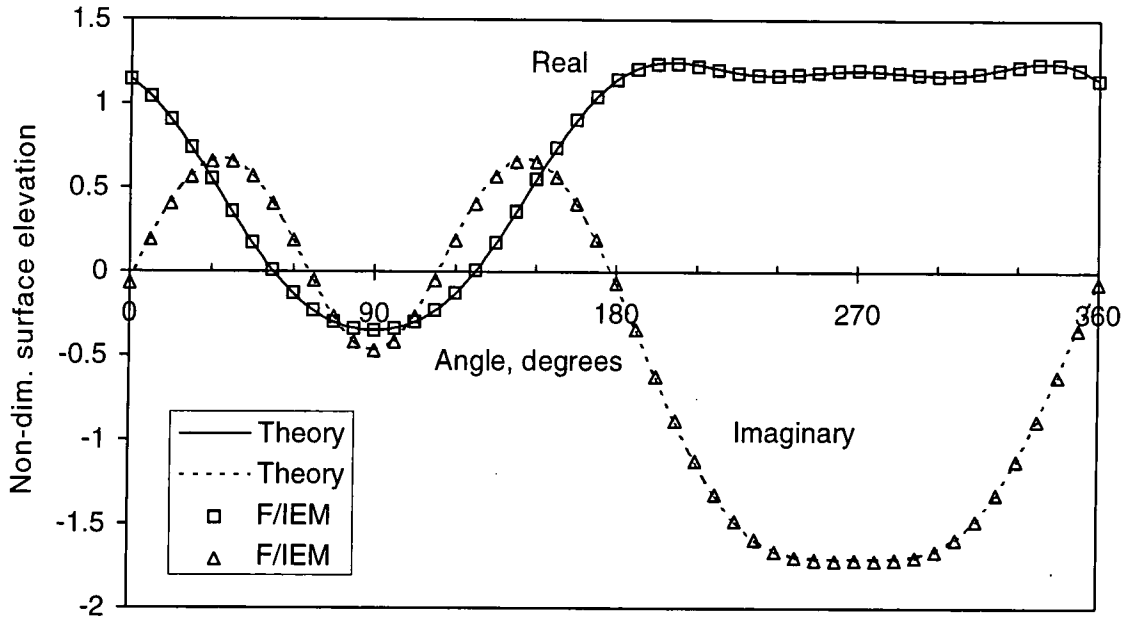

Figure 6.45: Real and imaginary parts of the surface elevations on elliptical cylinder as a function of angle around the cylinder ($b/a = 3$, $\theta_I = 90^o$)

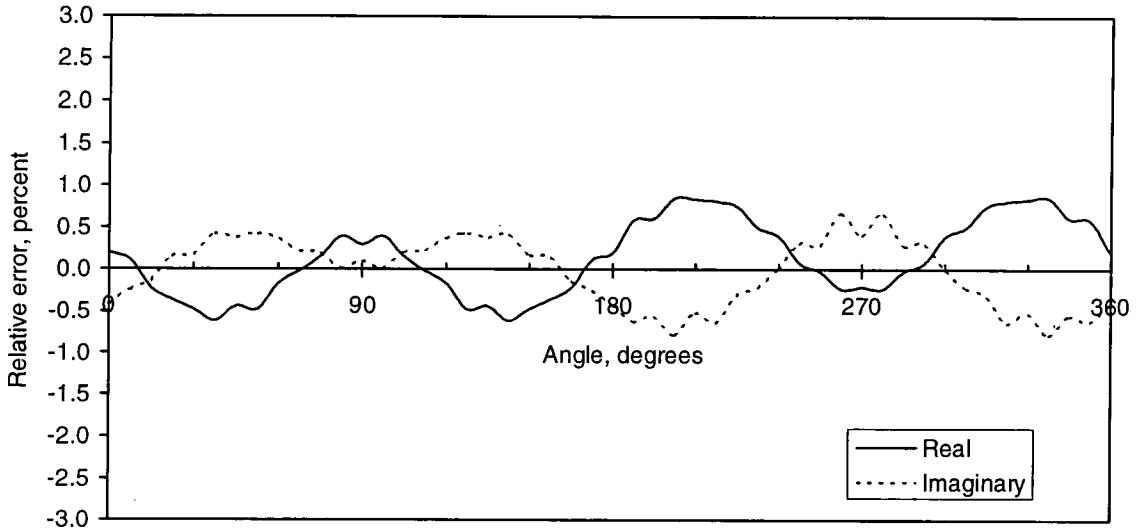

Figure 6.46: Errors in the real and imaginary parts of the solutions on the cylinder ($b/a = 3$, $\theta_I = 90^o$)

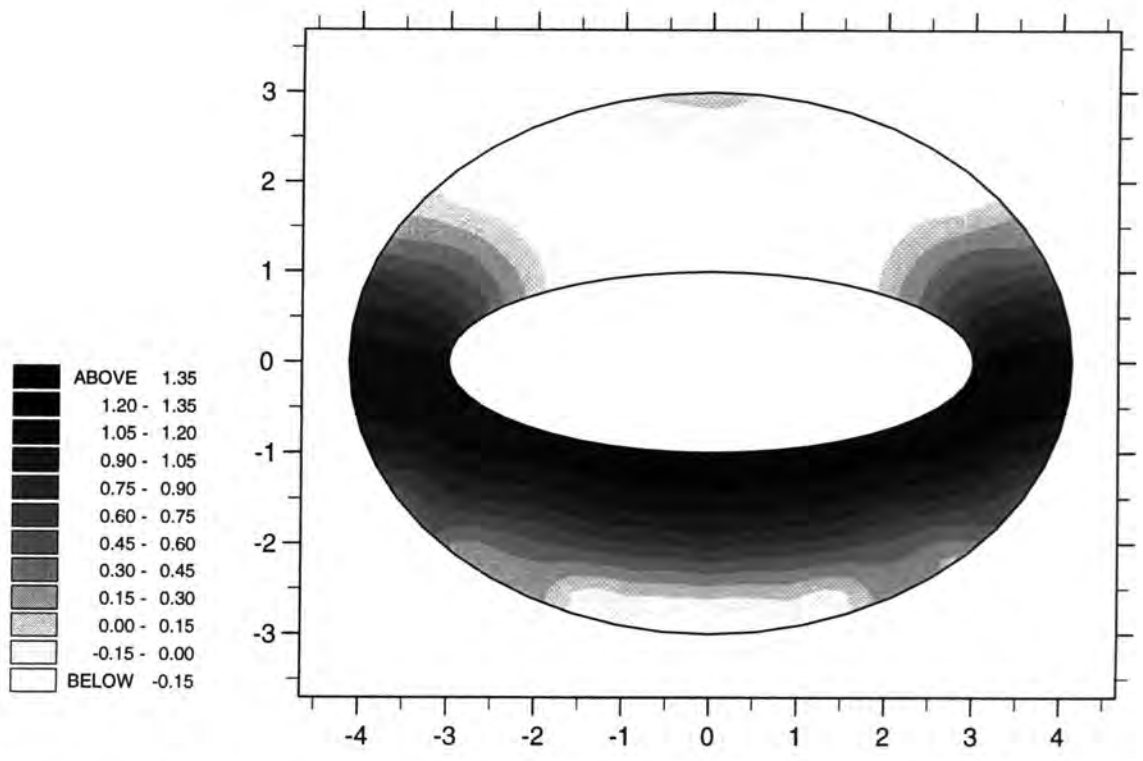

Figure 6.47: A contour plot of the non-dim. free-surface elevation around the cylinder, real part ($b/a = 3$, $\theta_I = 90^o$)

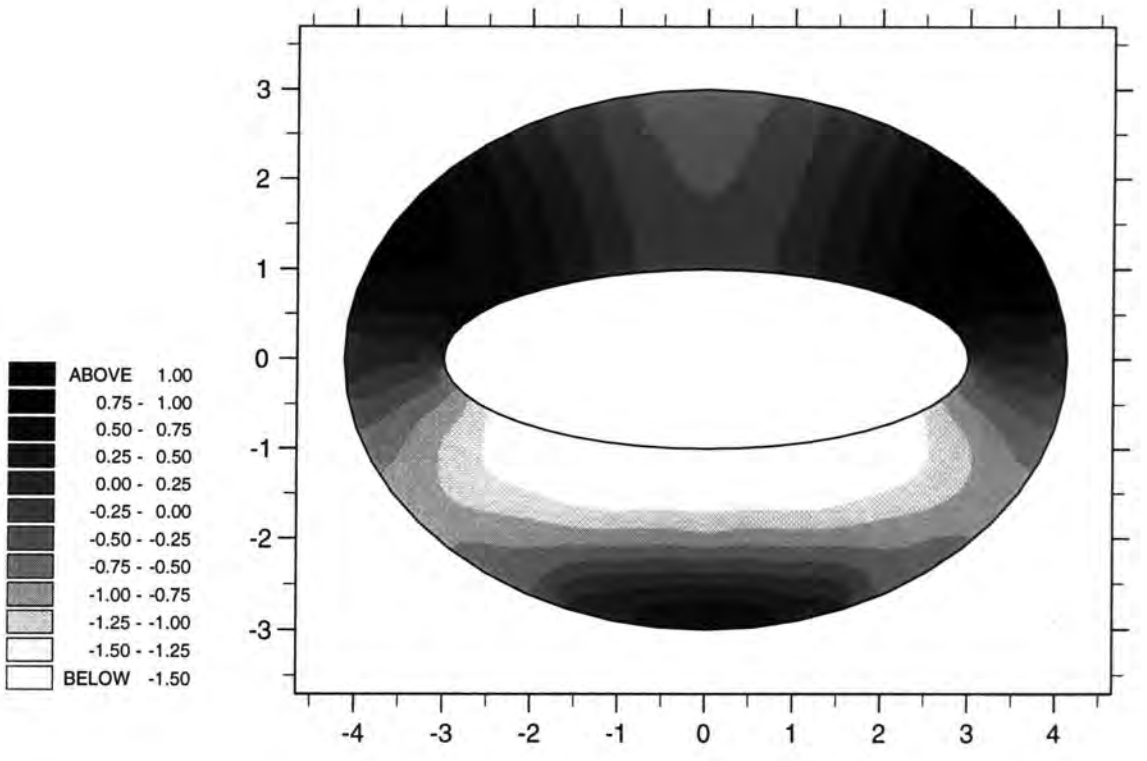

Figure 6.48: A contour plot of the non-dim. free-surface elevation around the cylinder, imaginary part ($b/a = 3$, $\theta_I = 90^o$)

6.4 Results for type 3 infinite element

In this section three test problems were solved using Type 3 infinite elements. First the basic problem of wave diffraction by a circular cylinder and then by an elliptical cylinder were solved and the solutions were compared with their equivalent analytical solutions presented in sections 3.2 and 3.3. Finally the problems of wave diffraction by arrays of circular cylinders were solved and the solutions were compared with their equivalent analytical solutions presented in section 3.4.

6.4.1 Problem of wave diffraction by a circular cylinder

A circular cylinder with radius a standing in open water with a plane surface wave incident upon it was analysed. The parameters for this problem were as follows:

$$d/a=1$$

$$\theta_I = 0^o$$

$$ka=1$$

A coarse mesh of finite and infinite elements is illustrated in Figure 6.49. It consists of one ring of finite elements and one ring of infinite elements (24 elements circumferentially). Figure 6.50 shows the comparison between the numerical and

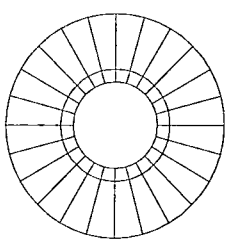

Figure 6.49: Mesh of finite and Type 3 infinite elements for circular cylinder, a=1

analytical solutions on the surface of the cylinder for both real and imaginary parts

of the free surface elevations. Figure 6.51 shows the relative errors around the cylinder which for the real part are not more than 0.4 percent and for the imaginary part are not more than 0.8 percent.

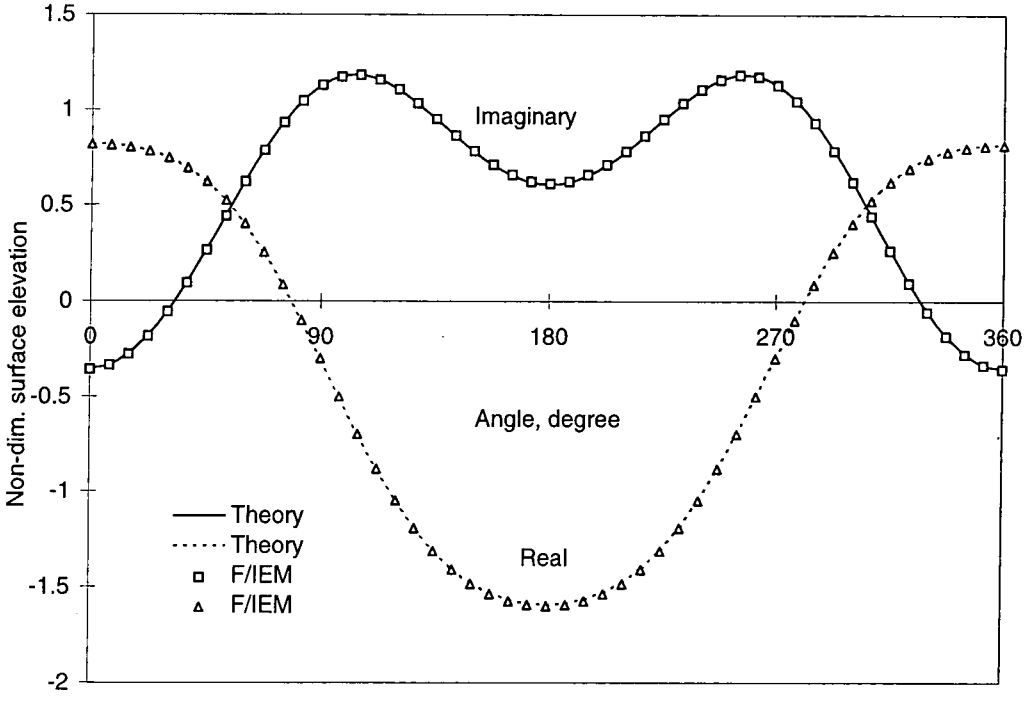

Figure 6.50: Real and imaginary parts of the surface elevations on circular cylinder as a function of angle around the cylinder, a=1

6.4.2 Problem of wave diffraction by elliptical cylinders

An elliptical cylinder standing in open water with a plane surface wave incident upon it was analysed. The parameters for this problem were as follows:

$$b/a=2$$

$$d/a=1$$

$$\theta_I = 0^o$$

$$ka=1$$

A coarse mesh of finite and infinite elements is illustrated in Figure 6.52 which

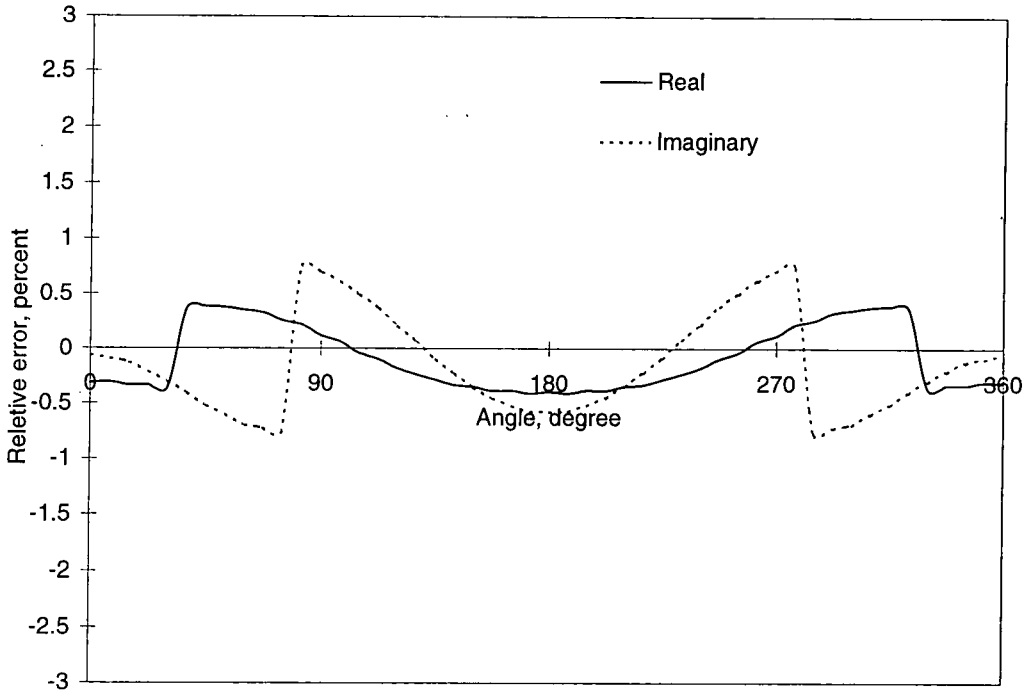

Figure 6.51: Errors in the real and imaginary parts of the solutions on the cylinder, a=1

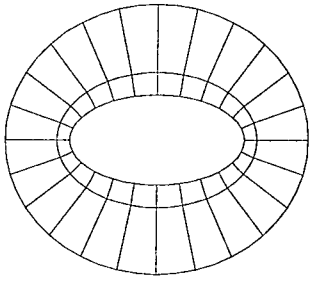

Figure 6.52: A coarse mesh of finite and Type 3 infinite elements for elliptical cylinder, b/a=2

again consists of only one ring of finite and one ring of infinite elements (24 elements circumferentially). The real and imaginary parts of the numerical solutions are compared to their analytical equivalents in Figure 6.53. The relative errors for real and imaginary components are plotted in Figure 6.54. As can be seen the errors are not greater than 2.6 percent for the real part and not more than 1.8 percent for the imaginary part. The infinite elements were next located reasonably far from the diffracting object (i.e. at a distance close to the half length of the

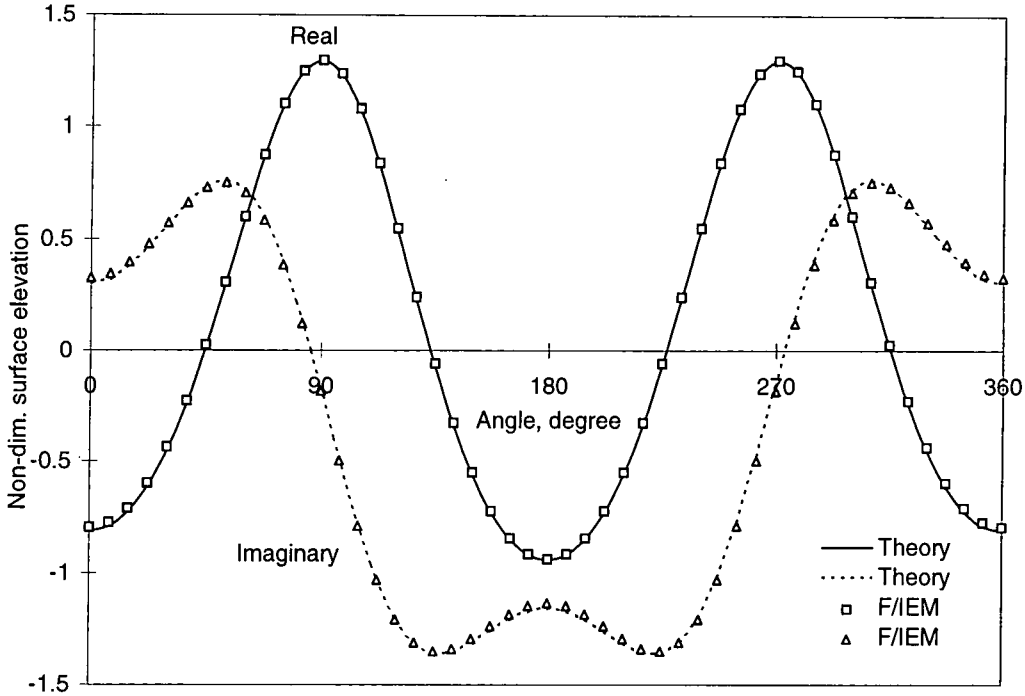

Figure 6.53: Real and imaginary part of surface elevations on elliptical cylinder as a function of angle around the cylinder (b/a=2, $\theta_I = 0^o$)

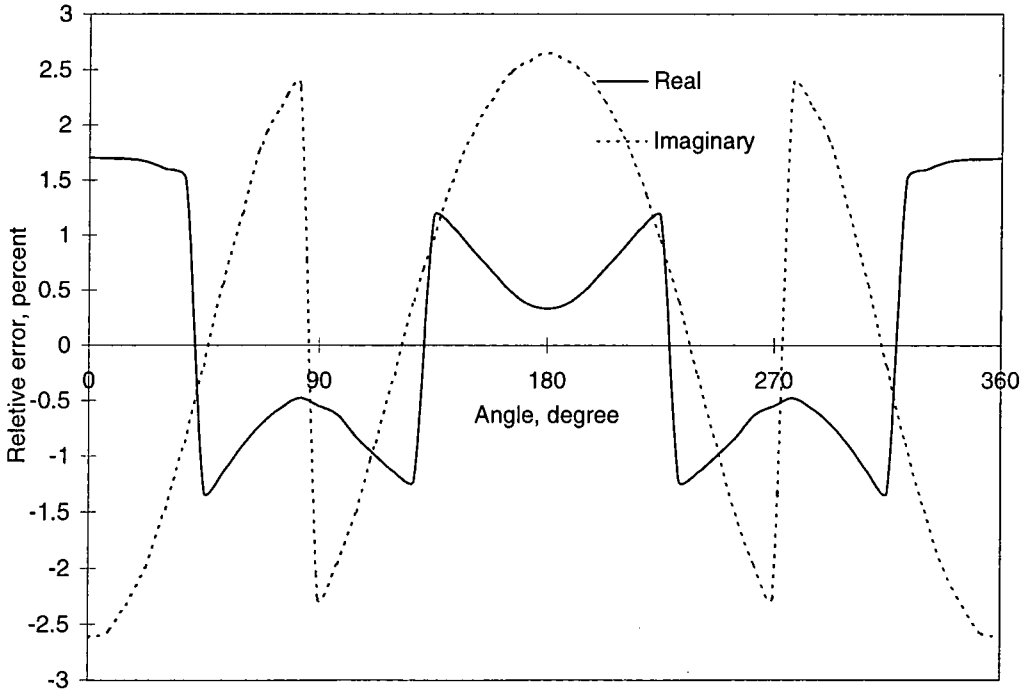

Figure 6.54: Errors in the real and imaginary parts of the solutions on the cylinder (b/a=2, $\theta_I = 0^o$)

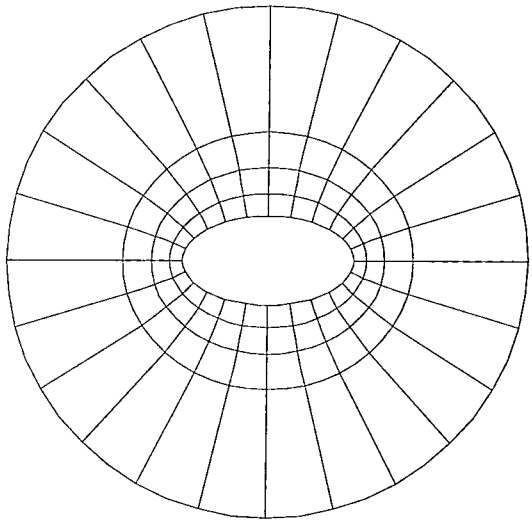

Figure 6.55: A fine mesh of finite and Type 3 infinite elements for elliptical cylinder, b/a=2

semi-major axis of the ellipse) to achieve more accurate results. A finer mesh of finite and infinite elements (three rings of finite and one ring of infinite elements) is illustrated in Figure 6.55. The relative errors for the real and imaginary parts are shown in Figure 6.56 which shows that the errors decrease and are now not more than 0.4 percent and 0.6 percent for the real and imaginary parts respectively. The infinite element was then tested for different cases of elliptical cylinder diffraction problem. The above problem was solved with the new following parameters:

$$\theta_I = 0^o, 30^o \text{ and } 90^o$$

$$b/a\text{=}4$$

A mesh of finite and infinite elements is illustrated in Figure 6.57. The real and imaginary parts of the numerical solutions are compared to their analytical equivalent in Figure 6.58. The relative errors for real and imaginary parts are plotted in Figure 6.59. As can be seen the errors are slightly greater than before (however not greater than 1.5 percent). Since the aspect ratio of the ellipse increased from 2 to 4, a larger number of elements are needed in the circumferential direction to maintain the same accuracy. A contour plot of the free-surface elevation around

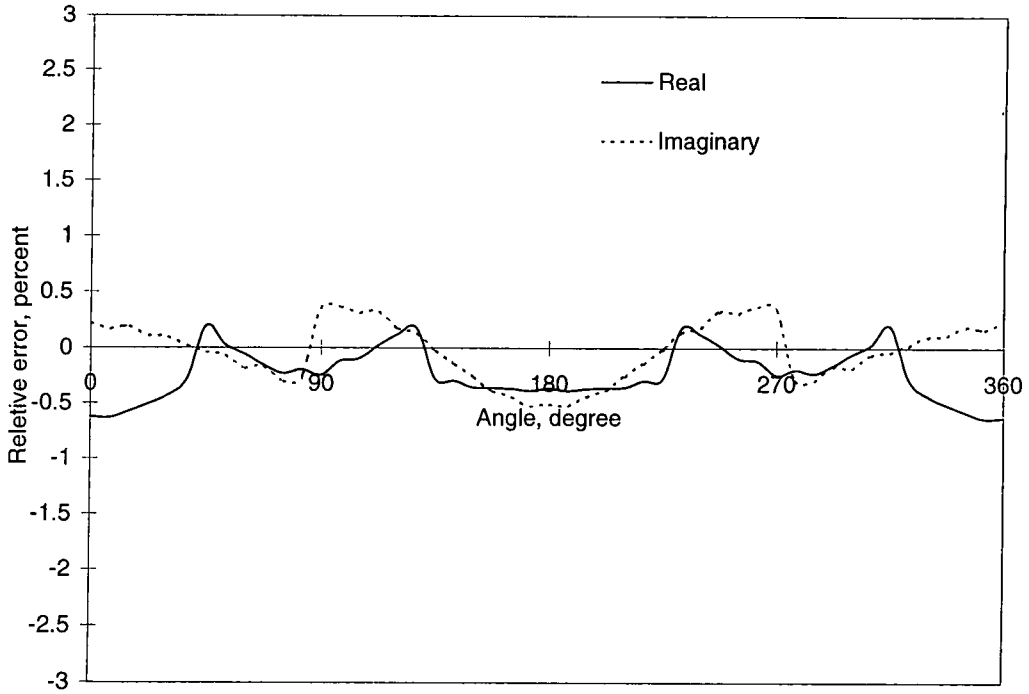

Figure 6.56: Errors in the real and imaginary parts of the solutions on the cylinder (b/a=2, $\theta_I = 0^o$)

is shown in 6.60 and 6.61 for real and imaginary parts respectively.

The same analysis was repeated for angles of incidence of 30 and 90 degrees. Results are shown in Figure 6.62 to 6.69. Figures 6.59, 6.63 and 6.67 demonstrate that the accuracy of the method remains almost the same for the different angles of incidence.

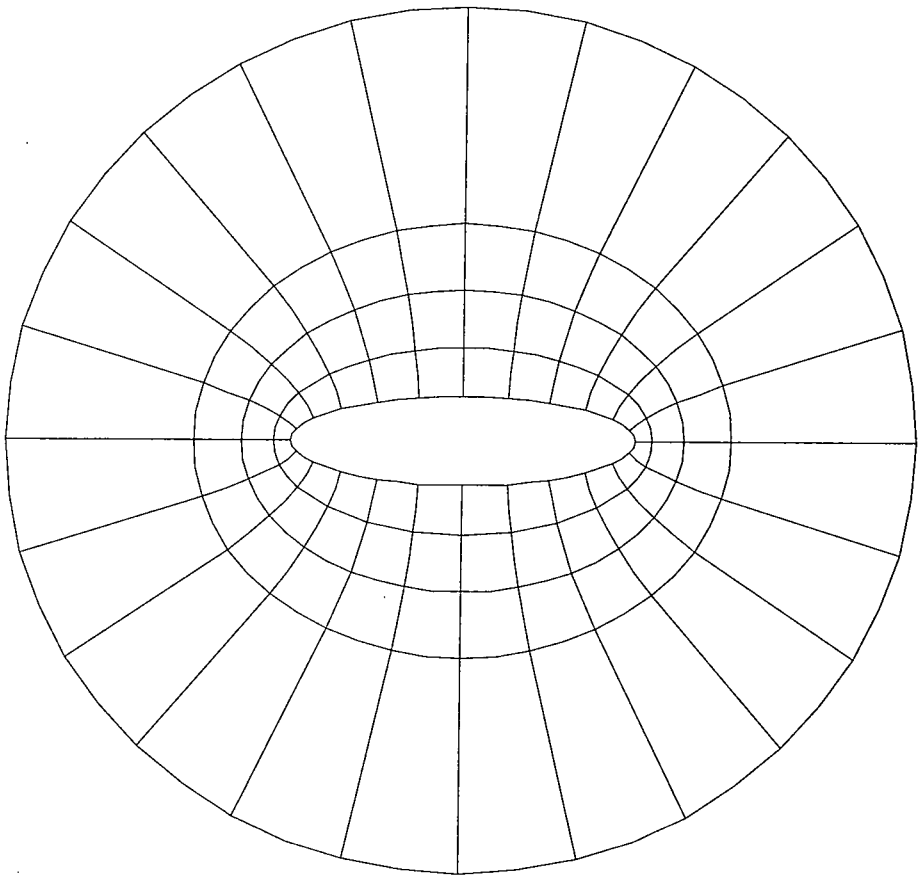

Figure 6.57: A mesh of finite and Type 3 infinite elements for elliptical cylinder, b/a=4

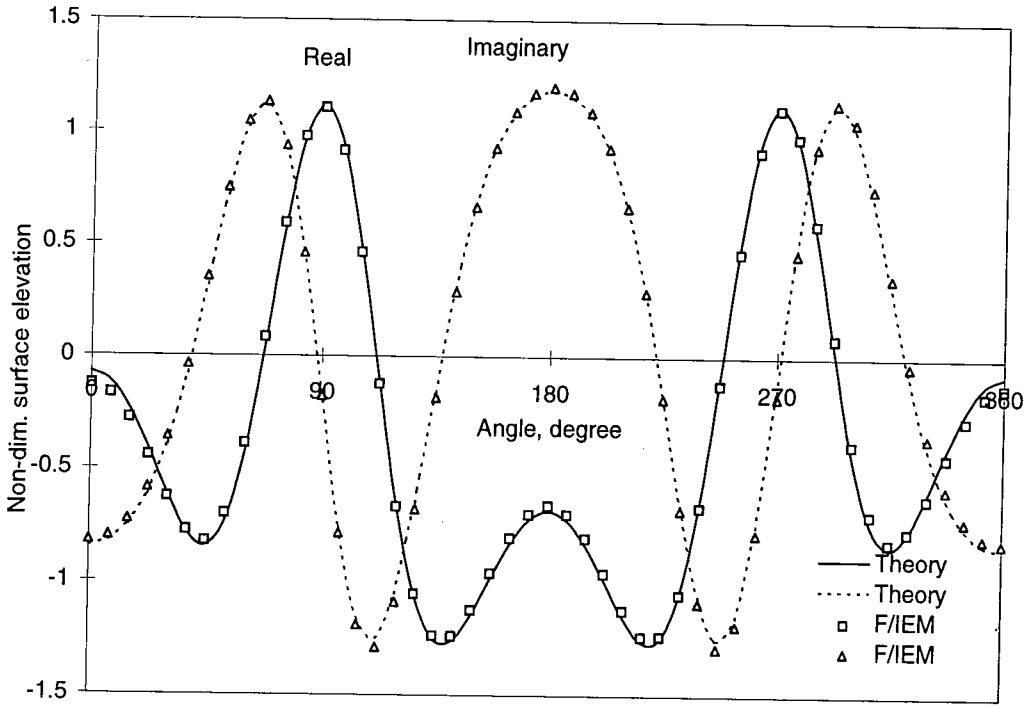

Figure 6.58: Real and imaginary parts of the surface elevations on elliptical cylinder as a function of angle around the cylinder (b/a=4, $\theta_I = 0^o$)

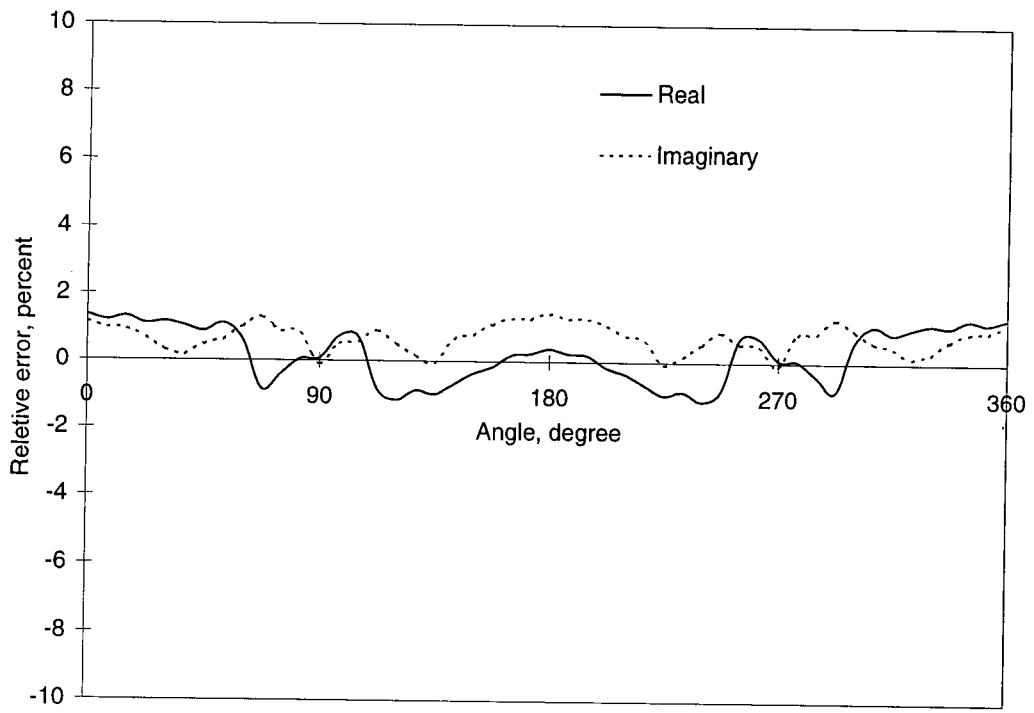

Figure 6.59: Errors in the real and imaginary parts of the solutions on the cylinder (b/a=4, $\theta_I = 0^o$)

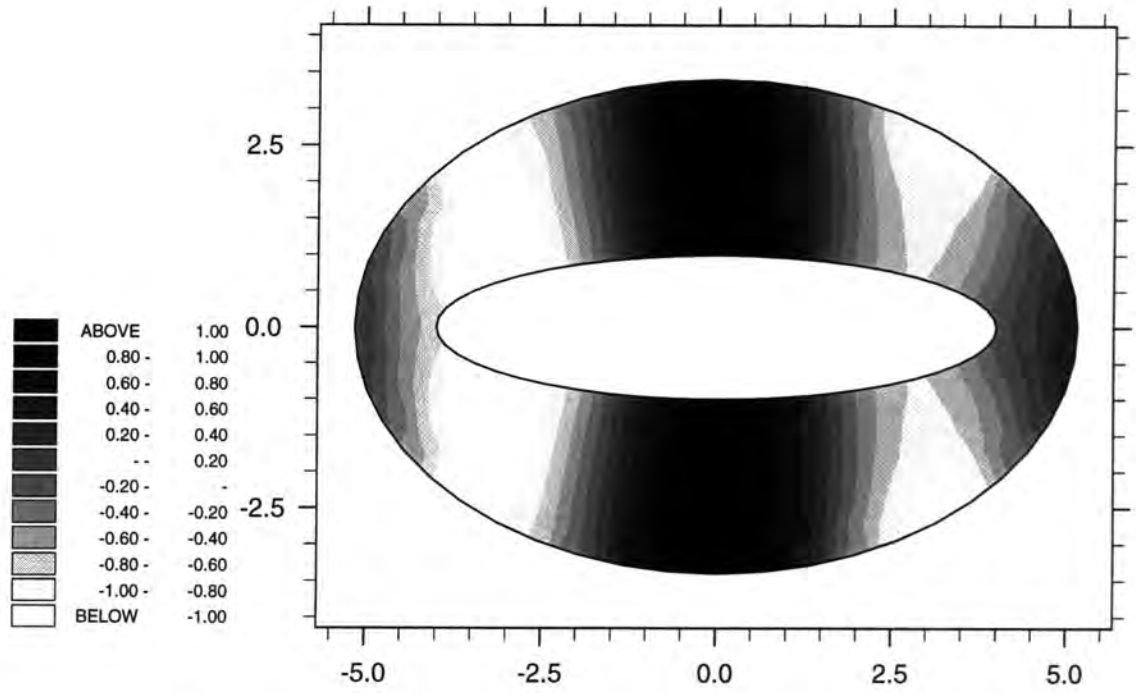

Figure 6.60: A contour plot of the non-dim. free-surface elevation around the elliptical cylinder, real part ($b/a = 4$, $\theta_I = 0^o$)

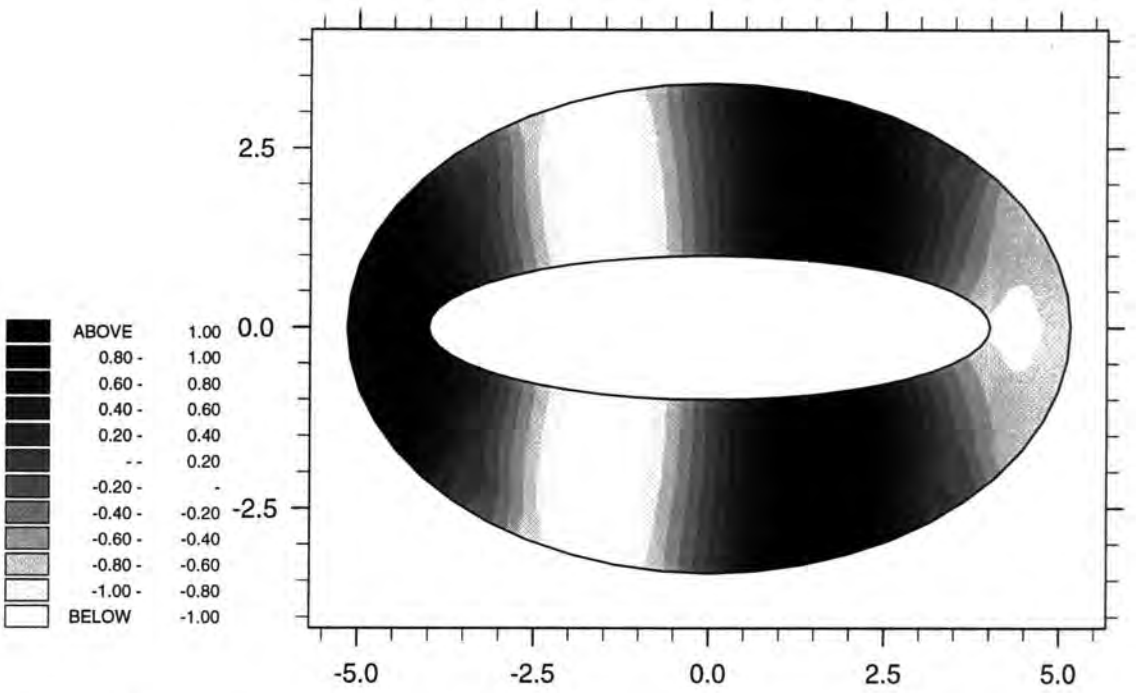

Figure 6.61: A contour plot of the non-dim. free-surface elevation around the cylinder, imaginary part ($b/a = 4$, $\theta_I = 0^o$)

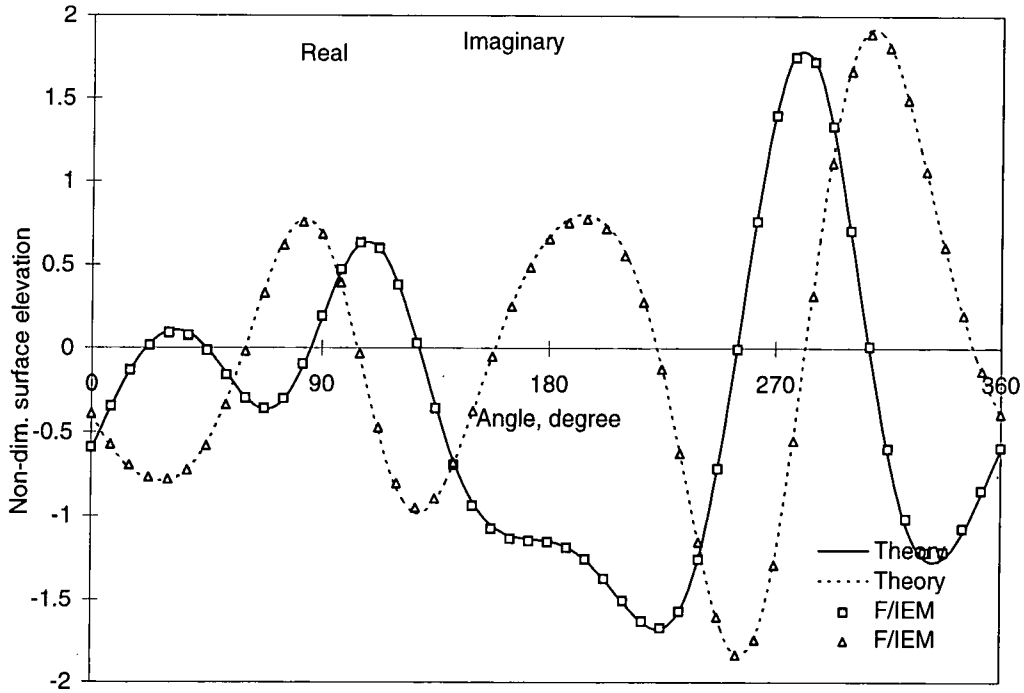

Figure 6.62: Real and imaginary parts of the surface elevations on elliptical cylinder as a function of angle around the cylinder (b/a=4, $\theta_I = 30^o$)

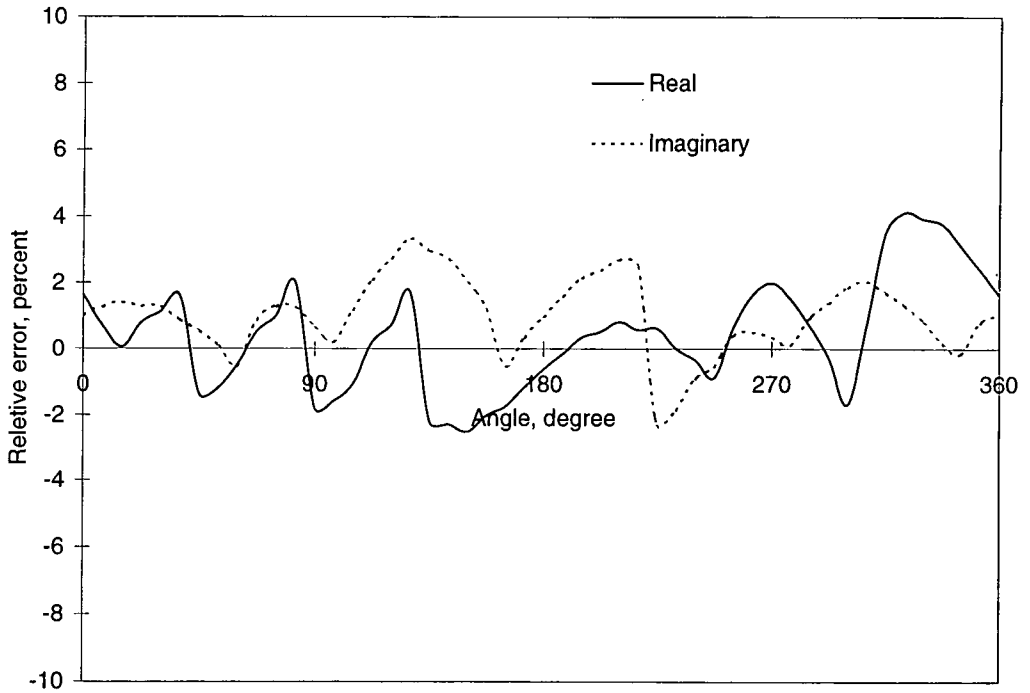

Figure 6.63: Errors in the real and imaginary parts of the solutions on the cylinder (b/a=4, $\theta_I = 30^o$)

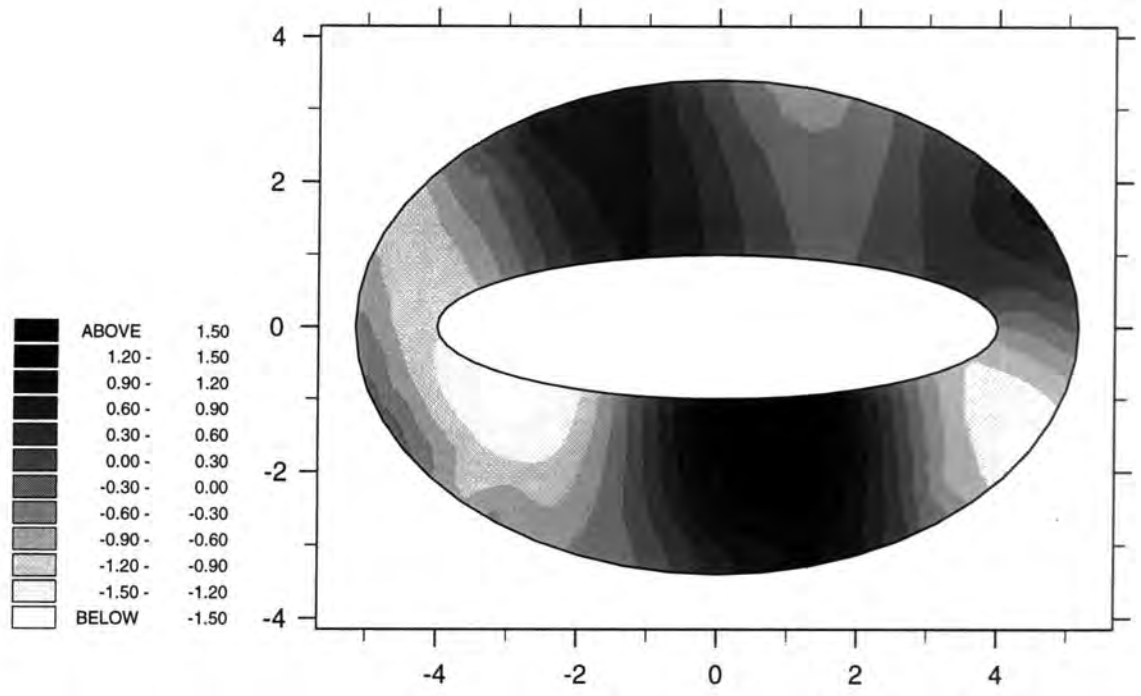

Figure 6.64: A contour plot of the non-dim. free-surface elevation around the elliptical cylinder, real part ($b/a = 4$, $\theta_I = 30^o$)

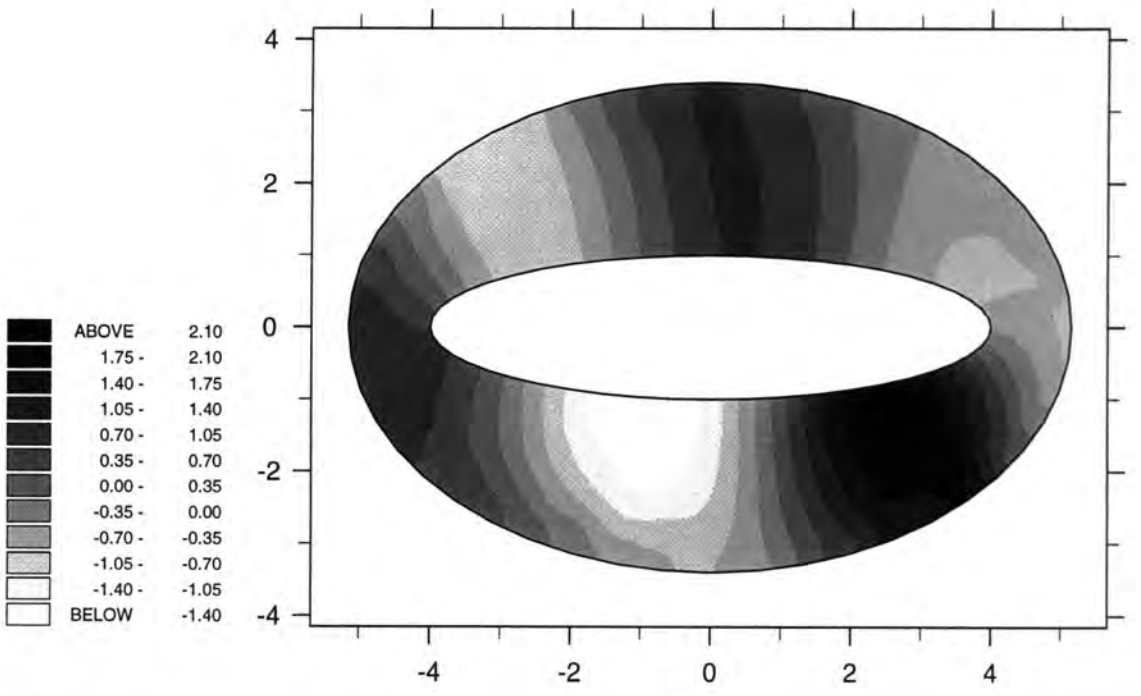

Figure 6.65: A contour plot of the non-dim. free-surface elevation around the cylinder, imaginary part ($b/a = 4$, $\theta_I = 30^o$)

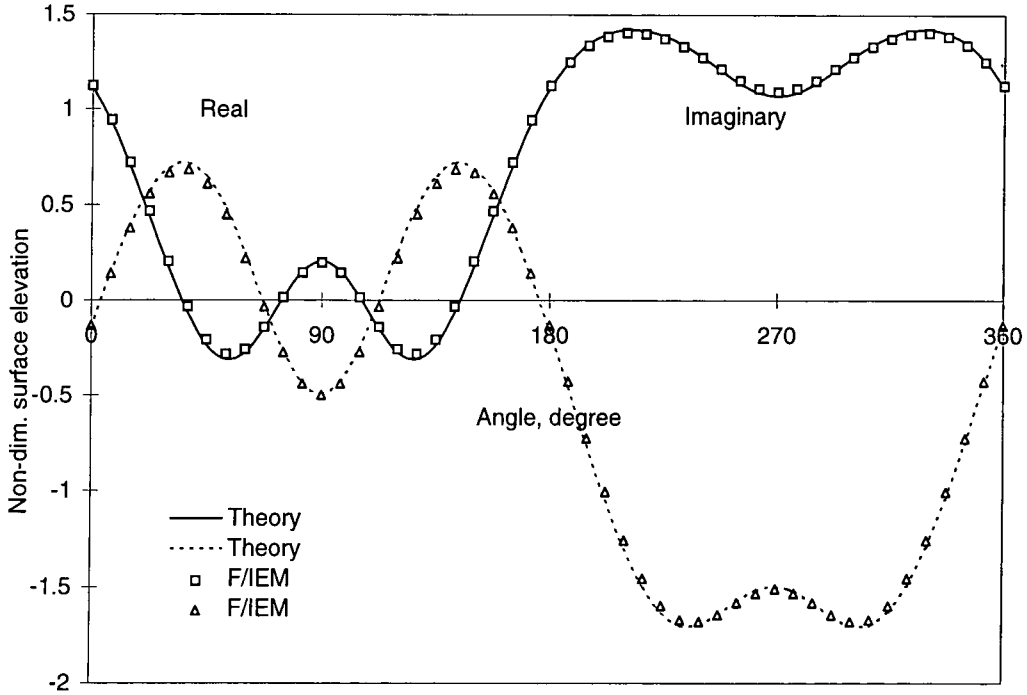

Figure 6.66: Real and imaginary parts of the surface elevations on elliptical cylinder as a function of angle around the cylinder (b/a=4, $\theta_I = 90^o$)

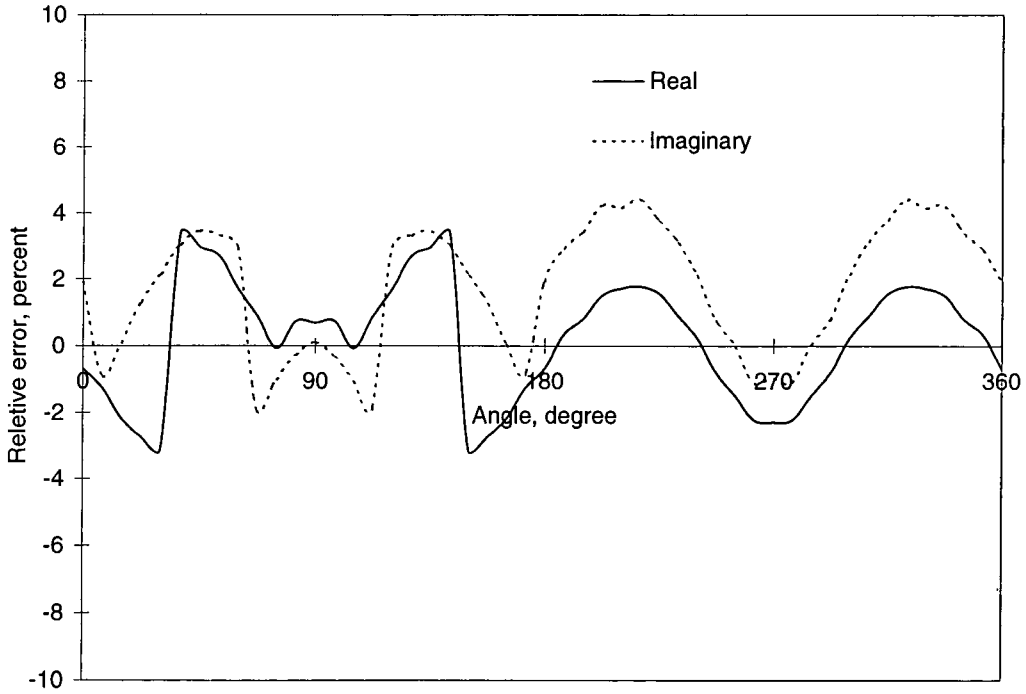

Figure 6.67: Errors in the real and imaginary parts of the solutions on the cylinder (b/a=4, $\theta_I = 90^o$)

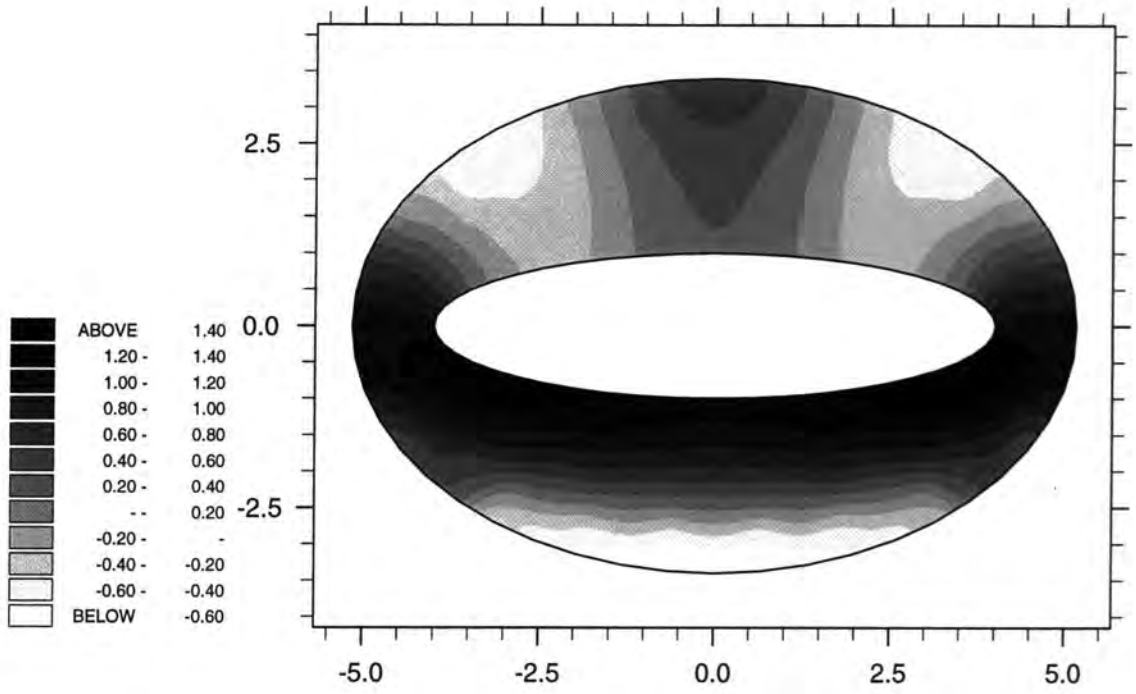

Figure 6.68: A contour plot of the non-dim. free-surface elevation around the elliptical cylinder, real part ($b/a = 4$, $\theta_I = 90^o$)

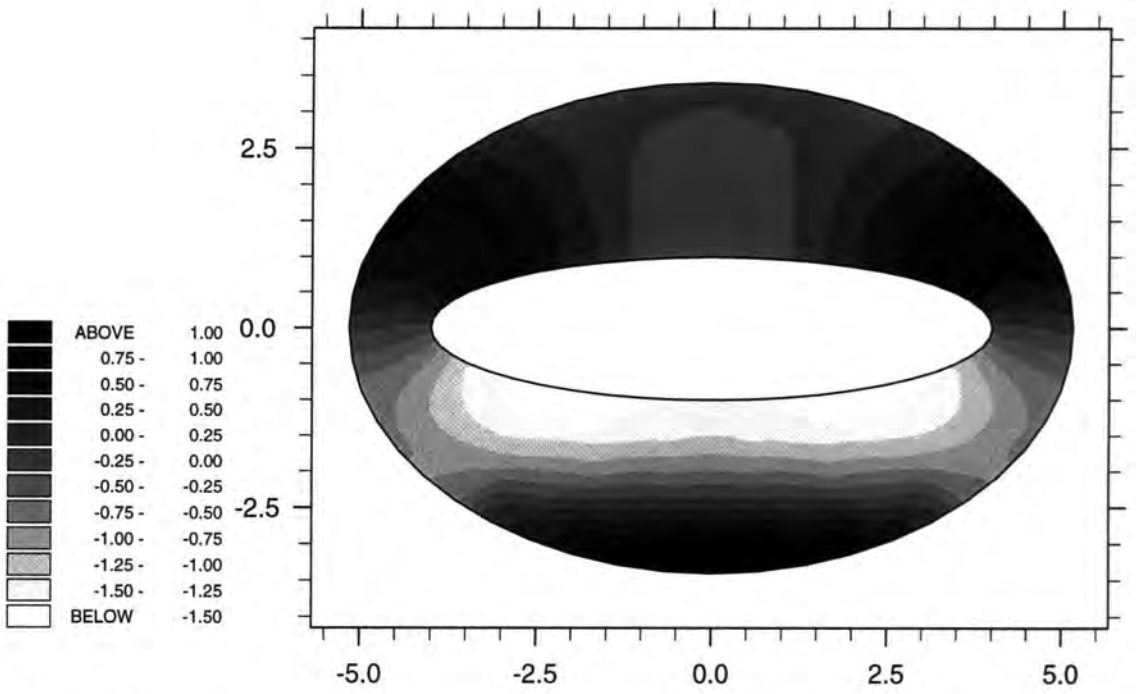

Figure 6.69: A contour plot of the non-dim. free-surface elevation around the cylinder, imaginary part ($b/a = 4$, $\theta_I = 90^o$)

6.4.3 Problems of wave diffraction by arrays of cylinders

As was explained in chapter 1 and section 2.1, wave diffraction effects (compared with viscous effects) become important when the dimension of the diffracting object is large enough to alter the pattern of the incoming waves. It is widely accepted that when $ka = 2a\pi/L > 0.2\pi$ the diffraction effects become dominant (see e.g. Sarpkaya *et al* [92], page 9-10). However, for a large ka (small wavelength) the minimum number of finite element nodes required to model the problem accurately increases. So in the following example problems a mesh of finite and infinite elements was first used to solve the problem for a small ka ($< 0.2\pi$) to test the general accuracy of the model. It must be emphasized that for small ka the viscous effect is dominant and so it must be taken into account for a real problem. However, the present model has only been developed for wave diffraction problems. The same mesh was then used to solve the problem for a large ka ($> 0.2\pi$) to illustrate the effect of wave diffraction by the objects. A finer mesh should be used to obtain more accurate results but was not possible in this research due to the constraints.

In this section, problems of diffraction of water waves by arrays of vertical circular and elliptical cylinders were solved. The finite and infinite element model was first fully tested for diffraction of wave by a pair of circular cylinders with different angles of wave incidence. First the angle of incidence, θ_I, (see figure 3.10) was taken to be zero degrees. The predicted free surface elevations on the cylinders were compared with their equivalent analytical solutions presented in section 3.4 and the errors were plotted. Then a contour plot of surface elevations around the pair of circular cylinders predicted by F/IE was compared with the equivalent

analytical solutions for angle of wave incidence of 0, 30 and 90 degrees. A problem of wave diffraction by an array of 4 (2 by 2) cylinders was then solved to test the model for more scattered geometry of objects. A real problem of wave diffraction by an array of 6 (2 by 3) circular cylinders was then solved. Finally an example problem of diffraction of waves by a 1 by 2 array of elliptical cylinder was solved.

Pair of cylinders

In this section, two vertical neighbouring circular cylinders with radius a standing in shallow water with a plane wave incident upon them were analysed. The parameters were as follows:

$$d/a=1$$

$$\theta_I = 0^o, 30^o \text{ and } 90^o$$

$$ka=0.2$$

A mesh of finite and infinite elements which consists of 284 elements (1003 nodes) is illustrated in Figure 6.70. First the angle of wave incidence was chosen to be zero (see figure 3.10). The real and imaginary parts of the numerical solutions on the first (left) cylinder were compared to their analytical equivalents in Figure 6.71. The relative errors for real and imaginary parts are plotted in Figure 6.72 for the first cylinder. As can be seen the errors are small being not greater than 0.5 percent for the real part and not more than 0.6 percent for the imaginary part. The same results are illustrated in Figures 6.73 and 6.74 for the second (right) cylinder which show that the errors are small being not greater than 0.35 percent for the real part and not more than 0.45 percent for the imaginary part. Contour plots of real and imaginary parts of the F/IE free surface elevations around the cylinders

are shown in Figures 6.76 and 6.78 and their equivalent analytical solutions are shown in Figures 6.75 and 6.77. A good agreement between the analytical and F/IE solutions can be observed .

The same problem was then solved for different angles of wave incidence (30 and 90 degrees). The contour plots of the real and imaginary parts of the analytical and F/IE solutions are shown in Figures 6.79, 6.80, 6.81, 6.82, 6.83, 6.84, 6.85 and 6.86. A good agreement between the analytical and F/IE solutions can be observed.

The same mesh, Figure 6.70, was then used to solve the problem for a larger ka ($> 0.2\pi$) with the following parameters:

$$d/a=20$$

$$\theta_I = 0^o$$

$$ka = 2$$

Contour plots of real and imaginary parts of the F/IE free surface elevations around the cylinders are shown in Figures 6.88 and 6.90 and their equivalent analytical solutions are shown in Figures 6.87 and 6.89. The figures show that unlike the previous example the pattern of the incoming wave has been significantly altered by the presence of the cylinders. The agreement between the analytical and F/IE solutions is reasonable but not as good as before. More finite element nodes are needed to achieve a better agreement.

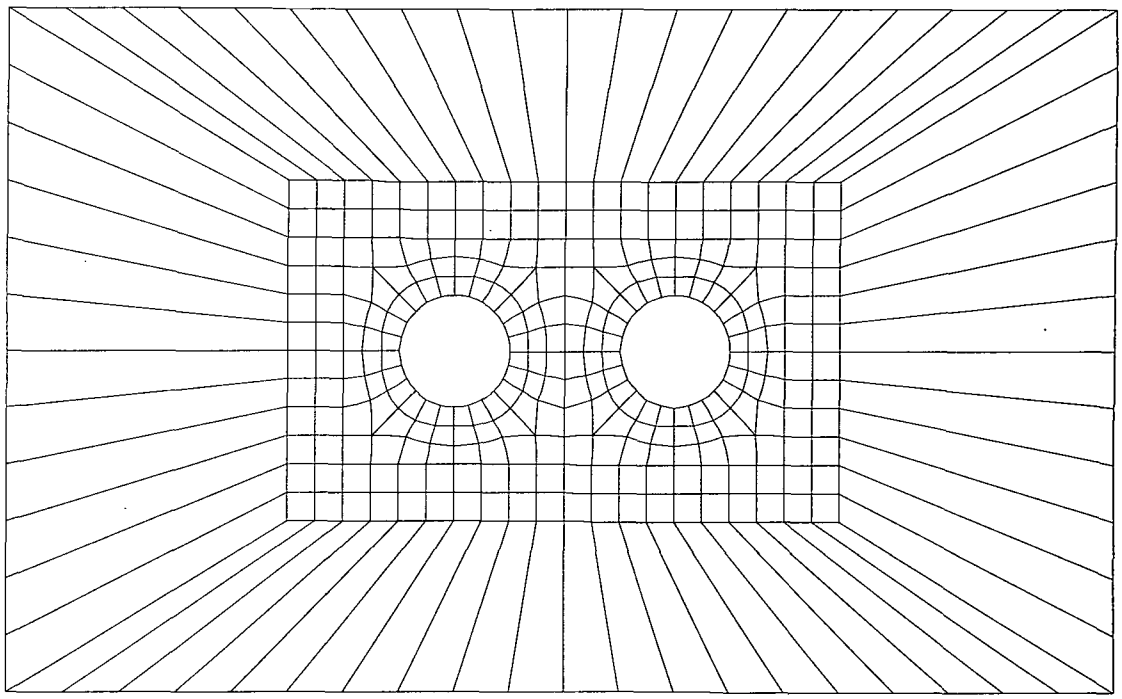

Figure 6.70: Mesh of finite and Type 3 infinite elements for double cylinder, a=1

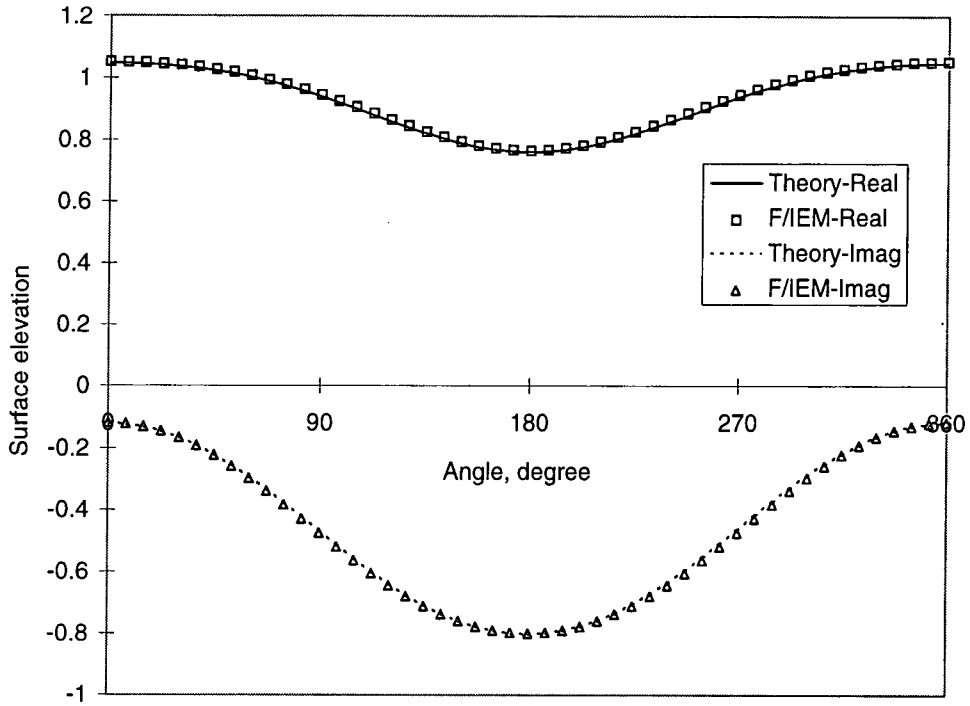

Figure 6.71: Real and imaginary part of non-dim. free-surface elevations on the first cylinder as a function of angle around the cylinder ($ka = 0.2$, $\theta_I = 0^o$)

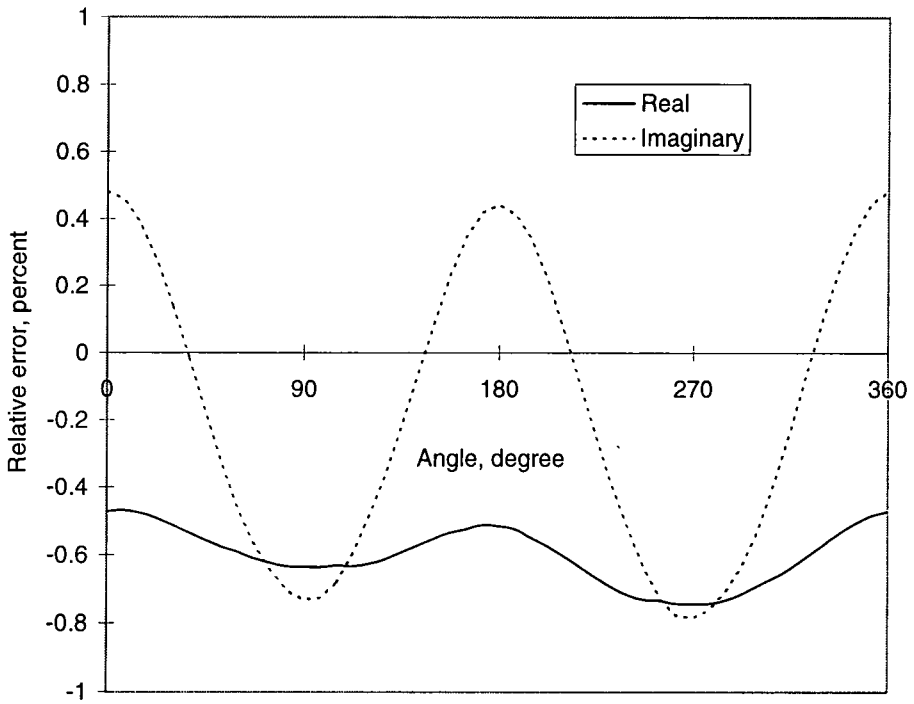

Figure 6.72: Errors in the real and imaginary parts of the solutions on the surface of first cylinder ($ka = 0.2$, $\theta_I = 0^o$)

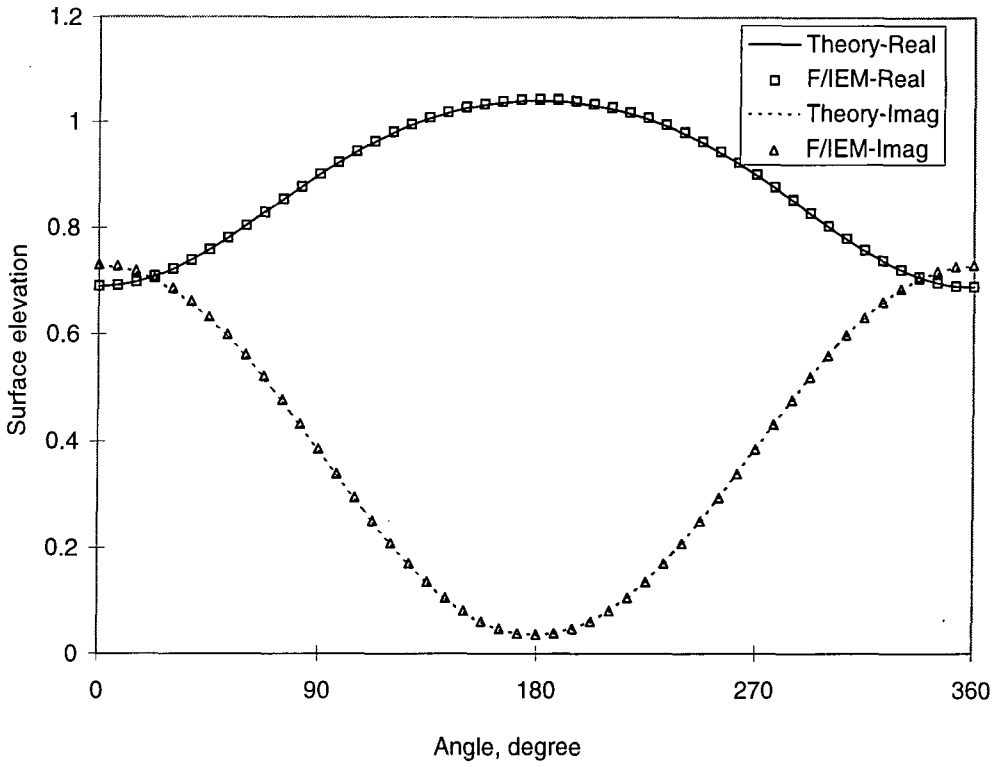

Figure 6.73: Real and imaginary part of non-dim. free-surface elevations on the second cylinder as a function of angle around the cylinder ($ka = 0.2$, $\theta_I = 0^o$)

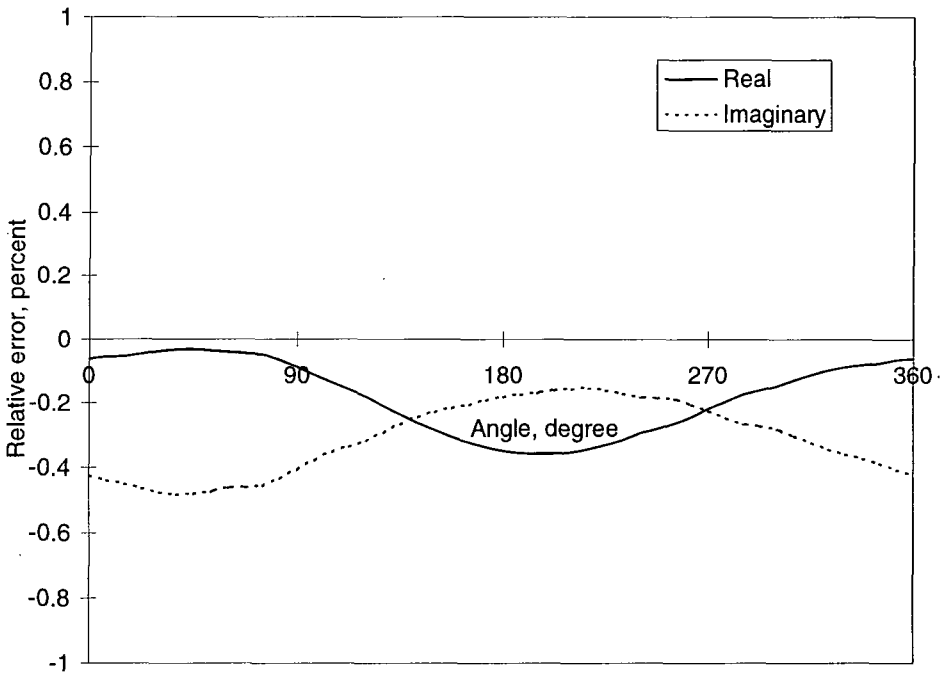

Figure 6.74: Errors in the real and imaginary parts of the solutions on the surface of second cylinder ($ka = 0.2$, $\theta_I = 0^o$)

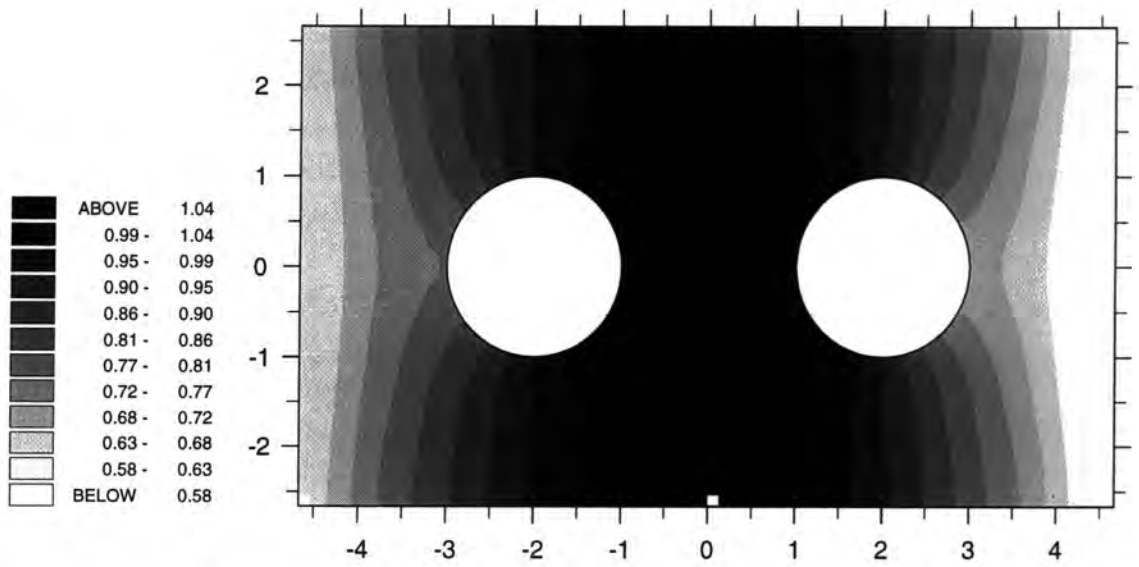

Figure 6.75: A contour plot of the non-dim. free-surface elevations around a pair of cylinders, real part of analytical solutions, ($ka = 0.2$, $\theta_I = 0^o$)

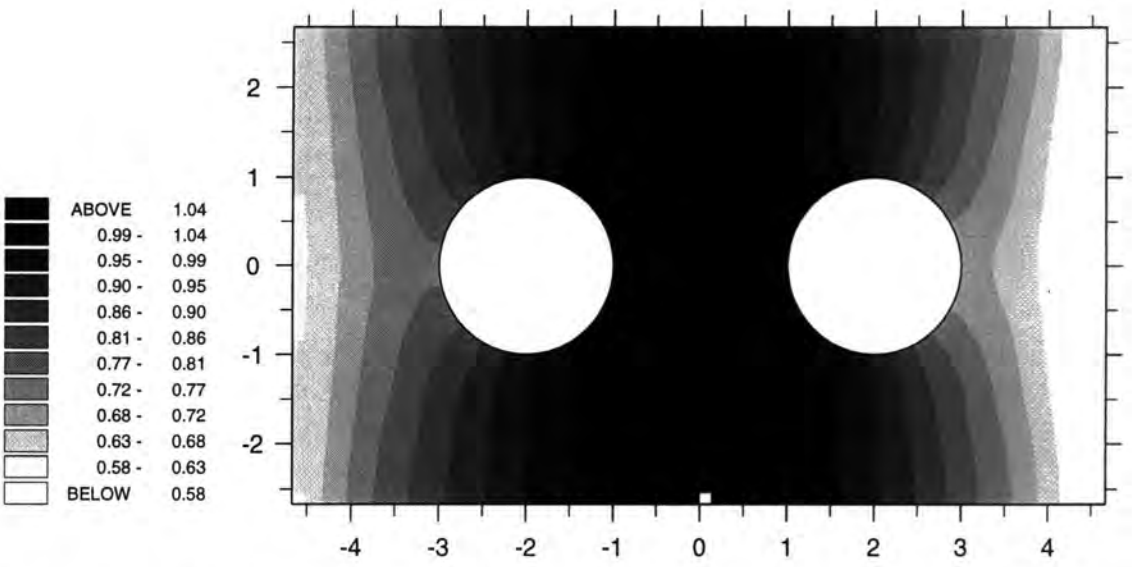

Figure 6.76: A contour plot of the non-dim. free-surface elevations around a pair of cylinders, real part of F/IE solutions ($ka = 0.2$, $\theta_I = 0^o$)

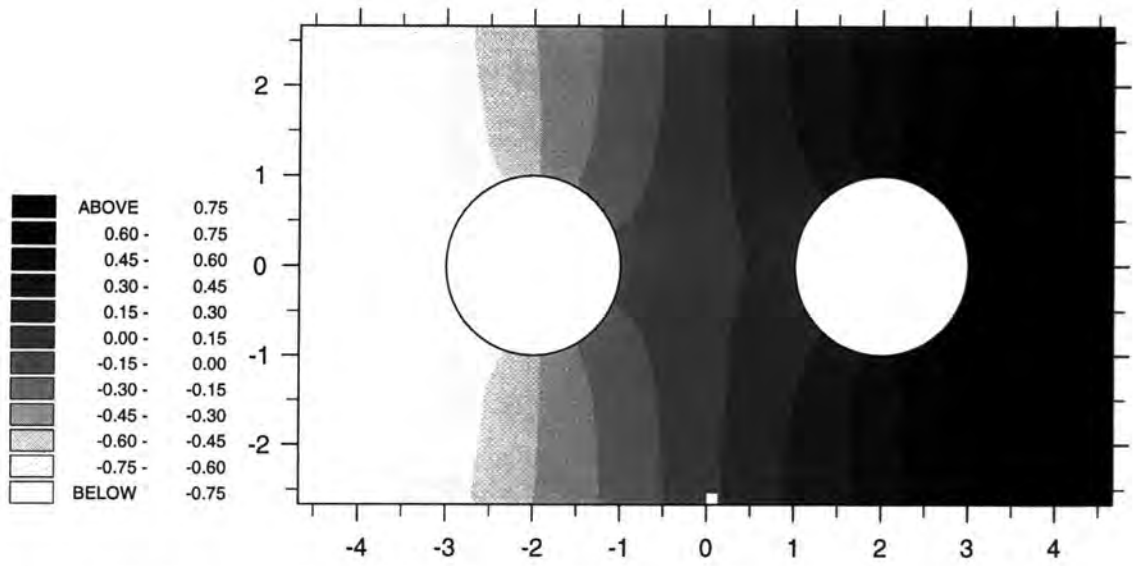

Figure 6.77: A contour plot of the non-dim. free-surface elevations around a pair of cylinders, imaginary part of analytical solutions ($ka = 0.2$, $\theta_I = 0^o$)

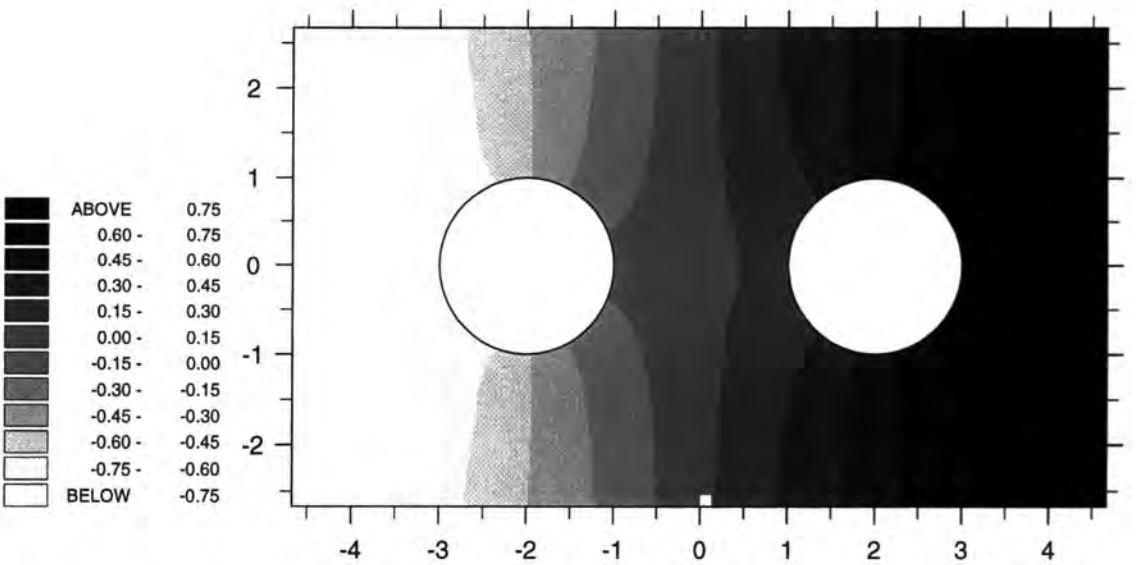

Figure 6.78: A contour plot of the non-dim. free-surface elevations around a pair of cylinders, imaginary part of F/IE solutions ($ka = 0.2$, $\theta_I = 0^o$)

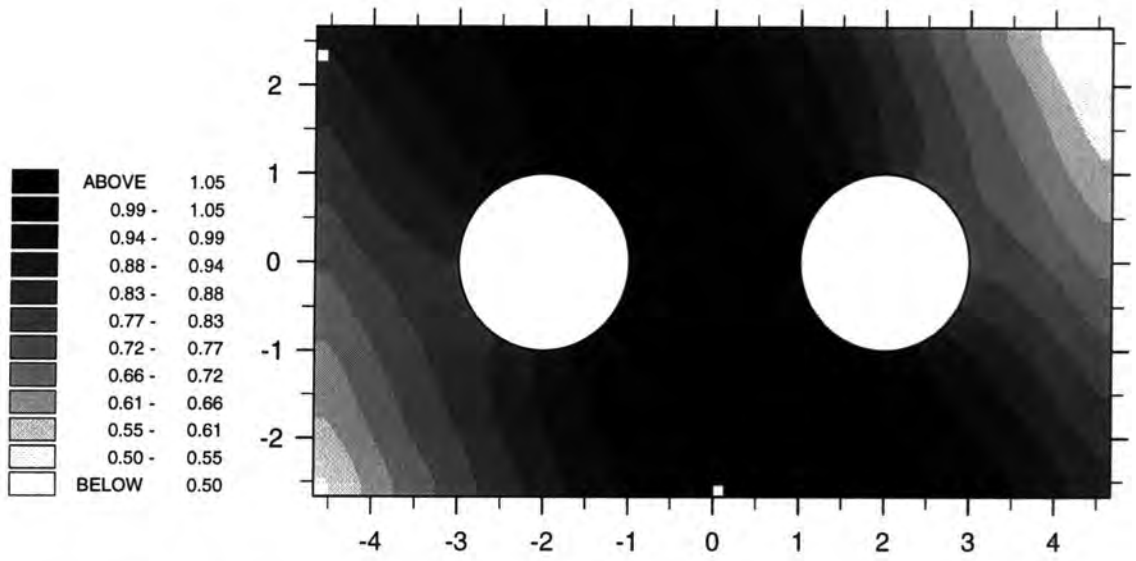

Figure 6.79: A contour plot of the non-dim. free-surface elevations around a pair of cylinders, real part of analytical solutions ($ka = 0.2$, $\theta_I = 30^o$)

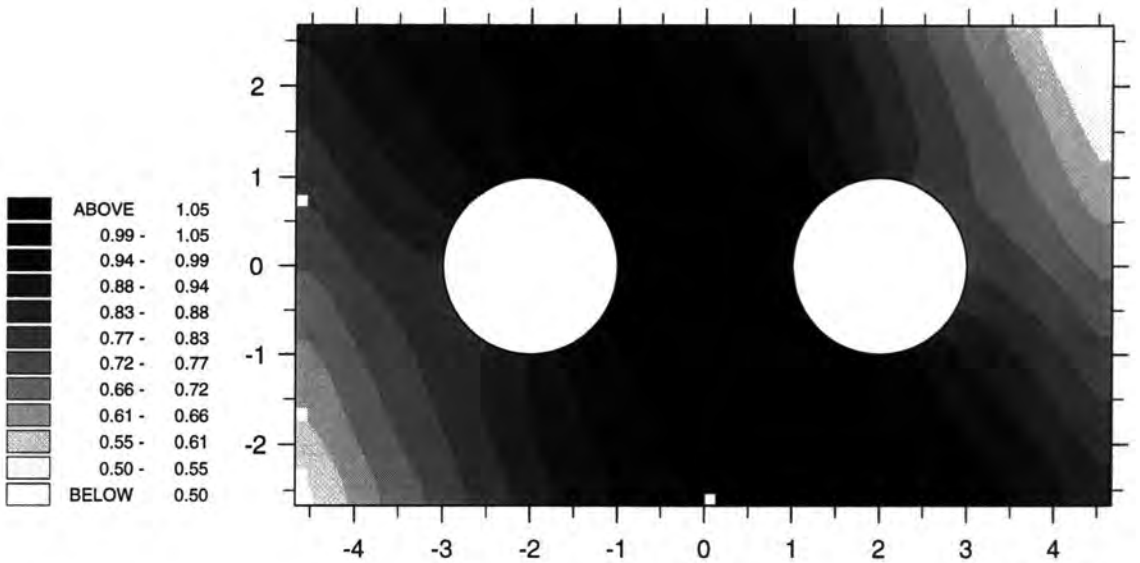

Figure 6.80: A contour plot of the non-dim. free-surface elevations around a pair of cylinder, real part of F/IE solutions ($ka = 0.2$, $\theta_I = 30^o$)

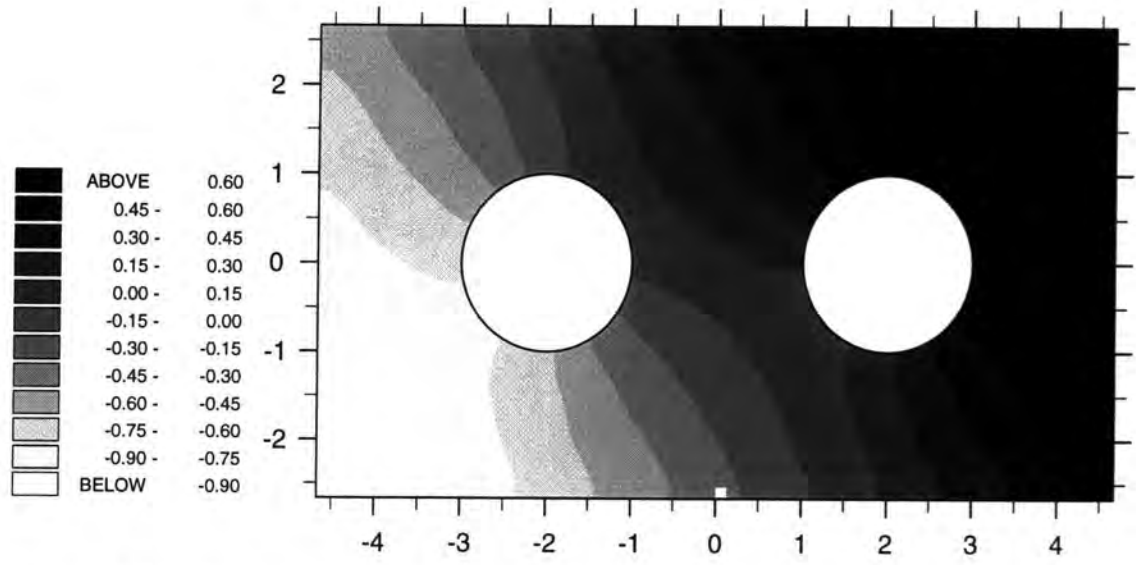

Figure 6.81: A contour plot of the non-dim. free-surface elevations around a pair of cylinders, imaginary part analytical solutions ($ka = 0.2$, $\theta_I = 30^o$)

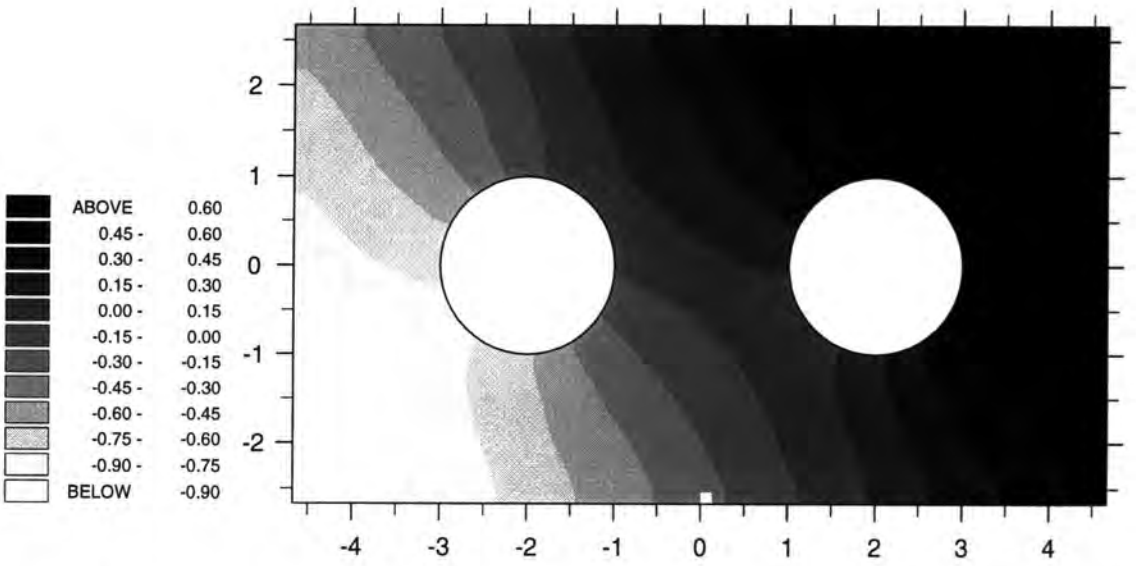

Figure 6.82: A contour plot of the non-dim. free-surface elevations around pair of cylinders, imaginary part F/IE solutions ($ka = 0.2$, $\theta_I = 30^o$)

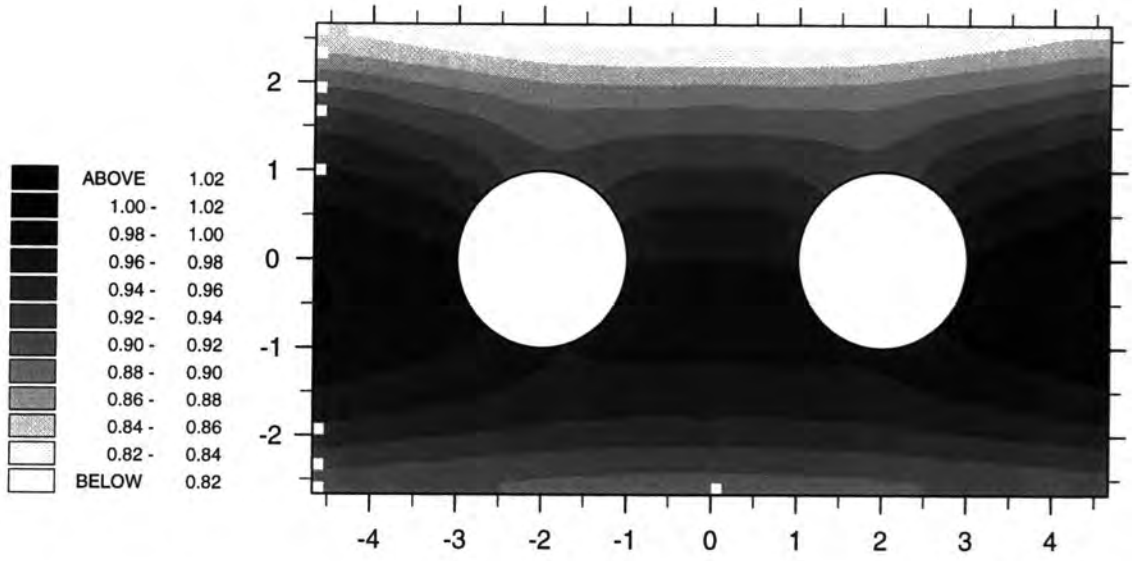

Figure 6.83: A contour plot of the non-dim. free-surface elevations around a pair of cylinders, real part of analytical solutions ($ka = 0.2$, $\theta_I = 90^o$)

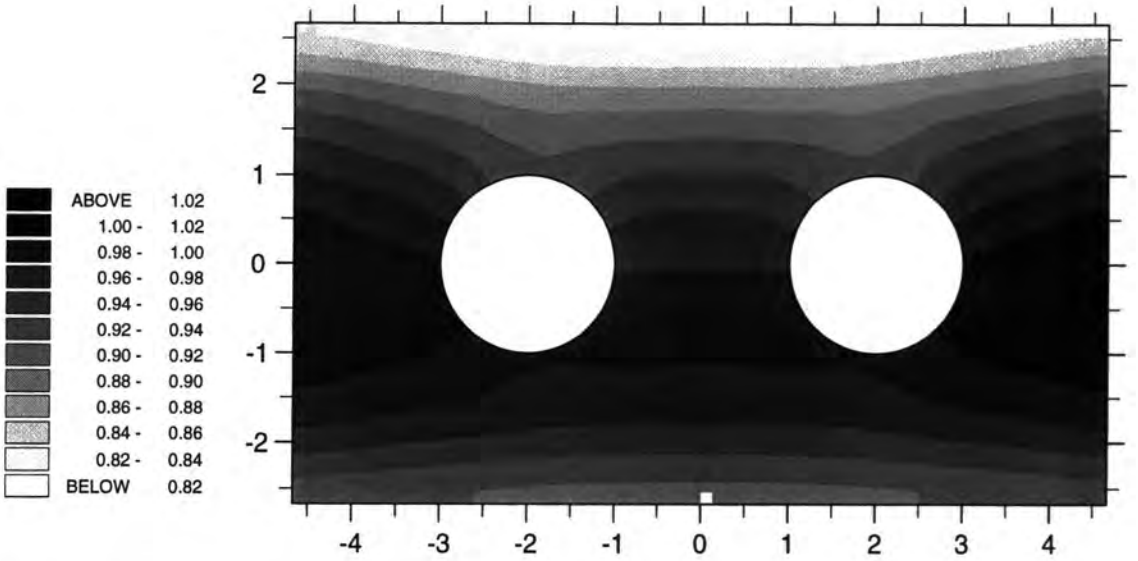

Figure 6.84: A contour plot of the non-dim. free-surface elevations around a pair of cylinder, real part of F/IE solutions ($ka = 0.2$, $\theta_I = 90^o$)

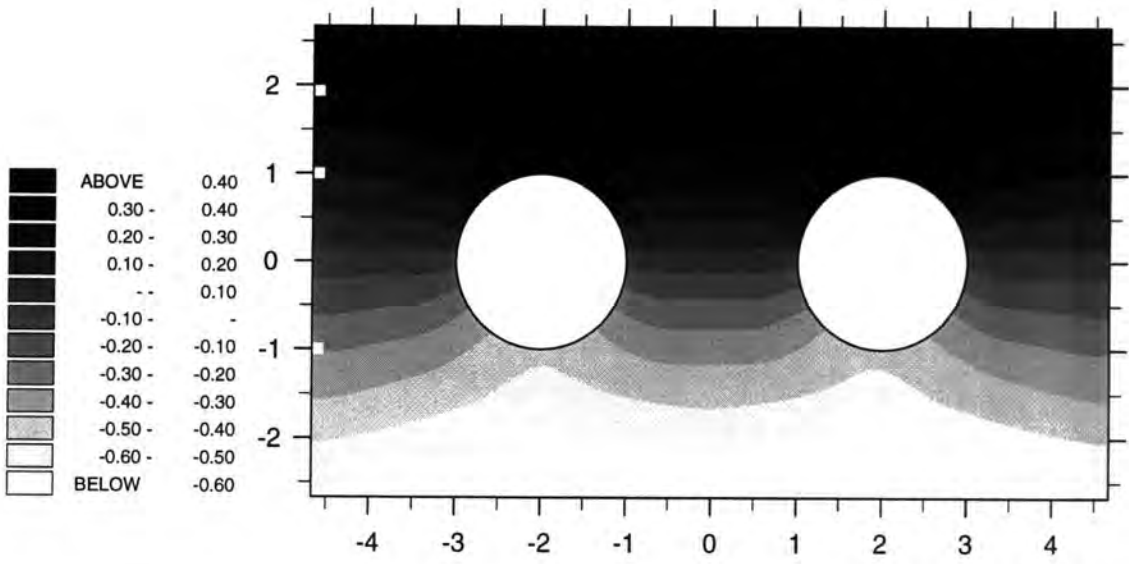

Figure 6.85: A contour plot of the non-dim. free-surface elevations around a pair of cylinders, imaginary part analytical solutions ($ka = 0.2$, $\theta_I = 90^o$)

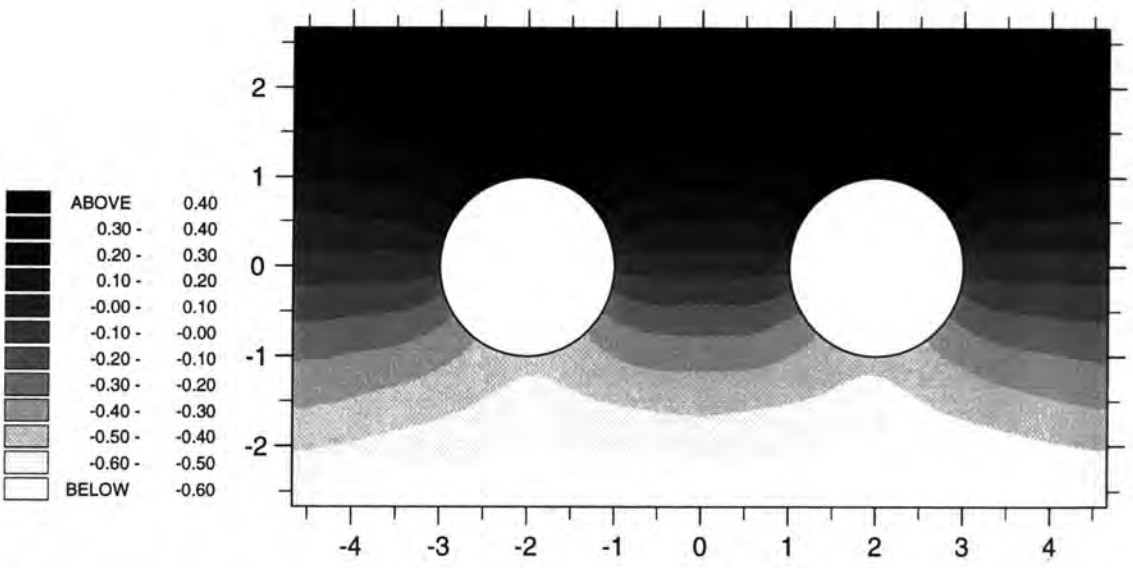

Figure 6.86: A contour plot of the non-dim. free-surface elevations around a pair of cylinders, imaginary part F/IE solutions ($ka = 0.2$, $\theta_I = 90^o$)

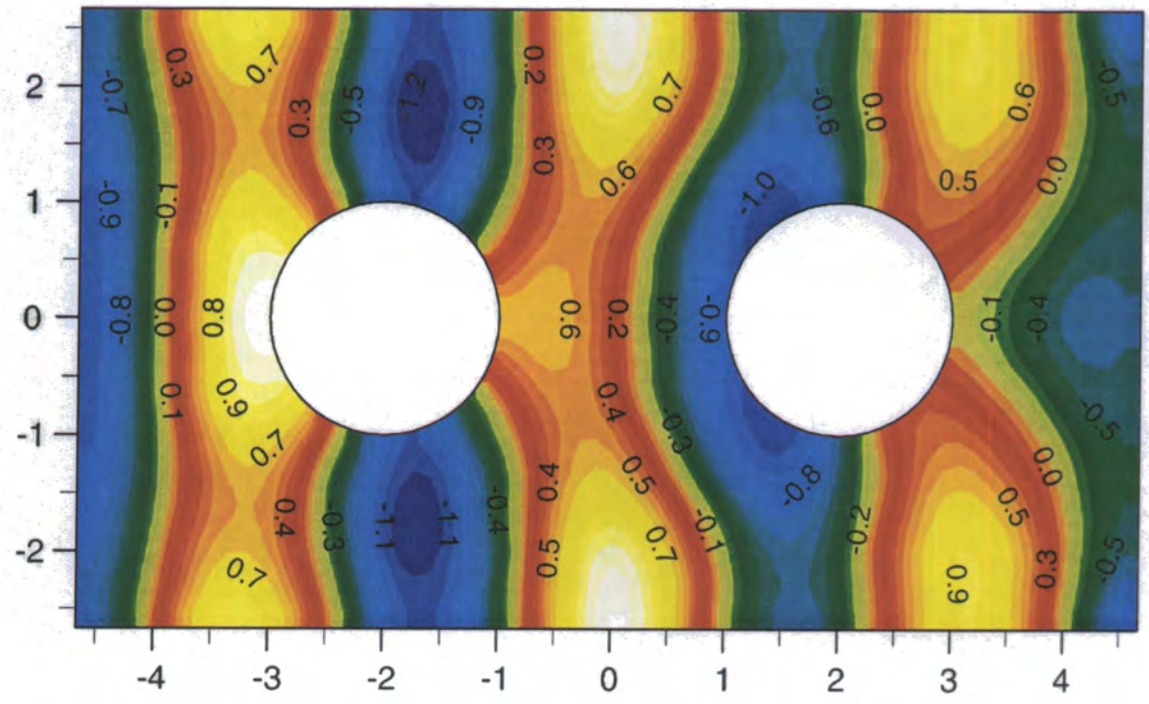

Figure 6.87: A contour plot of the non-dim. free-surface elevations around a pair of cylinders, real part of analytical solutions ($ka = 2$, $\theta_I = 0^o$)

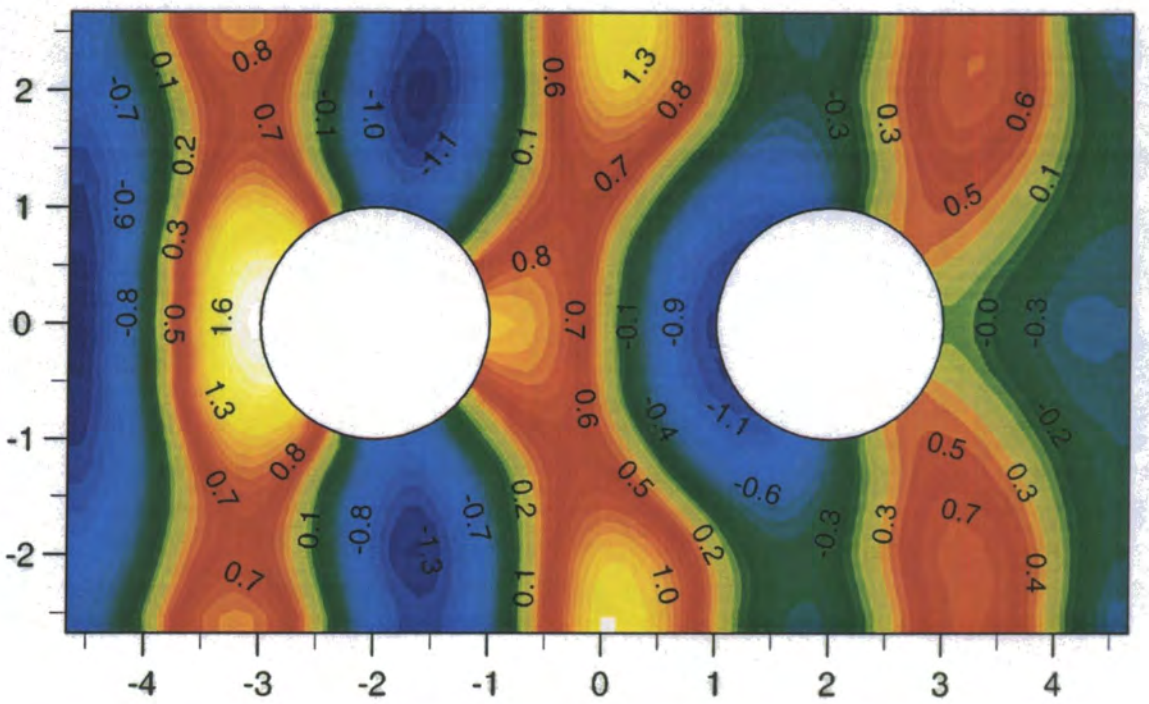

Figure 6.88: A contour plot of the non-dim. free-surface elevations around a pair of cylinders, real part of F/IE solutions ($ka = 2$, $\theta_I = 0^o$)

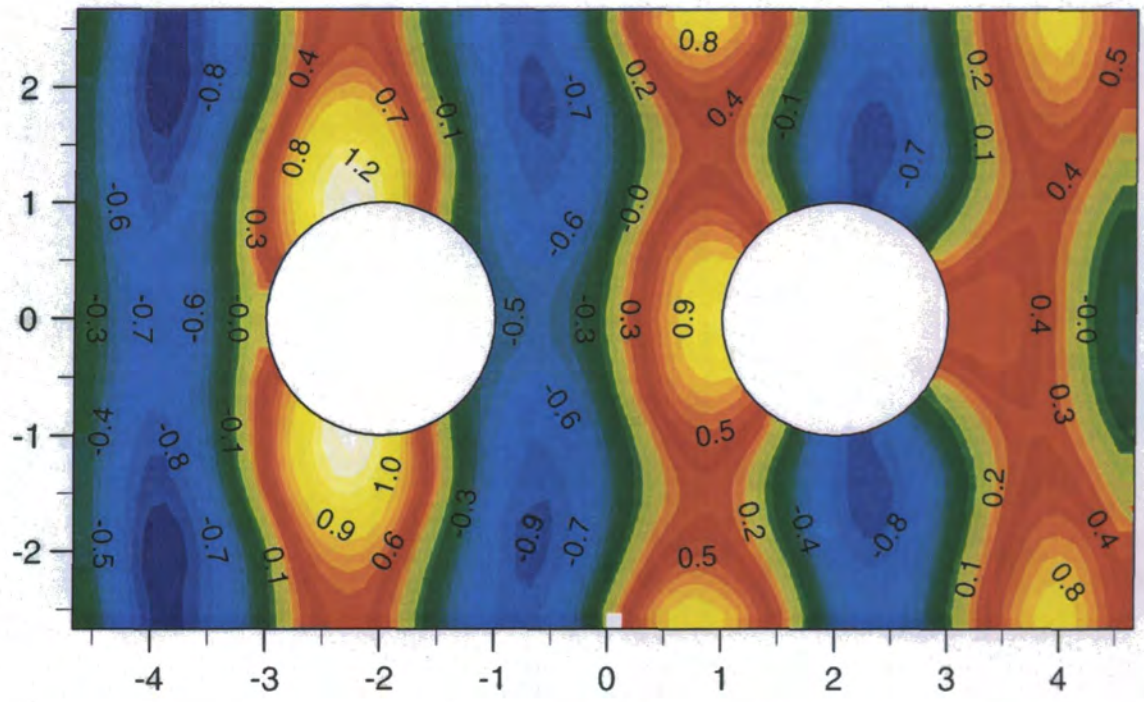

Figure 6.89: A contour plot of the non-dim. free-surface elevations around a pair of cylinders, imaginary part of analytical solutions ($ka = 2$, $\theta_I = 0^o$)

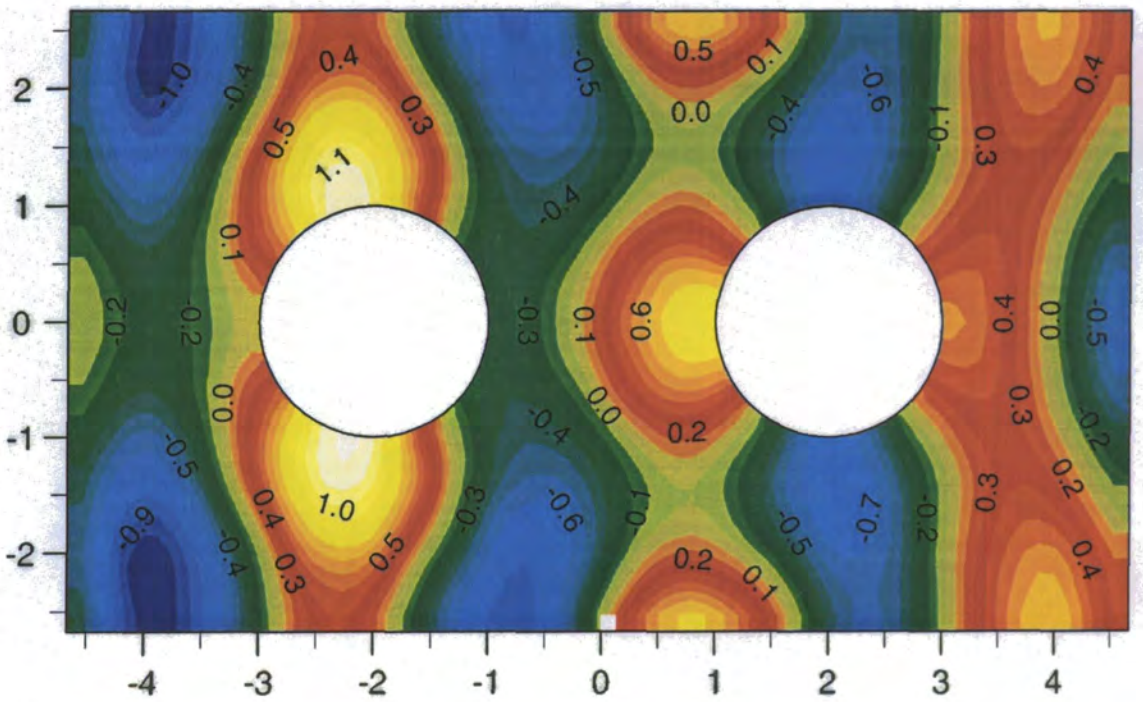

Figure 6.90: A contour plot of the non-dim. free-surface elevations around a pair of cylinders, real part of F/IE solutions ($ka = 2$, $\theta_I = 0^o$)

2 by 2 array of cylinders

A 2 by 2 array of equally spaced vertical circular cylinders (four identical cylinders with radius a) standing in shallow water with a plane wave incident upon them was analysed. The parameters were as follows:

$$d/a=1$$

$$\theta_I = 45^o$$

$$ka=0.2$$

A mesh of finite and infinite elements which consists of 464 elements (1613 nodes) is illustrated in Figure 6.91. Contour plots of real and imaginary parts of the analytical free surface elevations around the cylinders are shown in Figures 6.92 and 6.94 and their equivalent F/IE solutions are shown in Figures 6.93 and 6.95. A good agreement between the analytical and F/IE solutions can be observed.

The same mesh, Figure 6.91, was then used to solve the problem for a larger ka ($> 0.2\pi$) with the following parameters:

$$d/a=20$$

$$\theta_I = 45^o$$

$$ka = 2$$

Contour plots of real and imaginary parts of the analytical free surface elevations around the cylinders are shown in Figures 6.96 and 6.98 and their equivalent F/IE solutions are shown in Figures 6.97 and 6.99. The figures show that unlike the previous example the pattern of the incoming wave has been significantly altered by the presence of the cylinders. The agreement between the analytical and F/IE solutions is reasonable but not as good as before. More finite element nodes are needed to achieve a better agreement.

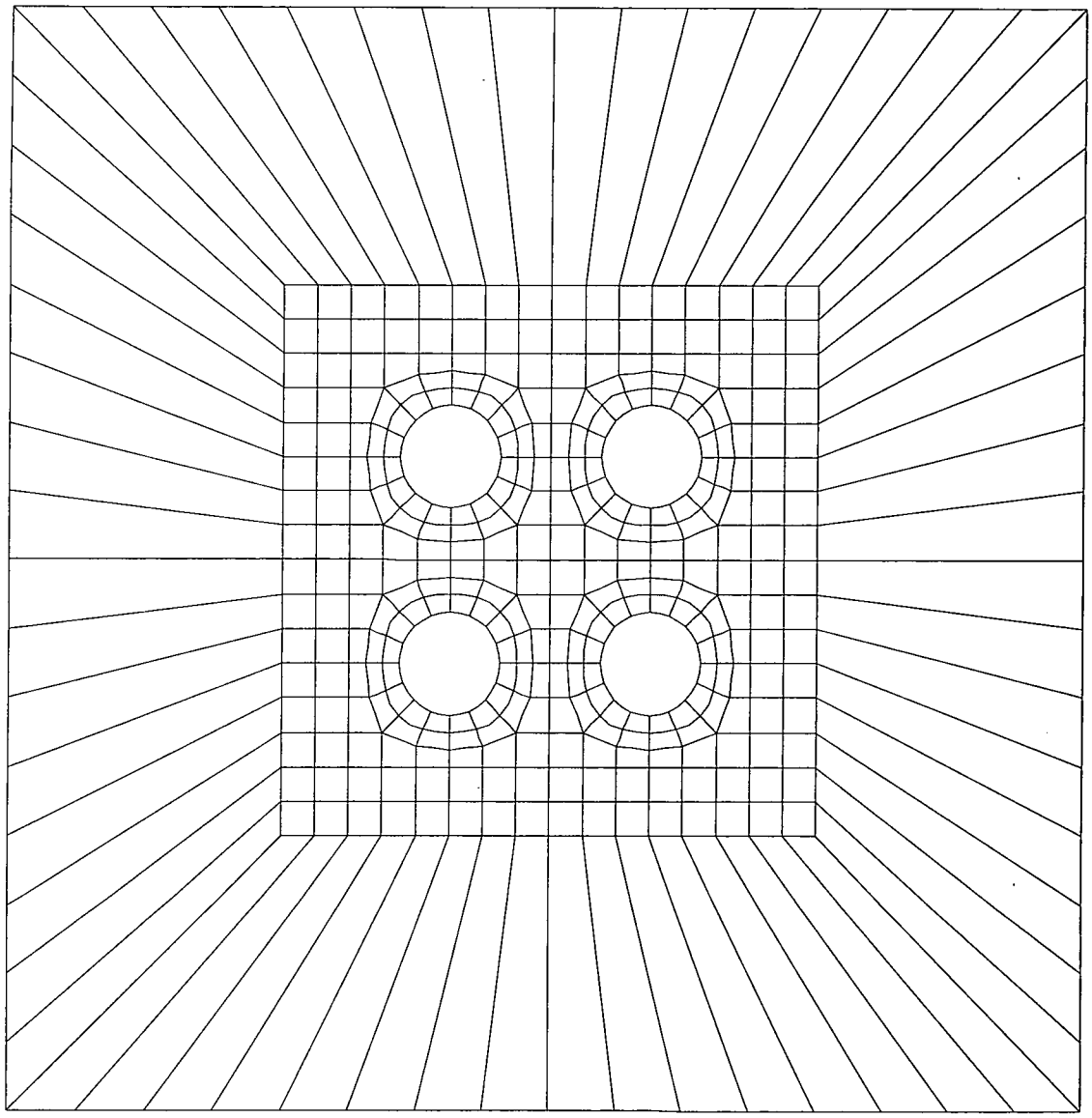

Figure 6.91: Mesh of finite and Type 3 infinite elements for 2 by 2 array of cylinders, a=1

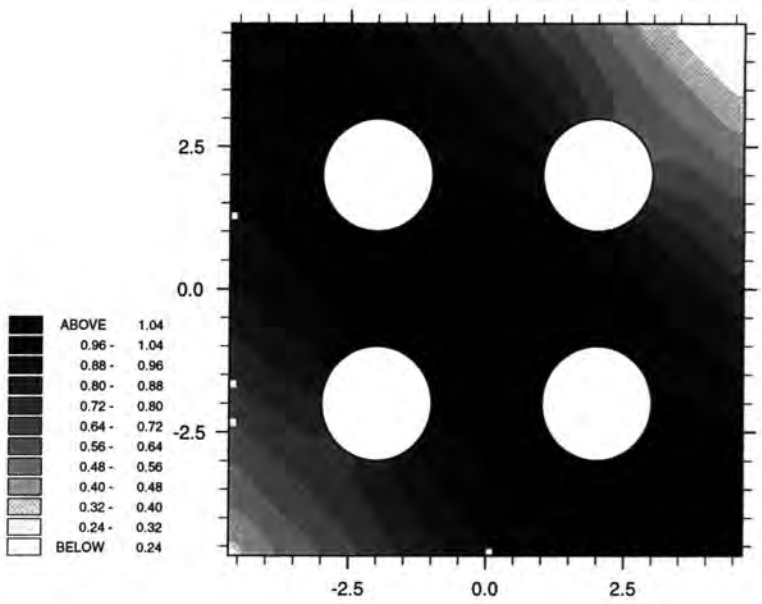

Figure 6.92: A contour plot of the non-dim. free-surface elevations around the cylinders, real part of the analytical solutions ($ka = 0.2$, $\theta_I = 45^o$)

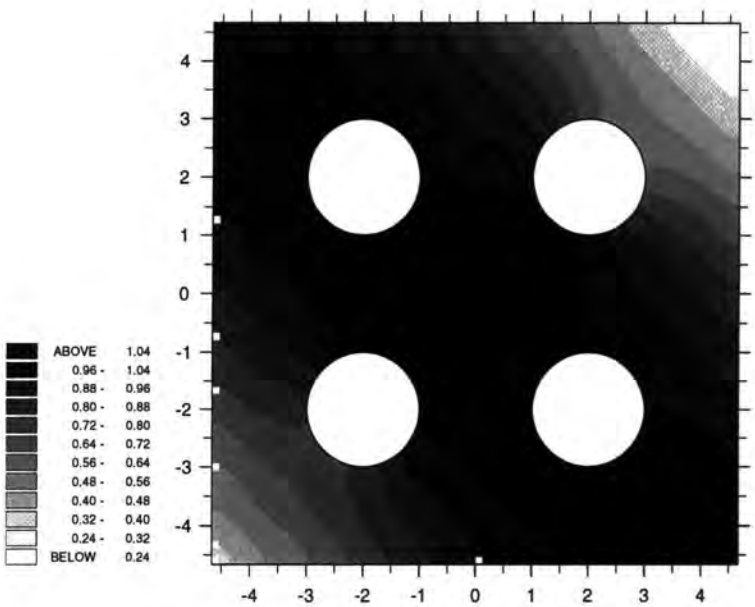

Figure 6.93: A contour plot of the non-dim. free-surface elevations around the cylinders, real part of F/IE solutions ($ka = 0.2$, $\theta_I = 45^o$)

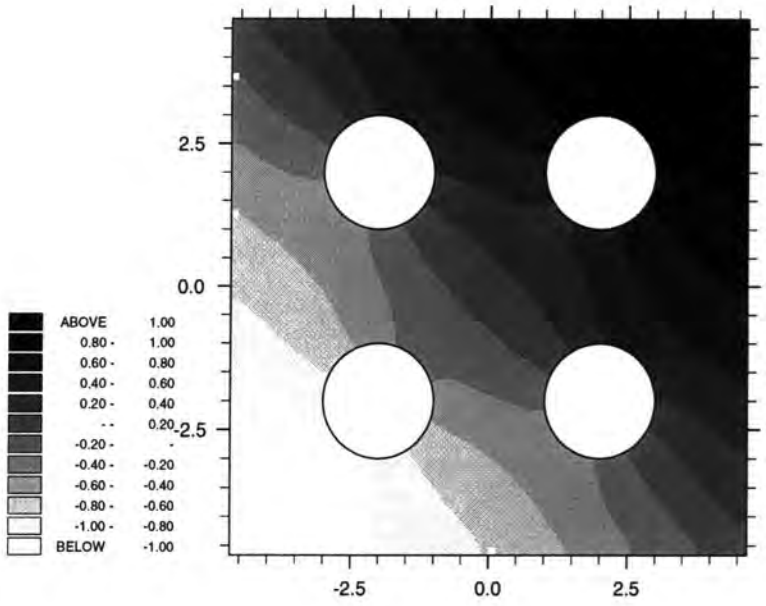

Figure 6.94: A contour plot of the non-dim. free-surface elevations around the cylinders, imaginary part of analytical solutions ($ka = 0.2$, $\theta_I = 45^o$)

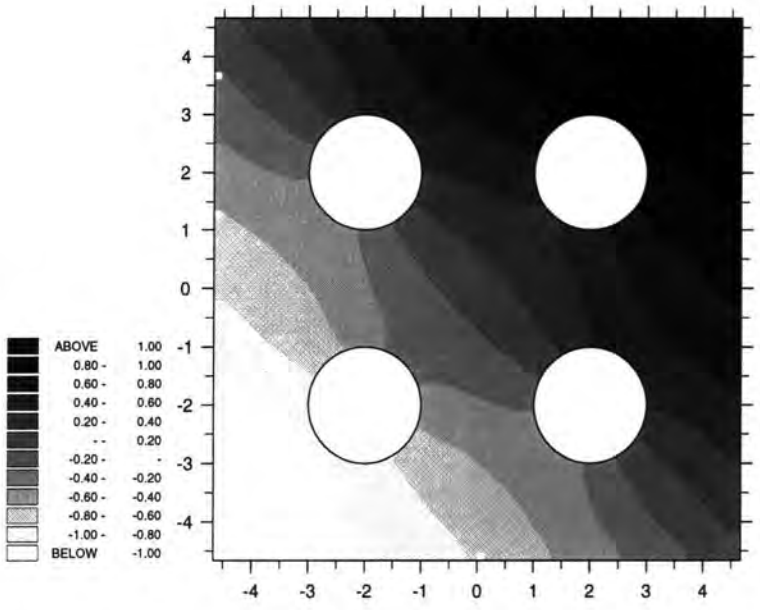

Figure 6.95: A contour plot of the non-dim. free-surface elevations around the cylinders, imaginary part of F/IE solutions ($ka = 0.2$, $\theta_I = 45^o$)

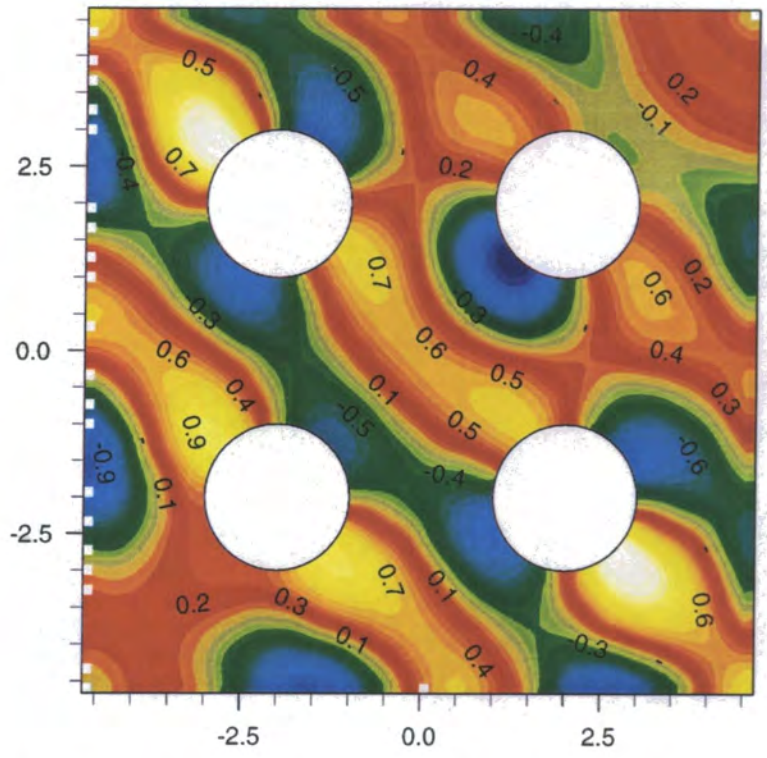

Figure 6.96: A contour plot of the non-dim. free-surface elevations around the cylinders, real part of the analytical solutions ($ka = 2$, $\theta_I = 45^o$)

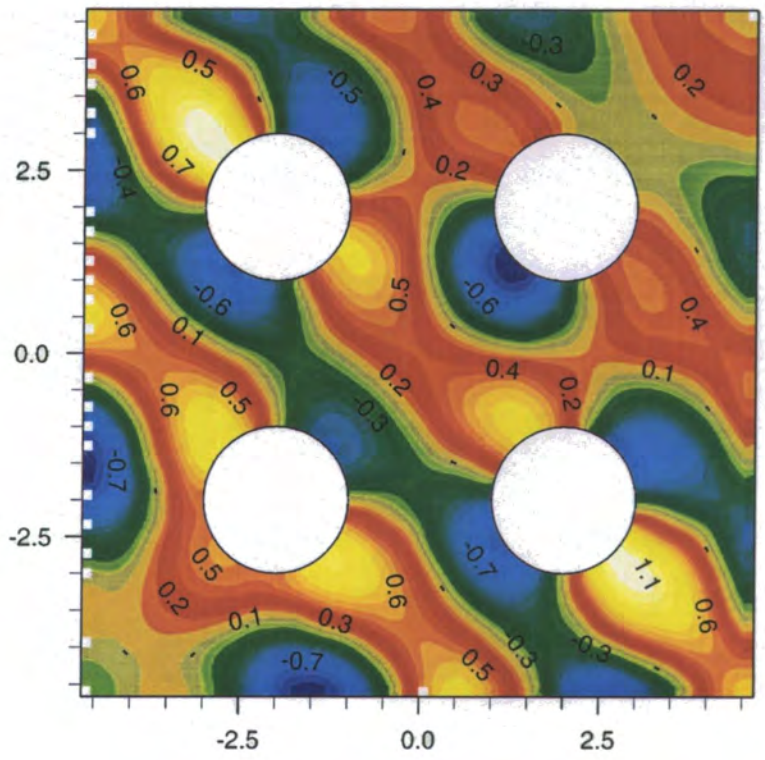

Figure 6.97: A contour plot of the non-dim. free-surface elevations around the cylinders, real part of F/IE solutions ($ka = 2$, $\theta_I = 45^o$)

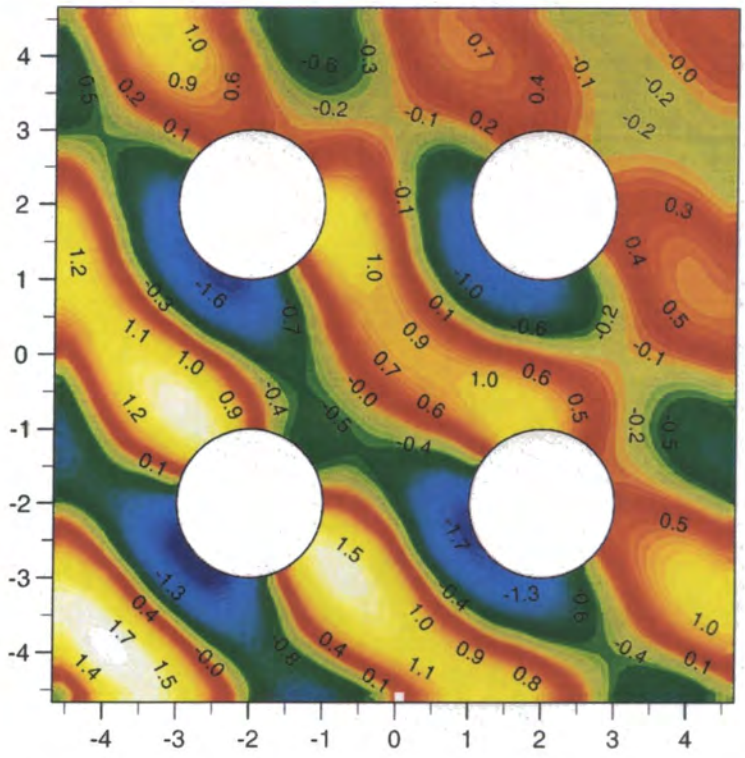

Figure 6.98: A contour plot of the non-dim. free-surface elevations around the cylinders, imaginary part of analytical solutions ($ka = 2$, $\theta_I = 45^o$)

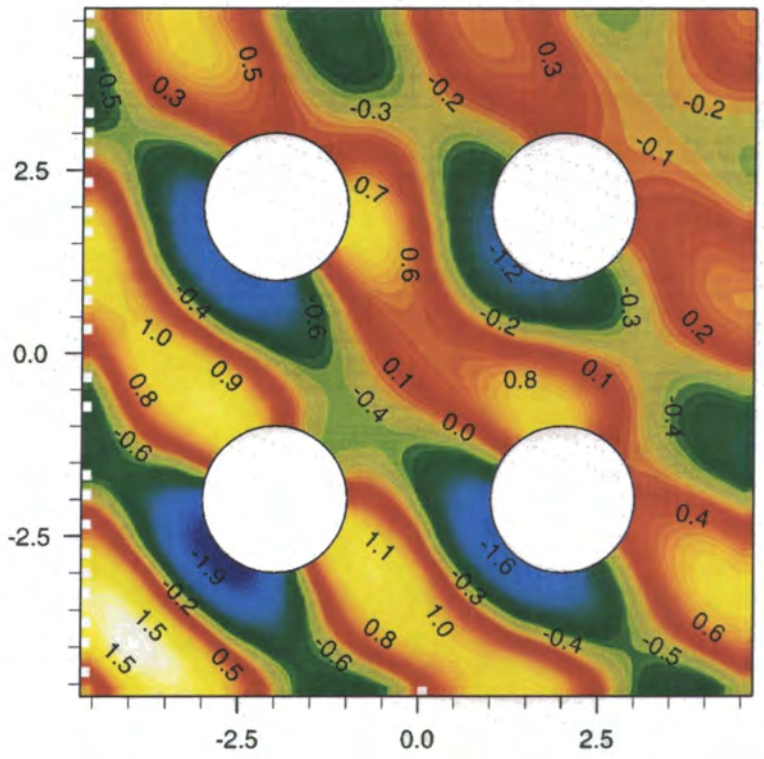

Figure 6.99: A contour plot of the non-dim. free-surface elevations around the cylinders, imaginary part of F/IE solutions ($ka = 2$, $\theta_I = 45^o$)

2 by 3 array of risers

A 2 by 3 array of equally spaced vertical circular risers (six identical cylinders with radius a), associated with a British Gas jacket structure in the North Sea [27], standing in open water with a plane wave incident upon them was analysed. The parameters were as follows:

Incident wave amplitude	A=4 m
Water depth	d=20 m
Wave frequency	ω=1.0 rad/s
Angle of the incident wave	$\theta_I = 0^o$
Acceleration due to gravity	g=9.81 m/s^2

Risers radius, a=0.36 m

The corresponding nondimensional parameters are:

$$d/a=55.556$$

$$ka=0.038$$

A mesh of finite and infinite elements which consists of 524 elements (1663 nodes) is illustrated in Figure 6.100. Contour plots of real and imaginary parts of the analytical free surface elevations around the cylinders are shown in Figures 6.101 and 6.103 and their equivalent F/IE solutions are shown in Figures 6.102 and 6.104. A good agreement between the analytical and F/IE solutions can be observed (note that the key to the real part of the F/IE solutions is different from the one to the analytical solutions).

For this real industrial problem the actual, rather than dimensionless, values of the free-surface elevations have been plotted. As can be seen the incident wave shows hardly any diffraction by the presence of the risers because the diffraction

parameter is very small ($ka = 0.038 << 0.2\pi$). Also $\frac{A}{D} = \frac{4}{0.72} > 0.75$. Hence for design purposes the viscous effect, which is dominant in this case, should be considered.

The same mesh, Figure 6.100, was then used to solve the problem for a larger ka ($= 0.72 > 0.2\pi$). Contour plots of real and imaginary parts of the non-dimensional. analytical free surface elevations around the cylinders are shown in Figures 6.105 and 6.107 and their equivalent F/IE solutions are shown in Figures 6.106 and 6.108. The figures show that unlike the previous example the pattern of the incoming wave has been significantly altered by the presence of the risers. The agreement between the analytical and F/IE solutions is reasonable but not as good as before. More finite element nodes are needed to achieve a better agreement. A three-dimensional view of the F/IE free surface elevations is shown in Figure 6.109 and 6.110.

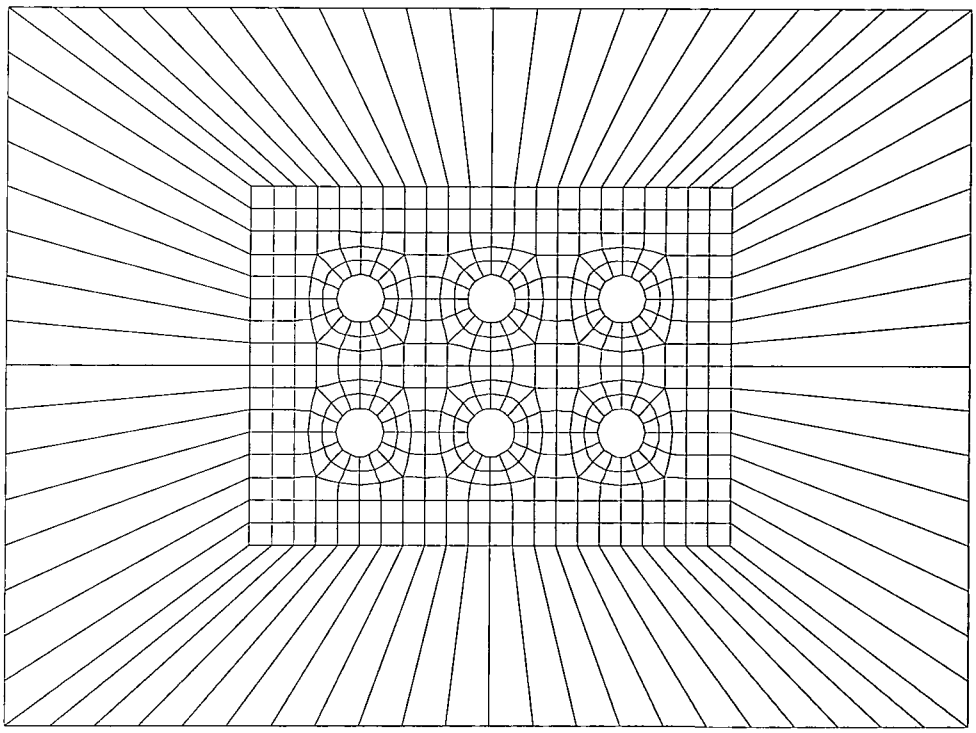

Figure 6.100: Mesh of finite and Type 3 infinite elements for 2 by 3 array of risers, a=0.36

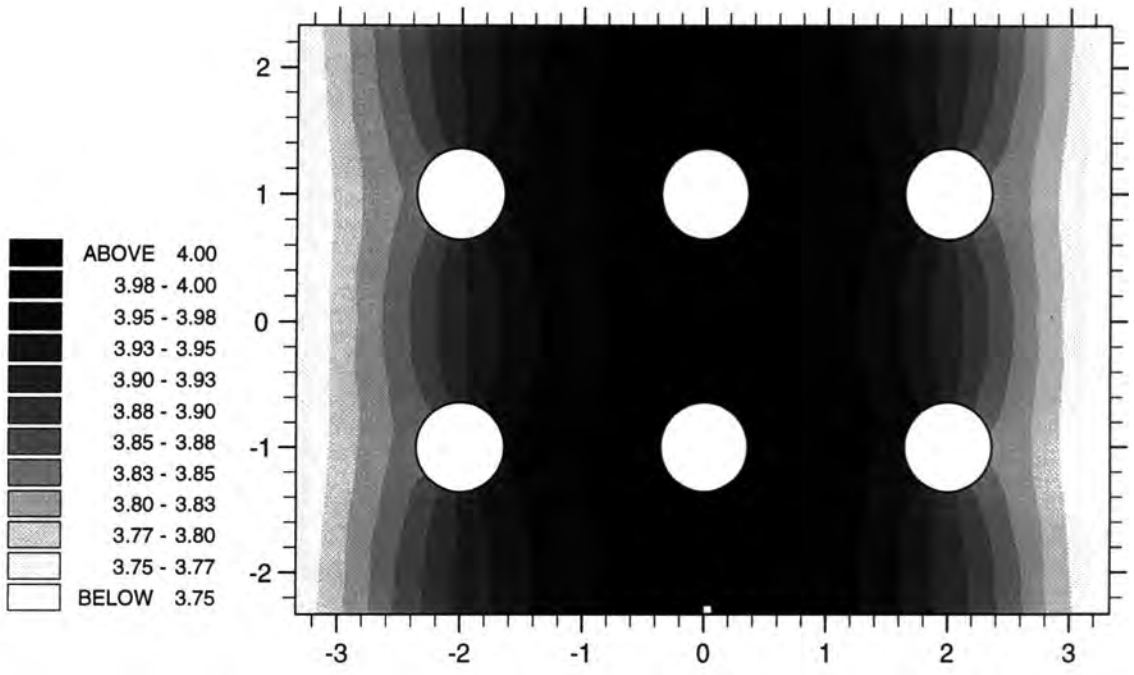

Figure 6.101: A contour plot of the free surface elevation around the cylinders, real part of the analytical solutions ($ka = 0.04$, $\theta_I = 0^o$)

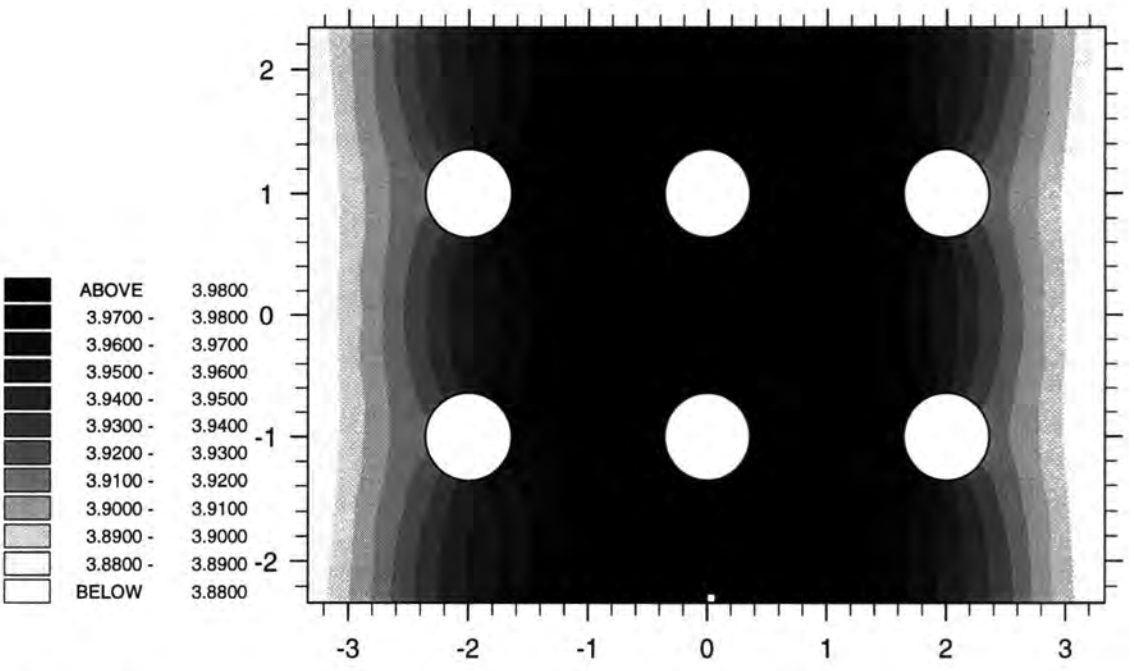

Figure 6.102: A contour plot of the free surface elevation around the cylinders, real part of F/IE solutions ($ka = 0.04$, $\theta_I = 0^o$)

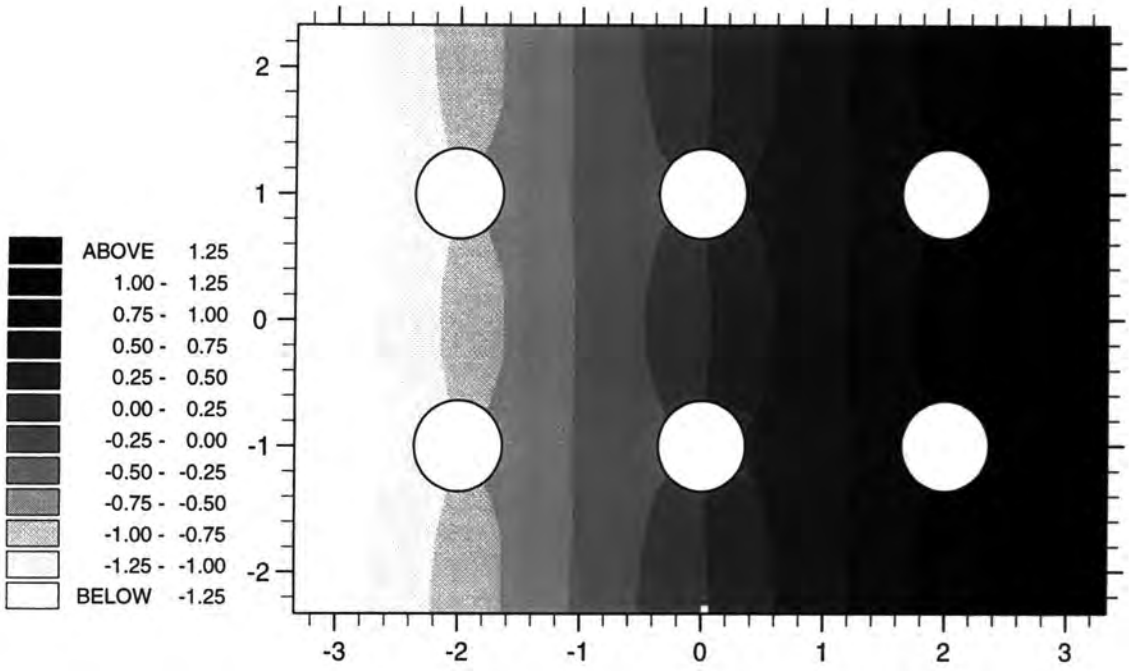

Figure 6.103: A contour plot of the free surface elevation around the cylinders, imaginary part of analytical solutions ($ka = 0.04$, $\theta_I = 0^o$)

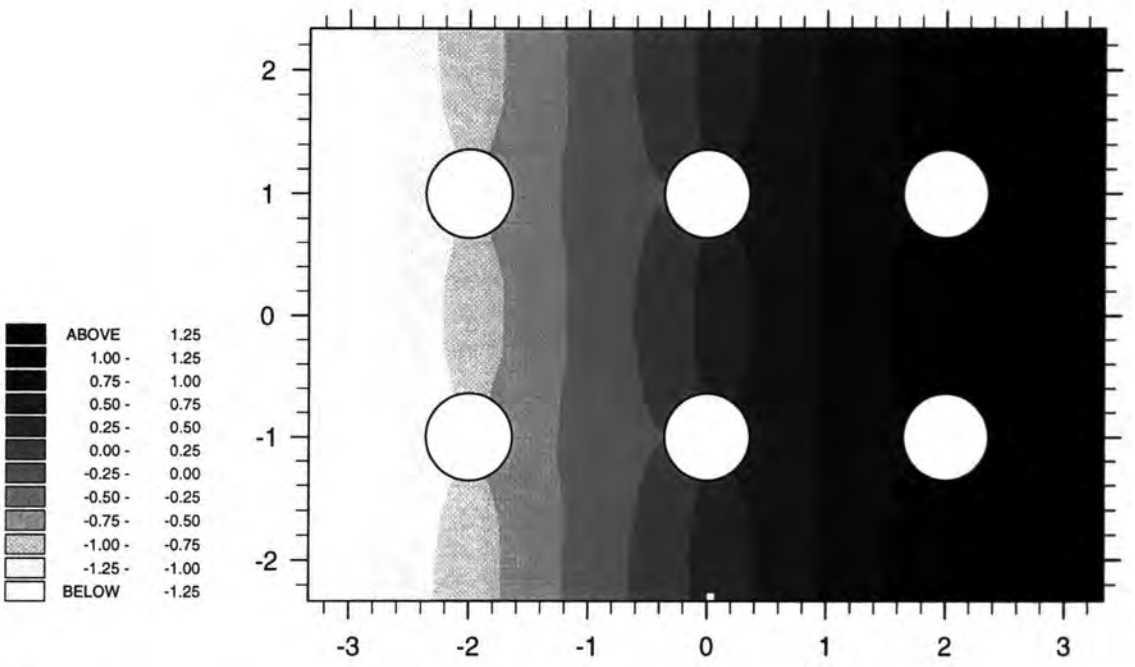

Figure 6.104: A contour plot of the free surface elevation around the cylinders, imaginary part of F/IE solutions ($ka = 0.04$, $\theta_I = 0^o$)

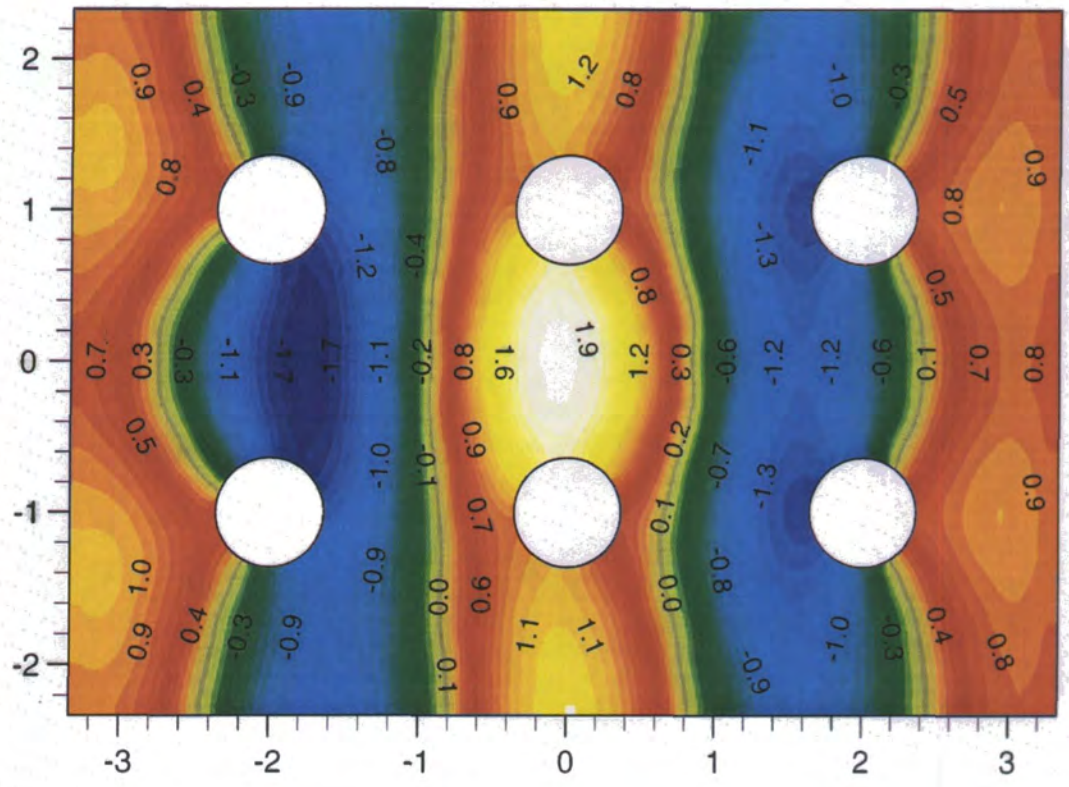

Figure 6.105: A contour plot of the non-dim. free surface elevation around the cylinders, real part of the analytical solutions ($ka = 0.72$, $\theta_I = 0^o$)

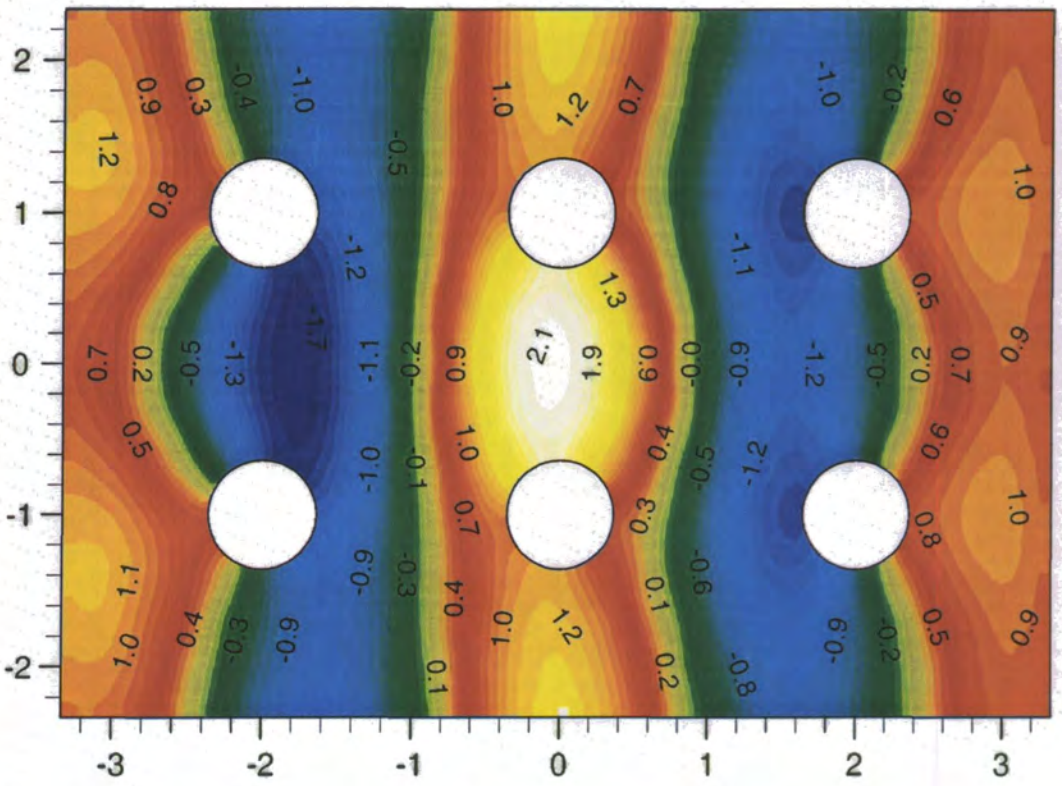

Figure 6.106: A contour plot of the non-dim. free surface elevation around the cylinders, real part of F/IE solutions ($ka = 0.72$, $\theta_I = 0^o$)

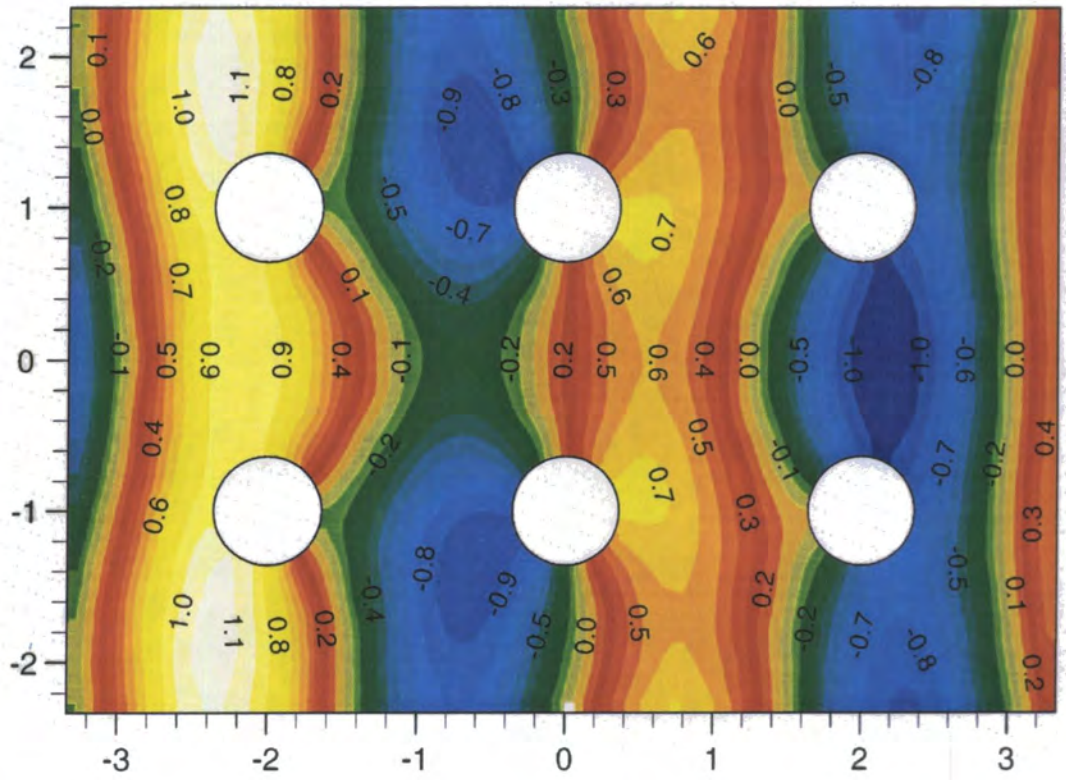

Figure 6.107: A contour plot of the non-dim. free surface elevation around the cylinders, imaginary part of analytical solutions ($ka = 0.72$, $\theta_I = 0^o$)

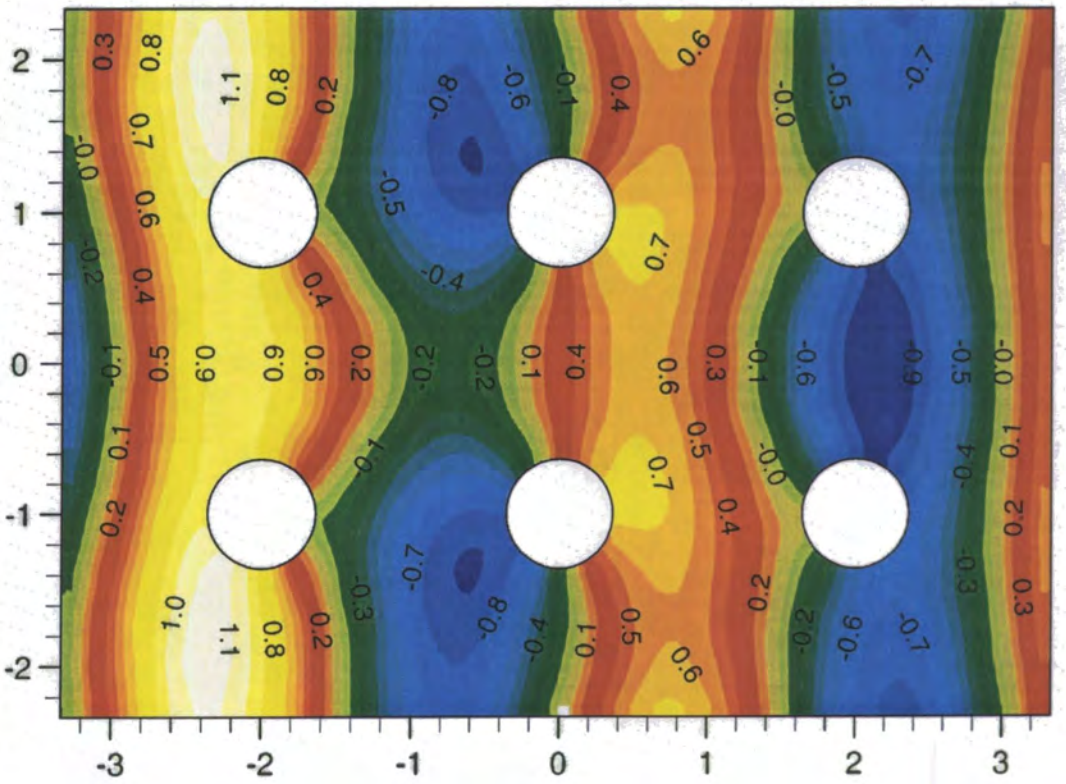

Figure 6.108: A contour plot of the non-dim. free surface elevation around the cylinders, imaginary part of F/IE solutions ($ka = 0.72$, $\theta_I = 0^o$)

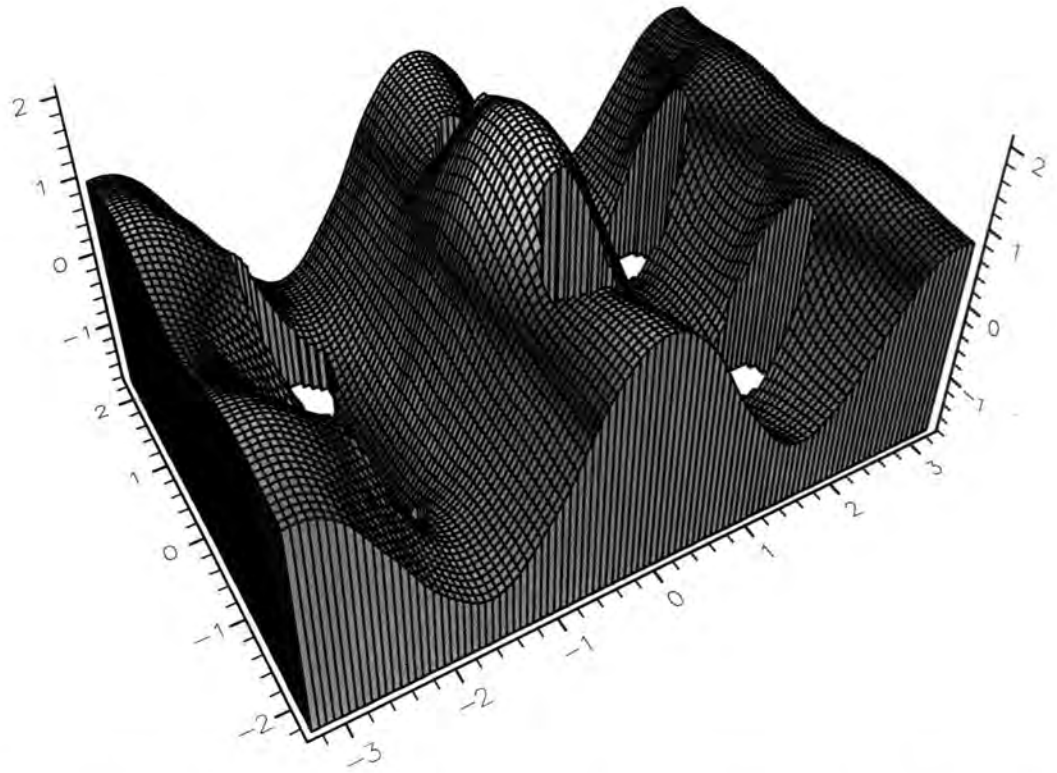

Figure 6.109: A three dimensional perspective view of the non-dim. free surface elevation, real part of F/IE solutions ($ka = 0.72$, $\theta_I = 0^o$)

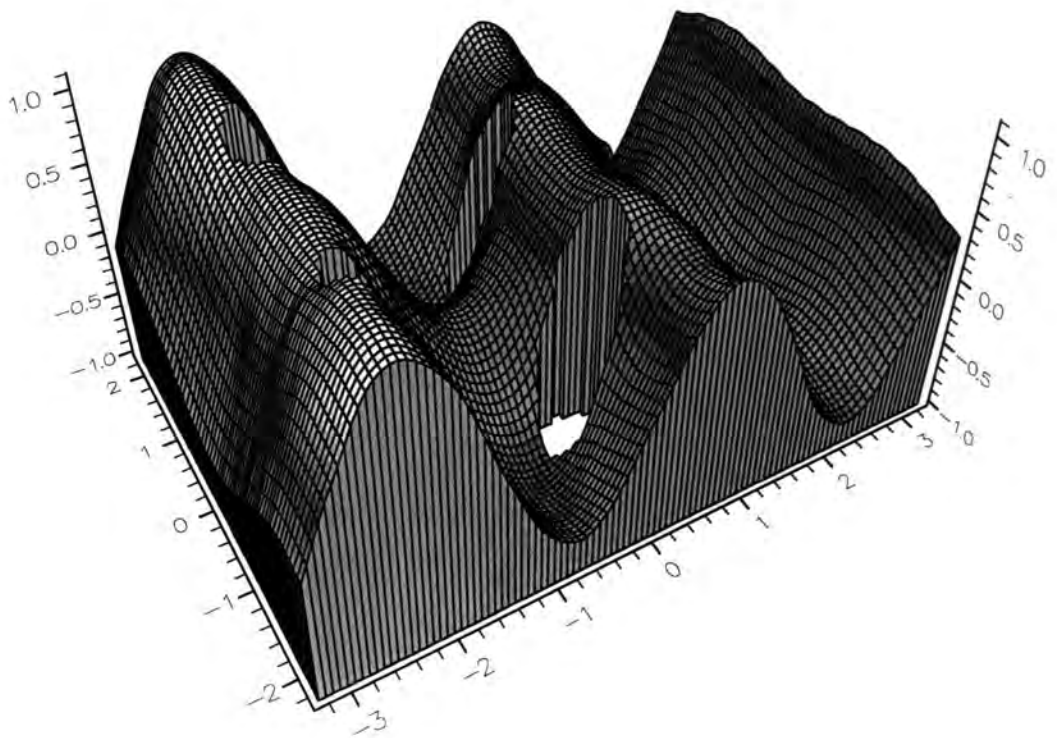

Figure 6.110: A three dimensional perspective view of the non-dim. free surface elevation, imaginary part of F/IE solutions ($ka = 0.72$, $\theta_I = 0^o$)

1 by 2 array of elliptical cylinders

Finally the problem of wave diffraction by multiple elliptical cylinders was considered. This can represent a number of enginering problems such as a pair of hulls. A 1 by 2 array of elliptical cylinders standing in shallow water with a plane wave incident upon them was analysed. The parameters were as follows:

$$b/a=3$$

$$d/a=1$$

$$\theta_I = 45^o$$

$$ka=0.2$$

A mesh of finite and infinite elements which consists of elements 328 (1031 nodes) is illustrated in Figure 6.111. Contour plots of real and imaginary parts of the F/IE solutions are shown in Figures 6.112 and 6.113.

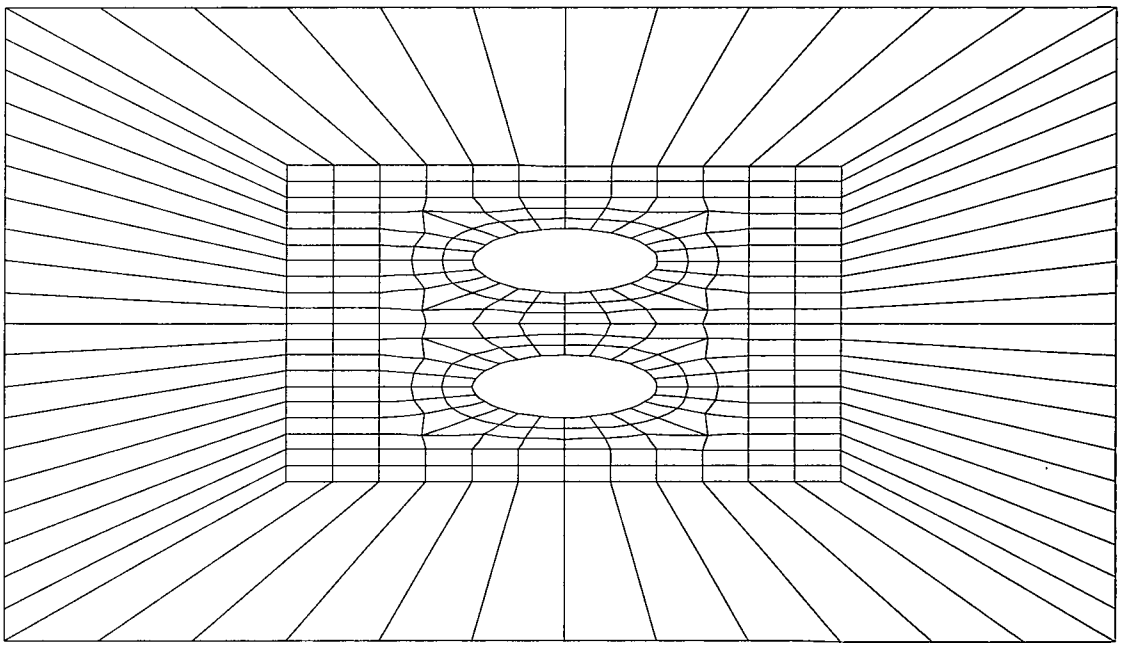

Figure 6.111: Mesh of finite and Type 3 infinite elements for 1 by 2 array of elliptical cylinders, b/a=3

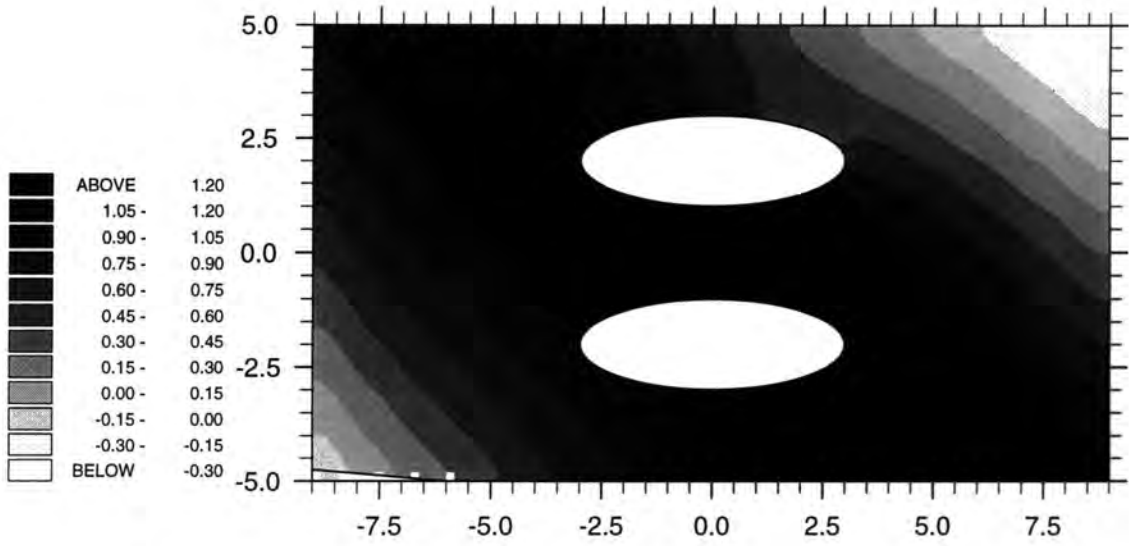

Figure 6.112: A contour plot of the non-dim. free-surface elevation around the cylinders, real part of F/IE solutions ($b/a = 3$, $ka = 0.2$, $\theta_I = 45^o$)

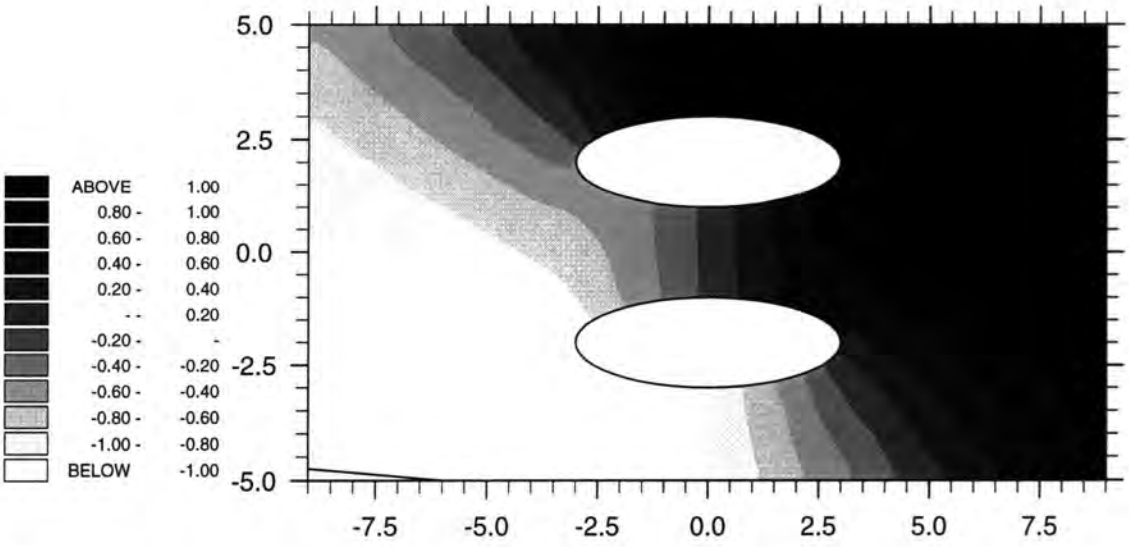

Figure 6.113: A contour plot of the non-dim. free-surface elevation around the cylinders, imaginary part of F/IE solutions ($b/a = 3$, $ka = 0.2$, $\theta_I = 45^o$)

6.5 Comparison of results obtained by three types of infinite elements

Three types of infinite elements, developed in this work, have been validated in the above sections. In this section, a comparison is made between the elements by solving example problems involving wave diffraction by circular and elliptical cylinders standing in shallow water with a plane wave incident upon them. The reason for choosing a shallow water problem is that the analytical solution for the elliptical cylinder problem given by Chen and Mei [39] is for this case. The wave diffraction parameter is selected to be small ($ka < 0.2\pi$) to minimize the errors resulting from finite elements, so that the three types of infinite elements can be compared correctly. The problem parameters were as follows:

$$d/a=1$$

$$\theta_I = 0^o$$

$$ka=0.2$$

First the problem of wave diffraction by a vertical circular cylinder of radius one unit was analysed using the three types of infinite elements. Coarse meshes of finite and infinite elements are illustrated in Figures 6.114 and 6.115. The real and imaginary parts of the relative errors in the calculation of surface elevations on the cylinder are plotted in Figure 6.116 and 6.117. The Type 1 infinite element appears to give the best results.

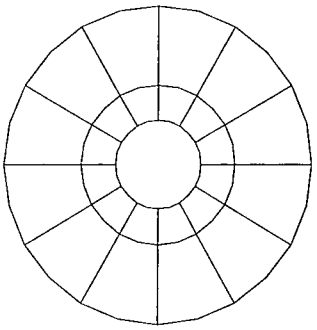

Figure 6.114: Mesh of finite and 6-node (Type 1/Type 3) infinite elements for circular cylinder

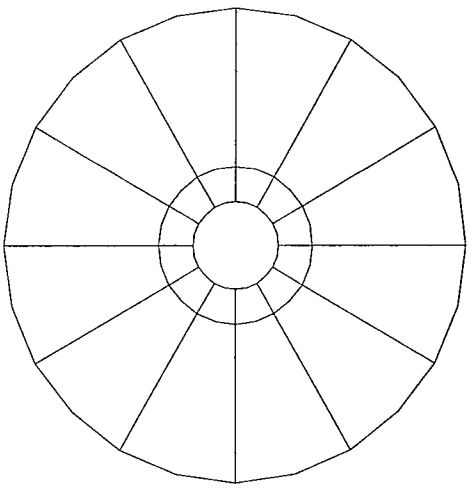

Figure 6.115: Mesh of finite and 9-node (Type 2) infinite elements for circular cylinder

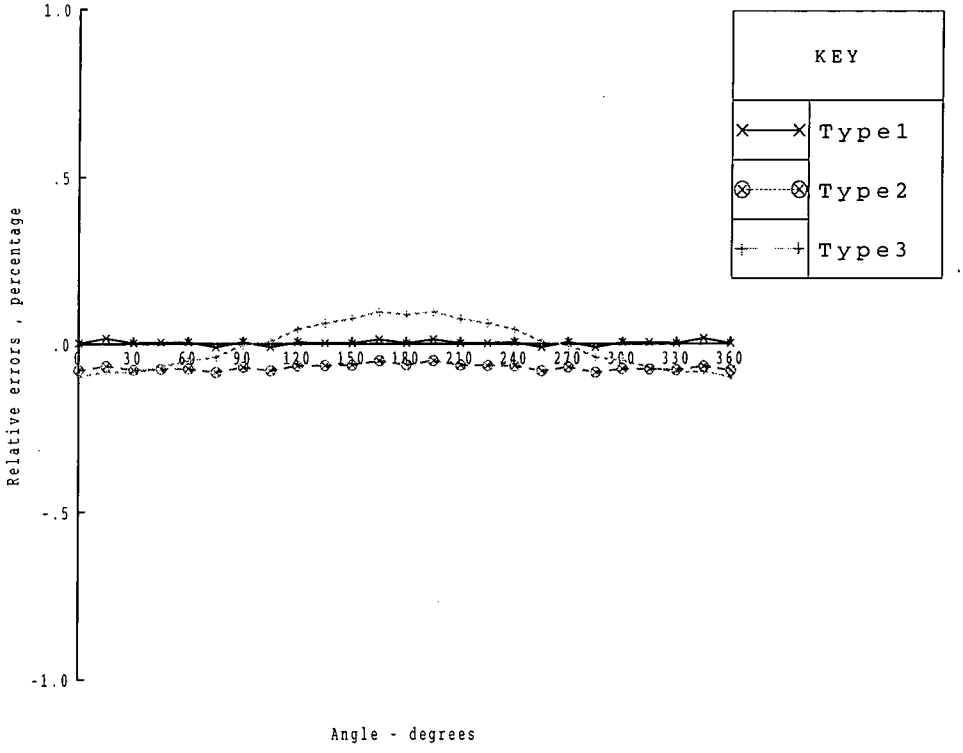

Figure 6.116: Comparison of errors in imaginary part of the solutions produced by 3 types of infinite elements

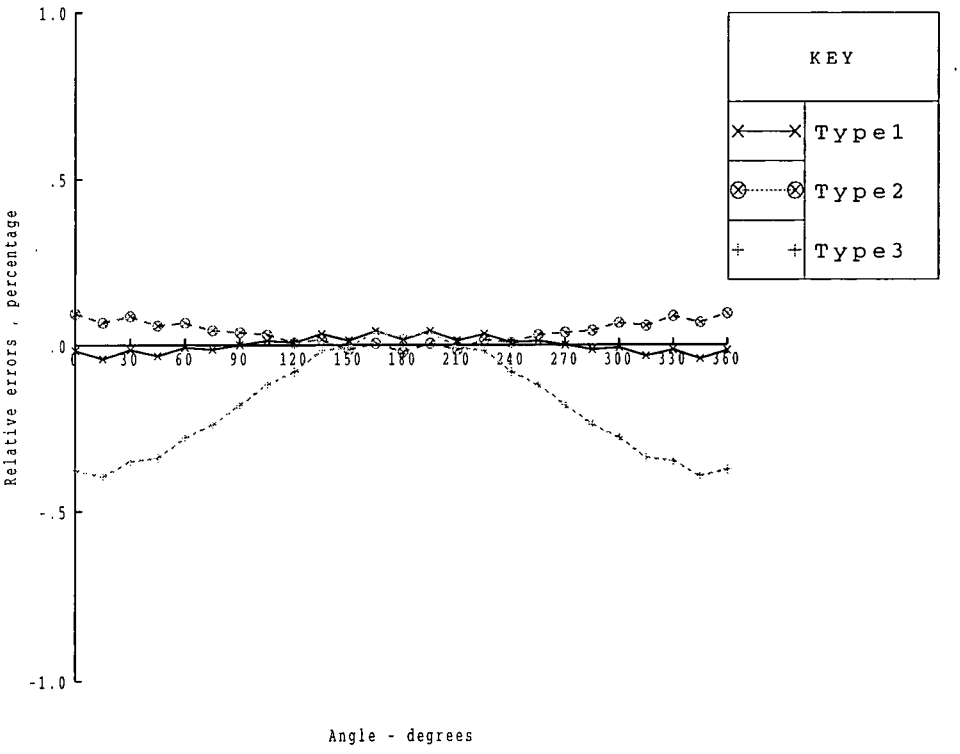

Figure 6.117: Comparison of errors in real part of the solutions produced by 3 types of infinite elements

Next the problem of wave diffraction by a vertical elliptical cylinder of aspect ratio 2 was analysed using the three types of infinite elements. Coarse meshes of finite and infinite elements are illustrated in Figures 6.118 and 6.119. The real and imaginary parts of the relative errors in the calculation of surface elevations on the cylinder are plotted in Figure 6.120 and 6.121. Again the Type 1 infinite element appears to give the best results.

Finally the aspect ratio of the ellipse was chosen to be 10. Coarse meshes of finite and infinite elements are illustrated in Figures 6.122 and 6.123. The real and imaginary parts of relative errors in the calculation of surface elevations on the cylinder are plotted in Figure 6.124 and 6.125. Again the Type 1 infinite element appears to give the best results. The finer meshes are illustrated in Figures 6.126 and 6.127. The real and imaginary parts of the relative errors in the calculation of surface elevations on the cylinder are plotted in Figure 6.128 and 6.129 which show that all three types of infinite elements give more or less the same results.

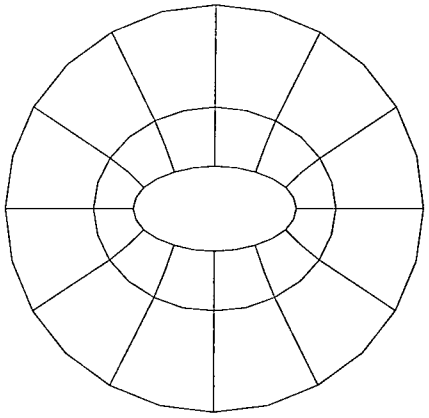

Figure 6.118: A coarse mesh of finite and 6-node (Type 1/Type 3) infinite elements for elliptical cylinder, b/a=2

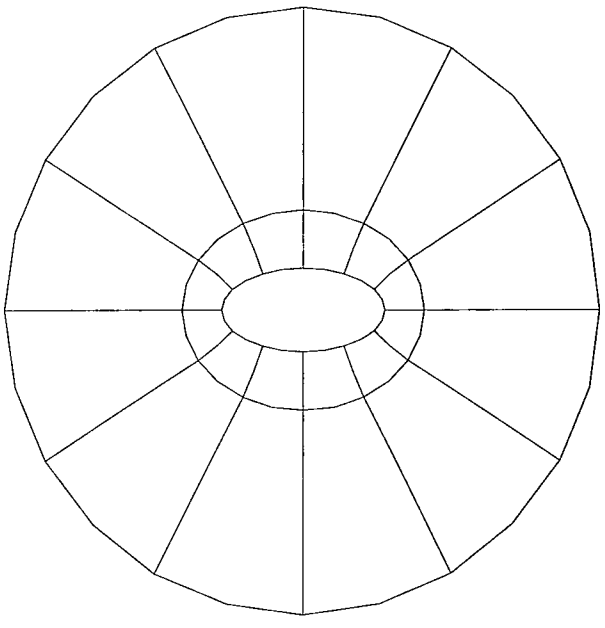

Figure 6.119: A coarse mesh of finite and 9-node (Type 2) infinite elements for elliptical cylinder, b/a=2

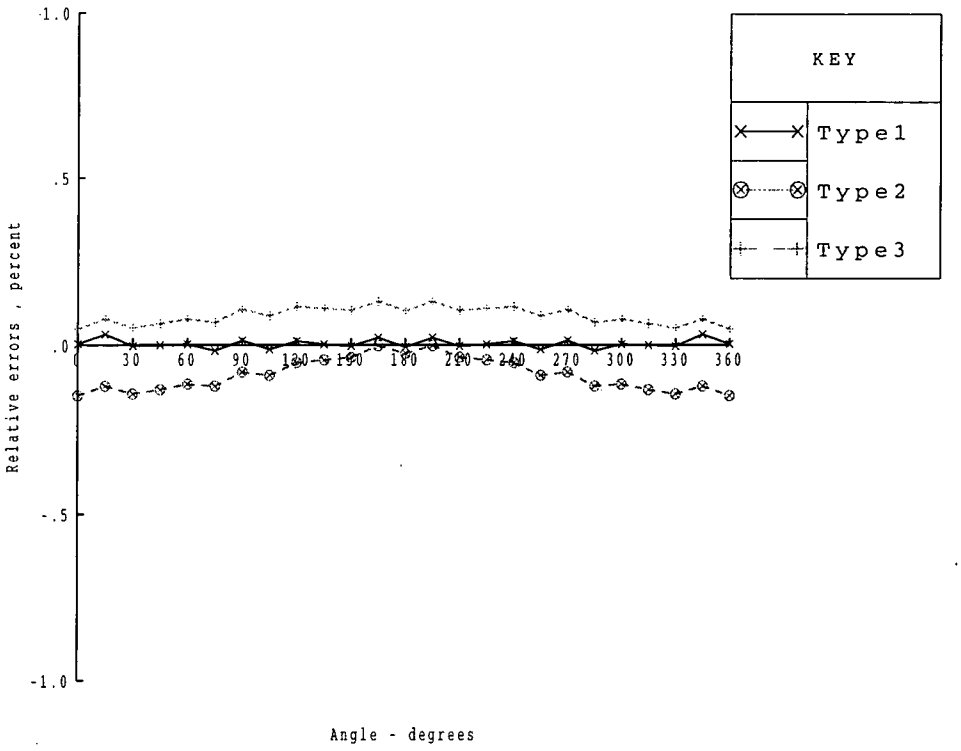

Figure 6.120: Comparison of errors in real part of the solutions produced by 3 types of infinite elements (b/a=2, $\theta_I = 0^o$)

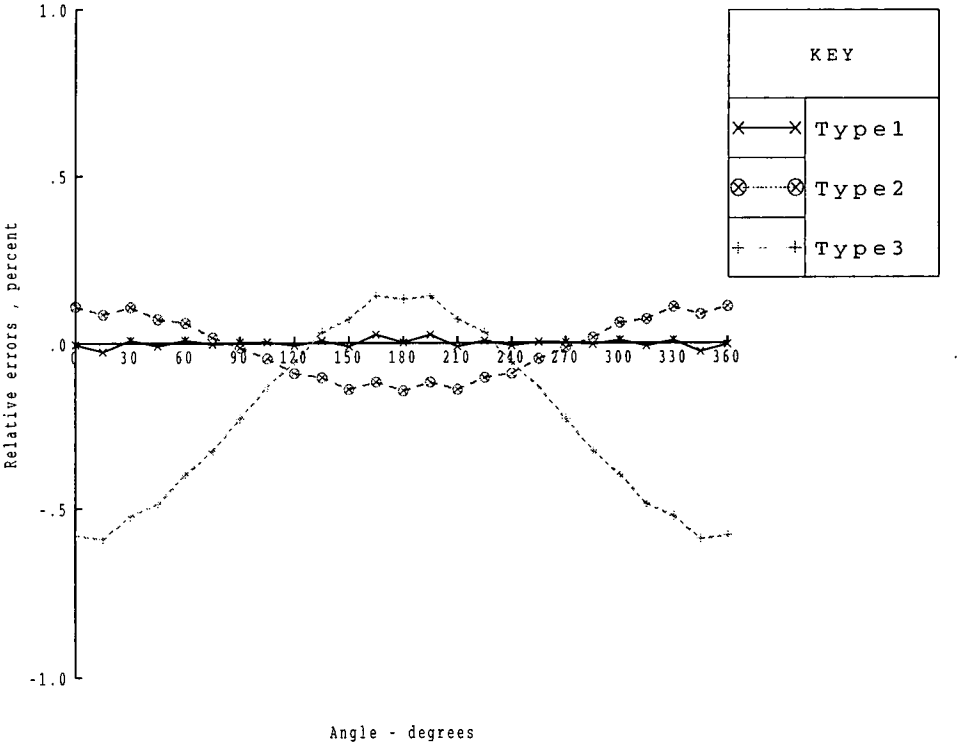

Figure 6.121: Comparison of errors in imaginary part of the solutions produced by 3 types of infinite elements (b/a=2, $\theta_I = 0^o$)

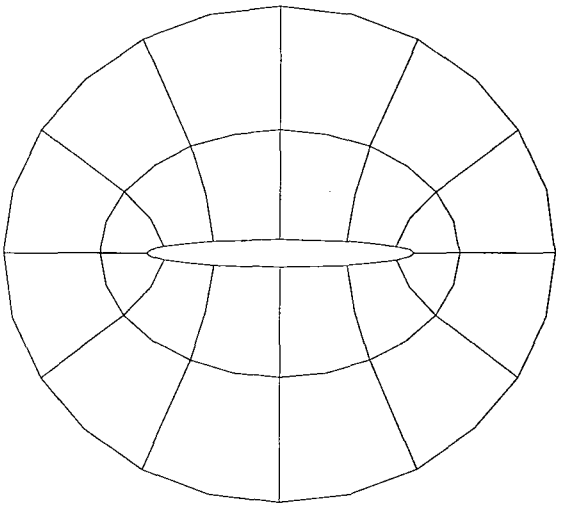

Figure 6.122: A coarse mesh of finite and 6-node (Type 1/Type 3) infinite elements for elliptical cylinder, b/a=10

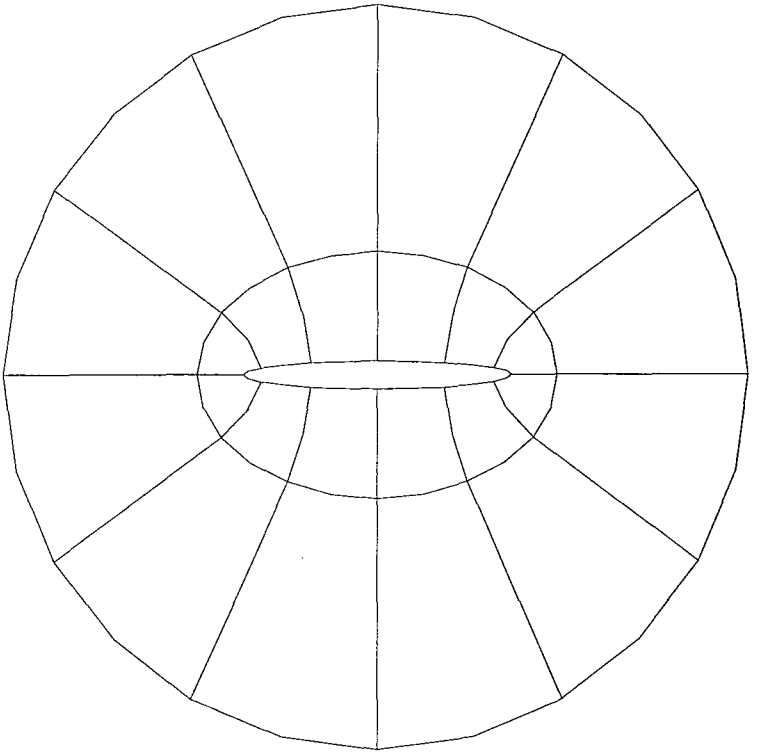

Figure 6.123: A coarse mesh of finite and 9-node (Type 2) infinite elements for elliptical cylinder, b/a=10

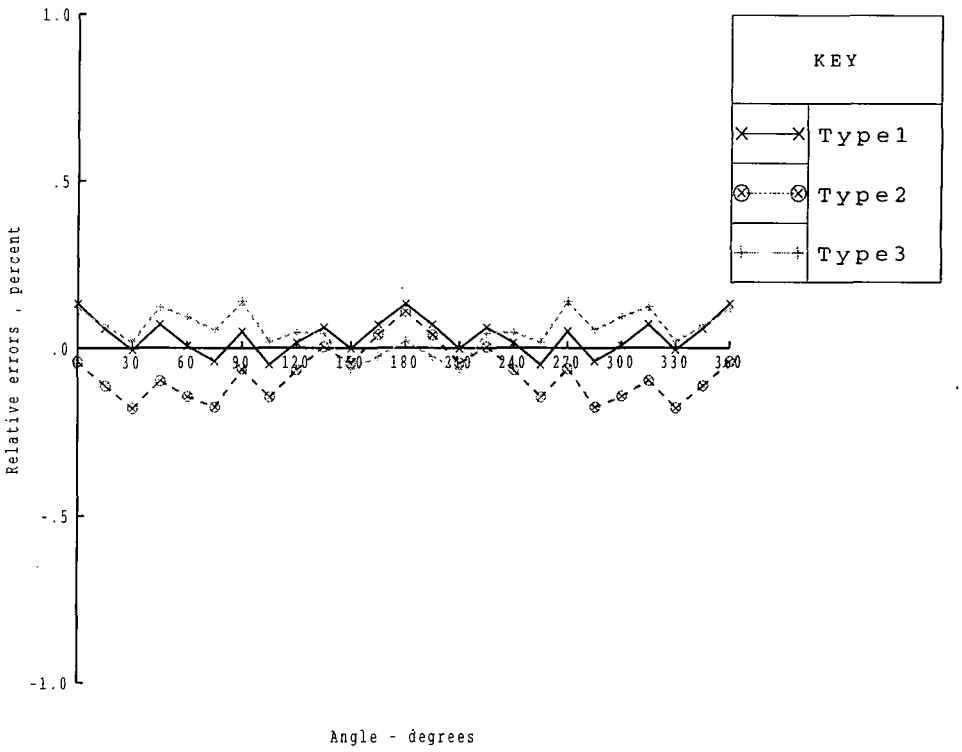

Figure 6.124: Comparison of errors in real part of the solutions produced by 3 types of infinite elements (b/a=10, $\theta_I = 0^o$)

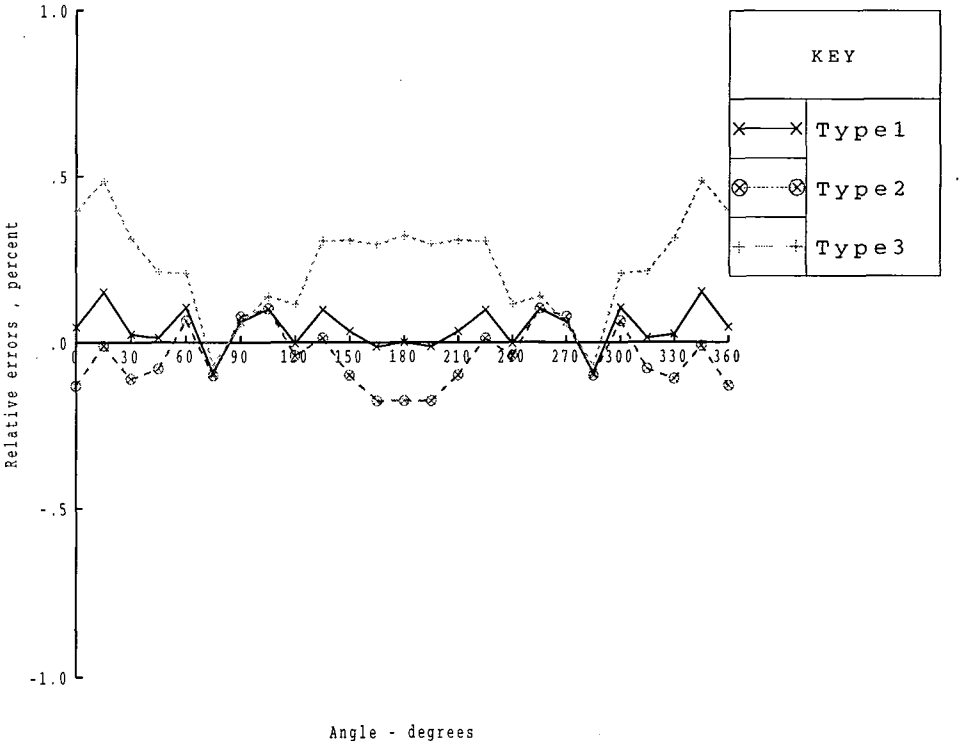

Figure 6.125: Comparison of errors in imaginary part of the solutions produced by 3 types of infinite elements (b/a=10, $\theta_I = 0^o$)

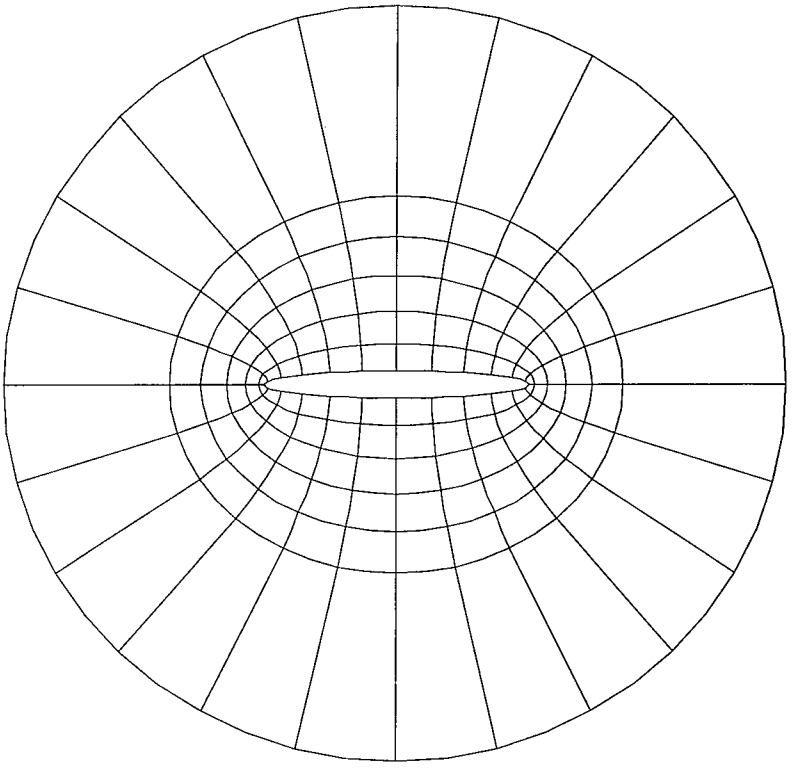

Figure 6.126: A finer mesh of finite and 6-node (Type 1/Type 3) infinite elements for elliptical cylinder, b/a=10

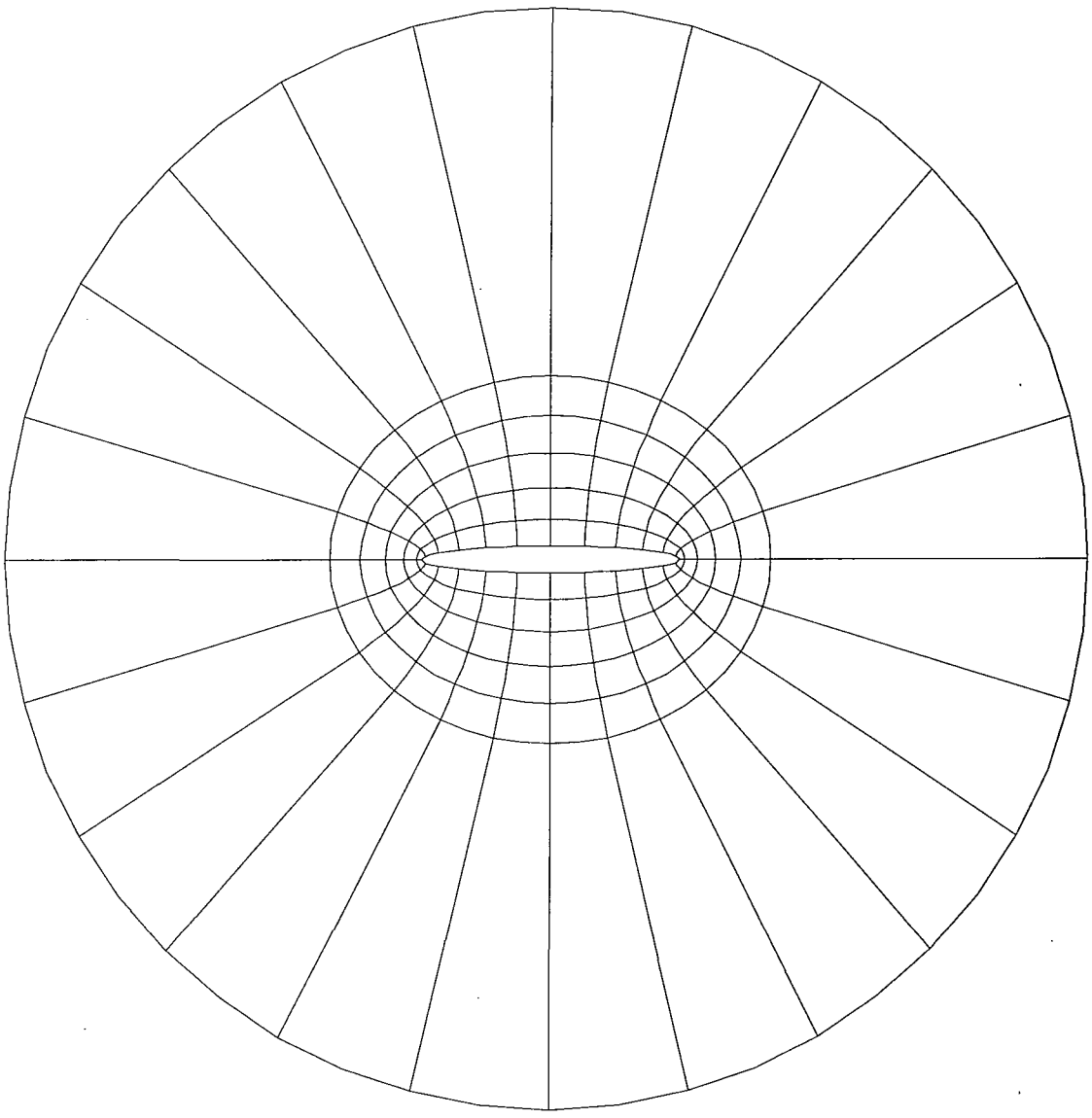

Figure 6.127: A fine mesh of finite and 9-node (Type 2) infinite elements for elliptical cylinder, b/a=10

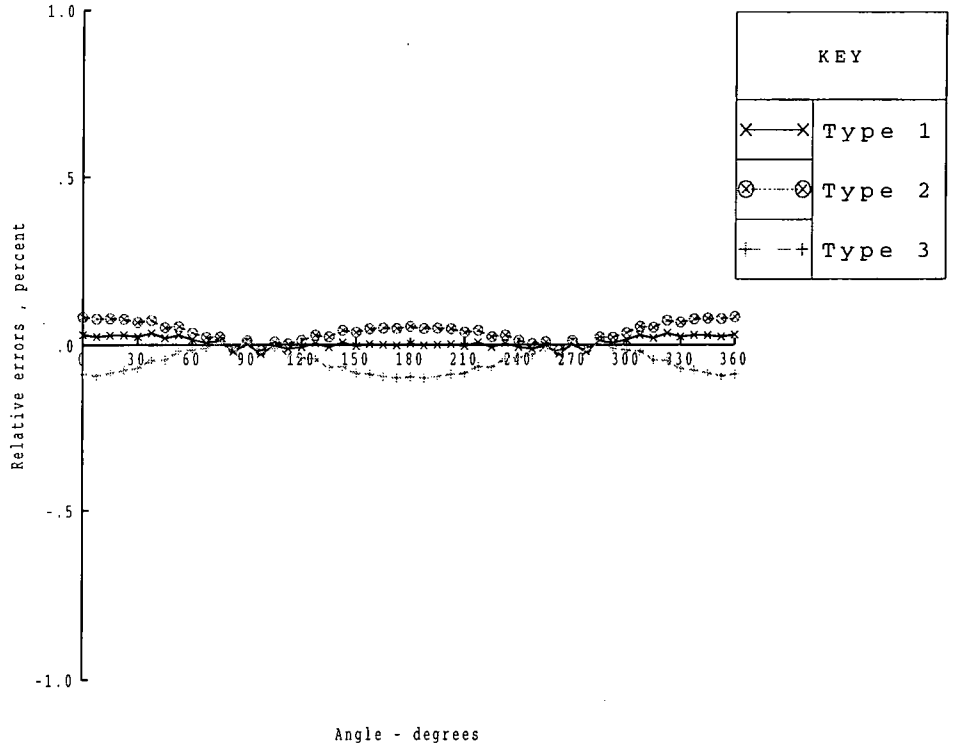

Figure 6.128: Comparison of errors in real part of the solutions produced by 3 types of infinite elements (b/a=10, $\theta_I = 0^o$)

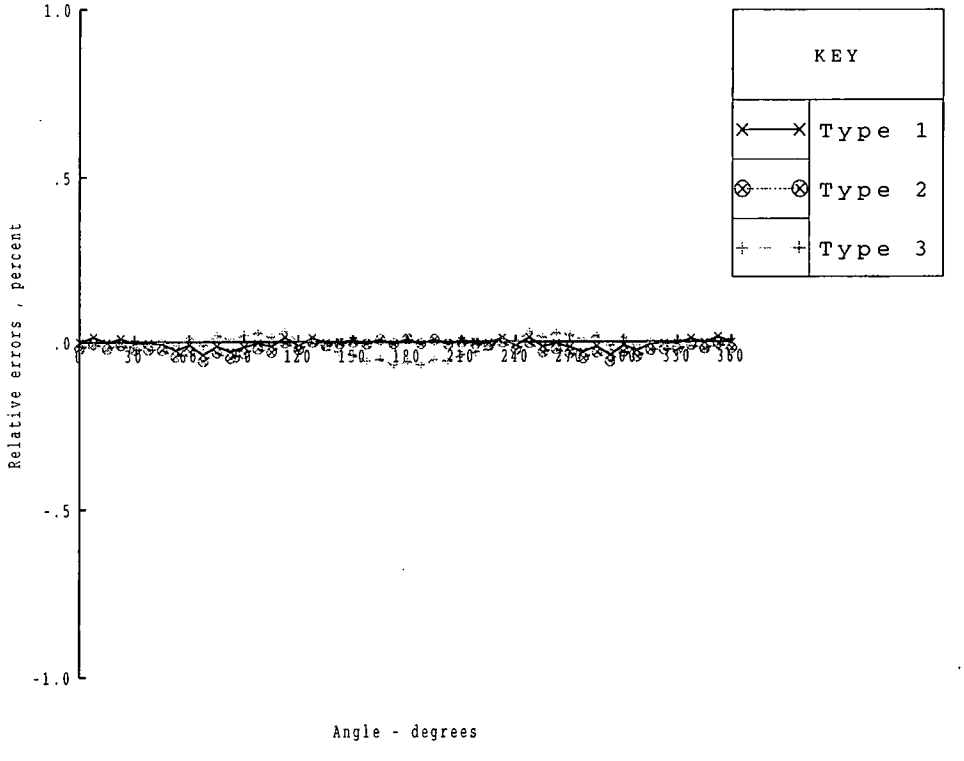

Figure 6.129: Comparison of errors in imaginary part of the solutions produced by 3 types of infinite elements (b/a=10, $\theta_I = 0^o$)

A comparison between the three types of infinite elements and CPU time of an HP series 730 workstation for solving the above example diffraction problem (ellipse with 10:1 aspect ratio modelled with a coarse mesh) can be found in the following table. As can be seen, for a given problem, the Type 1 infinite element method uses the least CPU time compared to the other types.

height

Different infinite elements	CPU time
Type 1	2.2 seconds
Type 2	7.3 seconds
Type 3	7.5 seconds

6.6 Summary

In this chapter, three types of infinite elements developed in this work have been validated using some special cases of wave diffraction problems for which analytical solutions exist. The predicted water surface elevations are compared with their equivalent analytical solutions. The errors in the calculation of the surface elevations on the diffracting objects have been calculated and plotted. A comparison is made between the contour plots of surface elevations predicted by F/IE models and their equivalent analytical solutions. Finally a comparison is made between the three types of infinite elements based on the errors and the CPU time in solving an example of a single body diffraction problem.

Chapter 7

Discussions, Concluding Remarks and Further Research

7.1 Introduction

The aim of this thesis has been to develop a series of infinite elements to be used in conjunction with conventional finite elements to solve the problem of wave diffraction by objects, in particular offshore structures. The first objective has been to improve the existing mapped infinite element, due to Zienkiewicz *et al* [102], so that it can model objects of large aspect ratio, say a submarine, more economically. The main objective has been to apply the idea of the wave envelope approach, due to Astley *et al* [9], to surface waves to develop a simple and efficient infinite element which gives accurate solutions both in the near and far fields.

A number of assumptions have been made to simplify the problem. They are

explained in chapter 2. Three main assumptions have been to reduce the problem to two-dimensions and to ignore the nonlinear and viscous effects. The governing equation has then become the well known Mild-Slope wave equation subjected to the natural and radiation boundary conditions.

The problem has been solved using the coupled finite and infinite element method. The unbounded solution domain has been divided into finite and infinite regions. Conventional finite elements have been used in the first region and infinite elements have been used in the latter region. Three types of infinite elements have been developed in this thesis.

Analytical solutions were presented in the literature for some special cases of water wave diffraction problems. They have been employed to validate the accuracy of the results produced by the infinite elements. All the analytical solutions presented in this thesis had been developed for water of constant depth and so the infinite elements have only been validated for the constant depth cases. If the time had been available it would have been possible to code other analytical solutions to validate the model for varying water depth problems.

7.2 Discussion of the results

The mapped infinite element presented originally by Zienkiewicz *et al* [102] is intended to be usable for solving diffraction of waves by any shape of the diffracting objects. It was assumed that the infinite elements were used on the exterior of a circle circumscribing the object. As Burnett [36] pointed out, for objects of

large aspect ratio this is computationally very inefficient which is contrary to the primary goal of introducing the infinite element. A remedy would be to use the infinite elements on the exterior of an ellipse circumscribing the object. However, as can be seen from Figures 6.5 and 6.6 the original formulation causes errors which will be more pronounced for objects with large aspect ratio, say 10. Therefore two approaches have been given in this thesis to remove the errors associated with the original formulation. The results illustrated in Figures 6.7 and 6.8 show that approach 1 gives very accurate results. It is very simple and easy to be inserted into existing codes, but it requires an assumption which is difficult to justify mathematically. As can be seen from Figures 6.9 and 6.10 approach 2 gives a robust solution to the problem reported by Burnett [36]. Therefore using approach 2, the mapped infinite element (Type 1) can now be applied to solve problems involving diffraction of waves by objects with large aspect ratio more economically. The solutions have been examined only for those located on the diffracting object. The parallel to Shirron's study [94] indicates that this formulation might produce very inaccurate solutions in the far field.

The next step was to develop a more simple infinite element (compared to the Type 1 infinite element) so that the complicated integration procedure would be avoided and at the same time would give accurate solutions both in the near and far fields. Furthermore, it can be used to model diffraction of waves by multiple bodies. Two more types of infinite elements emerged from this process.

The three types of infinite elements have then been validated and the discussion of their results is as follows:

Type 1 infinite elements appeared to give the best, i.e fastest and most accurate, results for a single circular and elliptical cylinder diffraction problems for solutions that are located on the diffracting object. This supports the comparison of unconjugated and conjugated infinite elements given by Shirron [94] (see chapter 1). It is faster, because, unlike Type 2 and Type 3, the resulting infinite element matrix is symmetric and hence only the half upper triangle of both finite and infinite elements matrices need to be calculated, stored and assembled into the global matrix equation which is solved to give the solutions. Therefore, a much smaller amount of computing resources are required to do the whole analysis. The reason for it being most accurate (for the solutions in the near field) is probably that a more correct rate of attenuation of wave amplitude towards infinity, i.e. $\frac{1}{\sqrt{r}}$, has been inserted into the shape and weighting functions.

The drawback of this infinite element, however, is that the computation of the element integrals, which involve complex exponential terms, is very complicated. The standard numerical integration schemes cannot be used to calculate these integrals and a new integration scheme is required (see e.g. Zienkiewicz *et al* [102]). Furthermore, this infinite element is very similar to Shirron's unconjugated infinite element [94], for which Shirron found that no reliable information about the solution can be achieved in the far field (i.e. outside the finite element domain).

The Type 2 infinite element solves the above problems by taking the weighting function to be the complex conjugate of the shape function so that the exponential terms cancel from the element integrals. Hence the standard Gauss-Legendre numerical scheme can be used to calculate the element integrals. Also this infi-

nite element is very similar to Shirron's conjugated infinite element [94], for which Shirron found that the solutions computed by the infinite element are accurate both in the near and far fields. The natural choice of the shape and weighting functions would be to use the Type 1 shape function and its complex conjugate. However as the line integral resulting from the integration by parts becomes undefined (see Appendix F), the shape and weighting functions are chosen such that the integrals, including the line integrals, are integrable (A similar problem was reported by Gerdes [59]). Hence the shape functions of some of the nodes decay like $\frac{1}{\sqrt{r}}$ and the others decay like $\frac{1}{\sqrt{r}}\frac{1}{r}$. Therefore the wave amplitude decays as a function of these two functions (see Appendix E)[1].

Results shown in Figures 6.120 and 6.121 show that for a single body diffraction problem, the errors are less than 0.2% but are slightly bigger than the ones using Type 1 infinite elements. This supports Shirron's finding [94]. The reason probably is that the shape function decays to zero more rapidly compared with Type 1 infinite elements. However, for a larger aspect ratio, Type 2 gives as accurate a result as Type 1 as shown in Figures 6.124 and 6.125. The disadvantage of this infinite element is that the element matrix is unsymmetric leading to an unsymmetric global matrix equation. This in turn means that more computing resources are required, compared to the Type 1 infinite element, to store and solve the global matrix equation. The Frontal solver employed in this study is slow. Other unsymmetric solvers, such as GMRES [23, 93], may be employed to decrease the computing time.

[1]However, the most accurate infinite element can be developed by choosing different shape functions for the different nodes of the element so that all the shape functions decay like $\frac{1}{\sqrt{r}}$ and at the same time the element line integrals remain integrable (see Appendix E).

The other drawback of this infinite element is that when formulating the element the outer boundary of infinite elements is taken as a circle. This could lead to some errors for problems in which this assumption can not easily be satisfied, such as the diffraction of waves by an array of diffracting objects. Thus a new, Type 3, infinite element has been developed.

For the Type 3 infinite element the shape function is chosen to be the same as the Type 1 infinite element shape function so that a slower rate of attenuation of wave amplitude towards infinity is considered. The weighting function is adopted such that the radiation matrix resulting from the line integral vanishes. Therefore the outer boundary of the infinite element is no longer required to be a circle. This infinite element, therefore, offers a more general solution to the wave diffraction problems. The only disadvantage of this infinite element is that the element matrix is unsymmetric which is similar to the situation for Type 2 infinite elements. Figures 6.120 and 6.121 show that the errors are slightly larger than the ones by using Types 1 and 2 infinite elements. As the shape function is chosen to be the same as the Type 1 shape function, this perhaps suggests that the selection of the weighting function, believed to be arbitrary, can also affect the solutions. Hence care must be taken when applying the method to other unbounded problems.

A drawback of all the three types of infinite elements is that the infinite element matrices are frequency-dependent and so the size of circumferential side (both inner and outer edges) of the elements must follow the usual rule of ten finite element nodes per wave length. This defect, as an example, is investigated for Type 1 infinite elements as is shown in Figures 6.2, 6.11, 6.12 and 6.13.

7.3 Concluding remarks

The new infinite elements presented in this thesis can now be used to solve the two-dimensional problem of diffraction of linear water wave by objects very accurately and economically. They have been validated using some known analytical solutions. This thesis will enable researchers as well as software engineers to use the new infinite elements in conjunction with conventional finite elements to solve their unbounded wave problems easily and economically. These ideas may be applied to other scientific and practical unbounded problems. The following recommendations may be made for using and developing infinite elements:

- Care should be taken in selecting both the shape and weighting functions for the infinite elements. A prior mathematical or experimental knowledge of the behaviour of the solution would help in this process.

- As the infinite elements are stretched to infinity in the radial direction, the size of the element in the circumferential direction requires the usual rule of ten finite element nodes per wavelength.

- A coarse mesh of finite and infinite elements gives good results. To get the best results Type 2 and 3 infinite elements should be placed at least half a length of the object away from it. However, this is not definitive and needs more investigation.

The results presented in chapter 6 show that the new infinite elements developed in this thesis can be used to solve the problem of wave diffraction by objects of any shape with some confidence. They show that all three types of infinite elements

can give accurate results for a given single diffracting object with less than 1.0% error for solutions on the object. Type 1 would be a preferable choice in situation where computing resource is the main concern and the reliable solutions are only required for the near field. Type 2 or 3 would be preferable choices when reliable solutions are required both in the near and far fields. Type 3 is the most suitable choice for modelling any number of arrays of individual geometries, number and configuration of bodies very accurately.

7.4 Further research

Although all three types of infinite elements presented here can now be used to solve problems of water wave diffraction with some confidence, there remain certain areas which would particularly benefit from further investigation. Recommendations for further research are listed below:

- The work should be extended to calculate other physical quantities of interest, particularly the hydrodynamic forces. This would make possible a more direct comparison between the numerical and experimental results.

- Although the finite/infinite element model has been developed for gradually varying water depth problems, it has only been validated for constant water depth problems. Therefore, further investigation is required to verify the model for problems with variable water depth.

- Trials should be conducted to investigate the accuracy of the solutions away from the diffracting objects, for all 3 types of infinite elements.

- A detailed comparative study is required to indicate in a wide variety of situations which of the infinite elements is most suitable.

- The application of the model to non-linear wave (steep wave) diffraction problems is another desired area for future research.

- Further work is required so as to employ a faster unsymmetric solver, such as GMRES. This would be more essential for a 3D model using Type 2 or Type 3 infinite elements.

- The extension of the infinite element to three dimensions is theoretically straight forward. More general problems can then be tackled. The sea bed friction effects (linear or nonlinear) can then be considered. Furthermore, floating bodies, such as a ship, may also be modelled.

- A demanding task for research would be to investigate the interaction of waves and current which makes the model more practical. This is mathematically straight forward. An extra term needs to be added to the governing equation (see e.g. Kirby [74]).

- Another direction for the research would be to develop a 3D infinite element to include the evanescent modes as well as the propagation modes which would offer the possibility of smaller three-dimensional meshes of elements, resulting in computational economies.

- There are many other scientific or practical problems with unbounded domain that can be solved using coupled finite and infinite elements, such as geo-mechanical or aerospace engineering problems.

Bibliography

[1] Abramowitz M. and Stegun I.A., *Handbook of Mathematical Functions*, Dover Publications Inc., New Yourk, 1965.

[2] Anderson D.L., Ungless R.L., 'Infinite Finite Elements', Intetrnational Symposium on Innovative Numerical Analysis in Applied Engineering Science, France, (1977).

[3] Astley R.J., 'Mapped Spheroidal Wave-Envelope Elements for Unbounded Wave Problems' , *International Journal for Numerical Methods in Engineering*, **41**, pp. 1235-1254, (1998).

[4] Astley R.J., 'Transient Wave Envelope Elements for Wave Problems', *Journal of Sound and Vibration*, **192**(1), pp. 245-261, (1996).

[5] Astley R.J., Macaulay J. and Coyette J.P., 'Mapped Wave Envelope Elements for Acoustical Radiation and Scattering', *Journal of Sound and Vibration*, **1**, pp. 97-118, (1994).

[6] Astley R.J. and Coyette J.P., 'Applications of Wave Envelope Elements to Acoustic Scattering', *Computational Acoustics*, **1**, pp. 145-161, (1993).

[7] Astley R.J., Bettess P. and Clark P.J. 'Letter to the editor' concerning Ref. [102], *International Journal for Numerical Methods in Engineering*, **32**, p.p. 207-209, (1991).

[8] Astley R.J., 'Wave Envelope and Infinite Elements for Acoustical Radiation', *International Journal for Numerical Methods in Fluids*, **3**, pp. 507-526, (1983).

[9] Astley R.J. and Eversman W., 'A Note on the Utility of a Wave Envelope Approach in Finite Element Duct Transmission Studies', *Journal of Sound and Vibration*, **76**, pp. 595-601, (1981).

[10] Atalianis C.A., 'Hydrodynamic Analysis of Structures by a Hybrid Method', *PhD thesis*, University of Newcastle uopn Tyne, UK, 1995.

[11] Atalianis C.A., 'Wave Forces on a Vertical Cylinder of Elliptical Shape', B.Eng. final year thesis, Dept. of Marine Tech., University of Newcastle upon Tyne, UK, 1990.

[12] Athanassoulis G.A., Belibassakis K.A.,'Water-Wave Green's Function for a 3D Uneven-Bottom Problems with Different Depths at $x \to +\infty$ and $x \to -\infty$, In: T. Geers, 'IUTAM Symposium on Computational Methods for Unbounded Domains', University of Colorado, USA, July 1997.

[13] Baghbani A., 'Comparative Study of Accuracy of Infinite Elements in Wave Diffraction Problems', Report prepared for the University of Durham, Durham, England, UK, 1995.

[14] Baghbani A., 'Infinite Mapped Wave Envelope Element for Unbounded Wave Problems', 17th International Conference on Ofshore Mechanics and Arctic Engineering, Lisbon, Portugal, July (1998).

[15] Baghbani A. *et al*, 'Modelling Wave Diffraction by Multiple Bodies Using Wave Envelope Infinite Elements', *Applied Ocean Research*, to be submitted.

[16] Bai K.J. snd Yeung R. 'Numerical solutions of free surface flow problems', *Proc. of 10th Symp. Naval Hydrodyn.*, Office Naval Res., Cambridge, Mass., pp. 609-647 (1974).

[17] Bando K, Sonu C.J., Grace P and Davidson D.D., 'Evalutaion of State-of-Art Numerical Models for the Analysis of Floating Breakwater', Proc. Ocean Structural Dynamics Symposium, Oregon State University, Corvallis, Oregon, USA, Sept. 9-11, 1986.

[18] Bando K. ,Bettess P. and Emson C., 'The Effectiveness of Dampers for the Analysis of Exterior Scalar Wave Diffraction by Cylinders and Ellipsoids', *International Journal for Numerical Methods in Fluids*, **4**, pp. 599-617, (1984).

[19] Beer G. and Meek J.L., 'Infinite Domain Elements', *International Journal for Numerical Methods in Engineering*, **17**, pp. 43-52, (1981).

[20] Berkhoff J.C.W., *Mathematical Models for Simple Harmonic Linear Water Waves Wave Diffraction and Refraction*, Delft Hydraulics Laboratory, Netherland, 1976.

[21] Berkhoff J.C.W., 'Linear Wave Propagation Problems and the Finite Element Method', In *Finite Elements in Fluids*, Eds. Gallagher R.H., Oden J.T., Taylor C., and Zienkiewicz O.C., **1**, pp. 251-280, Chichester, Wiley, 1975.

[22] Berkhoff J.C.W., 'Computation of Combined Refraction-Diffraction, 13th International Conference on Coastal Engineering, **1**, pp. 471-490, (1972).

[23] Borthwick A.G.L., Yiu K.F.C. and Anastasiou K., 'GMRES Solution of the Mild-Slope Equation on Quadtree Grids', *Proceedings of 27th IAHR Congress*, San Francisco, USA, p.p. 1322-1327, 10-15 August (1997).

[24] Bettess J.A. and Bettess P., 'New Mapped Wave Infinite Element for Diffraction of Waves by General Objects', *Proceedings of the ACME Conference*, Imperial College, University of London, April, (1997).

[25] Bettess J.A. and Bettess P., 'New Mapped Wave Infinite Element and Diffraction of Waves by Elliptical Cylinders of Varying Aspect Ratio', In: T. Geers, 'IUTAM Symposium on Computational Methods for Unbounded Domains', University of Colorado, USA, July 1997.

[26] Bettess P. and Chadwick E.A., 'Wave Envelope Examples for Progressive Waves', *International Journal for Numerical Methods in Engineering*, **38**, pp. 2487-2508, (1995).

[27] Bettess J.A. and Bettess P., 'Modelling of Flow Around Groups of Risers', Report for British Gas, Engineering Research Station Killingworth, England, UK, December 1993.

[28] Bettess P., *Infinite Elements*, Penshaw Press, Sunderland, UK, 1992.

[29] Bettess P., 'A Simple Wave Envelope Element Example', *Communications in Applied Numerical Methods*, **3**, pp. 77-80, (1987).

[30] Bettess P. and Bettess J.A., 'A Profile Matrix Solver with Built-in Constraint Facility', *Engineering Computations*, **3**(3), pp. 209-216, (1986).

[31] Bettess P., Emson C.R.I. and Chiam T.C., 'A New Mapped Infinite Element for Exterior Wave Problems', In *Numerical Methods in Coupled Systems*, Eds. Lewis R.W., Bettess P. and Hinton E., Chapter 17, Chichester, Wiley, 1984.

[32] Bettess P., 'Some Useful Techniques for Testing Infinite Elements', *Journal of Appl. Math. Modelling*, **6**, p.p. 436-440, (1982).

[33] Bettess P., 'More on Infinite Elements', *International Journal for Numerical Methods in Engineering*, **15**, pp. 53-64, (1980).

[34] Bettess P., 'Infinite Elements', *International Journal for Numerical Methods in Engineering*, **11**, pp. 53-64, (1977).

[35] Bettess P., and Zienkiewicz O.C., 'Diffraction and Refraction of Surface Waves Using Finite and Infinite Elements', *International Journal for Numerical Methods in Engineering*, **11**, pp. 1271-1290, (1977).

[36] Burnett D.S., 'A Three-Dimensional Acoustic Infinite Element Based on a Prolate Spheroidal Multiple Expansion', *Journal of the Acoustical Society of America*, **95**(5), pp. 2798-2816,

[37] Chadwick E.A. and Bettess P., 'Modelling of Progressive Short Waves Using Wave Envelopes', *International Journal for Numerical Methods in Engineering*, **40**, pp. 3229-3245, (1997).

[38] Chadwick E.A., Bettess P., Laghrouhe O., 'Diffraction of Short Waves Modelled Using New Mapped Wave Envelope Finite and Infinite Elements", *International Journal of Numerical Methods in Engineering*, Submitted.

[39] Chen H.S. and Mei C.C., 'Wave Forces on a Stationary Platform of Elliptical Shape', *Journal of Ship Research*, **17**(2), pp. 61-71, (1973).

[40] Chen H. S. and Mei C.C., 'Oscillations of Wave Forces in an Offshore Harbour', M.I.T. Report No. 190., 1974. (1994).

[41] Chu N., 'Wave Force Calculation with Consideration of Viscous Effects', *PhD thesis*, Strathclyde, UK, 1987.

[42] Cipolla J.L. and Butler M.J.,'Infinite Elements in the Time Domain Using Prolate Spheroidal Multipole Expansion', *International Journal for Numerical Methods in Engineering*, **43**, pp. 889-908, (1998).

[43] Clark P., 'The Finite Element Method Applied to Stokes Wave Diffraction', *PhD thesis*, University of Newcastle Upon Tyne, UK, 1993.

[44] Clark P.J., 'Recent Development in the Application of Infinite Element to Wave Diffraction', Dept. of Civil and Offshore Engineering, Heriot-Watt University, unpublished work, 1996.

[45] Cremeres L. and Fyfe K.R., 'A Variable Order Infinite Acoustic Wave Envelope Element', *Journal of the Acoustical Society of America*, **97**, pp. 2028-2040, (1995).

[46] Cremeres L. and Fyfe K.R., 'A Variable Order Infinite Acoustic Wave Envelope Element', *Journal of Sound and Vibration*, **171**(4), pp. 483-508, (1994).

[47] Curnier A., 'A Static Infinite Element', *International Journal for Numerical Methods in Engineering*, **19**, pp. 1479-1488, (1983).

[48] Demkowicz L., and Ihlenburg F.,'Proof of Convergence for the Coupled Finite/Infinite Element Methods for Helmholtz Exterior Boundary-Value Problems', In: T. Geers, 'IUTAM Symposium on Computational Methods for Unbounded Domains', University of Colorado, USA, July 1997.

[49] Demkowicz L.,'Asymptotic Convergence in Finite and Boundary Element Methods: Part1: Theoretical Results', *Computers and Mathematics with Apllications*, **27**, 12, pp. 69-84, 1994.

[50] Dingemans M. W., *Water Wave Propagation Over Uneven Bottoms: Part 1 - linear Wave Propagation*, World Scientific, London, 1997.

[51] Dingemans M. W., *Water Wave Propagation Over Uneven Bottoms: Part 2 - Non-linear Wave Propagation*, World Scientific, London, 1997.

[52] Eatock Taylor R., 'Analysis of non-linear wave-body interactions using finite elements', In: 'Waves and nonlinear processes in hydrodynamics', J. Grue, B. Gjevik and J.E. Weber (eds), Kluwer Academic Publishers, Dodrecht, 1996.

[53] Eatock Taylor R. and Teng B., 'The Effect of Corners on Diffraction/Radiation Forces and Wave Drift Damping', Proceedings of Offshore Technology Conference, Houston, OTC7187, pp. 571-581, 1993.

[54] Eatock Taylor R. and Chau F.P., 'Wave Diffraction-Some Developments in Linear and Non-Linear Theory', *Journal of Offshore Mechanics and Arctic Engineering*, **114**, pp. 185-194, (1992).

[55] Eatock-TaylorR. and Zietsman J.F.W., 'A Comparison of Localized Finite Element Formulations for Two-Dimensional Wave Diffraction and Radiation Problems', *International Journal for Numerical Methods in Engineering*, **17**, pp. 1355-1384, (1981).

[56] Faltinsen O.M. and Michelsen F.C., 'Motions of Large Structures in Waves at Zero Froud Number', Proc. Dynamics of Marine Vehicles and Structures in Waves, London, pp. 99-114, 1974.

[57] Garrison C.J.,'Hydrodynamic Loading of Large Volume Offshore Structures: Three-Dimensional Source Distribution Methods', *Numerical Methods in Offshore Engineering*, edited by O.C. Zienkiewicz *et al*, Wiley, Chichester, 1979.

[58] Geers T.,'IUTAM Symposium on Computational Methods for Unbounded Domains', University of Colorado, USA, July 1997.

[59] Gerdes K, 'Solution of the 3D Laplace and Helmholtz Equation in Exterior Domains of Arbitrary Shape using HP-Infinite-Finite Elements', *PhD Thesis*, University of Texas at Ausin, USA, 1996.

[60] Givoli D., *Numerical Methods for Problems in Infinite Domains*, Elsevier, Amesterdam, 1992.

[61] Gradshteyn I.S. and Ryzhik I.M., 'Table of Integrals', Series and Products, Academic, 1965.

[62] Greaves D.M., Borthwick A.G.L., Wu G.X. and Eatock Taylor R., 'A Moving Boundary Finite Element Method for Fully Nonlinear Wave Simulations', *Journal of Ship Research*, **41**, 3, pp.181-194, (1997).

[63] Harari I. and Hughes T.J.R., 'Studies of Domain Based Formulations for Computing Exterior Problems of Acoustics', *International Journal for Numerical Methods in Engineering*, **37**, pp. 2935-2950, (1994).

[64] Havelock T. H., 'The Pressure of Water Waves upon a Fixed Obstacle', *Proceedings Royal Society London*, Series A, No. 963, **175**, pp. 409-421, (1940).

[65] Hess J.L. and Smith A.M.O., 'Calculation of Non-Lifting Potential Flow about Arbitrary Three-Dimensional Bodies', *Journal of Ship Research*, **8**, pp. 22-44, (1964).

[66] Hogben N. and Standing R.G.,'Wave Loads on Large Bodies', Proc. Int. Symp. Dyn. Marine Vehicles and Structures in Waves, University College London, Inst. Mech. Eng., pp. 158-277, 1974.

[67] Hood P., 'Frontal Solution Program for Unsymmetric Matrices', *International Journal for Numerical Methods in Engineering*, **10**, pp. 379-399, (1976).

[68] Hood P., 'Erratum', *International Journal for Numerical Methods in Engineering*, **11**, pp. 1055, (1976).

[69] Homma S., 'On the Behavior of Seismic Sea Waves Around a Circular Island', *Geophysical Magasine*, **21**(3), pp. 199-208, (1950).

[70] Huebner K.H., Thornton, E.A. and Byrom, T.G., *The Finite Element Method for Engineers*, 3rd ed., Wiley & Sons, 1995.

[71] Irons B.M., 'A Frontal Solution Program for Finite Element Analysis', *International Journal for Numerical Methods in Engineering*, **2**, pp. 5-32, (1970).

[72] John F.,'On the Motion of Floating Bodies II', Comm. Pure App. Math., **3**, 45-101, (1950).

[73] Kakuno S., Nakata Y. and Liu P.L.-F.,'Wave Forces on an Array of Vertical Cylinders', *Journal of Waterways, Port, Coastal, and Ocean Engineering*, pp. 147-149, May/June (1996)

[74] Kirby J.T., 'A Note on Linear Surface Wave-Current Interaction over Slowly Varying Topography', *Journal of Geophysical Research*, **89**(C1), pp. 745-747, (1984).

[75] Korsmeyer F.T., Lee C.H., Newman J.N. and Sclavounous, P.D.,'The Analysis of Wave Effects on a Tension-Leg Platform', Proc. of Offshore Mechanics and Arctic Engineering, **2**, pp. 1-15, 1988.

[76] Lamb H., *Hydrodynamics*, Sixth edition, Cambridge University Press, 1924.

[77] Lewis P.E. and Ward J.P., *The Finite Element Method*, Addison-Wesley Publishing Company, 1991.

[78] Linton C.M. and Evans D.V., 'The Interaction of Waves with Arrays of Vertical Circular Cylinder', *Journal of Fluid Mevhanics*, **215**, pp. 549-569, (1990).

[79] Liu Y.H., Kim C.H., Kim M.H.,'The Computation of Mean Drift Forces and Wave Run-Up by Higher Order Boundary Element Method', Proc. of First International Offshore and Polar Engineering Conference, Edinburgh, UK, **3**, pp. 476-483, 1991.

[80] MacCamy R.C. and Fuchs R.A., 'Wave Forces on Piles: A Diffraction Theory', Beach Erosion Board, Corps of Engineers, Technical Memorandum No. 69, (1952).

[81] Marques J.M.M.C. and Owen D.R.J., 'Infinite Element in Quasi-Static Materially Non-Linear Problems', *Computers and Structures*, **18**(4), pp. 739-751, (1981).

[82] McIver P. and Evans D.V., 'Approximation of Wave Forces on Cylinder Arrays', *Applied Ocean Research*, **6**, pp. 101-107, (1984).

[83] Mei C.C., *The Applied Dynamics of Ocean Surface Waves*, World Scientific, Singapore, 1989.

[84] Mei C.C., 'Numerical Methods in Water-Wave Diffraction and Radiation", Annual Review of Fluid Mechanics, **10**, pp. 393-416, (1978).

[85] Morgan N.,'Marine Technology Reference Book', Butterworths, London, 1990.

[86] Morison J.R., 'The Forces Exerted by Waves on Marine Structures', Wave Project Report, Series 35, Issue 3, October 1950.

[87] Newman J.N., 'Marine Hydrodynamics', MIT Press, Camb. Mass., 1997.

[88] Orphanidou E.A., 'Application of transputers to surface wave problems in marine technology', M.Sc. Thesis No. S177, The University of Newcatle upon Tyne, 1991.

[89] Oslon L.G. and Bathe K.J., 'An Infinite Element for Analysis of Fluid-Structure Interaction', *Engineering Computations*, **2**, pp. 319-329 (1985).

[90] Penney W.G. and A.T. Price, 'The Diffraction Theory of Sea Waves and the Shelter Afforded by Breakwaters', *Philosophical Transanctions*, Royal Society of London, Series A, **224**, pp. 236-253, (1952).

[91] Pissanetzky S.,'An Infinite Element and a Formulation for Numerical Quadrature over an Infinite Interval', *International Journal for Numerical Methods in Engineering*, **19**, pp. 913-927, (1983).

[92] Sarpkaya T. and Isaacson M., *Mechanics of Wave Forces on Offshore Structures*, Van Nostrand Reinhold Company, New York, 1981.

[93] Saad Y. and Schults M.H., 'GMRES: A Generalised Minimal Residual Algorithm for Solving Nonsymmetric Linear Systems, *SIAM Journal of Scientific and Statistical Computing*, **7**(3): p.p. 856-869, (1986).

[94] Shirron J.J., 'Solution of Exterior Helmholtz Problems Using Finite and Infinite Elements', *PhD thesis*, University of Maryland College Park, USA, 1995.

[95] Sommerfeld A., *Partial Differential Equations in Physics*, New York, Academics Press, 1949.

[96] Teng B. and Eatock Taylor R., 'New Higher-Order Boundary Element Methods for Wave Diffraction/Raiation', *Applied Ocean Research*, **17**, pp. 71-77, (1995).

[97] Thompson L.L. and Pinsky P.M., 'A Space-Time Finite Element Method for the Exterior Structural Acoustics Problem : Time-Dependent Radiation Boundary Conditions in Two Space Dimensions', *International Journal for Numerical Methods in Engineering*, **39**, pp. 207-209, (1996).

[98] Ungless R.L., 'An Infinite Finite Element', *MA.Sc. thesis*, University of British Columbia, Canada, 1973.

[99] Yang Y.-B., Kuo S.-R. and Hung H.-H., 'Frequency-Independent Infinite Elements for Analysing Semi-Infinite Problems', *International Journal for Numerical Methods in Engineering*, **39**, pp. 3553-3569, (1996).

[100] Zienkiewicz O.C. and Taylor R.L., *The Finite Element Method*, Fourth ed., **1**, McGraw-Hill, London, 1991.

[101] Zienkiewicz O.C. and Taylor R.L., *The Finite Element Method*, Fourth ed., **2**, pp. 640, McGraw-Hill, London, 1991.

[102] Zienkiewicz O.C., Bando K., Bettess P., Emson C. and Chiam T.C., 'Mapped infinite elements for exterior wave problems', *International Journal for Numerical Methods in Engineering*, **21**, pp. 1229-1251, (1985).

[103] Zienkiewicz O.C., Emson C. and Bettess P., 'A Novel Boundary Infinite Element', *International Journal for Numerical Methods in Engineering*, **19**, pp. 393-404, (1983).

[104] Zienkiewicz O. C., Bettess P., Chiam T.C., Emson C. , 'Numerical Methods for Unbounded Field Problems and a New Infinite Element Formulation'. In *Computational Methods for Infinite Domain Media-Structure Interaction*, Wahington D.C., Edited by A. J. Kalinowski, The Applied Mechanics Division, ASME, pp. 115-148, 1981.

[105] Zienkiewicz O. C. and Bettess P., 'The Coupling of the Finite Element and Boundary Solution Procedure', *International Journal for Numerical Methods in Engineering*, **11**, pp. 355-375, (1977).

[106] Zienkiewicz O. C., Bettess P. and Kelly D.W.,'The Finite Element Method for Determinig Fluid Loading on Rigid Structures: Two and Three Dimensional Formulations', chapter 4 in *Numerical Methods in Offshore Engineering*, edited by O.C. Zienkiewicz *et al*, Wiley, London, 1977.

[107] Zienkiewicz O. C., Bettess P., 'Infinite Element in the Study of Fluid-Structure Interaction Problems', *Lecture Notes in Physics*, **58**, Eds. Ehlers J. *et al*, Springer-Verlag, Berlin, 1976.

[108] Zienkiewicz O.C. and Newton R.E., 'Coupled Vibrations of a Structure Immersed in a Compressible Fluid', In *Proceedings of Symposium on Finite Element Techniques*, Stuttgart, pp. 359-379, (1969).

[109] Zietsman J.F.W.,'Localized Finite Element Formulations for Ocean Wave Diffraction and Radiation Problems', *PhD thesis*, Dept. of Mechanical Engineering, University College London, 1982.

[110] Zietsman J.F.W. and Eatock Taylor R., 'The coupling of Finite and Bounday Integral Formulations for Two-Dimensional Hydrodynamic Analysis', MTC Report, OEG/80/2, University College London, 1980.

[111] Wang K.-H., Ren X.,'Interaction of Cnoidal Waves with Cylinder Arrays', *Ocean Engineering*, **26**, pp. 1-20, (1999).

[112] Wu G.X. and Eatock Taylor R.,'Finite Element Analysis of Two Dimensional non-linear wave radiation problem', *Ocean Engineering*, **22**, pp. 785-798, (1995).

[113] Wu G.X. and Eatock Taylor R.,'Finite Element Analysis of Two-Dimensional Non-Linear Transient Water Waves', *Applied Ocean Research*, Vol. 16, pp. 363-372, (1994).

Appendix A

Notation

Below is a list of symbols used in this thesis. All the matrices and vectors are shown by bold symbols. Some symbols have been used to represent more than one quantity.

$\mathbf{A}$	finite or infinite element (F/IE) matrix
A	wave amplitude
Ac_n, As_n	coefficients of the Mathieu functions
A_m^l, B_n	coefficients of the diffracted wave series
a, b	ellipse semi-major and semi-minor axis length
a_{ij}, b_j	element matrix and right hand side vector entries
C_h	diffraction coefficient
c	wave celerity
c_g	wave group velocity
$ce_n(\eta, q), se_n(\eta, q)$	periodic Mathieu functions of n^{th} order
d	water depth from the still water level to the sea bottom
e	element number
exp	exponential function
F_j, F	hydrodynamic force at point j and the total force
F_k	hydrodynamic Froude-Krylov force
g	acceleration due to gravity
H	wave height
h	interfocal distance of the ellipse
$H_n(kr)$	Hankel function of first kind of n^{th} order
I_j	phase factor associated with the jth cylinder
i	square root of -1 or node number
$\mathbf{J}$	Jacobian matrix
$\|\mathbf{J}\|$	determinant of the Jacobian matrix

$J_n(kr), Y_n(kr)$	Bessel functions of first and second kind and of n^{th} order
K, M, R	FE or IE stiffness, mass and radiation matrices
k	wave number
L	wave length
M	hydrodynamic overturning moment or number of terms used in series
$Mc_n(\xi, q), Ms_n(\xi, q)$	radial Mathieu functions of n^{th} order
$M_i(\xi), M_i(\xi, \eta)$	1D and 2D infinite element mapping functions for i^{th} node
m	number of dimensions or number of nodes per element
N	number of diffracting objects
$N_i(\xi, \eta), N_i(r)$	infinite element shape functions for i^{th} node
n	outward normal to the surface or number of nodes per element
ne	total number of elements in the finite/infinite element mesh
$P_i(\xi, \eta), P_i(\xi), P_i(\eta), P_i(r)$, $P_i^{"}(\xi), P_i^{*}(\eta), P_i^{"}(r)$	finite element shape functions for i^{th} node
p	total pressure
p_d	hydrodynamic pressure
$q = (kh/2)^2$	parameter of the Mathieu functions
R_{jl}	distance between the centres of objects j and l
r_0	radial distance between the inner node of an infinite element and its virtual source
r, θ	polar coordinates
T	wave period
t	time
u, v, w	velocity components in the x, y, z directions
x, y, z	Cartesian coordinates
x_j, y_j	local coordinates of object j
$Z(z)$	wave potential depth variation function
$W_i(\xi, \eta), W_i(r)$	infinite element weighting functions for i^{th} node

η, η_a	free surface elevations (numerical and analytical) from the still water level
ξ, η	elliptical coordinates or element local coordinates
ε	error in the numerical calculation of the free surface elevation
α_{jl}	angle between R_{jl} and positive x_j-axis
ω	wave angular frequency
Ω	unbounded two-dimensional (x-y) domain
Ω_1	finite two-dimensional region circumscrbing the object(s)
Ω_2	infinite two-dimensional region circumscrbing Ω_1
Γ	boundary between finite and infinite elements
Γ_0	boundary of diffracting object
Γ_∞	outer boundary of infinite elements
Γ_c	a boundary where the field variable changes
Φ	time dependent velocity potential
Φ_s	time dependent diffracted velocity potential
ϕ	time independent total velocity potential
ϕ_I	time independent incident velocity potential
ϕ_s	time independent diffracted velocity potential
ρ	water density
∇	gradient operator in two or three dimensions
θ_I	angle of wave incidence from the positive x-axis

Appendix B

Variational Formulation for Finite Elements

The weighted residuals equation for the governing equation over the Ω_1 region is given by equation 4.4 as

$$\iint_{\Omega_1} \nabla W c c_g \nabla \phi dx dy - \iint_{\Omega_1} W \frac{c_g}{c} \omega^2 \phi dx dy = 0 \tag{B.1}$$

Since the weighting function, W, is arbitrary, it may be taken as $W = \partial\phi$, so that the above equation is equivalent to the variational statement

$$\partial \Pi(\phi) = 0 \tag{B.2}$$

where

$$\Pi(\phi) = \frac{1}{2} \iint_{\Omega_1} \left(c c_g (\nabla \phi)^2 - \omega^2 \frac{c_g}{c} \phi^2 \right) dx dy \tag{B.3}$$

Now following the procedure which was first given by Bettess and Zienkiewicz [35], the field variable will be changed from the total wave potential, ϕ, to the diffracted wave potential ϕ_s. As a result a line integral arises which brings the incident wave into the formulation. As was explained in section2.4, the wave can be separated to the incident and scattered wave (equation (2.16))

$$\phi = \phi_I + \phi_s$$

substituting this into the equation (B.3) gives

$$\Pi(\phi) = \frac{1}{2}\iint_{\Omega_{12}} \left(cc_g(\nabla\phi_I + \phi_s)^2 - \omega^2 \frac{c_g}{c}(\phi_I + \phi_s)^2 \right) dx\, dy \tag{B.4}$$

Expansion gives

$$\Pi(\phi) = \frac{1}{2}\iint_{\Omega_{12}} \left(cc_g \nabla\phi_I^2 - \omega^2 \frac{c_g}{c}\phi_I^2 \right) dx\, dy +$$

$$\frac{1}{2}\iint_{\Omega_{12}} \left(cc_g \nabla\phi_s^2 - \omega^2 \frac{c_g}{c}\phi_s^2 \right) dx\, dy + \iint_{\Omega_{12}} \left(cc_g \nabla\phi_I \nabla\phi_s - \omega^2 \frac{c_g}{c}\phi_I\phi_s \right) dx\, dy \tag{B.5}$$

where Ω_{12} is the region between Γ_c and Γ where the field variable is changed to ϕ_s. The first term involves only the known incident wave which is not subject to variation and thus is discarded. By theorem:

$$u(\nabla v) = \nabla(uv) - v\nabla u \tag{B.6}$$

Taking $u = \nabla\phi_I$ and $v = \phi_s$, the last term of equation (B.5) can be written as

$$\iint_{\Omega_{12}} cc_g \nabla(\nabla\phi_I\phi_s)\, dx\, dy - \iint_{\Omega_{12}} \left(cc_g \nabla^2\phi_I + \omega^2 \frac{c_g}{c}\phi_I \right) dx\, dy\phi_s \tag{B.7}$$

As was explained in section 2.4, the incident wave is a known function which satisfies the wave equation and hence the last term is zero. By Green's theorem:

$$\oint (u dx + v dy) = \iint \left(\frac{\partial v}{\partial x} - \frac{\partial u}{\partial y} \right) dx\, dy \tag{B.8}$$

Taking $u = -\frac{\partial\phi}{\partial y}$ and $v = \frac{\partial\phi}{\partial x}$, the first term of equation (B.7) can be written as

$$\iint_{\Omega_{12}} cc_g \frac{\partial}{\partial x}\frac{\partial\phi_I}{\partial x} + \frac{\partial}{\partial y}\frac{\partial\phi_I}{\partial y}\, dx\, dy = \oint_{\Gamma_c} cc_g \left(-\frac{\partial\phi_I}{\partial y}dx + \frac{\partial\phi_I}{\partial x}dy \right) \tag{B.9}$$

Therefore the functional for finite elements becomes:

$$\Pi(\phi) = \iint_{\Omega_{12}} \frac{1}{2}\left(cc_g(\nabla\phi_s)^2 - \omega^2 \frac{c_g}{c}\phi_s^2 \right) dx\, dy + \oint_{\Gamma_c} cc_g \left(\frac{\partial\phi_I}{\partial x}\, dy - \frac{\partial\phi_I}{\partial y}\, dx \right) \phi_s \tag{B.10}$$

Following the above procedure, the variational statement, equation B.2, gives

$$\iint_{\Omega_{12}} (\nabla W c c_g \nabla \phi_s - \omega^2 \frac{c_g}{c} \phi_s) dx dy = \oint_{\Gamma_c} W c c_g \left(\frac{\partial \phi_I}{\partial x} dy - \frac{\partial \phi_I}{\partial y} dx \right) \tag{B.11}$$

The first integral gives the finite element matrix equation and the second integral brings the incident wave into the formulation.

Appendix C

Unsymmetric Complex Frontal Solver (UCFS)

Abstract

[1] An unsymmetric frontal solution program was presented by Hood [67, 68] to be used for the solution of unsymmetric matrix equations. The modified program is given to deal with situations when the matrix entries are complex numbers. This arises in certain application of the finite/infinite element method to unbounded problems. The global node numbering of the F/IE mesh can now be in an arbitrary manner. Different types of elements may also be used in the mesh. The original program has been parameterised so that it can be used for a mesh with any number of nodes or elements. The solver is fully validated using random numbers and using an existing symmetric frontal solver.

C.1 Introduction

A linear system of equations arises from finite element analysis as

$$\mathbf{A}_{m\times m}\mathbf{X}_{m\times 1} = \mathbf{b}_{m\times 1} \tag{C.1}$$

where $\mathbf{A}$ is a large matrix, $\mathbf{X}$ is the solution vector, $\mathbf{b}$ is the right hand side vector and m is the total number of nodes used in the analysis. The matrix $\mathbf{A}$ is a sum

[1] This work was carried out as part of the PhD research under supervision of Prof. P Bettess and was prepared as a report for the School of Engineering, University of Durham.

of individual finite element matrices

$$\mathbf{A} = \sum_{e=1}^{n} \mathbf{A}^{e} \tag{C.2}$$

where e is the element number and n is the total number of elements. The vectors $\mathbf{X}$ and $\mathbf{b}$ are also a sum of coresponding solution and right hand side vectors

$$\mathbf{X} = \sum_{e=1}^{n} \mathbf{X}^{e} \qquad \mathbf{b} = \sum_{e=1}^{n} \mathbf{b}^{e} \tag{C.3}$$

The global matrix, $\mathbf{A}$, resulting from wave diffraction analysis using the finite elements in conjunction with the wave envelope infinite elements is unsymmetric. The entries of the matrix and its right hand side vector are complex numbers. Therefore the solver, presented by Hood [67, 68], is modified to solve this kind of matrix equation. A new facility was inserted into the program to deal with cases where node numbering is not in ascending order. The solver was first tested thoroughly using random numbers and also against the existing symmetric frontal solver. It was then inserted into the finite infinite element wave diffraction code.

C.2 Pre-front

The pre-front parameters are defined and fully explained in the original paper by Hood [67]. Some parameters, such as mesh data or matrix entries, are generated by the main program. For testing the solver, these values are generated by a NAG random data generator. The assembly of the element matrices and the right hand side vectors is then done by the solver itself.

C.3 Testing for random data

The subroutine ABFIND is written to generate or read the element matrix and the right hand side vector for each element. The entries for each equation are then inserted into the correct location of the global right hand side vector according to the mesh node numbering scheme. The method of Bettess and Bettess [30] was used to test the solver. CALLs to a NAG subroutine generate random values for element matrix entries and the global solution vector entries. First the global solution vector, **X1** is generated in pre-front. Then the element matrix is multiplied by the appropriate solution vector for the element according to the global node numbering of the element to get the right hand side vector. Then using this right

hand side vector and the element matrix, the matrix equation is solved to get the new solution vector **X2**. Different test problems were solved. The difference vector, **DX= X2-X1**, had entries around 10E-15.

C.4 Node numbering scheme

The code was originally [67] written in such a way that the node numbering has to be in complete ascending order. As this is not practical for finite element programs the code was amended to work for any kind of node numbering. The only limitation is that the number of nodes given to the solver has to be set to the biggest node number used in the mesh.

C.5 Parameterizing the solver

The solver was set to work for only 70 nodes and 120 elements. It was desirable to get the solver to work for any number of nodes and elements. The code then was parameterised to work for any degrees-of-freedom and any number of elements.

C.6 Complex numbers

The entries of the element matrices and the right hand side vectors produced by the wave finite element program are complex numbers. Whereas the original solver works only for real numbers. It was necessary to modify the code to work for wave problems. The code was then tested for complex numbers. The procedure is almost the same as in section C.3. The only difference is that complex random entries for the solution vectors and the element matrices have to be created. Several example problems were solved. The difference vector DX has the entries of around (10E-15, 10E-15).

C.7 Testing against symmetric frontal solver (SFS)

A Symmetric Frontal Solver, due to Irons [71], was already working with the wave program succesfully. So the final test was to insert CUFS into the main wave program and solve an example problem using both SFS and CUSF. The velocity potentials and wave elevations produced by both solvers were the exactly the same.

The complex unsymmetric solver given here can be inserted to other programs with some confidence.

C.8 The FORTRAN code

Note that all lines, including statments, continued lines and so on, are printed from the first column by LATEX.

```
C*********************************************************************
      PROGRAM CHOOD
C
C***Test program for the Complex Version of P. Hood Unsymmetrical
C Frontal Solver.
C
C (C) Alireza Baghbani, Peter Bettess - November 1996
C
C NELL : element number.
C NBN(NELL) : Number of nodes for element NELL.
C NCN(NELL) : Number of degrees of freedom for element NELL.
C NOP(NELL,JMP) : Element conectivity data.
C JMP : Varies from 1 to the number of nodes per element.
C NE : Total number of elements.
C NH : Total number of nodes.
C NP : Total degress of freedom.
C MDF(I) : number of degrees-of-freedom at node I.
C IDF : number of degrees-of-freedom at the node.
C NEMAX : Maximum number of elements.
C NMAX : Maximum number of nodes.
C NBNMAX : Maximum number of nodes per element.
C IDFMAX : Maximum number of degree-of-freedom.
C
C
      INTEGER NEMAX, NMAX, NBNMAX, IDFMAX, DFMAX, NCNMAX
C
C***Problem dependent parameters.
C
      PARAMETER (NEMAX=120, NMAX=200,NBNMAX=9,IDFMAX=3)
      PARAMETER (DFMAX=IDFMAX*NMAX,NCNMAX=NBNMAX*IDFMAX)
C
      INTEGER ND1, NLP,NLR, NBN, NE, NH, IMP, JMP, MWGA, IDF, NCN
     1, NP, I, NCOD, NOP, NOPP, MDF, NTRA
      COMPLEX*16 BC, R1, XX1,DXX,SK,ESTIFM
      DOUBLE PRECISION TEM, G05CAF
```

```
      DIMENSION
     1 NOP(NEMAX,NBNMAX),NOPP(NMAX),MDF(NMAX)
     2,NCOD(DFMAX),BC(DFMAX),R1(DFMAX),XX1(DFMAX)
     3,SK(NMAX*NMAX),ESTIFM(NCNMAX,NCNMAX)
     4,NBN(NEMAX),NCN(NEMAX)
C
C
C***Open the files
C
      ND1 = 1
      NLP = 9
      NLR = 4
C
      OPEN(1,FORM='UNFORMATTED',STATUS='SCRATCH')
      OPEN(2,FORM='UNFORMATTED',STATUS='SCRATCH')
C
C***Channel 4 is the input channel
C
      OPEN(NLR,FILE='hood.dat')
C
C***Channel 9 is the output channel
C
      OPEN(NLP,FILE='hood.res')
C
C***Read in the necessary variables for test case, or bring them in from
C the FE code.
C
      READ(NLR,*)MWGA, NE, NH
      WRITE(NLP,6001)MWGA, NE, NH
C
C***Specify degrees-of-freedom for each node.
C
      DO 11 I=1, NH
      IF(MWGA.NE.0) THEN
      MDF(I) = 1
      ELSE
C
C***Insert your own maximum DOF for this problem instead of 3.
C
      MDF(I) =3
      ENDIF
      IDF = MDF(I)
      NOPP(1) = 1
      NOPP(I+1) = NOPP(I) + MDF(I)
   11 CONTINUE
C
C***Read in element conectivity data, or transfer it from FE code.
```

```
C
      DO 19 NELL = 1,NE
      READ(NLR,*) NBN(NELL),(NOP(NELL,JMP),JMP=1,NBN(NELL))
   19 CONTINUE
C
C***Write this data to output file.
C
      WRITE(NLP,6002)
      DO 40 NELL=1,NE
      WRITE(NLP,6007)NELL,NBN(NELL),(NOP(NELL,JMP),JMP=1,NBN(NELL))
   40 CONTINUE
C
C*** Calculate total DOF, assuming DOF is equall for each node.
C
      NP = NH * IDF
C
C*** Calculate DOF for each element.
C
      DO 111 NELL = 1, NE
      NCN(NELL) = NBN(NELL) * IDF
  111 CONTINUE
C
C*** Initialize boundary condition and the asociated vectors.
C
      DO 10 I=1,NP
      BC(I) = (0.0D0,0.0D0)
      NCOD(I) = 0
      R1(I) = (0.0D0,0.0D0)
   10 CONTINUE
C
      NTRA =1
C
C*** Read in initial solutions or create initial solutions using NAG
C random data generator.
C
C*** Initialize nag random generator.
C
      CALL G05CBF(0)
      TEM = 1.0D0
      DO 275 IROW=1,NP
      N = IROW
      XX1(N)= DCMPLX( G05CAF(TEM),G05CAF(TEM))
C READ(NLR,*) XX1(N)
  275 CONTINUE
      NELL = 0
C
C***Solve the equation using Complex Unsymetric Frontal Solver.
```

```
C
      CALL CFRONT(NEMAX,NMAX,NBNMAX,IDFMAX,DFMAX,NCNMAX
     1 ,NP,NH,NE,NBN,NCN,ND1,MWGA,NELL,NTRA,NLP
     2 ,NOP,NOPP,MDF,NCOD,BC,R1,SK,ESTIFM,XX1)
C
C*** Compare the calculated solutions with the itroduced ones.
C
C a) For all nodes
C
      WRITE(NLP,6003)
      DO 15 I= 1, NP
      DXX = XX1(I) - SK(I)
      WRITE(NLP,6004)I,XX1(I),SK(I),DXX
   15 CONTINUE
C
C
C***b) element by element.
C
      DO 37 I = 1, NE
      WRITE(NLP,422) I
      WRITE(NLP,6011)
      DO 38 J=1,NBN(I)
      IMP=ABS(NOP(I,J))
      DXX = XX1(IMP) - SK(IMP)
      WRITE(NLP,6010)J,IMP,XX1(IMP),SK(IMP),DXX
   38 CONTINUE
   37 CONTINUE
  422 FORMAT(/72('-')/,'ELEMENT NUMBER = ',I5)
  100 CONTINUE
 6001 FORMAT(/' Problem parameters '/
     1 ,'MWGA = ', I6/
     3 ,'Total No. of Elements = ',I6/
     4 ,'Total No. of Nodes = ',I6/)
 6002 FORMAT(/'ELE. NO., NO. of nodes per elemet, Node numbers ')
 6003 FORMAT(//'Node NO. — Int. Sols. — Comp. sols.—
     1DIFFERENCE',/72('-')/)
 6004 FORMAT(I5,5X,2D10.2,2D10.2,2D10.2)
 6007 FORMAT(10I5)
 6010 FORMAT(2I5,1X,2D10.2,1X,2D10.2,2D10.2)
      STOP
      END
C
      SUBROUTINE CFRONT(NEMAX,NMAX,NBNMAX,IDFMAX,DFMAX,NCNMAX
     1 ,NP,NH,NE,NBN,NCN,ND1,MWGA,NELL,NTRA,NLP
     2 ,NOP,NOPP,MDF,NCOD,BC,R1,SK,ESTIFM,XX1)
C
C
```

```
C FRONTAL ELIMINATION ROUTINE USING FULL PIVOTING
C
C***Reference: P.Hood, Frontal Solution Program for Unsymmetric matrices
C ,International Journal for Numerical Methods in
C Engineering, Volume 10, pages 379 to 399, 1976.
C
C***COMPLEX*16 version of the solver.
C
C***(C) Alireza Baghbani, Pete Bettess NOVEMBER 1996.
C
C
C
      INTEGER NEMAX, NMAX, NBNMAX,IDFMAX, DFMAX, NCNMAX
      COMPLEX*16 BC, R1, SK, ESTIFM
      COMPLEX*16 EQ, PVKOL, QQ, AA
      COMPLEX*16 FAC, PIVA, PIVOT, RHS,CZERO,CONE
      INTEGER KDEST, NK, LHED, KHED, KPIV, LPIV, JMOD
      INTEGER I, IDF, II, IR, IRR, J,
     1 K, KC, KH, KK, KPIVR, KPIVRO, KR, KRO, KROW, KRW, KT,
     2 L, LC, LCO, LCOL, LDEST, LH, LK, LL, LPIVC,
     3 LPIVCO, l1, M, MWGA, N,
     4 NBN, NCN, NCRIT, NE, NELL, NERROR, NH, NLAST, NLAST1,
     5 NLP, NN, NODE, NP, NTRA
      INTEGER NOP, NOPP, MDF, NCOD
      DIMENSION
     1NOP(NEMAX,NBNMAX),NOPP(NMAX),MDF(NMAX),NCOD(DFMAX),BC(DFM
     2,R1(DFMAX),XX1(DFMAX)
     3,SK(NMAX*NMAX),ESTIFM(NCNMAX,NCNMAX)
     4,NBN(NE),NCN(NE)
      DIMENSION
     1 LDEST(NCNMAX),KDEST(NCNMAX),NK(NCNMAX),AA(NCNMAX,NCNMAX)
     2 EQ(NMAX,NMAX),LHED(NMAX),KHED(NMAX),KPIV(NMAX),LPIV(NMAX),
     3 JMOD(NMAX),QQ(NMAX),PVKOL(NMAX)
C
      CZERO = DCMPLX(0.0D0,0.0D0)
      CONE = DCMPLX(1.0D0,1.0D0)
C
C PREFRONT
C
      NCRIT = NMAX - 30
      NELL = 0
D WRITE(NLP,400)
      IF(NTRA.EQ.0) GO TO 14
C
C FIND LAST APPEARANCE OF EACH NODE
C
      NLAST = 0
```

```
      DO 12 I = 1, NH
      DO 8 N = 1, NE
      DO 4 L = 1, NBN(N)
      IF(NOP(N,L).NE.I) GO TO 4
      NLAST1 = N
      IF(NLAST.NE.NLAST1) GO TO 3
      NERROR = 1
C WRITE(NLP,416) NERROR, N
      STOP
    3 CONTINUE
      NLAST = N
      L1 = L
    4 CONTINUE
CC WRITE(NLP,404) I, NLAST
    8 CONTINUE
      IF(NLAST.EQ.0) GO TO 12
C
      NOP(NLAST,L1) = -NOP(NLAST,L1)
      NLAST = 0
   12 CONTINUE
D WRITE(NLP,408)
C WRITE(NLP,412) (N,(NOP(N,L),L=1,NBN),N=1,NE)
D DO 315 N = 1, NE
D315 WRITE(NLP,412) N,(NOP(N,L),L=1,NBN(N))
C
C ASSEMBLY
C
   14 CONTINUE
      LCOL = 0
      KROW = 0
      DO 17 I = 1, NH
      DO 16 J = 1, NH
      EQ(J,I) = CZERO
   16 CONTINUE
   17 CONTINUE
   18 CONTINUE
      NELL = NELL + 1
      CALL ABFIND(NEMAX,DFMAX,NCNMAX,NBNMAX
     1 ,NP,NH,NE,NBN,NCN,ND1,NELL,NLP
     2 ,NOP,NCOD,BC,R1,AA,XX1)
      N = NELL
      KC = 0
      IF(MWGA.EQ.0) GO TO 21
      DO 20 I = 1, NBN(N)
      NK(I) = NOP(N,I)
   20 CONTINUE
      GO TO 23
```

```
   21 CONTINUE
      DO 22 J = 1,NBN(N)
      NN = NOP(N,J)
      M = IABS(NN)
      K = NOPP(M)
      IDF = MDF(M)
      DO 122 L = 1, IDF
      KC = KC + 1
      II = K + L - 1
      IF(NN.LT.0) II = -II
      NK(KC) = II
  122 CONTINUE
   22 CONTINUE
   23 CONTINUE
C
D WRITE(NLP,490)(NK(I),I=1,NP)
C
C SET UP HEADING VECTORS
C
      DO 52 LK = 1, NCN(NELL)
      NODE = NK(LK)
      IF(LCOL.EQ.0) GO TO 28
      DO 24 L = 1, LCOL
      LL = L
      IF(IABS(NODE).EQ.IABS(LHED(L))) GO TO 32
   24 CONTINUE
   28 LCOL = LCOL + 1
      LDEST(LK) = LCOL
      LHED(LCOL) = NODE
      GO TO 36
   32 CONTINUE
      LDEST(LK) = LL
      LHED(LL) = NODE
   36 CONTINUE
      IF(KROW.EQ.0) GO TO 44
      DO 42 K = 1, KROW
      KK = K
      IF(IABS(NODE).EQ.IABS(KHED(K))) GO TO 48
   42 CONTINUE
   44 CONTINUE
      KROW = KROW + 1
      KDEST(LK) = KROW
      KHED(KROW) = NODE
      GO TO 52
   48 CONTINUE
      KDEST(LK) = KK
      KHED(KK) = NODE
```

```
   52 CONTINUE
D WRITE(NLP,420) KROW, LCOL
D WRITE(NLP,424)
C WRITE(NLP,428) (KHED(K), LHED(K), K=1,NMAX)
D WRITE(NLP,428) (KHED(K), LHED(K), K=1,NP)
D WRITE(NLP,432)
D WRITE(NLP,428) (KDEST(K), LDEST(K), K=1,NCN(NELL))
      IF(KROW.LE.NMAX.AND.LCOL.LE.NMAX) GO TO 54
      NERROR = 2
      WRITE(NLP,417) NERROR
      STOP
   54 CONTINUE
      DO 57 L = 1, NCN(NELL)
      LL = LDEST(L)
      DO 56 K = 1, NCN(NELL)
      KK = KDEST(K)
      EQ(KK,LL) = EQ(KK,LL) + AA(K,L)
   56 CONTINUE
   57 CONTINUE
D WRITE(NLP,436) NELL
CC WRITE(NLP,440) ((EQ(I,J),J=1, NMAX), I=1,NMAX)
C
D DO 313 I=1,NP
D313 WRITE(NLP,440) (EQ(I,J),J=1, NP)
D WRITE(NLP,460)
D DO 314 I=1,NP
D314 WRITE(NLP,441)I, R1(I)
C
   IF(KROW.LT.NCRIT.AND.NELL.LT.NE) GO TO 18
C
C FIND OUT WHICH MATRIX ELEMENTS ARE FULLY SUMMED
C
   60 LC = 0
      DO 64 L = 1, LCOL
      IF(LHED(L).GE.0) GO TO 64
      LC = LC + 1
      LPIV(LC) = L
   64 CONTINUE
      IR = 0
      KR = 0
      DO 68 K = 1, KROW
      KT = KHED(K)
      IF(KT.GE.0) GO TO 68
      KR = KR + 1
      KPIV(KR) = K
      KRO = IABS(KT)
      IF(NCOD(KRO).NE.1) GO TO 68
```

```
      IR = IR + 1
      JMOD(IR) = K
      NCOD(KRO) = 2
      R1(KRO) = BC(KRO)
   68 CONTINUE
C
C MODIFY EQUATIONS WITH APPLIED BOUNDARY CONDITIONS
C
D WRITE(NLP,448) LC, KR
CC WRITE(NLP,428) (LPIV(K), KPIV(K), K=1,NMAX)
D WRITE(NLP,428) (LPIV(K), KPIV(K), K=1,NP)
   IF(IR.EQ.0) GO TO 71
D WRITE(NLP,456)
      DO 70 IRR = 1,IR
      K = JMOD(IRR)
D WRITE(NLP,428) K
      KH = IABS(KHED(K))
      DO 69 L = 1, LCOL
      EQ(K,L) = CZERO
      LH = IABS(LHED(L))
      IF(LH.EQ.KH) EQ(K,L) = CONE
   69 CONTINUE
   70 CONTINUE
   71 CONTINUE
      IF(KR.GT.0.AND.LC.GT.0) GO TO 72
      NERROR = 3
      WRITE(NLP,418) NERROR
      STOP
   72 CONTINUE
D WRITE(NLP,460)
D WRITE(NLP,464) (I,R1(I), I =1,NP)
C
C SEARCH FOR ABSOLUTE PIVOT
C
      PIVOT = CZERO
      DO 76 L = 1, LC
      LPIVC = LPIV(L)
      DO 74 K = 1, KR
      KPIVR = KPIV(K)
      PIVA = EQ(KPIVR, LPIVC)
      IF(ZABS(PIVA).LT.ZABS(PIVOT)) GO TO 74
      PIVOT = PIVA
      LPIVCO = LPIVC
      KPIVRO = KPIVR
   74 CONTINUE
   76 CONTINUE
C
```

```
C NORMALISE PIVOTAL ROW
C
      KRO = IABS(KHED(KPIVRO))
      LCO = IABS(LHED(LPIVCO))
D WRITE(NLP,452) KRO, LCO, PIVOT
      IF(ABS(PIVOT).LT.1.0E-08) WRITE (NLP,476)
      DO 80 L = 1, LCOL
      QQ(L) = EQ(KPIVRO,L) / PIVOT
   80 CONTINUE
      RHS = R1(KRO) / PIVOT
      R1(KRO) = RHS
      PVKOL(KPIVRO) = PIVOT
D WRITE(NLP,468)
D WRITE(NLP,440) (QQ(L), L = 1, LCOL)
C
C ELIMINATE THEN DELETE PIVOTAL ROW AND COLUMN
C
      IF(KPIVRO.EQ.1) GO TO 104
      KPIVR = KPIVRO - 1
      DO 100 K = 1, KPIVR
      KRW = IABS(KHED(K))
      FAC = EQ(K,LPIVCO)
D WRITE(NLP,480) FAC
      PVKOL(K) = FAC
      IF(LPIVCO.EQ.1.OR.FAC.EQ.CZERO) GO TO 88
      LPIVC = LPIVCO - 1
      DO 84 L = 1, LPIVC
      EQ(K,L) = EQ(K,L) - FAC * QQ(L)
   84 CONTINUE
   88 IF(LPIVCO.EQ.LCOL) GO TO 96
      LPIVC = LPIVCO + 1
      DO 92 L = LPIVC, LCOL
      EQ(K,L-1) = EQ(K,L) - FAC * QQ(L)
   92 CONTINUE
   96 R1(KRW) = R1(KRW) - FAC * RHS
  100 CONTINUE
  104 IF(KPIVRO.EQ.KROW) GO TO 128
      KPIVR = KPIVRO + 1
      DO 124 K = KPIVR, KROW
      KRW = IABS(KHED(K))
      FAC = EQ(K,LPIVCO)
D WRITE(NLP,480) FAC
      PVKOL(K) = FAC
      IF(LPIVCO.EQ.1) GO TO 112
      LPIVC = LPIVCO - 1
      DO 108 L = 1, LPIVC
      EQ(K-1,L) = EQ(K,L) - FAC * QQ(L)
```

```
  108 CONTINUE
  112 IF(LPIVCO.EQ.LCOL) GO TO 120
      LPIVC = LPIVCO + 1
      DO 116 L = LPIVC, LCOL
      EQ(K-1,L-1) = EQ(K,L) - FAC * QQ(L)
  116 CONTINUE
  120 R1(KRW) = R1(KRW) - FAC * RHS
  124 CONTINUE
  128 CONTINUE
C
C WRITE PIVOTAL EQUATION ON DISC
      WRITE(ND1)
     1 KRO,LCOL,LPIVCO,(LHED(L),QQ(L),L=1,LCOL),
     2 KROW,PIVOT,KPIVRO,(PVKOL(K),KHED(K),K=1,KROW)
      DO 129 K = 1, LCOL
      EQ(K,LCOL) = CZERO
  129 CONTINUE
      DO 130 K = 1, LCOL
      EQ(KROW,L) = CZERO
  130 CONTINUE
D WRITE(NLP,480) FAC
CC WRITE(NLP,440) ((EQ(I,J),J=1,NMAX),I=1,NMAX)
D WRITE(NLP,440) ((EQ(I,J),J=1,NP),I=1,NP)
D WRITE(NLP,460)
D WRITE(NLP,464) (I,R1(I),I=1,NP)
C
C RE-ARRANGE HEADING VECTORS
C
      LCOL = LCOL - 1
      IF(LPIVCO.EQ.LCOL+1) GO TO 136
      DO 132 l = LPIVCO, LCOL
      LHED(L) = LHED(L+1)
  132 CONTINUE
  136 CONTINUE
      KROW = KROW - 1
      IF(KPIVRO.EQ.KROW+1) GO TO 144
      DO 140 K = KPIVRO, KROW
      KHED(K) = KHED(K+1)
  140 CONTINUE
  144 CONTINUE
D WRITE(NLP,420) KROW, LCOL
D WRITE(NLP,424)
CC WRITE(NLP,428) (KHED(K),LHED(K),K=1,NMAX)
D WRITE(NLP,428) (KHED(K),LHED(K),K=1,NP)
C
C DETERMINE WHETHER TO ASSEMBLE, ELIMINATE OR BACK SUBSTI-
TUTE
```

```
C
      IF(KROW.GT.NCRIT) GO TO 60
      IF(NELL.LT.NE) GO TO 18
      IF(KROW.GT.1) GO TO 60
      LCO = IABS(LHED(1))
      KPIVRO = 1
      PIVOT = EQ(1,1)
      KRO = IABS(KHED(1))
      LPIVCO = 1
      QQ(1) = CONE
D WRITE(NLP,452) LCO, KRO, PIVOT
      IF(ABS(PIVOT).LT.1.0D-08) WRITE(NLP,476)
      R1(KRO) = R1(KRO) / PIVOT
C
      WRITE(ND1)
     1 KRO, LCOL, LPIVCO, LHED(1), QQ(1),
     2 KROW, PIVOT, KPIVRO, PVKOL(1), KHED(1)
C
      CALL BACSUB(NMAX,DFMAX,NCNMAX
     1,NP,NH,ND1,NLP,NOPP,MDF,NCOD,BC,R1,SK)
C
  400 FORMAT(' Node NLAST')
  404 FORMAT(1X,2I5)
  408 FORMAT(//' Nodal Numbering'/)
  412 FORMAT(9I5)
  416 FORMAT(/' NERROR = ',I5//I5,
     1 ' The element has more than one node with the '/
     2 ' same node number'/)
  417 FORMAT(/' NERROR = ',I5//
     1 ' The difference NMAX - NCRIT is not sufficiently large'/
     2 ' to permit the assembly of the next element — '/
     3 ' either increase NMAX or lower NCRIT'/)
  418 FORMAT(/' NERROR = ',I5//
     1 ' There are no more rows fully summed, this may be due to —'/
     2 ' 1. Incorrect coding of NOP or NK arrays '/
     3 ' 2. Incorrect value of NCRIT. Increase NCRIT to permit '/
     4 ' whole front to be assembled'/)
  420 FORMAT(/' KROW = ',I5,' LCOL = ',I5/)
  424 FORMAT(/' KHED LHED ')
  428 FORMAT(2I6)
  432 FORMAT(/' KDEST ',' LDEST ')
  436 FORMAT(/' EQ Matrix Element No. = ',I6/)
  440 FORMAT(20F5.2)
  441 FORMAT(I5,20F5.2)
  448 FORMAT(/' LC = ',I5/' KR = ',I5/' LPIV ',' KPIV'/)
  452 FORMAT(/' Pivotal Row = ',I4,' Pivotal Column = ',I4,
     1 ' Pivot = ',E16.8)
```

```
  456 FORMAT(/' JMOD'/)
  460 FORMAT(/' Right Hand Vector'/)
  464 FORMAT(I5,E16.8)
  468 FORMAT(/' Pivotal Row '/)
  476 FORMAT(/' Warning - Matrix Singular or Ill Conditioned ')
  480 FORMAT(/' FAC = ',E16.8)
  490 FORMAT(/' NK(I) = ',10I5)
      RETURN
      END
C
      SUBROUTINE BACSUB(NMAX,DFMAX,NCNMAX
     1 ,NP,NH,ND1,NLP,NOPP,MDF,NCOD,BC,R1,SK)
C
C
C Back substitution for full pivoting
C
      INTEGER NMAX, DFMAX, NCNMAX
      COMPLEX*16 PVKOL, QQ , BC, R1, SK, GASH, PIVOT,CZERO
C DOUBLE PRECISION PVKOL, QQ , BC, R1, SK, GASH, PIVOT
      INTEGER KDEST, NK, LHED, KHED, KPIV, LPIV, JMOD
      INTEGER NOPP, MDF, NCOD,NP,NH,ND1,NLP
      INTEGER I, IDF, J, K, KPIVRO, KRO, KROW,
      1 L, LCO, LCOL, LPIVCO
      DIMENSION
     1 LDEST(NCNMAX),KDEST(NCNMAX),NK(NCNMAX)
     2 ,LHED(NMAX),KHED(NMAX),KPIV(NMAX),LPIV(NMAX),
     3 JMOD(NMAX),QQ(NMAX),PVKOL(NMAX)
      DIMENSION
     1 NOPP(NMAX),MDF(NMAX),NCOD(DFMAX),BC(DFMAX)
     2,R1(DFMAX)
     3,SK(NMAX*NMAX)
C
C Back substitution
C
      CZERO = DCMPLX(0.0D0,0.0D0)
C
      DO 4 I = 1, NP
      SK(I) = BC(I)
    4 CONTINUE
      DO 32 IV=1,NP
      BACKSPACE ND1
      READ(ND1)
     1 KRO,LCOL,LPIVCO,(LHED(L),QQ(L),L=1,LCOL),
     2 KROW,PIVOT,KPIVRO,(PVKOL(K),KHED(K),K=1,KROW)
      BACKSPACE ND1
D WRITE(NLP,404)
D WRITE(NLP,408) KRO, LCOL, LPIVCO
```

```
D WRITE(NLP,408) (LHED(L), L = 1,LCOL)
D WRITE(NLP,412) (QQ(L), L = 1, LCOL)
      LCO = IABS(LHED(LPIVCO))
      IF(NCOD(LCO).GT.0) GO TO 24
      GASH = CZERO
      QQ(LPIVCO) = CZERO
      DO 16 L = 1, LCOL
      GASH = GASH - QQ(L) * SK(IABS(LHED(L)))
   16 CONTINUE
      SK(LCO) = R1(KRO) + GASH
      GO TO 32
   24 CONTINUE
      NCOD(LCO) = 1
   32 CONTINUE
D WRITE(NLP,416)
      DO 36 L = 1, NH
      J = NOPP(L) - 1
      IDF = MDF(L)
D WRITE(NLP,420) L, (SK(J+I), I = 1, IDF)
   36 CONTINUE
  404 FORMAT(' Tape Contents')
  408 FORMAT(10I5)
  412 FORMAT(5E16.8)
  416 FORMAT(' Results')
C 420 FORMAT(I5, 6E18.9)
  420 FORMAT(I5, 12F7.2)
  RETURN
  END
C
      SUBROUTINE ABFIND(NEMAX,DFMAX,NCNMAX,NBNMAX
     1 ,NP,NH,NE,NBN,NCN,ND1,NELL,NLP
     2 ,NOP,NCOD,BC,R1,ESTIFM,XX1)
C
C Routine to give an element matrix, fixed bondary
C condition and force vector(rhs).
C
      INTEGER NEMAX, NBNMAX,DFMAX, NCNMAX
      COMPLEX*16 BC, R1, ESTIFM,XX1,TXX1
      INTEGER NOP, NCOD
      INTEGER NP,NH,NE,NBN,NCN,ND1,NELL,NLP
      DOUBLE PRECISION HARVEST, G05CAF
      INTEGER IROW, JCOL
      DIMENSION
     1 NOP(NEMAX,NBNMAX),NCOD(DFMAX),BC(DFMAX)
     2,R1(DFMAX),XX1(DFMAX),TXX1(DFMAX)
     3,ESTIFM(NCNMAX,NCNMAX)
     4,NBN(NE),NCN(NE)
```

```
C
      HARVEST = 1.0D0
C
C*** Initialize nag random generator.
C
      CALL G05CBF(0)
C
C***Process all columns and rows.
C
      DO 200 IROW = 1, NCN(NELL)
      DO 100 JCOL = 1, NCN(NELL)
C
C***Generate random element matrix using NAG. This will be calculated by
C the FE codes as well as right hand side vector, when inserting the
C the solver as a subroutine to the FE program.
C
      ESTIFM(IROW,JCOL) = DCMPLX(G05CAF(HARVEST),G05CAF(HARVEST))
C
  100 CONTINUE
  200 CONTINUE
C
      DO 260 IROW=1,NCN(NELL)
C
      N = ABS(NOP(NELL,IROW))
C
C*** Store corresponding solution for this element in a vector.
C
      TXX1(IROW) = XX1(N)
C
  260 CONTINUE
C
C***Multiply element matrix by the initial solution vector to get the
C right hand side vector, BC()
C
      CALL MATMUL(ESTIFM, NCNMAX, TXX1,NCNMAX , BC, NCNMAX,
NCN(NELL)
     1, NCN(NELL))
C
C*** Assemble the right hand side vector.
C
      DO 265 IROW=1,NCN(NELL)
      N = ABS(NOP(NELL,IROW))
      R1(N) = R1(N) + BC(IROW)
  265 CONTINUE
C
C*** Set NCOD(I) to unity if node I has fixed boudary condition.
C
```

```
D WRITE(NLP,6001)NELL
C DO 11 IROW=1,NCN(NELL)
C IF(BC(IROW).NE.0.d0)NCOD(IROW)=1
C 11 CONTINUE
C
C 6001 FORMAT(//'Element Number = ',I5)
      RETURN
      END
      SUBROUTINE MATMUL(A, IA, B, IB, C, IC, L, M, N)
C *** Subroutine MATirx MULtiplication
C ***(c) Peter and Jacqueline A. Bettess, 1986
C
C PURPOSE :
C Post multiplies matrix A by matrix B to give matrix C.
C
C HISTORY :
C Written June 1986.
C Modified by Christine Barbier, August 1989.
C Modified by Alireza Baghbani, October 1996
C (B and C are column vectors).
C
C ARGUMENTS IN :
C
C A : Matrix A.
C IA : First dimension of matrix A.
C B : Matix B.
C IB : First dimension of matrix B.
C IC : Number of rows in C.
C L : Number of rows used in A and C.
C M : Number of columns used in B and C.
C N : Number of columns used in A and rows used in B.
C
C ARGUMENTS OUT :
C
C C : Product matrix, C = A * B
C
C
      COMPLEX*16 A, B, C
      INTEGER IA, IB, IC, IL, IN, L, M, N
      DIMENSION A(IA,IA), B(IB), C(IC)
C
C***process rows in A and C
C
      DO 30 IL = 1, L
C
      C(IL) =(0.0D0,0.0D0)
C
```

```
C***form inner product
C
      DO 10 IN = 1, N
      C(IL) = C(IL) + A(IL,IN) * B(IN)
   10 CONTINUE
   30 CONTINUE
      RETURN
      END
```

C.9 Test Example

A test example is solved. The mesh data is read from a data file which consists of 3 elements and 17 nodes. Each node is assumed to have 1 degree-of-freedom. The initial solution vector and the element matrix entries (all complex numbers) are generated by NAG random data generator. The node numbering is not in a complete ascending order. The total number of nodes is set to the bigest node number in the mesh (=27). Two types of elements are used in the mesh (8-node and 9-node elements). The solution produced by the solver and the difference with the introduced ones are given element by element.

Example data file:

```
1  3  27
8  1  2  3  9  15  14  13  7
9  3  5  6  12  18  17  15  9  11
8  13  14  15  21  27  26  25  19
```

Results:

```
Problem parameters
MWGA = 1
Total No. of Elements = 3
Total No. of Nodes = 27
```

```
Element number = 1
NO., Node NO. —— Int. Sols. ——— Comp. Sols. ———— Difference
```

1	1	.80D+00	.23D+00	.80D+00	.23D+00	.14D-14	-.23D-14
2	2	.37D+00	.23D+00	.37D+00	.23D+00	-.32D-14	-.14D-14
3	3	.88D+00	.47D-01	.88D+00	.47D-01	-.89D-15	-.21D-16
4	9	.35D+00	.49D+00	.35D+00	.49D+00	.56D-16	.28D-15
5	15	.90D+00	.43D+00	.90D+00	.43D+00	-.10D-14	.17D-14
6	14	.40D+00	.62D+00	.40D+00	.62D+00	-.56D-15	.21D-14
7	13	.39D-01	.23D-01	.39D-01	.23D-01	.40D-15	-.12D-14
8	7	.64D+00	.69D+00	.64D+00	.69D+00	.12D-14	-.11D-15

ELEMENT NUMBER = 2

NO.,	Node NO.	—— Int. Sols.	———	Comp. Sols.	———	Difference	
1	3	.88D+00	.47D-01	.88D+00	.47D-01	-.89D-15	-.21D-16
2	5	.39D-01	.58D+00	.39D-01	.58D+00	.15D-14	.11D-15
3	6	.95D+00	.62D+00	.95D+00	.62D+00	.40D-14	.17D-14
4	12	.89D-01	.54D-01	.89D-01	.54D-01	.28D-15	.10D-14
5	18	.64D+00	.45D+00	.64D+00	.45D+00	.16D-14	-.28D-15
6	17	.24D+00	.62D+00	.24D+00	.62D+00	.14D-15	.26D-14
7	15	.90D+00	.43D+00	.90D+00	.43D+00	-.10D-14	.17D-14
8	9	.35D+00	.49D+00	.35D+00	.49D+00	.56D-16	.28D-15
9	11	.78D+00	.87D+00	.78D+00	.87D+00	-.29D-14	-.48D-14

ELEMENT NUMBER = 3

NO.,	Node NO.	—— Int. Sols.	———	Comp. Sols.	———	Difference	
1	13	.39D-01	.23D-01	.39D-01	.23D-01	.40D-15	-.12D-14
2	14	.40D+00	.62D+00	.40D+00	.62D+00	-.56D-15	.21D-14
3	15	.90D+00	.43D+00	.90D+00	.43D+00	-.10D-14	.17D-14
4	21	.60D+00	.46D+00	.60D+00	.46D+00	.44D-15	-.61D-15
5	27	.93D+00	.44D+00	.93D+00	.44D+00	-.18D-14	-.12D-14
6	26	.82D+00	.62D+00	.82D+00	.62D+00	.22D-15	-.78D-15
7	25	.24D-01	.71D+00	.24D-01	.71D+00	-.97D-16	-.89D-15
8	19	.86D+00	.13D+00	.86D+00	.13D+00	.36D-14	.15D-14

Appendix D

Some Useful Functions

There are some functions that satisfy the wave equations and the relevant boundary conditions for some simple shape of the diffracting objects. Some of these are used in chapter 3 to give the analytical solutions for the problem. All these functions need to have two certain characteristics to describe the physical behaviour of wave propagation. They have harmonic (sinusoidal) behaviour and decay as they travel outwards from the pole. Therefore these functions are a function of *cos* or *sin* functions

$$W(r) = f(cos(r)) \qquad or \qquad W(r) = g(sin(r)) \tag{D.1}$$

or a combination of f and g. The solutions for the wave equation and its boundary conditions are complex for real values of r. An example of the complex function is $e^{(ir)} = cos(r) + sin(r)$ and its plot is given below:

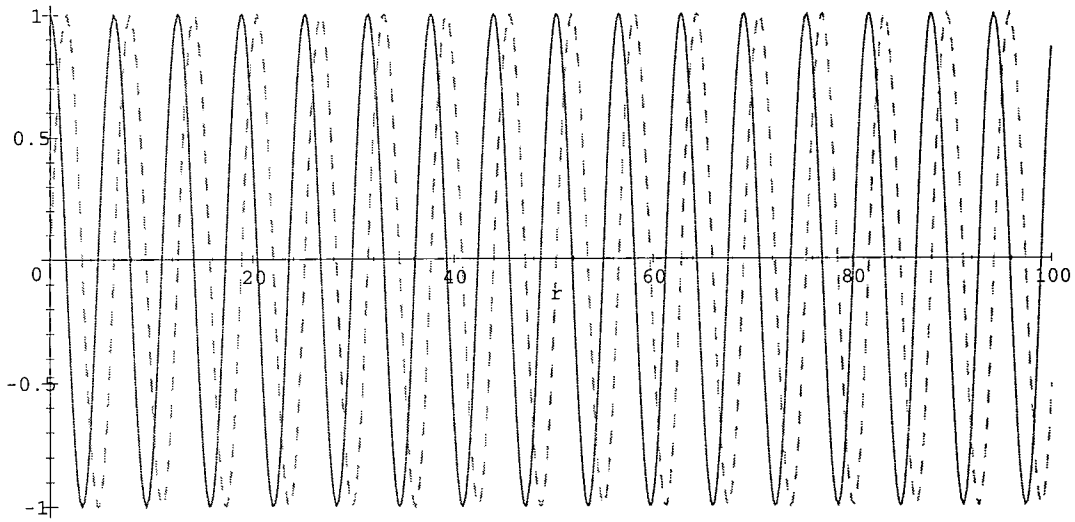

Figure D.1: solid line is $cos(r)$ and dashline is $sin(r)$)

The waves travel outwards and decay to zero at infinity due to media damping. The decay or damping function varies depends on the material in which the waves travel and the dimension of the problem. Plots of two example functions are given below:

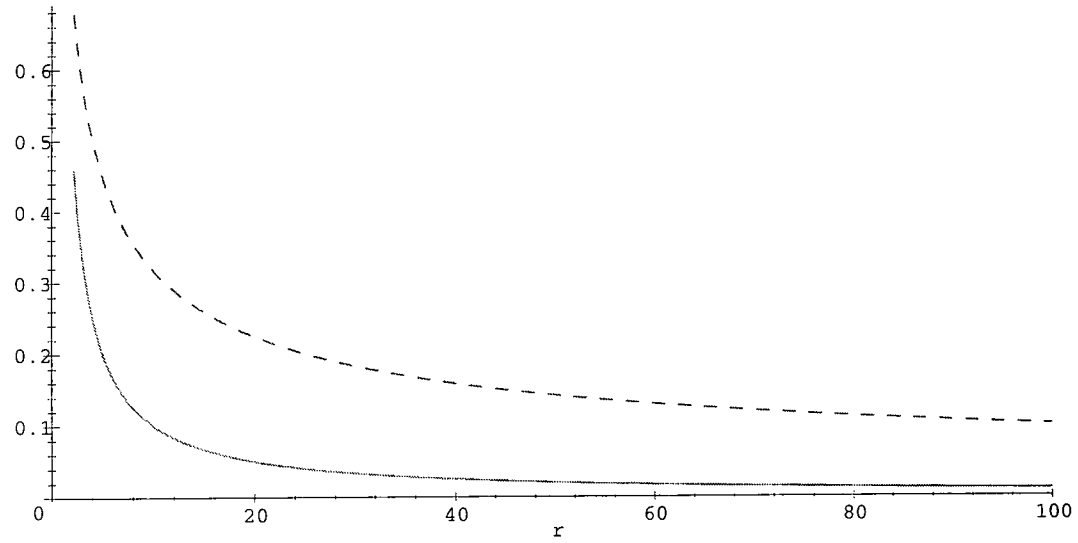

Figure D.2: solid line is $1/r$ and dashline is $1/\sqrt{r}$)

So another term has to be added to the wave function giving

$$W(r) = f(r)d(r) \tag{D.2}$$

Plots of two example functions are given below:

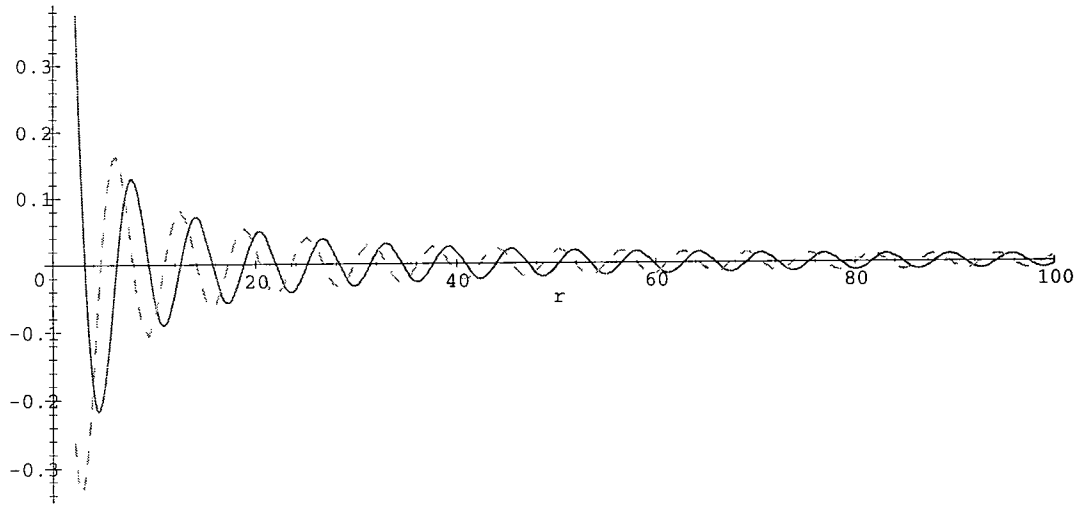

Figure D.3: solid line is $cos(r)/r$ and dashline is $sin(r)/r$)

From the literature we can find some functions that behave as above. Some of them are Bessel, Hankel and Mathieu functions. Bessel and Hankel functions

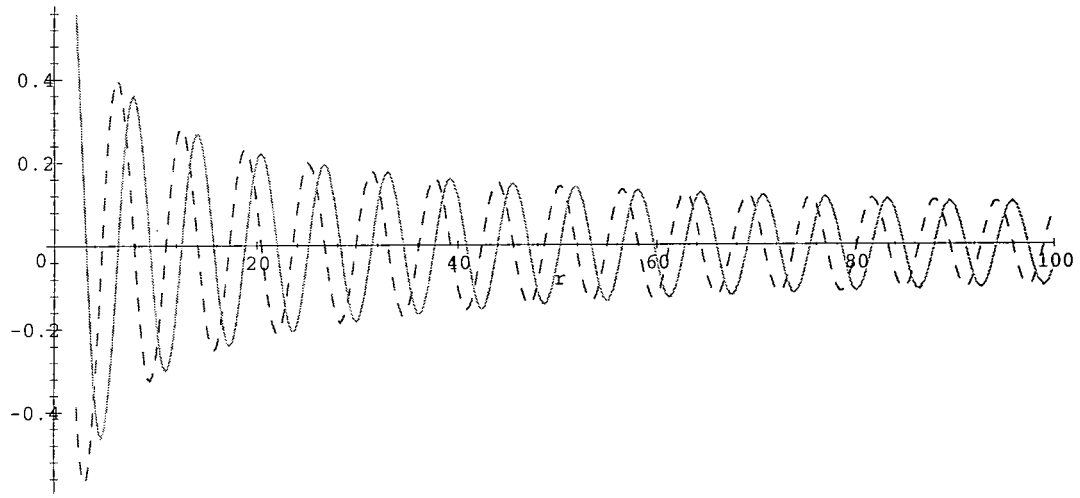

Figure D.4: solid line is $cos(r)/\sqrt{r}$ and dashline is $sin(r)/\sqrt{r}$)

satisfy the wave and boundary conditions when the solid boundary has a circular cross section. Mathieu functions satisfy these equations when this is an ellipse. They are given in standard text books (see e.g. Abramowitz and Stegun [1]). A brief description of these functions and their plots is given here for easy access as well as visual understanding of the wave functions.

D.1 Bessel functions

The Bessel function of the **first kind** of order n is one of above mentioned functions (Abramowitz and Stegun [1], page 227)

$$J_n(r) = r^n \sum_{m=0}^{\infty} \frac{-1^m r^{2m}}{2^{2m+n} m!(n+m)!} \tag{D.3}$$

for large value of r this gives (Abramowitz and Stegun [1], page 228)

$$J_n(r) \approx \sqrt{\frac{2}{\pi r}} cos(r - \frac{n\pi}{2} - \frac{\pi}{4}) \tag{D.4}$$

The Bessel function of the **second kind** of order n is one of the other functions that satisfy the requirements (Abramowitz and Stegun [1], page 238)

$$Y_n(x) = \frac{1}{sinn\pi}[J_n(x)\cos n\pi - J_{-n}(x)] \tag{D.5}$$

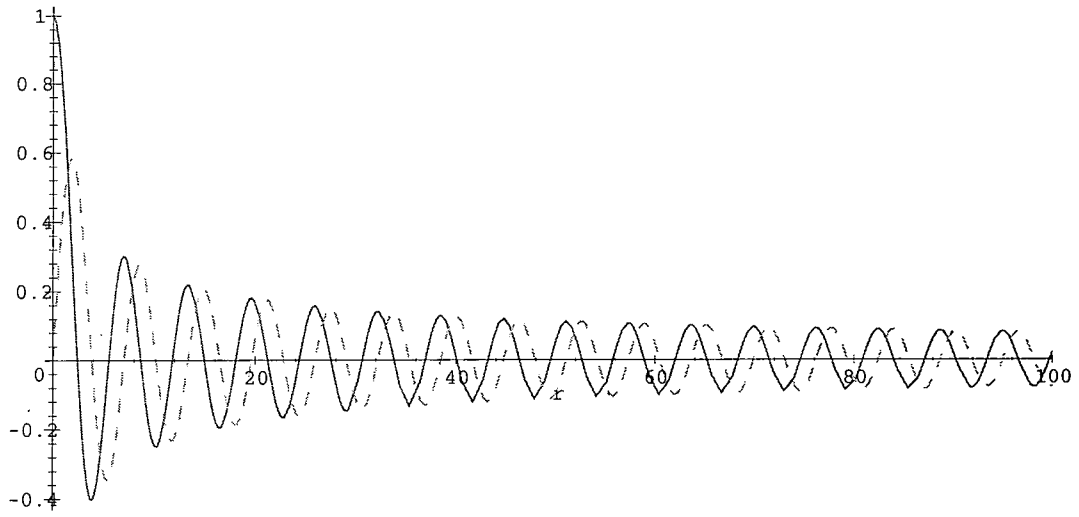

Figure D.5: Bessel function of the first kind of order 0 and 1 (solid line is J_0, dashline is J_1)

D.2 Hankel functions

As was mentioned above, the solutions for wave equations are complex for real values of r. For this reason a linear combination of Bessel functions of the first and second kind is used as

$$H_n^{(1)}(r) = J_n(r) + iY_n(r) \tag{D.6}$$

where $H_n^{(1)}$ are called Bessel functions of the third kind of order n or the **first Hankel** functions of order n.

As can be seen from Figure D.8, the absolute value of the first Hankel function of zero order decays like $2/\sqrt{\pi r}$.

D.3 Mathieu functions

Mathieu functions satisfy the wave equation and the boundary conditions when the diffracting body has an elliptical cross section. The mathematical properties of these functions are given by Abramowitz and Stegun ([1], page 721-744). Plots of these functions are given below:

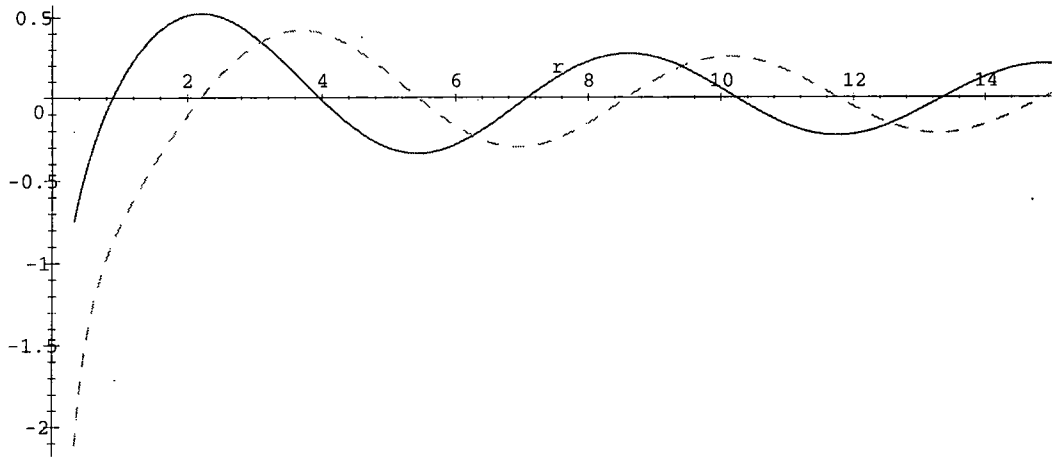

Figure D.6: Bessel function of the second kind of order 0 and 1 (solid line is Y_0, dashline is Y_1)

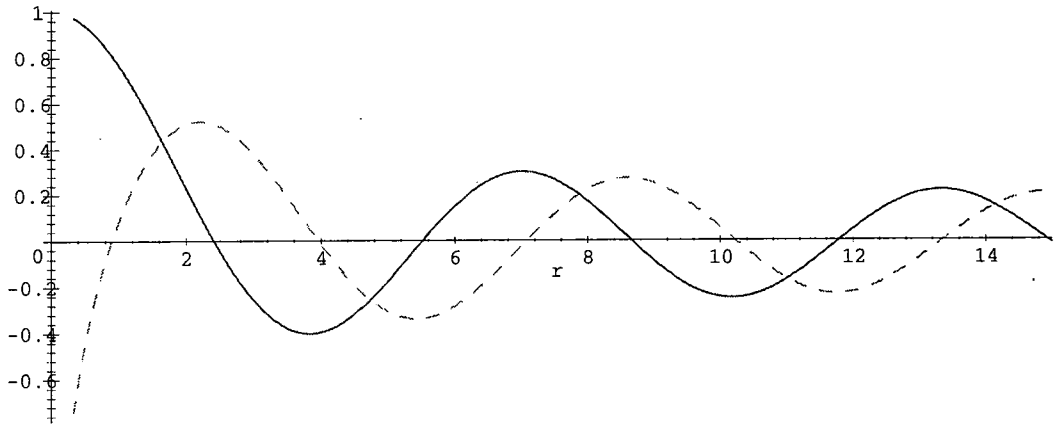

Figure D.7: Hankel function of the first kind of order 0- solid line the real and dashline is the imaginary part

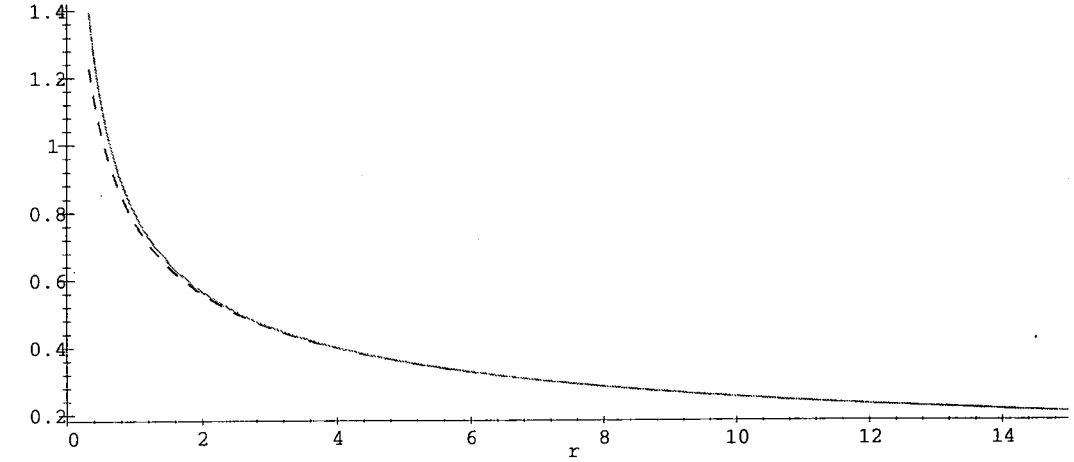

Figure D.8: Solid line is $|H_0^{(1)}|$ and dash line is $2/\sqrt{\pi r}$

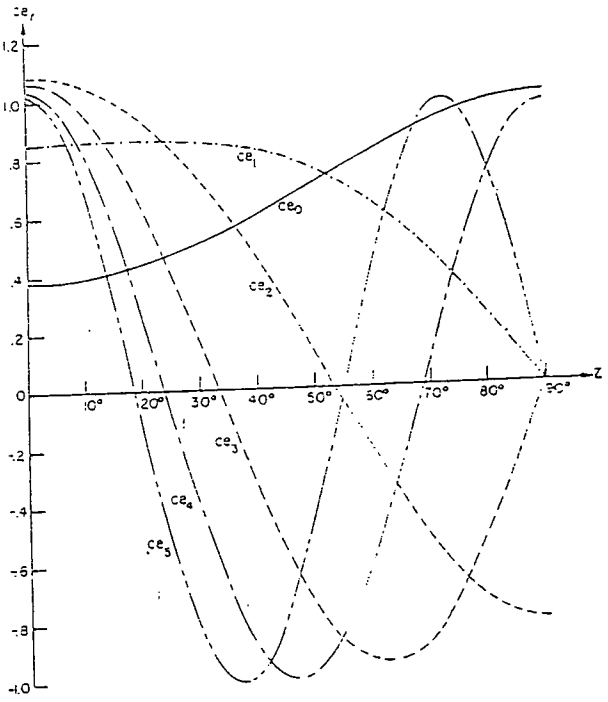

Figure D.9: Even Periodic Mathieu Functions (ce), order 0-5, $q = 1$

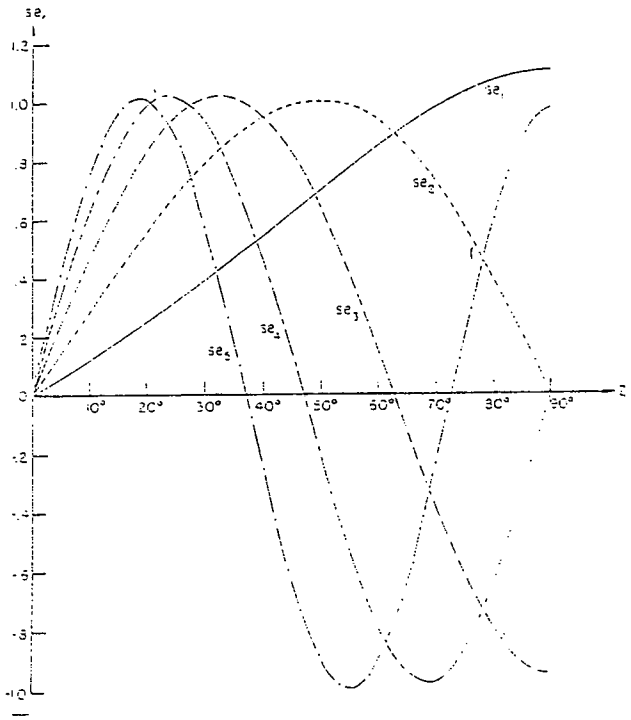

Figure D.10: Odd Periodic Mathieu Functions (se), order 0-5, $q = 1$

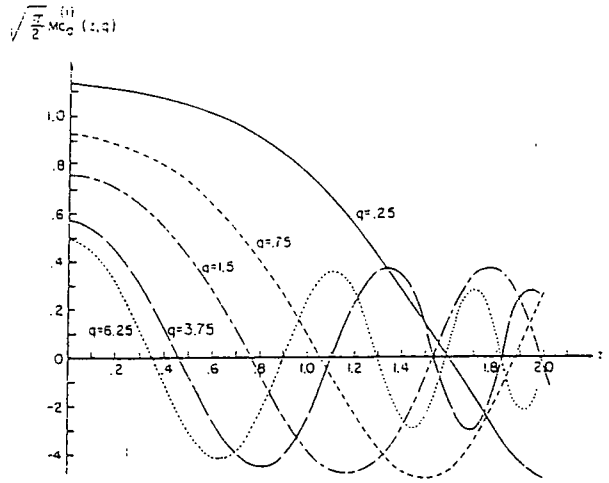

Figure D.11: Radial Mathieu Function of the first kind ($Mc^{(1)}$)

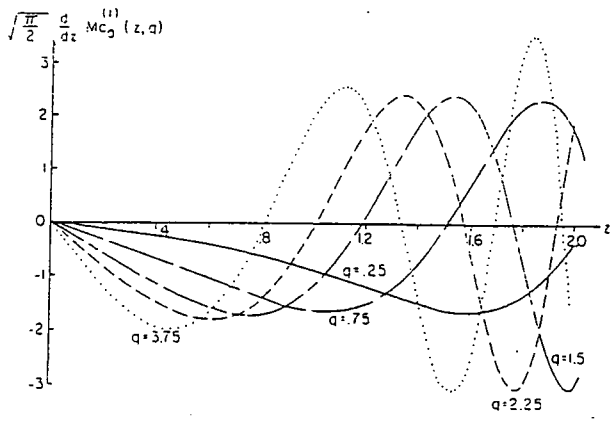

Figure D.12: Derevetive of the Radial Mathieu Function of the first kind

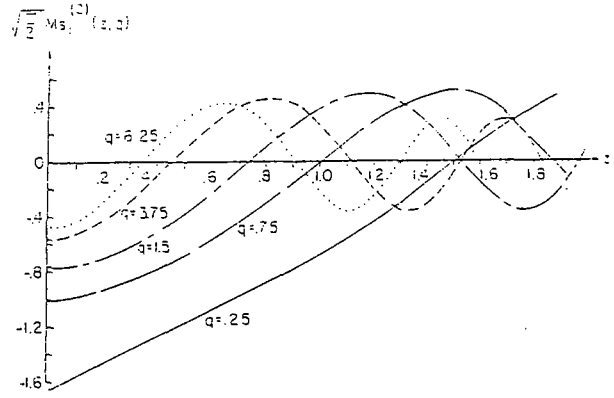

Figure D.13: Radial Mathieu Function of the second kind ($Ms^{(2)}$)

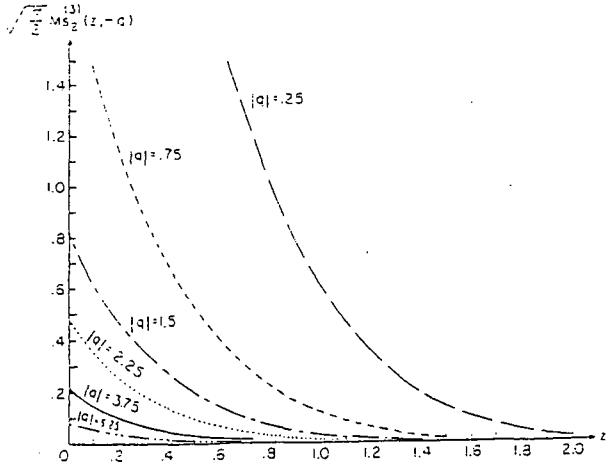

Figure D.14: Radial Mathieu Function of the third kind ($Ms^{(3)}$)

Appendix E

A Note On the Construction of Infinite Element Shape Functions

The construction of an infinite element shape function was explained in section 5.3. As was explained there, the diffracted wave amplitudes for 2D problems decay approximately as $1/\sqrt{r}$. In that section, it was concluded that in using a quadratic polynomial as a parent shape function in the infinite direction, the amplitude decay of $\frac{1}{r}$ was achieved. Therefore the base function was multiplied by a factor of $\sqrt{r}$ to achieve a decay of $\frac{1}{\sqrt{r}}$. Now consider shape functions of a quadratic one dimensional finite element (Figure 5.1).

$$P_1(\xi) = -0.5\xi(1-\xi)$$

$$P_2(\xi) = (1+\xi)(1-\xi)$$

$$P_3(\xi) = 0.5\xi(1+\xi) \tag{E.1}$$

The finite to infinite geometry mapping is given by equation (5.11) as

$$\xi = 1 - \frac{2r_0}{r} \tag{E.2}$$

Substituting this into equation (E.1) gives

$$P_1(r) = -\frac{r_0}{r} + \frac{2r_0^2}{r^2}$$

$$P_2(r) = \frac{-4r_0}{r} + \frac{4r_0^2}{r^2}$$

$$P_3(r) = 1 - \frac{3r_0}{r} + \frac{2r_0^2}{r^2} \tag{E.3}$$

Now if P_1 or P_2 is taken as the base function, then an appropriate infinite element shape function may be achieved by multiplying the finite element shape function by a factor of $\sqrt{r}$, giving

$$N(r) = P(r)\sqrt{r} \tag{E.4}$$

where $N(r)$ is the infinite element shape function. However, if P_3 is taken as the base function, then an appropriate infinite element shape function may be achieved by multiplying the finite element shape function by a factor of $r^{-1/2}$, giving

$$N(r) = P(r)\frac{1}{\sqrt{r}} \tag{E.5}$$

Equations (E.4) and (E.5) are the base functions for Type 1 and Type 2 infinite elements respectively. Therefore, in using either of the infinite elements, only some of the shape functions decay as $\frac{1}{\sqrt{r}}$.

Perhaps, the most accurate method would be to use different factors for different nodes so that all the shape functions of the infinite element decay like $\frac{1}{\sqrt{r}}$. A similar procedure was employed by Astley *et al* [7] to explain the calculation of the radiation matrix for Type 1 infinite elements. However, in the above reference's formulation a troublesome term, an exponential term of the form $\exp i2kr$, appears in the formulation. This term becomes undefined as r tends to infinity. The upper limit of the integral was ignored to overcome this problem. Although the results produced by this method are very satisfactory, there is no mathematical justification for this. Fortunately, in using the the wave envelope approach the troublesome term disappears from the formulation thus giving the most accurate and mathematically justified infinite element.

By adding the harmonic term (see section 5.3.2) and applying the finite and infinite element compatibility criteria (see section 5.3.3) the final shape function

for the Type 2 infinite element would then become

$$N(r) = P(\frac{r_0}{r})^{1/2} \exp ik(r - r_0) \tag{E.6}$$

Appendix F

Radiation Matrix for Pre-Type 2 Infinite Element

A natural way of developing wave envelope mapped infinite elements for wave diffraction problems seems to be to use the usual mapped infinite element shape function as its shape function and the complex conjugate of it as the element weighting function (this element termed here as Pre-Type 2 infinite element). However, these shape and weighting functions lead to undefined radiation matrix integrals which are explored below.

Consider the radiation matrix, equation (5.34)

$$\mathbf{R}^e = \int_{\Gamma_\infty^e} \mathbf{W}^T c c_g \frac{\partial \mathbf{N}}{\partial n} d\Gamma \tag{F.1}$$

The usual mapped infinite element shape function is given by equation (5.22) as

$$N(r) = P(\frac{r}{r_0})^{1/2} \exp ik(r - r_0) \tag{F.2}$$

Using the wave envelope approach the weighting function is the complex conjugate of the shape function so that

$$W(r) = P(\frac{r}{r_0})^{1/2} \exp -ik(r - r_0) \tag{F.3}$$

$\frac{\partial N}{\partial n}$ in equation (F.1) is given by equation (5.55) as

$$\frac{\partial N}{\partial n} \approx \frac{\partial N}{\partial r} = \left(\frac{\partial P}{\partial r} + \frac{P}{2r} + ikP\right)\left(\frac{r}{r_0}\right)^{1/2} \exp ik(r - r_0) \tag{F.4}$$

where P is the finite element shape function and this for the nodes which are located at the infinite edge of the element can be written as

$$P = P^*(\eta)P_3^{"}(\xi) \tag{F.5}$$

where P^* is the finite element shape function for a quadratic line element in the η direction given by equation (4.36) and $P_3^{"}$ is the finite element shape function for a quadratic line element in the ξ direction (i.e. shape function for node 3 in Figure 5.1). $P_3^{"}$ is therefore

$$P_3^{"}(\xi) = 0.5\xi(1+\xi) \tag{F.6}$$

Substituting finite to infinite geometry mapping equation (5.23) to this gives

$$P^{"}(r) = 1 - \frac{3r_0}{r} + \frac{2r_0^2}{r^2} \tag{F.7}$$

and its derivative as

$$\frac{\partial P^{"}}{\partial r} = \frac{3r_0}{r^2} - \frac{4r_0^2}{r^3} \tag{F.8}$$

The equation (F.5) can be rewritten as

$$P = P^*(\eta)P^{"}(r) \tag{F.9}$$

and similarly equation (F.3) can be rewritten as

$$W(r) = P^*P^{"}(\frac{r}{r_0})^{1/2}\exp -ik(r-r_0) \tag{F.10}$$

and equation (F.4) as

$$\frac{\partial N}{\partial n} \approx \frac{\partial N}{\partial r} = P^*\left(\frac{\partial P^{"}}{\partial r} + \frac{P^{"}}{2r} + ikP^{"}\right)\left(\frac{r}{r_0}\right)^{1/2}\exp ik(r-r_0) \tag{F.11}$$

Substituting equations (5.44), (5.47), (F.7), (F.8), (F.10) and (F.11) into equation (F.1) gives

$$\mathbf{R} = \int_{-1}^{+1} \mathbf{P}^{*T}[\frac{ik}{r_0}r^2 + (\frac{1}{2r_0} - 6ik)r + 13ikr_0]\mathbf{P}^* f(\eta)d\eta \tag{F.12}$$

where $f(\eta)d\eta = d\theta$ as given in equation (5.47). At infinity r tends to infinity and therefore the line integral is undefined. The same result was achieved by calculating

the line integrals using Maple mathematical software.